THE UNIVERSITY
of EDINBURGH

This thesis has been submitted in fulfilment of the requirements for a postgraduate degree (e.g. PhD, MPhil, DClinPsychol) at the University of Edinburgh. Please note the following terms and conditions of use:

This work is protected by copyright and other intellectual property rights, which are retained by the thesis author, unless otherwise stated.
A copy can be downloaded for personal non-commercial research or study, without prior permission or charge.
This thesis cannot be reproduced or quoted extensively from without first obtaining permission in writing from the author.
The content must not be changed in any way or sold commercially in any format or medium without the formal permission of the author.
When referring to this work, full bibliographic details including the author, title, awarding institution and date of the thesis must be given.

Investigating the Role of Semaphorin7a in Paracetamol Induced Liver Injury

Eilidh Livingstone

Doctor of Philosophy

The University of Edinburgh

2019

Declaration

I declare that this thesis has been composed solely by myself and that it has not been submitted, in whole or in part, in any previous application for a degree. Except where stated otherwise by reference or acknowledgment, the work presented is entirely my own.

I confirm that this thesis does not exceed the 100,000 word limit set by the University of Edinburgh

Signed by Eilidh Livingstone Date: 6th September 2019

Lay Summary

Paracetamol overdose is responsible for 46% of drug-induced liver injury in the Western world, causing 200 deaths in the UK and 500 deaths in the USA per annum. The current therapy, N-Acetyl-Cysteine, is only effective within 12 hours after overdose. When the overdose is moderate, it is still possible for the liver to recover through its innate healing process. However, after a severe overdose this is not the case. Severe liver injury prevents the liver from performing vital tasks. This results in multiple organ failure and fatality. The only effective option for treatment is a liver transplantation, which is limited by organ availability and associated transplant related morbidity. New therapies are needed outside the initial 12 hour window to improve the outcome of paracetamol induced liver injury.

The liver's innate healing process involves immune cells which remove debris caused by paracetamol injury and promote liver regeneration. Understanding how immune cells promote these healing processes and how to manipulate the immune cells to perform these healing therapies, may lead to the development of new regenerative therapies for paracetamol overdose.

In this thesis, I investigate the role the signalling protein Semaphorin 7a, which has previously been shown to manipulate the immune system. I show that Semaphorin 7a is expressed by liver cells which act to contain the spread of damage caused by paracetamol injury. A deficiency of Semaphorin 7a, results in more paracetamol induced liver injury and inflammation.

This work builds on previous knowledge on how Semaphorin 7a modulates the immune system and demonstrates a novel role where Semaphorin 7a limits the spread of damage caused by paracetamol. By understanding how the liver protects and repairs itself following paracetamol injury, we can continue to develop innovative therapies that improve the outcome after a paracetamol overdose.

Abstract

Paracetamol (Acetaminophen, APAP) overdose is responsible for 46% of drug induced liver injury in the Western world, causing 200 deaths in the UK and 500 deaths in the USA per annum. The current treatments for APAP overdose are N-Acetyl-Cysteine, which is only effective in the first 12 hours after overdose, or in most serious cases a liver transplantation. Novel therapies are needed outside of this 12 hour window. After a moderate APAP overdose, patients will recover. This process involves macrophages which phagocytose necrotic cells and secrete signals which stimulate hepatocyte proliferation. Understanding and manipulating pathways involved in this endogenous repair process may lead to new therapeutic strategies.

Semaphorins are a diverse group of signalling proteins that modulate axon guidance and immune responses. Semaphorin 7a (Sema7a) is a chemoattractant for dendritic cells, monocytes and macrophages. It can also modulate if macrophages secrete pro- or anti- inflammatory cytokines. This thesis investigates the role of Sema7a during APAP injury.

24 hours after a 350 mg/kg APAP overdose, Sema7a was expressed by viable Hnf4α+ peri-necrotic hepatocytes. To further examine the role of Sema7a during APAP injury, mice deficient for Sema7a (Sema7a KO) were compared to wild type (WT) mice, during a time course of APAP injury and recovery. Histological analysis displayed increased injury and necrosis in the Sema7a KO mice, with significantly more neutrophils in the necrotic area at 24 hours post APAP administration. In addition, Sema7a KO mice had increased serum levels of the pro-inflammatory cytokines IL-6 and CXCL1, in comparison to WT mice. These findings demonstrate novel roles of Sema7a reducing injury and inflammation caused by APAP overdose.

Acknowledgements

I would like to thank my supervisors, Stuart Forbes and Luke Boulter and my PhD committee for their advice and support over the last four years. I am indebted to Lara Campana, for taking me under her wing, endless patience and knowledge and being there every step of the way, it would have been a very different project without you. I would also like to thank all the members of the Forbes lab, past and present, for making my PhD enjoyable, and for answering all my questions over the years. I am also hugely grateful to Ben Dwyer for all the life chats and editing skills, and to Phil Starkey Lewis who taught me the APAP experiments. Thank you, Janet Man and Rhona Aird who tirelessly work to keep the Forbes lab ship shape. I would like to extend my huge thanks to Jennifer Cartwright, working with you was a delight and many of these experiments could not have happened without you. Special thanks go to Amy Pegg, Duncan Godwin and Prof Clare Blackburn who encouraged me to start a PhD.

I would also like to thank Fiona Rossi for all her expertise and help with flow cytometry over the years. Theresa, Audrey, Helen and Marilyn who work tirelessly in tissue culture and at the autoclave, we are so lucky to have you. To Bertrand Vernay and Matthieu Vermeren for confocal imaging, and to Eoghan O' Duibhir who taught me how to perform image analysis with the Operetta microscope.

I would also like to thank my incredible parents who have encouraged and supported me throughout my education. I couldn't have done any of this without you. I am hugely grateful to my brother Callum, Auntie Sheena, family and dear friends who cheered me along the way through the good and bad times. Huge thanks go to my fellow PhD students Paul Rouse and Katie Ember, the trials of the PhD were much more enjoyable with your wonderful companionship. Lastly, Rose Rae, my long suffering, but very supportive, flatmate.

Contents

Abbreviations

%PKH+	Frequency of phagocytosis
AILI,	Acetaminophen Induced Liver Injury
AJ	Adherens Junctions
AKT	Protein Kinase B
ALP	Alkaline Phosphatase
ALT	Alanine Transaminase
ALF	Acute liver failure
ANOVA	Analysis of variance
Apaf-1	Apoptotic protease factor -1
APAP	Acetaminophen, Paracetamol
ApopTs	Apoptotic thymocytes
ASK-1	Apoptosis Signalling-Regulating Kinase 1
AST	Aspartate Transaminase
ATP	Adenosine Triphosphate
AWERB	Animal Welfare and Ethical Review Body
BAL	Bronchoalveolar Lavage
BMDMs	Bone Marrow Derived Macrophages
BrdU	Bromodeoxyuridine
CCl2	C-C Motif Chemokine Ligand 2, also known as MCP1
CD	Cluster of Differentiation
CD11b	Integrin alpha M
CK19	Cytokeratin19
CMTMR	CMTMR, an orange fluorescent dye;
CSF1	Macrophage Colony-Stimulating Factor

CSF1R	Colony Stimulating Factor 1 Receptor
CV	Central Vein
Cx	Connexins
CX_3CR1	C-X3-C Motif Chemokine Receptor 1
CXCL1	Chemokine (C-X-C motif) Ligand 1
CXCL2	Chemokine (C-X-C motif) Ligand 2, (MIP-2)
CXCR2.	C-X-C Chemokine Receptor Type 2
Cyp2E1	Cytochrome P450 2E1
DAB	3,3′-Diaminobenzidine
DAMPs	Danger Associated Molecular Patterns
DAPI	4′, 6-diamidino-2-phenylindole. Nuclear stain.
DC	Dendritic Cells
DILI	Drug induced liver injury
DMSO	Dimethyl Sulfoxide
DNA	Deoxyribonucleic acid
DNase	Deoxyribonuclease
DSS	Dextran Sodium Sulfate
EAE	Experimental Autoimmune Encephalomyelitis
ECM	Extra Cellular Matrix
EDTA	Ethylenediaminetetraacetic acid
EGF	Epidermal Growth Factor
ELISA	Enzyme-linked immunosorbent assay
ERF	Est2-Repressor Factor
FACS	Fluorescent Activated Cell Sorting
FFPE	Fixed in formalin overnight and paraffin embedded

FMO	Fluorescent Minus One
FP	Formylated Peptides
FPR1	FP Receptor 1
GTP	Guanosine-5'-triphosphate
GAP	GTPase activating protein.
GATA6	GATA-binding protein 6
$GdCl_3$	Gadolinium Chloride
GLDH	Glutamate Dehydrogenase
GnRH	Gonadotropin-Releasing Hormone
gPCR	Genomic DNA PCR.
GPI	Glycophosphatidylinositol
GSCF	Granulocyte-Colony Stimulating Factor
GSH	Glutathione
H&E	Haematoxylin and Eosin
HA	Hepatic Artery
HGF	Hepatocyte Growth Factor
HH	Hypogonadotropic Hypogonadism
HIF-1	Hypoxia-Inducible Factor
HMECs	Human Mammary Endothelial cells
HMGB1	High Mobility Group Box Protein 1
Hnf4α	Hepatocyte nuclear factor alpha
HSCs	Hepatic stellate cells
HSP	Heat Shock Protein
ICAM-1	Intercellular Adhesion Molecule 1(CD54)
Id3	Inhibitor of DNA binding 3
IFNγ,	Interferon Gamma

IHC	Immunohistochemistry
IL-	Interleukin -
iNKT	Invariant Natural Killer T cells
i.p	intraperitoneal
IPT	Immunoglobulin–Plexin–Transcription factor
IVC	Inferior Vena Cava
JAMs	Junction Adhesion Molecules
JMH	John Milton Hagan
JNK	c-Jun N-Terminal Kinase
KCs	Kupffer cells
KO	Knock Out
L/D	Live/Dead
LFT	Liver Function Test
LIMK	LIM Kinase
LPS	Lipopolysaccharide
LSECs	Liver Sinusoidal Endothelial Cells
MAC-1	Integrin αMβ2
MCP-1	Monocyte Chemoattractant Protein 1, CCL2
M-CSF	Macrophage Colony Stimulating Factor
MerTK	Mer Tyrosine Kinase
MFI	Mean Fluorescent Intensity
MIP-2	Macrophage Inflammatory Protein-2
MKK4/7	Mitogen-Activated Protein Kinase Kinase 4/7
MLKL	Mixed-Lineage Kinase Domain-Like Protein
MMPs	Matrix Metalloproteinases
MPT	Mitochondrial Permeability Transition

MAPK	MAP Kinase
MPO	Myeloperoxidase
mRNA	Messenger RNA
MSD	Meso Scale Diagnostics
mSema7a	Recombinant mouse Sema7a
MSI	Multispectral Imaging
Mϕ	Macrophages
NAC	N-Acetylcysteine
NAPQI	N-acetyl-p-benzoquinone imine
Nec-1	Necrostatin-1
NETs,	Neutrophil Extracellular Traps
NK	Natural Killer
NPCs	Non-Parenchymal Cells
Nrp	Neuropilin
FAK	Protein Tyrosine Kinase
OCT	Optimal Cutting Temperature
OPC	Oligodendrocyte Precursor
P/S	Penicillin/Streptomycin
pAKT	Phosphorylated Protein kinase B
PBS	Phosphate Buffered Saline Solution
PBST	PBS 0.1% Tween 20
PEC	Peritoneal Exudate Cells
pERK	Phosphorylated Extracellular-Regulated Kinase, also known as MAPK
p-FAK	Phosphorylated Protein Tyrosine Kinase 2
PGE2	Prostaglandin E2

PHx	Partial Hepatectomy
PKH	PKH26L a phagocytic dye
PMN	Polymorphonuclear leukocytes
POD	Paracetamol Overdose
PPIA1	Peptidyl-prolyl cis-trans isomerase
PSI	Plexin-Semaphorin- Integrin
PT	Portal Triad
PV	Portal Vein
QMRI	Queens Medical Research Institute
qRT-PCR	Quantitative Reverse Transcription Polymerase Chain Reaction
RAGE	Receptor for Advanced Glycation End products
RBD	Rho-GTPase Binding Domain
RIPK	Receptor-Interacting Protein Kinase
RNA	Ribonucleic Acid
ROS	Reactive Oxygen Species
RPMI	Rosewell Park Memorial Institute, culture medium
RT	Room Temperature
Sab	SH3 homology-associated BTK-binding protein
Sema	Semaphorin
Sema7a	Semaphorin 7a
Sema7a KO	Semaphorin 7a knock out mouse
SGZ	Subgranular zone
SLPI	Secretory Leucocyte Protease Inhibitor
SuRF	Shared university Research Facilities
TRCs	Taste Receptor Cells
TGF	Transforming Growth Factor

TGFβR1	TGFβ Receptor 1
T_H1	T helper 1 Cell
Tim2	T-cell immunoglobulin and mucin domain protein 2
TLR	Toll Like Receptor
TNFα,	Tumour Necrosis Factor α,
T_{regs}	regulatory T cells
TUNEL	Terminal deoxynucleotidyl transferase dUTP nick end labelling
VEGF	Vascular Endothelial Growth Factor
WT	Wild Type
ZO	Zonal Occludin proteins

Chapter 1- Introduction

Introduction

Paracetamol (Acetaminophen, APAP) is a widely used analgesic and antipyretic. Whilst safe at therapeutic doses, APAP overdoses cause 46% of acute liver failure in the western world. This equates to 50,000 emergency room visits, 26,000 hospitalisations and 500 deaths in the USA and 200 deaths in the UK per annum [1,2]. Overdosing on APAP occurs intentionally but is more commonly accidental, through patients taking a combination of painkillers for acute and chronic pain syndromes [3].

An overdose of APAP induces hepatocyte necrosis and inflammation. The clinical outcome can vary from a complete recovery to cerebral oedema, coagulopathy and death. In the short term, patients can be treated with N-acetylcysteine (NAC) which restores intracellular levels of glutathione, an antioxidant essential for APAP metabolism. Unfortunately, NAC is only truly effective in the first 12 hours after ingestion of APAP [3]. In extreme cases, the only viable therapy is a liver transplantation, but donor organs are in short supply. Research is therefore needed to find a suitable therapy to prevent liver failure after the initial 12 hour time window [3,4].

Basic liver anatomy

The liver is the largest internal organ with over 500 functions. It main roles include: filtering nutrient rich blood from the intestines, detoxification of xenobiotics and drugs, bile synthesis, glucose and lipid metabolism [5].

To facilitate these diverse functions the liver has a unique vasculature system consisting of densely packed fenestrated capillaries, termed sinusoids. Blood is supplied to the liver through both the hepatic artery (HA), which supplies oxygenated blood; and the portal vein (PV), which delivers nutrient rich blood from the intestine, to be filtered by the liver. The terminal branches of the HA and PV are associated with a biliary ductule, forming the portal triad (PT) (Figure 1. 1). Blood flows from the PT along the sinusoids and is collected by the central vein (CV), forming an oxygen concentration gradient. Adjacent to the sinusoids are cords of hepatocytes, the major epithelial cells of the liver, which perform the liver's functions. In between the hepatocytes are the bile canaliculi, which collect bile and excretory products from the hepatocytes. The bile canaliculi drain into the bile ductule in the PT. The bile is then transported to the gallbladder for storage (Figure 1. 1) [5].

Hepatocytes located along the PT to CV axis are heterogeneous in function and can be separated into three zones. These functional zones correlate with the oxygen concentration gradient (highest at the PT, zone 1) and an opposing Wnt signalling gradient (highest at the CV, zone 3) (Figure 1. 1) [6]. Zone 1 periportal hepatocytes contain high levels of the antioxidant glutathione. Zone 1 hepatocytes perform oxygen demanding roles such as gluconeogenesis and urea synthesis. Zone 2 is poorly defined and is often seen as a transient zone between the highly distinct zones of 1 and 3. Zone 3 centrilobular hepatocytes contain high levels of cytochrome P450, which enables the metabolism of drugs such as APAP and alcohol. However, hepatocytes within zone 3 contain low levels of the antioxidant glutathione, making them susceptible to reactive oxygen species (ROS) (Figure 1. 1) [5].

Hepatocytes have exceptional proliferative capacity, making the liver a highly regenerative organ. After 70% partial hepatectomy, the liver regenerates through hyperplasia. Mice will restore their liver mass within one week, and be fully functional within a month [7]. However, if the insult or damage to the liver outweighs its regenerative capacity, the liver cannot regenerate. In chronic liver injury, this results in fibrosis and cirrhosis [8]. In acute injury such as APAP overdose, this results in acute liver failure (ALF) and potentially death [3].

Figure 1. 1 Liver microstructure and zones

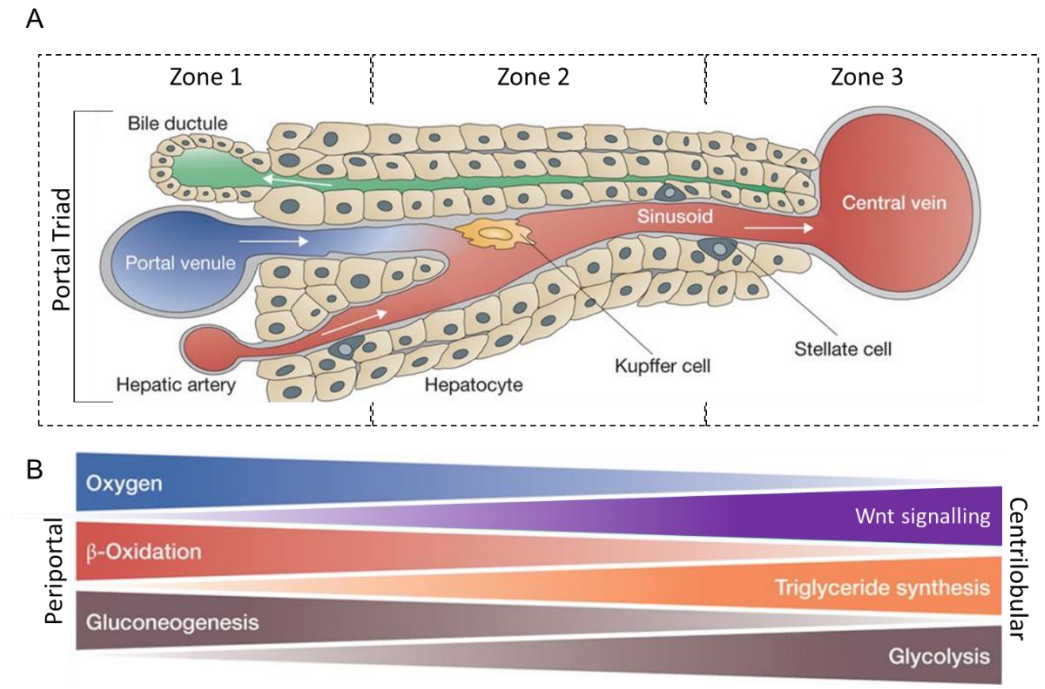

Figure 1. 1

A) The liver has a dual blood supply from the hepatic artery (red) and the portal vein (blue), which are accompanied by a bile ductule (green) to form the portal triad (PT). Blood flows along the sinusoids from the PT to the central vein. Adjacent to the sinusoids are hepatocytes. Hepatocytes secrete bile into the bile canaliculi, which flows in the opposite direction to the blood (white arrows) and is collected by the bile ductule. Kupffer cells are the liver's resident macrophage. They scavenge the sinusoids for pathogens and damaged blood cells.

B) Opposing oxygen and Wnt signalling gradients separate the hepatocytes into three functional zones. Zone 1 hepatocytes surrounding the PT perform β-oxidation and gluconeogenesis. Zone 3 hepatocytes perform glycolysis, triglyceride synthesis and drug metabolism.

CV, Central vein; HA, hepatic artery; PT, portal triad; PV, portal vein.

Adapted from: Birchmeier, W. (2016) 'Orchestrating Wnt signalling for metabolic liver zonation', *Nature Cell Biology*, Nature Publishing Group, 18(5), pp. 463–465. [9]

Pathophysiology and treatment of APAP induced liver injury

APAP is a dose related toxin that causes 46% of ALF in the USA and the UK [3]. ALF is defined as the abrupt loss of hepatocellular function resulting the sudden onset of coagulopathy and encephalopathy, in a patient with no prior history of liver disease [10]. In patients, APAP toxicity is worsened by several factors including starvation and alcohol abuse [11–13]. Over the past few decades, the hepatotoxicity pathway has been well described.

Ingested APAP passes from the small intestine to the liver after a few hours of consumption. At safe doses, 90% of APAP is readily esterified by glucuronic acid and sulfotransferases to form glucuronate and sulfate conjugates, respectively, which are safely excreted through the bile or urine [3,14]. Once the esterification capacity is saturated, APAP is oxidised by cytochrome P450 2E1 (Cyp2E1), to generate a toxic intermediate: N-acetyl-p-benzoquinone imine (NAPQI). Glutathione S-transferase converts NAPQI into a safe inactive form by conjugating it to the antioxidant glutathione (GSH), to form 3-glutathionyl acetaminophen. This safe metabolite can then be excreted from the body (Figure 1. 2) [3,4,14].

In the overdose scenario, the esterification process becomes saturated, and APAP is predominantly metabolised by Cyp2E1. As a result, GSH becomes depleted from the cytosol and mitochondria of hepatocytes, and NAPQI accumulates [14]. NAPQI is a highly reactive metabolite and will covalently bind to free cysteines to form protein adducts. This includes NAPQI binding complex I and III in the electron transport chain, halting adenosine triphosphate (ATP) production, and enhancing the formation of ROS.

ROS can be dismutated into hydrogen peroxide and molecular oxygen in the mitochondria, or react with endogenous nitric oxide to form peroxynitrite [15]. Both hydrogen peroxide and peroxynitrite are detoxified by GSH, further depleting the GSH supply. As peroxynitrite accumulates it nitrates tyrosine residues in mitochondrial DNA and proteins to form 3-nitrotyrosine proteins. Nitrated proteins are a biomarker for nitrogen stress, and correlate with APAP injury [16,17].

Figure 1. 2 The APAP induced hepatotoxicity pathway

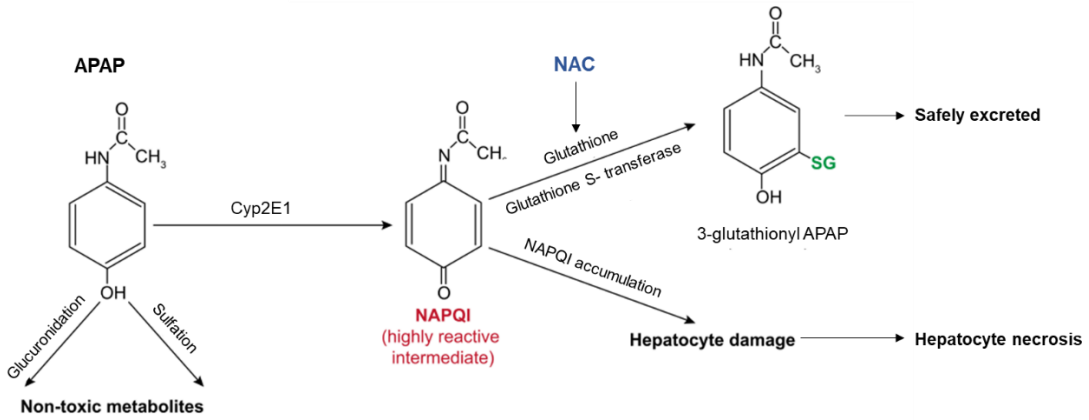

Figure 1. 2

APAP is converted into NAPQI, a toxic metabolite, by the Cyp2E1 enzyme. If there is sufficient glutathione (GSH) available, it is conjugated to NAPQI by Glutathione S-transferase, to form an inactive reduced compound, 3-glutathionyl APAP, which is safely secreted from the body. In the overdose setting, GSH becomes depleted, allowing NAPQI to accumulate. This leads to the formation of protein adducts, reactive oxygen species, mitochondrial dysfunction and hepatocyte death. NAC, the only current therapy, is a precursor to GSH, and limits APAP injury by restoring GSH levels.

APAP, acetaminophen, paracetamol; GSH, glutathione; NAC, N-acetylcysteine; NAPQI, N-acetyl-p-benzoquinone imine.

Adapted from: Lee, W. M. (2017) 'Acetaminophen (APAP) hepatotoxicity-Isn't it time for APAP to go away?', *Journal of hepatology*, 67(6), pp. 1324–1331.

ROS activates the c-Jun N-terminal kinase (JNK) pathway which induces the mitochondrial permeability transition (MPT) pore to open, which ultimately leads to necrotic cell death. Hydrogen peroxide causes the activation of apoptosis signalling-regulating kinase 1 (ASK-1) which phosphorylates mitogen-activated protein kinase kinase 4/7 (MKK4/7), which phosphorylates JNK. The phosphorylation of JNK results in an activated form of the protein that can translocate to the mitochondria. Once within the mitochondria, JNK phosphorylates SH3 homology-associated BTK-binding protein (Sab). Sab activation leads to the dysfunction of the electron transport chain, and further increases ROS production. As ROS increases it creates a self-sustaining feedback loop with JNK. Continual activation of JNK causes the phosphorylation and activation of bax. Bax translocates into the mitochondria, where it initiates MPT pore opening. This causes the depolarisation of the inner mitochondrial membrane. The loss of structural integrity prevents adequate ATP production, increases oxidative stress, and release of intermembrane mitochondrial proteins including endonuclease G, which triggers DNA fragmentation and necrotic cell death [14,15,17].

Cyp2E1 is expressed by zone 3 hepatocytes, which metabolises APAP. Consequently, zone 3 hepatocytes are the first to succumb to APAP toxicity. The resultant centrilobular cell death is a hallmark of APAP injury [17]. In addition to hepatocyte death, centrilobular liver sinusoidal endothelial cells (LSECs) are also damaged. APAP toxicity causes LSECs to swell, and to become permeable [18,19]. This results in reduced perfusion, erythrocytes extravasation [20,21], coagulation and more liver injury [15,17]. In severe APAP overdose, hepatocytes in zone 2 and even 1 can undergo cell death, ultimately leading to liver failure as necrosis spreads through the liver.

Cell death in APAP injury

Cell death can occur through several distinct mechanisms including: apoptosis, necrosis and necroptosis. Apoptosis is an energy dependant controlled method of cell death mediated by a tightly regulated caspase cascade [22]. During APAP injury, ATP depletion prevents apoptosis. This is confirmed in mouse models where pan caspase inhibitors did not protect or prevent cell death [23,24].

Necrosis is a passive, uncontrolled, energy independent form of cell death. Necrosis occurs after a toxic or hypoxic injury, when cells are depleted of energy. It is characterised by mitochondrial dysfunction, organelle and cell swelling and a loss of cellular integrity. As the cell membrane ruptures, it leaks its contents into the

surrounding tissue, releasing damage-associated molecular patterns (DAMPs) (for example ATP, DNA fragments and high mobility group box protein 1 (HMGB1)), which activates the innate immune system. Cellular leakage and infiltrating immune cells can cause substantial collateral damage to the surrounding tissue and systemic injury [22,25].

Necroptosis is a controlled mechanism of cell death, with similar characteristics to necrosis; swelling, loss of cell integrity, cell leakage, release of DAMPs, and the consequent pro-inflammatory response [25]. Unlike necrosis, necroptosis occurs through a specific pathway: in the absence of caspase 8 activity, receptor interacting protein kinase 1(RIPK1) recruits RIPK3 to form the necrosome, which recruits and phosphorylates the mixed-lineage kinase domain-like protein (MLKL). MLKL then destabilises the plasma membrane and initiates cell lysis [26]. In addition, RIPK3 activates pathways to induce ROS production and mitochondrial fission [25].

As the mechanisms of necroptosis and necrosis are morphologically similar, it has been debated which mechanism is involved in APAP induced cell death. Sensitive antibodies for necroptosis are unavailable. RIPK1 inhibitors (necrostatin -1 (Nec-1), or the more sensitive Nec-1s), have been used to study necroptosis in APAP injury, but as Nec-1 is unstable in vivo, and RIPK1 is involved in both apoptosis and necroptosis these studies gave conflicting results [22,27,28]. However, studies using mice deficient for either RIPK3 or MLKL, proteins specific for necroptosis, had no protection from APAP induced cell death as the mice displayed the same levels of necrosis and alanine transaminase (ALT) as wild type (WT) mice [27,29]. This data demonstrates APAP cell death is mediated by necrosis.

Treatment of APAP overdose in the clinic

The only viable treatment for APAP overdose is NAC, which restores the depleted GSH. NAC is only effective with in the first 12 hours of APAP overdose (Figure 1. 2), or in select cases a liver transplantation [3,4]. APAP overdose is either intentional with patients ingesting over 12 grams of APAP in a single time point, or accidental. Accidental overdose patients typically ingest 6-10 grams/ day over several days [3], either as APAP tablets or in combinatorial painkillers. The most common reasons for an accidental overdose are: postoperative pain or to treat pancreatitis, toothache or chronic back pain [3]. Patients who unintentionally overdose on APAP, arrive later to hospital than intentional overdose patients, and are more likely to be outside the 12

hour window that NAC is effective and therefore have worse outcomes from APAP overdose.

APAP injury evolves rapidly in a dose dependant manner, with patients initially suffering from nausea and abdominal pain. These symptoms are associated with extremely high levels of aspartate transaminase (AST) and alanine transaminase (ALT) which are markers of hepatocellular injury. As injury continues, liver function is compromised. This leads to hyperammonaemia, coagulopathy, acute kidney injury, encephalopathy, and cerebral oedema [3,30]. In the healthy state, the liver acts as a 'firewall' to prevent commensal bacteria and pathogens absorbed by the intestines from spreading around the body [31]. During APAP injury, the liver loses this function, allowing intestinal bacterial translocate into the bloodstream causing sepsis [4,32]. If multi-organ failure does not occur from the effects of APAP injury, patients have a chance of recovering with no lasting side effects [3]. Resolution of APAP-mediated injury is as rapid as its onset, with 64% of patients making spontaneous recoveries, and 7% recover with the aid of liver transplant surgery. The remaining 28.5% die either of multi-organ failure or whilst awaiting a liver transplant [3]. New therapies are needed to prevent fatality and reduce the number of patients requiring a liver transplant.

The innate immune system during APAP injury

The innate immune system is crucial during both APAP injury and recovery. However, the roles of the innate immune system are still being clarified, with many controversies over roles and benefits of different cell types. This section will focus on neutrophils and macrophages during APAP injury and recovery.

Kupffer cells during homeostasis

Every minute 30% of the total blood volume passes through the liver, carrying 100 million peripheral blood lymphocytes per 24 hours [33]. A third of the liver's blood supply is oxygenated blood from the hepatic artery. The remaining two thirds is delivered by the portal vein. It carries nutrient rich blood and potential pathogens from the intestines. One of the primary roles of the liver is to filter this blood, by removing any ingested toxins and pathogens [34]. As such, the liver hosts a large population of resident liver macrophages known as Kupffer cells (KCs). For every 100 hepatocytes there is an estimated 20 – 40 KCs in healthy rodent livers [35], constituting 20% of the non-parenchymal cell (NPC) fraction of the liver [33].

Kupffer cells are predominantly stationary, self-renewing phagocytes. KCs originate from colony stimulating factor 1 receptor (CSF1R) + erythromyeloid progenitors in the yolk sac that seed the liver from embryonic day 10.5 in mice [36,37]. Once seeded in the foetal liver, the inhibitor of DNA binding 3 (Id3) mediates the differentiation of erythromyeloid progenitors towards adult KCs [37].

KCs are located on the luminal side of the hepatic sinusoids (Figure 1. 1). They sense and scavenge their environment with long cytoplasmic protrusions, and efficiently phagocytose cellular debris and pathogens, maintaining homeostasis in the liver and prevent unnecessary inflammatory reactions [35]. During homeostasis, KCs are continually bombarded by commensal and dietary bacteria from the gut, which it phagocytoses [31]. To prevent continual initiation of an inflammatory reaction to these bacteria, KCs respond to bacterial endotoxin by producing the anti-inflammatory cytokine interleukin- (IL-)10 [38,39]. This prevents the production of the pro inflammatory cytokines Interferon gamma (IFN-γ), IL-12, and Tumour-like necrosis factor α (TNFα) [40]. In addition, KCs preferentially present antigens of phagocytosed bacteria to regulatory T cells (T_{regs}), which also produce IL-10 and to promote tolerance [38,39].

Recent findings indicate resident tissue macrophages “cloak” single cell microlesions created by mechanical stress. Hiding these microlesions from neutrophils prevents them initiating an immune response. Uderhardt *et al.* used a laser to damage a single cell in the peritoneal wall. Resident tissue macrophages “cloaked” these microlesions with their pseudopods and scavenged for any inflammatory molecules released by the dying cell. This prevented patrolling neutrophils from detecting the damage and initiating an inflammatory response. However, if multiple cells were ablated by the laser to form a “macrolesion”, the resident tissue macrophage could not cloak the damage, and an inflammatory response was initiated [41]. This data demonstrates how resident tissue macrophages limit neutrophil driven inflammation to non-apoptotic cell death of a single cell. Most of these experiments were performed on the peritoneal wall, or muscle fibres which may be more subjected to mechanical stress than other tissues. It will be interesting to see if these cloaking events are performed by tissue resident macrophages in dense organs such as the liver, which are subjected to less mechanical stress. However, this is outside the scope of my project.

KCs are also capable of mounting rapid immune responses to both injury and pathogens by releasing cytokines to activate the immune system. The threshold between promoting tolerance and initiating an immune response against pathogens depends on Toll like receptor (TLR) signalling. The TLRs detect bacterial proteoglycans or foreign RNA and DNA structures. If a high concentration of their cognate ligand is detected, or if several TLRs are simultaneously activated, an immune response will be activated [42,43]. In the context of necrotic cell death, DAMPs are detected by KCs. KCs initiate the inflammasome, an intracellular multiprotein complex, which activates IL-1β and IL-18, and triggers the innate immune system. In APAP injury, the inflammasome is activated by DAMPs including ATP, HMGB1 and mitochondrial DNA [43,44].

Roles of monocytes and macrophages during APAP injury

Experimental APAP overdose mouse models have been used to study the roles of KCs. During APAP injury, KCs act as the first line of defence for the innate immune system. Necrosis of the hepatocytes causes DAMPs to be released, including DNA, ATP, HMGB1 and heat-shock protein-70 (HSP-70). KCs detect the DAMPs and become activated to secrete a plethora of cytokines including: TNFα, IL-6, IL-1α and IL-18 to activate and recruit the innate immune system [4,45]. TNFα also acts to prime hepatocytes for apoptosis, enhancing hepatocyte loss [46,47]. During APAP injury, KCs are depleted by the APAP toxicity. Macrophages and neutrophils infiltrate the liver, tripling the total number of leukocytes in the liver [48–51], and gravitate towards necrotic areas [48,52,53].

To examine if reducing inflammation induced by KCs was protective against APAP injury, KC depletion studies have been performed. Gadolinium chloride ($GdCl_3$) inactivates KC ROS production and phagocytosis [54]. Pre-treatment of mice with $GdCl_3$ reduced ALTs, and enhanced survival [55,56], but mice had more acetaminophen-protein adducts [57]. In addition, mice deficient for ROS production showed no protection [58–60], suggesting that KCs do not produce ROS to enhance APAP injury. Liposomal clodronate macrophage depletion reduced TNFα and IL-1β secretion. However, treated mice had increased ALTs throughout APAP injury, and reduced IL-10 secretion [61,62]. Together, macrophage depletion reduces pro-inflammatory cytokine secretion, but delays recovery as mice had persistent APAP adducts or raised ALTs, and reduced IL-10.

In mice, KCs become depleted during APAP injury [48–51]. The dwindling KC population is replaced by highly plastic infiltrating monocytes [48]. There are two major populations of circulating monocytes in the blood. In mice they are the patrolling pro-inflammatory population, which is identified by: CCR2+ CX_3CR1^{lo} $Ly6C^{hi}$; and the anti-inflammatory population, which is identified by CCR2- CX_3CR1^{hi} $Ly6C^{lo}$ [45]. From here on referred to as $Ly6C^{hi}$ and $Ly6C^{lo}$ monocytes, respectively. CCL2 (also known as monocyte chemoattractant protein-1 (MCP-1)) attracts $Ly6C^{hi}$ monocytes to the mouse liver via CCR2 [48,49,63]. Once the $Ly6C^{hi}$ monocytes have entered the liver they can differentiate into Ly6C+ macrophages [64].

After peak APAP injury in mice, the depleted KC population is restored by either self-renewal [48], or the infiltrating macrophages can occupy the KC niche and adopt a phenotype similar to KCs. For example, when the KC population is completely

abolished by a diphtheria toxin [65], irradiation [66], or liposomal clodronate [67], infiltrating macrophages convert into a resident phenotype and repopulate the liver.

During APAP injury, infiltrating monocytes/ macrophages have been shown as both harmful and beneficial. In the initial stages of APAP injury (6 - 24 hours post overdose in mice) Ly6C^{hi} monocytes secrete pro-inflammatory cytokines such as IFNγ, IL-6, TNFα and IL-1α, further enhancing inflammation and hepatocyte damage [4,35,68]. In support of this deleterious role, preventing Ly6C^{hi} infiltration by antagonising or genetically depleting CCR2 in mice reduced necrosis and ALTs [49]. However, these CCR2 Knock Out (KO) mice had persistent necrosis after APAP injury [51]. Pre-treatment with liposomal clodronate to ablate macrophages reduced IL-1α secretion and enhanced survival of mice in the early stages of APAP injury [68]. However, by 72 hours of 550 mg/kg APAP treatment, liposomal clodronate treated mice had 100% mortality compared to 50% survival of the WT controls [68]. In a different study, total macrophage ablation by treating CCR2 KO mice with liposomal clodronate, prevented vascular restoration and liver regeneration [21]. Therefore, the initial wave of inflammation mediated by infiltrating monocytes and potentially resident macrophages, contributes to hepatocyte damage and necrosis. Conversely, without this infiltration of monocytes, and without resident macrophages there is a lack of tissue repair, persistent necrosis, reduced regeneration and revascularisation.

There is a possible third source of macrophages during hepatic injury. The surrounding peritoneal cavity is home to a complex milieu of immune cells which monitor the visceral organs and mesothelium [69]. The two dominant peritoneal macrophages populations are the large mature F4/80+ and the F4/80^{lo} MHC II^{hi} small peritoneal macrophages [69,70]. Recently, GATA-binding protein 6 (GATA6)+ F4/80+ peritoneal macrophages have been shown to infiltrate the liver 1 hour after a sterile thermal injury [71]. These GATA6+ macrophages are recruited by ATP and hyaluronan released by necrotic cells. At the site of injury, these GATA6+ macrophages adopt a restorative phenotype, as characterised by the expression of arginase and the mannose receptor, CD206. They then proliferate, dismantle the necrotic nuclei, and aid revascularisation. Specific deletion of GATA6 only delayed the time it took for these peritoneal macrophages to arrive at the site of injury, but ablation of all peritoneal macrophages delayed necrosis resolution. An oral dose of CCl_4 to induce acute liver injury caused GATA6+ macrophage recruitment into the liver. Liposomal clodronate prior to CCl_4 depletion prevented recovery of and mice had to be

euthanised [71]. It will be interesting to see how these GATA6+ macrophages behave in the context of sterile APAP liver injury, where there is mass necrosis across the whole liver, and not at a focal point in near the mesothelium. It would also be interesting to see how these peritoneal macrophages interact with hepatic macrophages or modulate cytokine production during APAP injury. Understanding these mechanisms may develop into new therapeutics through the modulation of different macrophage populations.

Roles of monocytes and macrophages during APAP recovery

Recovery from APAP injury requires several factors: an end to necrosis, removal of necrotic debris proliferation of the remaining hepatocytes, and resolution of inflammation. As professional phagocytes, macrophages remove debris and secrete anti-inflammatory cytokines which reduce inflammation and prime hepatocytes to proliferate. The importance of macrophages during recovery from APAP is shown in macrophage depletion studies. Depleting the infiltrating macrophages delays recovery from APAP injury [21,48,51].

Kupffer cells are a source of the anti-inflammatory cytokine IL-10 [62,72]. IL-10 together with IL-13 and IL-4 dampen pro-inflammatory events and promote expression of anti-inflammatory genes [73–75]. Mice treated with liposomal clodronate, but not $GdCl_3$, did not express *IL-10* during APAP injury [62]. The importance of IL-10 and IL-13 during APAP injury is highlighted in IL-10 KO and IL-13 KO mice, which have continually higher ALT and necrosis and reduced survival during APAP injury [73,76,77]. During recovery, infiltrating macrophages convert from $Ly6C^{hi}$ macrophages to a $Ly6C^{lo}$ restorative phenotype [48,78]. These restorative macrophages also secrete anti-inflammatory factors to inhibit neutrophil activation and recruitment such as prostaglandin E2 (PGE2) [48,79].

Macrophages are professional phagocytes which remove the necrotic debris after APAP injury. They also phagocytose apoptotic neutrophils [80,81]. The act of phagocytosis also converts macrophages from a pro-inflammatory to a restorative phenotype [72,82]. Phagocytosing macrophages secrete IL-10 [72], to reduce inflammation. Depleting monocytes from the liver with either a MC21 antibody or CCR2 KO mice, delays neutrophil clearance from the liver and recovery from APAP injury [48]. Recently, a subset of restorative KCs have been identified in both humans

and mice that express Mer tyrosine kinase (MerTK) [81]. These MerTK+ macrophages release secretory leukocyte protease inhibitor (SLPI) to induce infiltrating macrophages and KCs towards the pro-restorative phenotype and enhance phagocytosis of neutrophils *in vitro*. Mice deficient in MerTK display delayed liver regeneration after APAP injury [81].

To restore the liver parenchyma, a scaffold of extracellular matrix (ECM) must be prepared, the microvascular restored and the remaining hepatocytes must proliferate to replace those lost. Macrophages express factors such as matrix metalloproteinases (MMPs) which can remodel the ECM to facilitate wound closure [48,83] and vascular endothelial growth factor (VEGF) to restore the vasculature [21,48]. Macrophage ablation delayed vascular regrowth, with treated mice having highly permeable vasculature at 48 and 72 hours post APAP administration, compared to control mice [21].

Macrophages also secrete TNFα and IL-6, which prime hepatocytes to be more responsive to hepatocyte mitogens [84,85]. These mitogens include hepatocyte growth factor (HGF), Transforming Growth Factor Alpha (TGFα) and Epidermal Growth Factor (EGF). In the presence of growth factors, TNFα activates NF-κB to enhance the activation of hepatocyte proliferation genes. It was previously mentioned that TNFα can cause hepatocyte apoptosis. This occurs in the absence of NF-κB, and in the presence of stress factors including free radicals and depleted cellular energy levels. Hepatocyte proliferation and microvascular regrowth is a collaborative process, with hepatocytes secreting VEGF and LSECs secreting HGF to stimulate liver regeneration [17,86].

The possibility of using macrophages as a cellular therapy have been examined during chronic liver disease. Injection of BMDMs ameliorated liver fibrosis in mice in two separate studies [87,88]. In both studies, the injected BMDMs reduced the number of activated HSCs and produced MMP-9 and 13 to degrade collagen scars. The BMDMs also recruited endogenous macrophages which amplified and extended these beneficial effects [87,88]. The second study demonstrated that BMDMs were polarised to the pro-inflammatory phenotype by LPS and IFN-γ were responsible for these beneficial effects. In addition, the polarised BMDMs significantly promotes hepatocyte proliferation [88]. Hepatocyte proliferation was detected in the original study, but not at significant level [87]. The injected BMDMs only survived for a short time in the liver, therefore repeated injections may be needed for continued efficacy [87–89].

In APAP injury, administration of CSF1-Fc to mice at 12 hours APAP injury promotes recovery. CSF1-Fc enhanced Ly6C^{hi} monocyte recruitment, promotes KC and infiltrating macrophage proliferation and macrophage phagocytosis [32]. However, injection of macrophages into healthy mice induces biliary epithelial expansion, a process normally restricted to the chronic liver injury setting [90]. Therefore, understanding how to control or direct macrophage behaviour during liver injury will lead to novel therapeutic tools.

Roles of neutrophils during APAP injury

Neutrophils are short lived polymorphonuclear leukocytes, which originate in the bone marrow and are key effectors of the innate immune system. These cells patrol the body for invading microbes or DAMPs. Neutrophils react rapidly upon appropriate stimulation; migrating to areas of inflammation as the first leukocytes arriving at the site of injury [91].

Classical recruitment of neutrophils to injured tissue has been well defined in mice [91–94]. Endothelial cells capture neutrophils from the circulation through P and E selectin. The neutrophils then roll along the endothelium in the direction the blood flow [95–97]. Endothelial cells express cytokines such as TNFα and IL-1β which prime neutrophils for maximum neutrophil activation and release [98,99]. Chemokines including CXCL1, 2 and 5 (IL-8 in humans) are also expressed by endothelial cells and bind to chemokine receptor 2 (CXCR2) on the neutrophils, causing them to activate and to firmly adhere to the endothelial wall. This firm adhesion is facilitated by endothelial intercellular adhesion molecule-1 (ICAM-1) binding to Integrin αMβ2 (MAC-1) on the neutrophil [52,91,95,100]. The neutrophil then crawls along the endothelium following a chemotactic gradient. Neutrophils exit the vessel by transmigrating between or directly through the endothelial cells. The exact mechanisms of neutrophil migration and extravasation is organ and context dependent [52,91,94,101]. For details on how neutrophils migrate through the liver during sterile injury, see below.

At the site of injury, activated neutrophils can phagocytose debris and pathogens, modify tissue architecture via proteases or directly kill bacteria through the release of ROS, antibacterial granules or neutrophil extracellular traps (NETs). These neutrophil weapons have poor specificity and can cause collateral damage to the host tissue

[91,92]. Neutrophils also recruit and activate monocytes by the secretion of proteins such as azurocidin and cathepsin G. Neutrophils also modulate vasculature permeability and release IL-6 to promote endothelial cell expression of CCL2 and adhesion molecules (VCAM) which facilitate transmigration of monocytes into the injured tissue [102–104]. Activated neutrophils have longer lifespans than their non-activated counterparts, ensuring the presence of activated neutrophils at the site of injury [105–107]. With these pro-inflammatory effects, neutrophils are typically seen as detrimental during injury. However, ablation of neutrophils prevents the clearance of infection [91]. In humans, reduced numbers of neutrophils in the blood causes immunodeficiency [108,109].

During APAP injury, neutrophils are recruited to necrotic sites by a plethora of chemokines secreted by macrophages and DAMPs released by dying hepatocytes [4]. Key DAMPs include: formylated peptides (FP) which bind to the FP receptor 1 (FPR1) [52]; HMGB1 which binds to the receptor for advanced glycation end-products (RAGE) on neutrophils [53]; and free DNA received by TLR9 [110].

During sterile injury in the mouse liver, neutrophils do not roll along the highly fenestrated sinusoids, but immediately adhere to the LSECs, by binding to ICAM-1 via MAC-1 (CD11b/ CD18) [52,91,101]. The neutrophils then crawl along the LSECs towards a hierarchy of chemokines and DAMPs. In a model of sterile thermal injury, neutrophils crawl along the LSECs and towards an intravascular gradient of CXCL1 in mice and CXCL2 (also known as macrophage inflammatory protein-2; MIP-2) via CXCR2. This chemokine gradient guides the neutrophils to within 100-150 μm of the necrotic injury. From here, DAMPs dominate over chemokines secreted from healthy cells to precisely direct neutrophils into the necrotic zone [52,111].

The precise roles of neutrophils during APAP injury are still being defined, with conflicting opinions on whether their activities are beneficial or detrimental. Activated neutrophils can promote hepatocyte loss by releasing ROS [110,112]. Marques *et al.* argue that neutrophils are detrimental during APAP injury [110,113]. By reducing neutrophil recruitment during APAP injury with either CXCR2 or FPR1 antagonists or TLR9 KO mice, the authors showed there was a reduction in serum ALTs, CXCL1 and CXCL2, and the pro-inflammatory cytokines IL-1β and TNFα [110,113]. In accordance with this, mice with a hepatocyte deletion of HMGB1 had less infiltrating neutrophils and reduced necrosis and ALTs during APAP injury [53]. Depletion of neutrophils by pre-treatment with a Gr-1 antibody also reduced serum ALT and necrosis and

improved survival of APAP treated mice [112,113]. These results suggest that recruited neutrophils are detrimental during APAP injury, and release ROS to induce hepatocyte death.

However, pre-treating mice with neutropenia – inducing antibodies have been shown to be protective. The antibody tagged neutrophils become trapped in the LSECs and phagocytosed by KCs. Subsequently, KCs and hepatocytes temporarily produce protective genes and making them resistant to APAP injury [114,115]. Depleting neutrophils with a Ly6G antibody after APAP administration [60]; or genetically preventing neutrophil production with granulocyte-colony stimulating factor (GSCF) KO mice [60]; or preventing neutrophil recruitment with CD18 deficient mice [116]; had the same levels of ALT and necrosis during APAP injury. In addition, mice with defective ROS production had the same ALTs as WT mice during APAP injury, but prolonged recovery times [59,60]. These later studies suggest that neutrophils are not detrimental during APAP.

Roles of neutrophils during APAP recovery

As neutrophils are the first responders to injury, they have been primarily studied as pro-inflammatory mediators of injury. However, there is mounting new evidence that neutrophils promote recovery by phagocytosing bacteria, removing cellular debris, promoting revascularisation and remodelling the ECM to facilitate wound closure [91,117]

In a mouse model of thermal sterile injury, Wang *et al*. demonstrated that neutrophils can remove small fragments of DNA and dismantle phagocytose and damaged LSECs [117]. Neutrophils also deposited collagen in the necrotic area, forming a framework for tissue regeneration. Depletion of neutrophils with a Ly6G antibody 24 hours prior to injury, delayed revascularisation. Necrosis was still present 4 weeks later in neutrophil depleted mice, whereas control mice had recovered [117]. However, the authors also demonstrated that if neutrophils do not reverse migrate back into the circulation when required, tissue regeneration and revascularisation is delayed.

In support of their revascularisation role, neutrophils express vascular endothelial growth factor A (VEGF-A) a mitogen for endothelial cells. Pro-angiogenic neutrophils, which constitute 3% of the circulating neutrophil population [118], release 10-fold more matrix MMP-9 than other neutrophil populations. MMP-9 is required to degrade the ECM to create tunnels for the new blood vessels, and to promote blood vessel growth

by releasing matrix bound VEGF [119]. Therefore, neutrophils facilitate tissue regeneration and revascularisation, but must be cleared from the site of injury for the tissue to recover.

Neutrophils are cleared from the tissue by reverse migration or by macrophages phagocytosing apoptotic or necrotic neutrophils. These actions are performed by the neutrophils themselves, or in cohesion with monocytes/ macrophages [93,120,121]. Neutrophils recruit circulating monocytes by secreting chemokines, and aid monocyte extravasation. IL-6 complexes from neutrophils cause endothelial cells to upregulate adherent molecules and CCL2 to specifically recruit monocytes [91]. Apoptotic neutrophils also release “find me” signals that target them for phagocytosis [91]. Phagocytosing monocytes and macrophages switch from a pro-inflammatory to an anti-inflammatory phenotype [72], thus aiding regeneration.

Neutrophils can also reverse migrate out of the inflamed tissue, by remodelling the ECM. They then travel through the circulation or lymphatics back to the bone marrow or lymph nodes, where they apoptose and can be recycled [93,117]. In zebra fish, macrophages directly contact neutrophils at a wound, promoting neutrophil reverse migration [122].

In experimental mouse models of APAP injury, neutrophils infiltrate the liver from 4 hours post APAP and accumulate until peak injury, defined by levels of ALT and necrosis, at 24 hours post APAP administration. From this time onwards, the number of neutrophils in the liver decreases, but a reduced population of neutrophils is retained until 72 hours following APAP overdose [59]. New evidence suggests that these persistent neutrophils secrete factors including ROS to promote monocytes and macrophages to switch between phenotypes that can be described by Ly6C activity. Distinct pro- and anti-inflammatory phenotypes occur in monocytes and macrophages with high and low Ly6C expression, respectively. Ly6G antibody depletion of neutrophils six hours after APAP administration, or genetically with GCSF KO mice, reduced hepatocyte proliferation and necrosis resolution at 72 hours post APAP. There were also less $Ly6C^{lo}$ monocytes and macrophages present in the livers of the neutrophil depleted mice. Yang *et al*. demonstrate that the delayed recovery in these mice was mediated by a lack of ROS secretion from neutrophils, as mice treated with the Ly6G antibody could be rescued by adoptively transferring WT polymorphonuclear leukocytes (PMNs) from WT mice, but not ROS defective PMNs [60].

Figure 1. 3 Inflammation during APAP injury

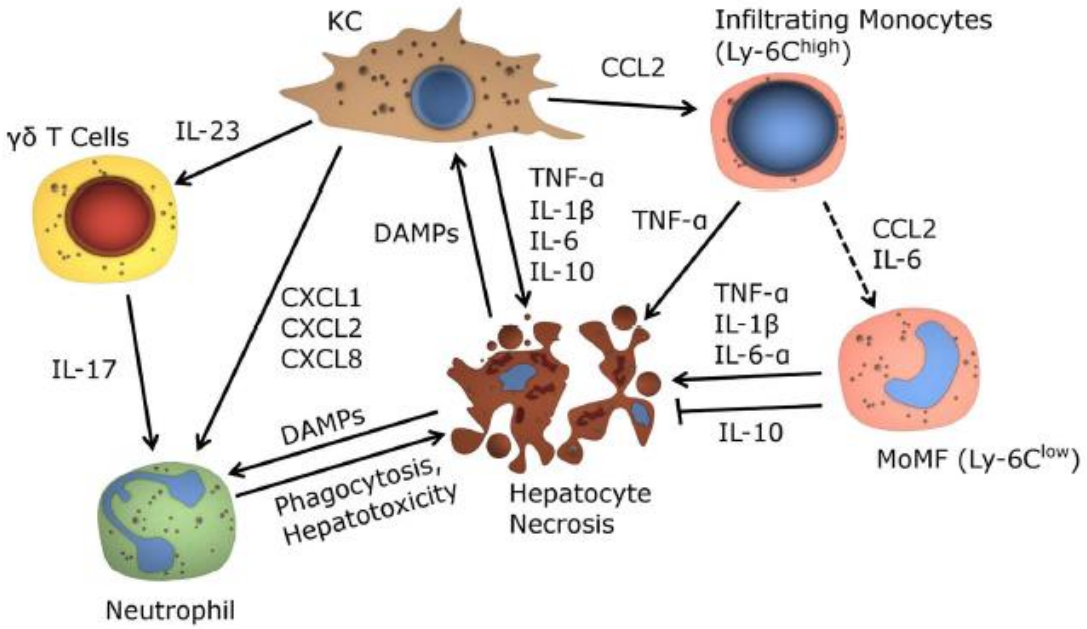

Figure 1. 3

APAP induces hepatocyte necrosis. This causes the passive release of DAMPs (HMGB1, HSp70, free DNA) which are detected by KCs and patrolling neutrophils. This leads to the activation of KCs and neutrophils. Activated KCs secrete pro-inflammatory cytokines including CCL2, CXCL1, CXCL2, CXCL8, TNFα, IL-1β and IL-6 which activate and recruit the innate immune system to the liver. CCL2 specifically recruits infiltrating macrophages. CXCL1, CXCL2 and CXCL8 recruit neutrophils. KCs also secrete IL-23 which activates γδ T cells, which further activate neutrophils through IL-17 secretion. TNF-α also promotes hepatocyte apoptosis.

Infiltrating Ly6C^{hi} monocytes are likely to mature into Ly6C^{lo} macrophages under the influence of CCL2 and IL-6. Restorative KC and infiltrating macrophages secrete IL-10 to reduce inflammation and promote recovery.

MoMF, monocyte derived macrophage

Adapted from: Krenkel, O., Mossanen, J. C. and Tacke, F. (2014) 'Immune mechanisms in acetaminophen-induced acute liver failure.', *Hepatobiliary surgery and nutrition*, 3(6), pp. 331–43.

Regulation of tissue and barrier integrity

During APAP injury, the spread of necrosis and toxic solutes must be contained to prevent collateral damage in healthy tissue. Cell junctions maintain tissue integrity, cellular polarity, epithelial barriers, mechanical strength and intracellular communication, and have been suggested to have a role in preventing the spread of toxicity. There are four different types of cell junctions: Tight junctions, adherens junctions (AJ), desmosomes and gap junctions.

Tight junctions are apical connections of epithelial cells which form a physical barrier to control the lateral flux of solutes, and maintain apical- basal cell polarity [123]. Cell polarity is essential to asymmetrically organise components of a cell. This polarisation propagates across the tissue, optimising tissue function [123,124]. Tight junctions consist of membrane proteins including occludins, claudins and Junction Adhesion Molecules (JAMs). Zonal occludin proteins (ZO 1-3) attach the tight junction complex to the actin cytoskeleton [125,126]. During APAP injury tight junctions within the liver become disrupted in a dose dependant manner [127,128]. It was suggested that this permitted the spread of APAP toxicity. Although this was not demonstrated.

Adherens junctions are formed by cadherins and catenins. They form strong intracellular connections to maintain lateral integrity of the epithelial cell layer, and regulate cytoskeletal networks to facilitate cell movement [129]. In the vasculature, vascular endothelial (VE)-cadherin maintains the permeability barrier of the vessel [130]. In APAP injury, the sinusoids become damaged and more permeable, resulting in the extravasation of erythrocytes [18,20]. It is likely that the VE-cadherin junctions become destabilised during APAP injury, but this has not been examined.

Gap junctions are intracellular channels which allow the exchange of ions and small metabolites, including ROS and GSH, between cells. Gap junctions are composed of six connexin (Cx) proteins. These transmembrane proteins oligomerise to form a six protein hemi channel known as a connexon. Connexons on adjacent cells align to form a gap junction. Gap junctions are essential for cell differentiation growth and metabolic co-ordination [131,132]. Opening and closure of Gap junctions is influenced by pH, calcium ions, transmembrane voltage and phosphorylation of the intracellular domains of the connexons [133–135]. Outside of their channel function, gap junctions can influence the cytoskeleton to regulate cell morphology and movement [131,132].

In the liver the predominant Cx protein is Cx32 [136]. During APAP injury, it has been proposed that Cx32 transmits toxic APAP solutes between cells, increasing liver injury. Genetic deletion of Cx32, or application of the Cx32 small inhibitor, 2-ABP, prevents the spread of APAP induced necrosis [137]. However, a different study indicated the protective effects of 2-ABP were partially mediated by the hepatoprotective factor dimethyl sulfoxide (DMSO), and a reduction of JNK signalling, and not a block of Cx32 junctions [138]. In another study Cx32 KO mice were not protected from APAP injury, but had less APAP protein adducts at 6 hours post APAP administration [139]. Nevertheless, *in vitro*, deletion of the Cx32-Cx26 gap junction in coupled hepatocytes prevented synchronised necrotic cell death. Furthermore, fusing a single female hepatocyte, which are naturally resistant to APAP toxicity, to a single male hepatocyte, which are more susceptible to APAP toxicity, prevented cell death of the male hepatocyte [140].

Cx43 is upregulated during APAP injury, and Cx43 $^{+/-}$ mice had elevated ALT and increased IL-1β and TNFα secretion at 24 hours post APAP injury, suggesting Cx43 protects against APAP injury [141]. Together these results indicate APAP toxicity may spread through gap junctions.

Macrophages also have protective barrier roles. This function has been observed in CX_3CR1+ macrophages lining the synovial cavity in healthy mice. RNA_{seq} analysis revealed these cells have an anti-inflammatory and an epithelial-like profile. They expressed the tight junction proteins JAM1, ZO-1 and claudin 5. They also expressed *Fat4* and *Vangl2* which are required for planar polarity. In a model of arthritis, these barrier macrophages became active and entered the synovial joint leading to reduced inflammation, independent of infiltrating PMNs or monocytes. Selective ablation of the barrier macrophages accelerated PMN influx and exacerbated the early stages of arthritis [142]. These results reveal that specialist barrier macrophages protect the synovial joint and reduce the onset of inflammation injury. Future investigations could examine if the protective role of these macrophages could be upregulated to prevent arthritis. It will be fascinating to see if these macrophages also “cloak” microtears in the joint to prevent inflammation, as reported in the peritoneum and muscle [41]. It would also be interesting to explore if KCs or infiltrating macrophages can form a barrier against the spread of APAP toxicity within the liver.

What shifts the balance between injury and recovery?

Recovery from APAP injury requires several processes. These include: preventing the spread of necrosis, a switch from promoting inflammation to promoting restoration, clearance of necrotic debris and proliferation of the remaining hepatocytes to restore the parenchyma (Figure 1. 4).

Necrosis will end once the APAP has been metabolised and cleared from the body, as to when this happens is dose dependant. Currently there is little knowledge on how the spread of necrosis is limited. Epithelial cells form barriers through cellular junctions. Tight junctions are down regulated during APAP injury, but the effects of this is unknown. Preventing the spread of APAP toxicity through the gap junction Cx32 has been investigated but with conflicting results. For an epithelial barrier to be sustained, the cells in the barrier must stay alive. Potentially this is maintained by cell cycle arrest.

Cell cycle arrest or senescence is induced during times of oxidative stress or DNA damage to prevent damaged cells from replicating. Senescent cells also secrete factors which attract the immune system. Senescence is marked by p21 and other bona fide markers, which can be induced by TGFβ signalling in times of cellar stress [143,144]. Senescence can be beneficial, as it can prevent the spread of damage and mass cell death during tissue insult [145]. However senescence can be detrimental if it persists and prevents tissue regeneration [143,144,146].

In APAP injury, peri-necrotic p21 expression correlates with the degree of injury in both humans and mice [144,147]. Macrophages secrete TGFβ to induce cell cycle arrest in peri-necrotic hepatocytes and prevents hepatocyte proliferation required for APAP recovery. Preventing TGFβ macrophage secretion, TGFβR1 inhibition, or genetically deleting p21 increased hepatocyte proliferation. However, p21 KO mice had elevated serum ALTs, a marker for hepatocyte injury. The area of necrosis in the p21 mice was not reported [144]. p21 expression might be needed to prevent peri-necrotic hepatocyte cell death, and therefore prevent the spread of necrosis.

To recover from APAP injury, the innate immune system must switch from promoting inflammation to an anti-inflammatory, restorative machine. Macrophages and monocyte are highly plastic cells which easily switch from Ly6C^{hi} pro-inflammatory to a Ly6C^{lo} pro-restorative phenotype. This is mediated by several factors including:

colony-stimulating factor-1 (CSF-1, also known as M-CSF) [32], IL-4, IL-6, IL-13 [148]; and the act of phagocytosis [72,149].

Restorative macrophages secrete IL-10 to reduce inflammation, phagocytose debris and secrete IL-6 and TNFα to prime the hepatocytes for proliferation [21,62,72,82,84,85]. They are also responsible for secreting Wnt and TGFβ, which induce regeneration or senescence respectively [144,150]. Manipulating the actions of macrophages may be a novel and powerful approach to treat APAP injury.

Hepatocyte proliferation is synchronised with the microvasculature restoration, with hepatocytes secreting VEGF to promote angiogenesis and LSECs secreting HGF to stimulate hepatocyte proliferation [17,86,147]. Wnt/ β- catenin signalling is important in liver regeneration in both APAP injury and chronic liver injury [147,150]. Bhushan *et al*. compared mice which recover from APAP injury, by using a 300 mg/kg dose of APAP, to mice treated with 600 mg/kg APAP, which do not recover [147]. In the 300 mg/kg APAP treated mice, mRNA expression of Wnt4 and Wnt5a were elevated 6 hours post APAP injury, and β-catenin localised to the nucleus between 12 and 24 hours post APAP injury. However, in the 600 mg/kg treated mice, Wnt/ β-catenin signalling was not induced [147]. What promotes Wnt signalling is unknown. Mice with forced nuclear β-catenin signalling had more hepatocyte proliferation, but ALT and necrosis was unchanged, compared to control mice [147]. This suggests Wnt -β-catenin signalling promotes hepatocyte proliferation but does not protect against APAP injury. In chronic injury, macrophages secrete Wnt to differentiate hepatic progenitor cells into hepatocytes [150].

Whilst the aforementioned factors are important during recovery from APAP injury, it is still unknown what shifts the balance from the injury setting, to the recovery setting during APAP injury (Figure 1. 4). The cellular source and specific type of Wnt present during APAP injury and recovery remains to be investigated, it is also not clear why or how Wnt signalling was initiated in the 300mg/kg APAP treated mice and not the 600 mg/kg APAP treated non-regenerative mice. The mechanisms underlying TGFβ signalling, and the TGFβ mediated senescence were not fully examined. It is still unclear what prevents the spread of necrosis during APAP injury. In addition, factors that orchestrate the innate immune system to shift from a pro-inflammatory phenotype to a restorative phenotype remain to be elucidated. Understanding these processes will lead to novel regenerative therapies.

Figure 1. 4 What shifts the balance between injury and regeneration?

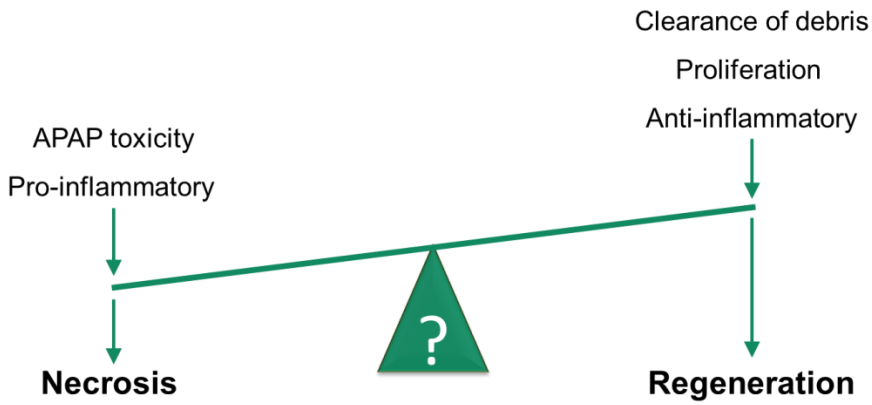

Figure 1. 4
During the injury phase, APAP toxicity promotes inflammation and necrosis. Regeneration of the liver requires the necrotic debris to be removed, inflammation to resolve and convert to the anti-inflammatory restorative phenotype, and hepatocytes to proliferate.

After peak APAP injury there is a shift from APAP induced necrosis to a recovery phase. What mediates this shift is unknown.

Semaphorins

The semaphorins are a diverse family of over 20 signalling proteins. They were originally identified as axon guidance molecules but have since been found to mediate a diverse array of functions from immune responses, axon migration and bone homeostasis [151,152].

The structure of semaphorins

All semaphorins contain a conserved 500 residue 'sema' domain at their N- terminus. Adjacent to the sema domain is the cysteine-rich plexin-semaphorin- Integrin (PSI) domain, named after the similarity to the beta chain of integrins and regions found within the Plexin family [153].

The semaphorin family is divided into 8 classes, based on defining structural features. Within each class the semaphorins are labelled alphabetically (e.g. Sema3a) (Figure 1. 5). Class 1 and 2 semaphorins are exclusively expressed in invertebrates. Classes 3 – 7 are expressed by vertebrates. Class 3 semaphorins are secreted; Classes 4, 6 and 7 are membrane associated [152]. Classes 3, 4, 7 and V have Ig like domains. Class 5 semaphorins are defined by their thrombospondin repeats. In Class 6, the sema-PSI domain constitutes the whole of the extracellular domain of the protein. Class 8 or V are viral semaphorins, which are a structural mimics of Sema7a (Figure 1. 5) [153], [154].

Crystal structures of Sema3a [155], Sema4d [156], Sema6a [157], and Sema7a [158] reveal that the sema domain consists of a seven bladed β propeller fold, which forms a stable platform for homodimerisation of the semaphorin which is required for sema function. The sema domain also facilitates binding, with one homodimer binding to two receptor proteins. So far no heterodimers of semaphorins have been found [152].

Semaphorin receptors

The main semaphorin receptors are plexins and neuropilins. Plexins are large transmembrane receptors which contain an extracellular sema - PSI domain and three immunoglobulin–plexin–transcription factor (IPT) domains, but unlike the semaphorins, the plexin's sema domains do not dimerise to be active. Currently 11 vertebrate plexins have been identified: Plexin A1-4, B1-3, C1, and D1 [152,159]. The β propeller fold in the plexin's sema domain inserts into the semaphorin's β propeller fold, with the angle and length of insertion defining receptor-ligand specificity [158,160] (Figure 1. 5). Semaphorin - plexin binding induces conformational changes which triggers signalling [161].

Membrane bound semaphorins in classes 4 - 7 directly bind to activate their respective Plexin receptor. As class 3 semaphorins are secreted, a neuropilin (Nrp) co-receptor is required to stabilise the Sema3- Plexin A interaction [152], the exception being Sema3e which can bind directly to Plexin D1 [153]. Downstream signalling is mediated by the intracellular region of the plexin which contains a conserved GTPase activating protein (GAP) domain. This conducts signalling through activation of protein kinases, GTPases and cytoskeleton associated proteins [152].

Nrps are membrane spanning glycoproteins with a short intracellular domain, making them unable to transmit semaphorin signalling independently [161]. However, Nrp can determine the outcome of downstream semaphorin signalling. For example, during neurone development, secreted Sema3e repels ventrolateral and striatal axons by binding to Plexin D1. However, in subicular axons, Sema3e acts as a chemoattractant, when received by Plexin D1 and Nrp1 [162].

Nrps can act as co-receptors to a diverse range of signalling proteins outside of the plexins, where they direct downstream signalling. The best characterised is Nrp acting as a co-receptor for VEGF with VEGFR on endothelial cells to promote angiogenesis [163]. Nrp1 can also bind to TGFβ, and increase its affinity to TGFβR receptors in T cells [164]. In myofibroblasts, binding of Nrp1 to TGFβR2 directs TGFβ signalling away from SMAD 1/5/8 to SMAD 2/3 signalling, causing myofibroblasts to activate [165]. Nrp1 and 2 can also bind to hepatocyte growth factor (HGF) in endothelial cells to promote angiogenesis [166].

Figure 1. 5 The Semaphorin Family and their Receptors

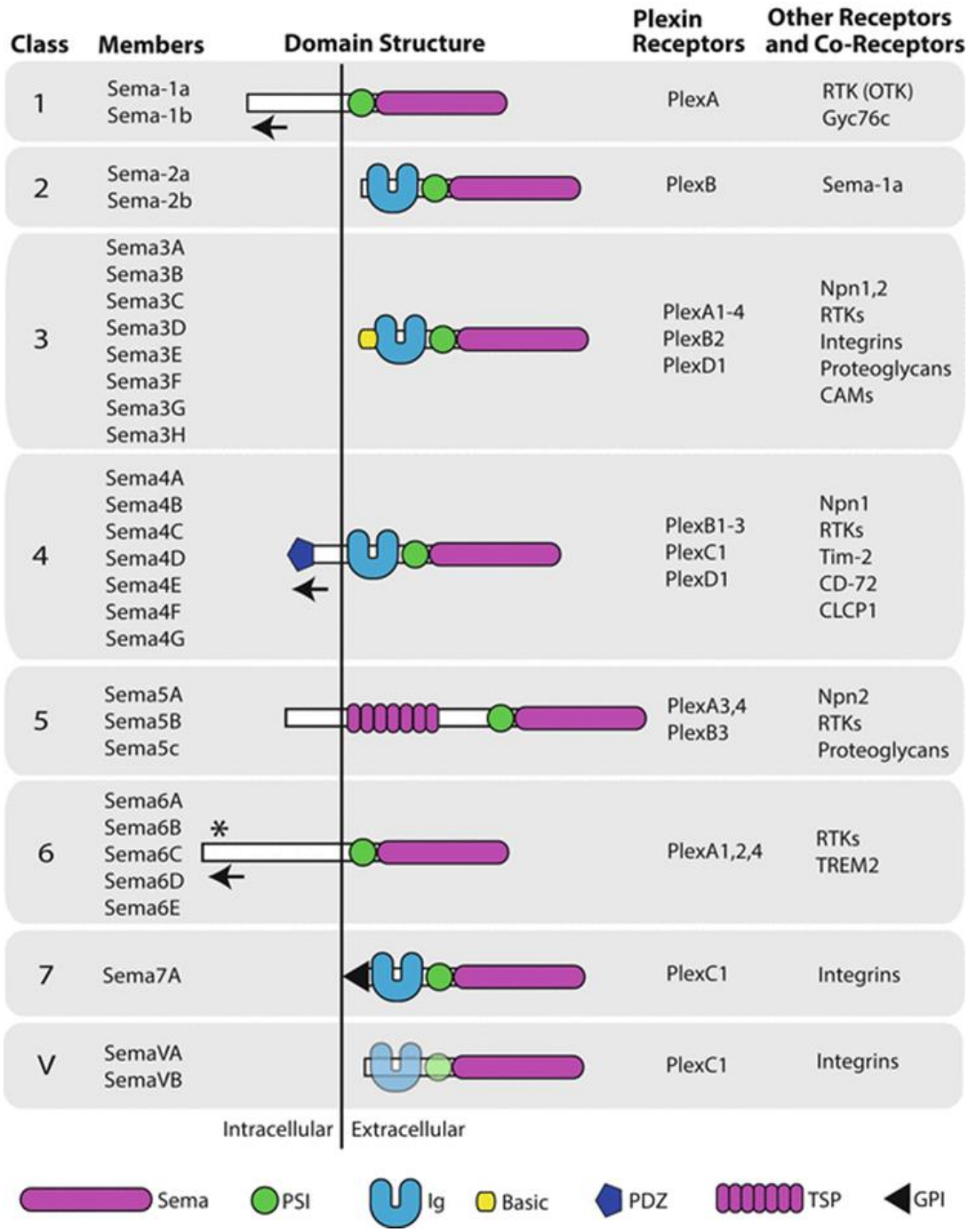

Figure 1. 5
Semaphorins all have a conserved 500 amino acid 'Sema' domain and can bind to plexins, Integrin s or neuropilins (Npn). Adjacent to this is the PSI domain.
Class 1, 2 are found in invertebrates
Class 3 semaphorins are secreted and bind to the Plexin A neuropilin 1 complex to regulate neurone growth and immune cell trafficking.
Class 4 are transmembrane proteins which bind to Plexin Bs to repel neurones or activate immune cells.
Class 6 semaphorins are transmembrane proteins which bind to plexin A1 in cohesion with either VEGFR during development, or TREM-2 or DAP2 to modulate immune system function
Class 7 has a single member, Sema7a. It is linked to the cell membrane by a GPI linker, and binds to Plexin C1 or Integrin β 1 in the immune and nervous system.
Class V are viral semaphorins

From: Alto L.T., Terman J.R. (2017) Semaphorins and their Signalling Mechanisms. In: Terman J. (eds) Semaphorin Signalling. Methods in Molecular Biology, vol 1493. Humana Press, New York, NY [153]

Roles of semaphorins

Semaphorins were originally identified as axon guidance molecules which fine tune neurone guidance during development and in adults. Semaphorins have since been found to have roles in angiogenesis and the immune system.

During development semaphorins guide neurones to their final destination to ensure the correct wiring of the neuronal network. This is achieved by chemoattraction and chemorepulsion of neurones, or promoting and inhibiting of neurone outgrowth (Table 1. 1). For example, Sema4d triggers the growth cone collapse through Plexin B1 and Rho GTPase signalling [167].

Semaphorins can promote opposite actions in their target cell by binding different receptors. Sema3e attracts axons by binding Nrp1 and Plexin D1 but repels neurones by binding exclusively to Plexin D1 [168]. Being able to bind two distinct receptors diversifies the functions of the semaphorins, and enables the delicate fine tuning needed to assemble the neuronal network.

In the adult, semaphorins can guide axons during neurogenesis and injury. Piaton *et al*. investigated the potential role of semaphorins in multiple sclerosis. In their murine demyelination model, they found that Sema3a prevents oligodendrocyte precursor (OPCs) cell recruitment, whereas Sema3f enhanced recruitment of the OPCs and increased the remyelination rate [169].

Table 1. 1 Roles of Semaphorins in the nervous system

Semaphorin	**Receptor**	**Function**	**Reference**
Sema3a	Plexin A1	Growth cone collapse, repulsion of OPCs	[169–171]
Sema3b	Nrp2	Attraction and repulsion of neurones	[172]
Sema3e	Nrp1 and Plexin D1	Attracts axons	[168]
Sema3e	Plexin D1	Repels axons	[168]
Sema3f	Nrp2	Axon guidance of cranial nerve, recruitment of OPCs	[169,173]
Sema3g	Nrp2	Repels axons in the cerebellum	[174]
Sema4d	Plexin B1	Growth cone collapse	[167]
Sema5a	Plexin A1	Inhibits growth of retinal ganglion cells	[175]
Sema7a	Integrin β1	Axon outgrowth and branching. Guidance of GnRH neurones	[176–180]

Semaphorins can also directly regulate angiogenesis, by binding to Nrp1 with VEGFR as a co-receptor. During development, Sema3a and Sema3e repel the developing microvasculature to ensure the correct vascular patterning of the embryo [181,182]. Class 3 semaphorins also reduce angiogenesis by competing with VEGF for is receptor [161]. In the adult, Sema3a inhibits VEGF mediated angiogenesis, and destabilises VE cadherin junctions to induce microvascular permeability [183,184]. Preventing Sema3a induced permeabilisation with Sema3a KO mice, reduced brain haemorrhage and ischemic damage in a stroke injury model [185].

In the adult liver, Sema3e is transiently secreted by damaged hepatocytes, after an acute CCl_4 injury. It binds to Plexin D1 on LSECs and causes them to contract. After the expression of Sema3a diminishes from its peak at 24 hours post injury, the LSECs expand and reform their radial pattern around the central vein, a process which is absent in mice with persistent Sema3e [186].

Class 4 and 7 semaphorins promote angiogenesis, independent of VEGFR. Sema4d binds to Plexin B1 on endothelial cells to induce angiogenesis. *In vitro,* porcine aortic endothelial cells treated with Sema4d migrate and form tube like structures that mimic angiogenesis [187]. With its pro-angiogenic roles, Sema4d facilitates tumour growth through angiogenesis. Treatment with a Sema4d blocking antibody reduced tumour growth, even in tumours resistant to anti-VEGF treatment [188].

To conclude, semaphorins regulate axon outgrowth or retraction, and the direction of growing axons. These actions are not class specific. In contrast, semaphorins regulate vasculature growth and permeability in a class dependant manner. Class 3 semaphorins prevent angiogenesis, repel the growing vasculature and induce vascular permeability by destabilising VE-cadherin. Sema4d and Sema7a promote angiogenesis, particularly during tumour development (Table 1. 2).

Table 1. 2 Roles of Semaphorins in the vasculature system

Semaphorin	**Receptor**	**Function**	**Reference**
Sema3a (embryo)	Plexin A1	Repels the sprouting tips of the vasculature microvasculature	[181]
Sema3a (embryo)	Integrin αvβ3	Vascular remodelling by inhibiting endothelial cell attachment to the ECM	[189]
Sema3a (adult)	Plexin A1	Inhibits VEGF mediated angiogenesis, and induces microvascular permeability, by destabilising VE cadherin junctions	[183,184]
Sema3e	Plexin D1	Repels Plexin D1 expressing endothelial cells, in a Nrp1 independent mechanism	[182]
Sema3e	Plexin D1	LSEC contraction during liver fibrosis	[186]
Sema5a	Plexin B3	Angiogenesis in the cranium and tumours	[190]
Sema4d	Plexin B1	Works in cohesion with VEGF to promote *in vivo* angiogenesis, during development and cancer	[187,188]
Sema7a	Integrin β1	Angiogenesis in mammary tumours	[191]

Immune functions of semaphorins

Semaphorins have diverse roles in the immune system and have been implicated in inflammatory diseases. The outcome of semaphorin signalling are defined by the receptor which receives the semaphorins and the location and cell type. For a summary see Table 1. 3.

Sema4d (or CD100) was the first semaphorin to be discovered as an immune semaphorin [192]. It has since been shown to have pro- and anti-inflammatory roles, and can act as a transmembrane protein or a secreted molecule [193]. On human B cells, Sema4d binds to CD72 or Plexin B1 to promote proliferation and antibody generation [193]. Sema4d signalling in human monocytes promotes the secretion of the pro-inflammatory cytokines TNFα and IL-6 [194,195]. Conversely, when neutrophil Sema4d binds to Plexin B2 on endothelial cells, neutrophil activation is prevented [196].

Sema4a drives T helper 1 (T_H1) differentiation and stabilises T_{regs}. DCs express Sema4a which binds to Tim-2 receptor on T cells, promoting T cell activation and proliferation [197]. Sema4a is highly expressed by during T cell differentiation into T_H1 cells, suggesting Sema4a might act in an autocrine manner to promote T cell differentiation [193]. In Sema4a KO mice, the differentiation of naive T cells to T_H1 is impaired [197]. The experimental autoimmune encephalomyelitis (EAE) mouse model is commonly used to study multiple sclerosis, an autoimmune disease driven by T cell inflammation [198]. Blocking Sema4a with an antibody reduced the progression of EAE [197], indicating Sema4a as a driver for T cell activation and inflammation.

Sema4a also stabilises T_{regs} by binding to Nrp1 [199]. T_{reg} expression of Sema4a is required to limit IL-13 secretion from T_H2 cells, which drives pulmonary inflammation in an asthmatic model. Sema4a KO mice have increased IL-13, and reduced T_{regs}, but were rescued by treatment with recombinant Sema4a [200,201]. Together, Sema4a promotes inflammation through the activation and differentiation of T_H1 cells but reduces inflammation of T_H2 cells through the action of T_{regs}.

Class 3 semaphorins also modulate the actions of T cells. Sema3a binds to Plexin A4 and Nrp1 to on T cells to prevent T cell priming and proliferation [202]. Plexin 4A KO mice had exacerbated EAE inflammation [203], underscoring that Sema3a limits T cell activation. Conversely, Sema3a can indirectly activate T cells by promoting DC migration into the lymph nodes.

Activated dendritic cells (DCs) migrate from the peripheral tissues into the lymphoid organs, where they activate T cells. Lymphatic endothelial cells secreted Sema3a and binds to Plexin A1 and Nrp1 on the DC. This causes the phosphorylation of the myosin light chain within the DC, causing the DC to contract allowing it to squeeze through the small gaps between lymphatic endothelial cells. Genetic deletion of Sema3a or Plexin A1 impairs T cell activation in the lymph node [204].

Class 3 semaphorins can cause macrophages to be pro-inflammatory. LPS challenge induces peritoneal macrophages to express Sema3a. Sema3a binds to Plexin A4, inducing optimal cytokine production in macrophages. Plexin A4 KO mice were protected from LPS induced septic shock, with improved survival from LPS treatment and polymicrobial peritonitis [205]. In dietary obesity, Sema3e is expressed by adipose tissue and chemoattracts macrophages to the tissue by binding to macrophage Plexin D1. This results in macrophage infiltration to the tissue and TNFα production. Plexin D1 knock down with a short hairpin RNA, prevented macrophage infiltration [206].

Sema3e prevents inflammation by repelling neutrophils and preventing neutrophil cytokine secretion. In human neutrophils, Sema3e binds to Plexin D1 and acts a chemorepellent. Sema3e also prevents neutrophils migrating towards IL-8 [207], a known neutrophil chemoattractant [52]. Treating mice with Sema3e during an allergic asthma model, reduced the presence of neutrophils in the lungs [207].

Sema6d is expressed by Natural Killer cells (NKs), T and B cells. The receptor for Sema6d is PlexinA1. Sema6d contributes to CD4+ T cell endogenous signalling. When Sema6d is received by DCs, they produce IL-12, a cytokine which promotes the development of T_H1 T cells. Although no defect in T cell priming was detected in Sema6d KO mice [151,193,208].

Overall, semaphorins promote and reduce inflammation, in a context dependant manner. The Sema3a- Plexin A4 axis prevents T cell activation but promotes macrophages to secrete pro-inflammatory cytokines. Sema3e-Plexin D1 signalling attracts macrophages but repels neutrophils. Sema4a promotes the production of T_H1 and also stabilises T_{reg} cells to reduce pulmonary inflammation. Sema4d stimulated pro-inflammatory cytokine production from monocytes and antibody production from B cells. In APAP injury, the innate immune system is activated, and semaphorins may help modulate the immune system. In line with this, a microarray detected *Sema4a* and *Sema4d* expression by restorative $Ly6C^{hi}$ monocytes during APAP injury [48]. Although the function of these semaphorins was not described.

Table 1. 3 Roles of semaphorins in the immune system

Semaphorin	**Receptor**	**Immune cell**	**Function**	**Reference**
Sema3a	Plexin A4 and Nrp1	T cells	Prevention of T cell priming and proliferation	[202]
Sema3a	Plexin A4 and Nrp1	DC	DC contraction to facilitate migration into the lymph node	[204]
Sema3a	Plexin A4	Macrophages	Pro-inflammatory cytokine production from macrophages during LPS challenge	[205]
Sema3e	Plexin D1	Macrophages	Macrophage infiltration into adipose tissue and TNFα production	[206]
Sema3e	Plexin D1	Neutrophil	Neutrophil chemorepellent	[207]
Sema4a	Tim-2	T cells	Induces T cell proliferation and the production of IL-4 and IL-17	[197]
Sema4a	Nrp1	T_{reg}	Maintains T_{reg} stability via during inflammation	[199]
Sema4d	Plexin B1	B cells	Proliferation and antibody regeneration	[193]
Sema4d	Plexin B2	Monocytes	Secretion of TNFα and IL-6	[194,195]
Sema4d	Plexin B2	Neutrophils	Prevent neutrophil activation	[196]
Sema6d	Plexin A1	T cells	Contributes to CD4+ T cell endogenous signalling	[151]

Semaphorin 7a

Semaphorin 7a (Sema7a, CD108) is the only semaphorin in class 7, as it is the only semaphorin to be linked the membrane via a GPI linker. *Sema7a* is located on human chromosome 15 (25kb) and mouse chromosome 9B (22kb), both comprise of 14 exons [209]. The Sema7a protein in human and mice is composed of 666 and 664 amino acids respectively, with 89.5% sequence identity [210]. The mouse Sema7a consists of a short 19 amino acid GPI linker, attached to a 602 amino acid extracellular domain, which contains the sema, PSI and Ig domains of Sema7a. Contained within Sema7a's sema domain, is a RGD motif that facilitates binding to Integrin α -β1 dimers [158].

Sema7a expression is promoted in human endothelial cells (HMECs) by IL-6 and TNFα signalling or during hypoxia by Hypoxia-Inducible Factor 1α (HIF-1α) [211,212]. These factors converge on Nf-κB signalling to promote Sema7a expression. Furthermore, Sema7a promotes IL-6 and TNFα expression in HMECs, indicating it is part of a positive feedback loop [212]. Sema7a expression can also be repressed by Est2-repressor factor (ERF) [213].

The Sema7a receptors are Integrin β1 and Plexin C1. Both Sema7a and Plexin C1 have large extracellular domains which are highly glycosylated [158]. The cytoplasmic domain of Plexin C1 contains a Rho-GTPase binding domain (RBD), and two GAP domains to facilitate downstream signalling.

Typically, Plexin C1 signalling prevents cell adhesion and spreading, by preventing cofilin activation. Cofilin depolymerises F-actin at the slow growing end of the actin filament, providing new actin monomers for actin polymerisation. Phosphorylation by LIMK I and II inhibits cofilin [214,215]. Sema7a - Plexin C1 - LMKII signalling inactivates cofilin and prevents melanocyte and dendritic cell spreading and adhesion [216–219].

SemaVa (or A39R) synthesised by the vaccinia small pox virus, and SemaVb (or AHV-1) produced by alcelaphine herpes virus type 1, are structural mimics of Sema7a, and bind to Plexin C1 [154]. A39R has evolved to bind to Plexin C1 with a 10 fold higher affinity [158]. A39R and AHV-1 bind to Plexin C1 expressed by dendritic cells. This prevents cytoskeleton rearrangements required to phagocytose the virus, allowing the virus to thwart the immune system [218,219]. Like all semaphorins, Sema7a was originally identified as an axon guidance molecule, it has since been shown to have roles in the immune response, angiogenesis and cancer.

Figure 1. 6 The structure of the Sema7a / Plexin C1 complex

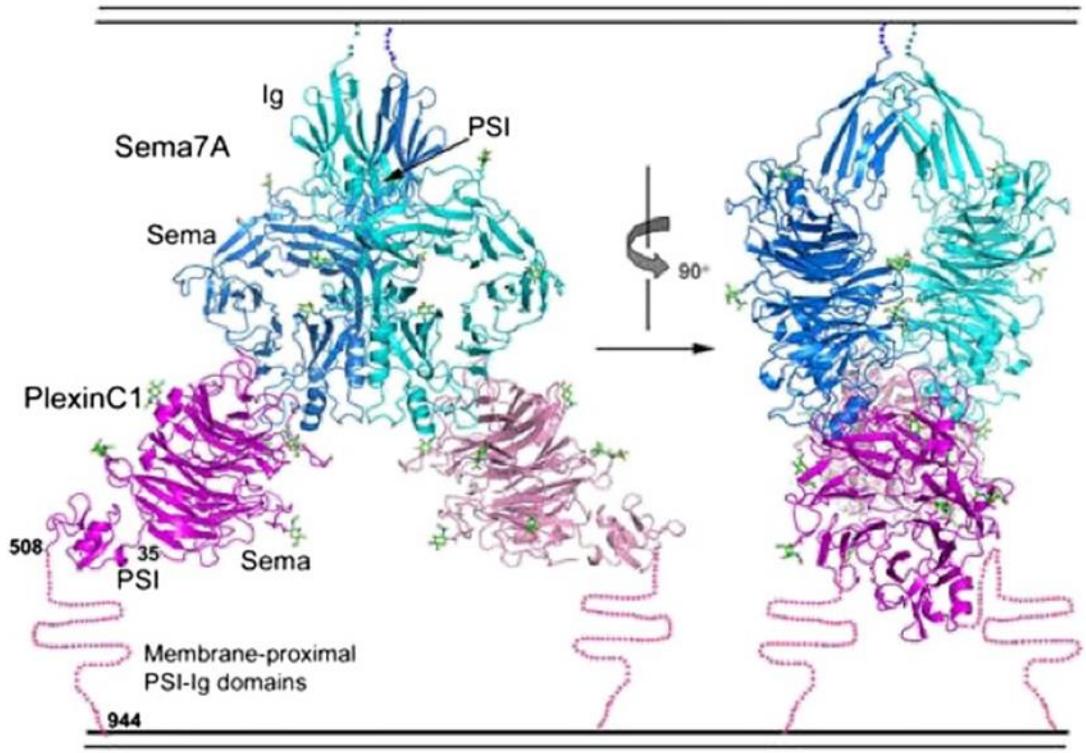

Figure 1. 6

Ribbon models of the Sema7a / PlexinC1 complex.
Sema7a (blue and cyan) is bound to the plasma membrane by a GPI linker. It forms a homodimer via its PSI and sema domains to bind two Plexin C1 (pink and magenta) receptors. Binding depends on a 'loop in groove' conformation.
Plexin C1 is bound to the membrane by Ig domains.
Sema7a and Plexin C1 are highly glycosylated. The N-linked glycans are shown (green).

Black lines, position of cell membranes. Front view (left) and side view (right). Sema, sema domain; PSI, plexin-semaphorin- integrin domain.

Adapted from Liu, H. et al. (2010) 'Structural Basis of Semaphorin-Plexin Recognition and Viral Mimicry from Sema7A and A39R Complexes with Plexin C1', Cell. Elsevier Ltd, 142(5), pp. 749–761 [158]

Sema7a as an axon guidance molecule

Sema7a was first identified to promote axon outgrowth in the olfactory bulb *in vitro* and *in vivo* [176]. Sema7a binds to Integrin β1 on the neurone, which phosphorylates FAK and ERK to promote outgrowth [176]. Sema7a also promotes outgrowth of cortex and dorsal root ganglia axons *in vitro* [176]. Since this discovery, Sema7a has been shown to promote neurone branching, migration and integration in both embryos and adults. For a summary, see Table 1. 4.

Sema7a promotes axon branching of thalamocortical neurones by Integrin β1 [220]. Or branching of dendrites and cortical neurones by Arg (Abelson family non receptor tyrosine kinases related gene) mediated cytoskeletal rearrangements [177]. Conversely, when Sema7a binds to Plexin C1 on dopaminergic neurones it restricts neurone growth. Sema7a KO mice had more Plexin C1+ axons extending dorsally into the dorsal striatum [221].

To restrict Sema7a signalling during neural development, Sema7a is cleaved into an inactivate form by Caspase 9. Caspase 9 is activated by apoptotic protease factor -1 (Apaf-1) and is independent of apoptosis and Caspase 3 activation. It has been proposed that the Apaf-1 /Caspase 9 signalling is part of a bigger developmental program which regulates axon wiring in the olfactory bulb. Mice deficient for Apaf-1 or Caspase 9 had abnormal olfactory sensory neurone axon trajectories, maturation and synapse formation [222,223].

In the adult central nervous system, Sema7a- PlexinC1 signalling prevents proliferation of neural progenitors. Neurogenesis in the adult is tightly controlled and restricted to the subventricular zone and the subgranular zone (SGZ) of the dentate gyrus. Early progenitors in the SGZ express Plexin C1, this binds Sema7a which represses progenitor proliferation. At subsequent stages of neurogenesis, the new neurones must integrate into the existing neural network. Sema7a binds to Integrin β1 to facilitate dendrite outgrowth, spine development and the functional integration of the new born neurone [178].

Sema7a also precisely guides new sweet taste receptor cells (TRCs) in the taste buds to its corresponding sweet ganglion, which relays the information to the CNS. TRCs are replaced every 5 – 20 days, but their corresponding ganglions last a lifetime. Therefore, Sema7a is constantly acting in the tongue to integrate new TRCs. Bitter TRCs are guided by Sema3a. Misexpression of Sema3a in sweet TRCs causes bitter

ganglion neurones to bind to sweet TRCs, with the ganglion responding to both the sweet and bitter stimuli. Repeating the experiments with Sema7a gave the same results but in the sweet pathway [224]. Therefore, Sema3a and Sema7a work independently of each other. Presumably, this specificity is receptor dependant, but receptor expression was not examined. It was not shown if Sema7a was secreted or membrane bound, which may also determine specificity.

Following spinal cord injury, astrocytes become activated express Sema7a. The end feet of these astrocytes which highly express Sema7a bind to Integrin α1β1 on macrophages. It has been proposed that the activated macrophages and astrocytes prolong injury and fibrosis, to form a scar which prevent neurone regeneration [225].

Sema7a directs Gonadotropin-releasing hormone (GnRH) neurones during development and regulate their actions in the adult. GnRH neurones are the master regulators of reproductive functions. They secrete GnRH into the bloodstream which carries GnRH to the anterior pituitary gland. This causes the release of reproductive hormones into the circulation including testosterone, luteinising hormone and follicle stimulating hormone. They also integrate olfactory sensory signals such as pheromones, to elicit attraction. The development and migration of GnRH neurones is tightly controlled by spatial-temporal expression of growth factors and adhesion molecules. In humans, defects in this system leads to hypogonadotropic hypogonadism (HH), a condition characterised by the reduction or failure of sexual competence [226]. Patients with HH have mutations in the *SEMA7A* gene [227].

Sema7a guides GnRH migration during development. GnRH neurones originate at the nasal placode. At the start of their migration, GnRH neurones only express Integrin β1. However, when the GnRH neurones enter the ventral forebrain, they only express Plexin C1 which hinders migration [179]. This switch in receptor expression may be required for the precise guidance of GnRH neurones to their final location.

The correct wiring of the GnRH neurones is required for reproduction in adult mice. Sema7a KO mice have less GnRH neurones and reduced fertility. Males have reduced testicular size and lower testosterone levels than WT mice. When exposed to male pheromones, the male Sema7a KO mice elicited the same attractional response, mediated by c-fos signalling, as female mice. Testosterone administration restored the typical male pattern response to male pheromones. These results imply the correct formation of GnRH neurones and testosterone circulation are required for male reproduction [180].

In female adult mice, progesterone causes cyclic Sema7a expression in tanycytes. Tanycytes cover the pituitary portal vessels to insulate them from GnRH nerve terminals during dioestrus. Progesterone binds to its receptor on the tanycyte which promotes TGF β expression. TGF-β upregulates Sema7a in the tanycyte. Autocrine - Sema7a – Integrin β1 – pFAK – pERK – pAKT signalling promotes the outgrowth and elongation of the tanycyte, so that it covers the portal vessel. In addition, Sema7a is secreted from the tanycyte, and binds to Plexin C1 expressed on GnRH neurones. Plexin C1 – pFAK – pERK causes GnRH neurone retraction. These mechanisms together prevent GnRH neurones from signalling into the vasculature at peak progesterone levels. Mice deficient for Plexin C1 or Sema7a have abnormal GnRH innervation, ovulation and cyclic fertility [227].

In summary, Sema7a controls axon outgrowth and contraction by binding to structurally distinct receptors. When Sema7a binds to neural Integrin β1, FAK and ERK signalling activates axon outgrowth. When Sema7a binds to neural Plexin C1 cofilin becomes inhibited; reducing migration and proliferation during neurogenesis, or neurone contraction. Sema7a receptor expression is often spatially and temporally controlled. This tight regulation is crucial for the correct neuronal wiring.

Table 1. 4 Roles of Sema7a in the nervous system

Receiving neurone	**Sema7a Receptor**	**Function**	**Reference**
Adult de novo neurones	Integrin β1	Dendrite outgrowth and functional integration of new neurones in the adult	178
Adult neural progenitors	Plexin C1	Prevents proliferation of neural progenitors	178
Cortex and dorsal root ganglia axons	Integrin β1	Axon outgrowth	176
Dendrites and cortical neurones	?	Axon branching, mediated by Arg	177
Dopaminergic neurones	Plexin C1	Restriction of neurone growth	221
GnRH neurones	Integrin β1 at the nasal placode Plexin C1 as the neurone reaches its destination	Neurone migration	179
GnRH neurones	Plexin C1	Neurone contraction during dioestrus, to prevent aberrant hormonal signalling	227
Olfactory bulb	Integrin β1	Axon outgrowth, By pERK-pFAK signalling	176
Tanycyte	Integrin β1	Tanycyte extension during dioestrus, to prevent aberrant hormonal signalling	227
Taste receptor cells (TRC)	?	Integration of new sweet TRCs with existing sweet ganglions	224
Thalamocortical neurones	Integrin β1	Axon branching	220

Roles of Sema7a in the immune system

Sema7a has pro- and anti-inflammatory roles in the immune system. It is expressed by activated dendritic cells, T cells and macrophages; it attracts dendritic cells, monocytes and macrophages [228–230]; and promotes monocyte activation. Most of the actions of Sema7a converge on the pFAK – pERK signalling pathway. Like all semaphorins, the receptor which receives Sema7a defines the overall outcome. For a summary see Table 1. 5.

Sema7a is expressed by activated T cells. Sema7a on T cells binds to Integrin α1β1 on macrophages to form a stable immunological synapse. This binding induces macrophage IL-6 and TNFα secretion (Figure 1. 7). This Sema7a expression on activated T cells was crucial for the effector phase of T cell mediated inflammation *in vivo*, as Sema7a KO mice were resistant to EAE [231].

In rheumatoid arthritis, Sema7a forms a positive feedback loop to promote inflammation. Synovial monocytes secrete ADAM- 17, which cleaves Sema7a from the cell surface of T cells. This shed Sema7a promotes the differentiation of T_H1 and T_H17 cells. Shed Sema7a also binds to Integrin β1 on monocytes in the arthritic joint, this induces the monocytes to secrete pro-inflammatory IL-6, TNFα and more ADAM-17, completing the pro-inflammatory feedback loop. In rheumatoid arthritis patients, Sema7a in the synovial fluid and serum correlates with the degree of arthritis. Blocking Sema7a in mice reduced inflammation in the joint in the collagen induced arthritis model [232].

In human blood, Sema7a is expressed on human platelets [233] and erythrocytes where it carries John Milton Hagen (JMH) group antigens [234]. *In vitro* studies suggest the JMH antigens activate T cell proliferation and secretion of the pro-inflammatory cytokines IL-8 and IFN-γ [235].

In addition to the pro-inflammatory roles, Sema7a can have anti-inflammatory roles on macrophages. In a model of dextran sodium sulfate (DSS)-induced colitis, intestinal epithelial cells express Sema7a which binds directly to Integrin αvβ1 on intestinal macrophages. This induces the macrophages secrete the cytokine IL-10 and reduces inflammation and injury (Figure 1. 7). Furthermore, Sema7a KO mice had severely reduced survival compared to WT mice [236].

Figure 1. 7 Sema7a has pro- and anti-inflammatory effects on macrophages

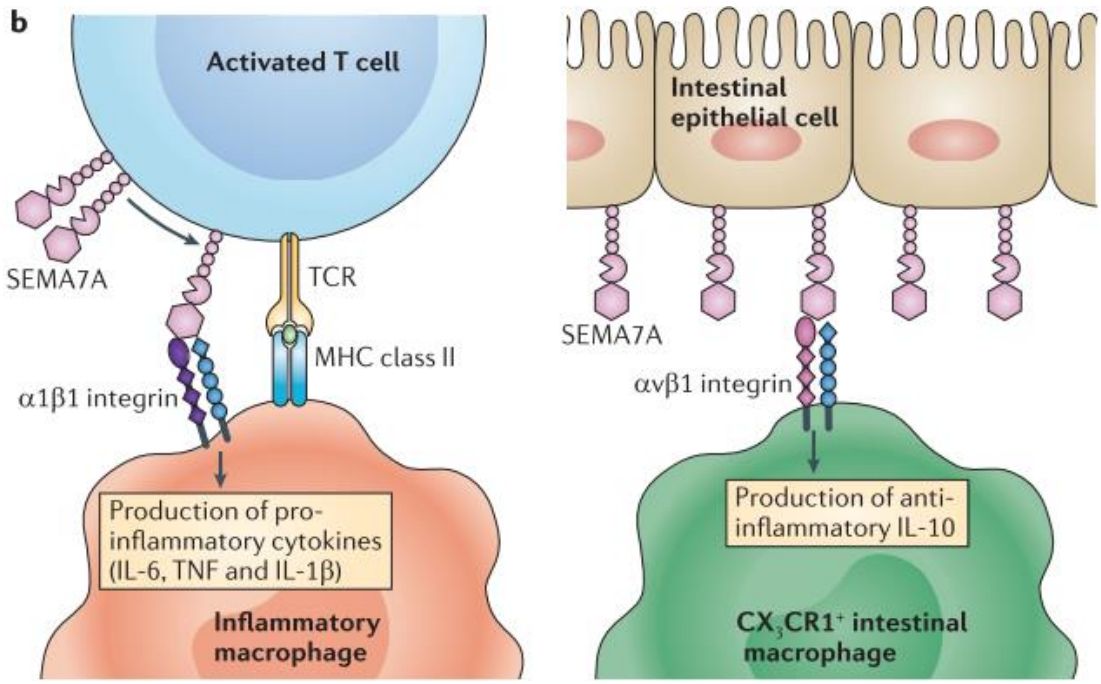

Figure 1. 7

Left: Sema7a on activated T cells binds to Integrin α1β1 inflammatory macrophages to promote the secretion of IL-6 and TNFα.
Right: Intestinal epithelial cells express Sema7a, which binds to Integrin αvβ1 on intestinal macrophages to promote the secretion of the anti-inflammatory cytokine IL-10

CX_3CR1, CX3 C-chemokine receptor 1; TRC, T cell receptor.

Adapted from: Kumanogoh, A. and Kikutani, H. (2013) 'Immunological functions of the neuropilins and plexins as receptors for semaphorins.', *Nature reviews. Immunology*. Nature Publishing Group, 13(11), pp. 802–14. [151]

Sema7a also facilitates the transmigration of PMNs across an endothelial layer. Treating HMECs with a siRNA to knock down Sema7a reduced PMN transmigration, whereas HMEC transfection with a viral promoter enhanced transmigration [211]. Sema7a KO mice had less myeloperoxidase (MPO) activity in the lungs after hypoxia, or LPS inhalation. Bone marrow transfer experiments indicated the effects are not mediated by immune cells [211,212].

Follow up studies indicated that Plexin C1 on PMNs facilitates their transmigration into the lung during forced ventilation pulmonary injury. Plexin C1 KO mice, or WT mice with a Plexin C1 KO bone marrow transplant, had a reduced number of infiltrating cells in the bronchoalveolar lavage (BAL), and a lower expression of: IL-1β, TNFα, IL-6 and CXCL1 [237].

The same lab demonstrated Plexin C1 KO mice have less inflammation in a zymosan-induced peritonitis model. Again, Plexin C1 expression on immune cells binds to Sema7a to facilitate infiltration and inflammation in the peritoneum [238]. However, they did not show where Sema7a was expressed in relation to the peritoneum or characterise the peritoneal exudate cells.

Sema7a is highly upregulated on mature DCs but is virtually absent on resting DCs. In Sema7a KO mice, DCs mature but have less actin based protrusions, lower adherence and cannot migrate in response to CCL21, a DC chemoattractant [230].

Sema7a prevents DC phagocytosis. The herpes virus AHV-1 and the vaccinia poxvirus (A39R) produce a structural mimic of Sema7a, which binds to Plexin C1 expressed by DCs [218,219]. Sema7a - Plexin C1 signalling inhibits cofilin and prevents phosphorylation of FAK. This prevents the cytoskeletal rearrangements required for the DCs to adhere and to form the cellular protrusions required to perform phagocytosis of the virus. Thus the virus can thwart the immune system [218,219,239].

Overall, Sema7a activates T cells, facilitates neutrophil migration across an endothelial barrier to promote acute pulmonary inflammation, and reduced DC adhesion, migration and phagocytosis. Sema7a also regulates if macrophages secrete pro- or anti-inflammatory cytokines, in a receptor dependant manner. If macrophages use Integrin α1β1 to bind to Sema7a on T cells, the macrophage secretes IL-6 and TNFα. Conversely, when macrophages use Integrin αvβ1 as the receptor for Sema7a expressed on intestinal epithelial cells, the macrophage secretes IL-10 (Figure 1. 7).

Table 1. 5 Immune functions of Sema7a

Cell expressing Sema7a	**Receptor**	**Receiving cell**	**Function**	**Reference**
Dendritic cells	-	-	Dendritic cell adherence and migration in response to CCl21	230
Herpes virus AHV-1 and the vaccinia poxvirus	Plexin C1	Dendritic cell	Prevents cytoskeletal rearrangements required for phagocytosis	218,219,239
Activated T cells	Integrin α1β1	Macrophages	IL-6 and TNFα secretion	231
Intestinal epithelial cells	Integrin αvβ1	Macrophages	Secretion of IL-10 Reduction of inflammation	236
Spinal cord astrocytes	Integrin α1β1	Macrophages	Pro-inflammation, prolonging injury and fibrosis	225
Shed Sema7a from T cells	Integrin β1	Monocytes	Secretion of IL-6, TNFα Secretion of ADAM-17, which cleaves Sema7a on T cells creating a pro-inflammatory loop	232
?	Integrin β1	Monocytes and macrophages	Chemoattraction	228,229
Endothelial cells	Plexin C1	PMNs	Transmigration of PMNs into the lung	211,237
Shed Sema7a from T cells	?	T cells	Differentiation of T_H1 and T_H17 cells	232
Erythrocytes, JMH antigens	?	T cells	T cell proliferation and secretion IL-8 and IFN-γ	235

Roles of Sema7a in cancer

Sema7a expression in breast cancer patients is associated with a poor prognosis. Sema7a is promotes mammary tumour cell motility and invasion via Integrin β1 [240]. It also facilitates angiogenesis in mammary tumours [191]. Inhibiting Sema7a with a short hairpin reduced tumour growth *in vivo* [241].

Sema7a is expressed in human oral squamous cell carcinoma. *In vitro,* Sema7a -pERK-pAKT signalling promotes cell growth and proliferation in human oral squamous cell carcinoma derived cells lines. In addition, Sema7a induced the expression of MMP2 and 9 which are required to breakdown the ECM during invasion. The authors also implied these effects were mediated by TGFβ signalling [242]. It would be interesting to see if blocking Sema7a or TGFβ reduces oral squamous cell tumour growth *in vivo*.

Together, Sema7a promotes tumour growth by promoting angiogenesis and metastasis. Sema7a often induces contrasting affects through its receptors Integrin β1 or Plexin C1. In breast cancer Integrin β1 promotes cell invasion [240]. In melanoma, Plexin C1 is expressed in primary tumours, and inhibits melanocyte proliferation and migration. Plexin C1 is downregulated during metastasis, which allows melanoma migration and proliferation, with depth of invasion inversely correlating with Plexin C1 expression [217,243,244]. Futures studies could examine if treatment with Plexin C1 prevents Sema7a induced metastasis.

Roles of Sema7a in the liver and TGFβ mediated lung fibrosis

Very little known about the roles of Sema7a in the liver. Previous to this project Sema7a has been studied in the context of ischemia reperfusion injury [245] and chronic liver injury [246]. In human liver samples, Sema7a is upregulated with either alcoholics liver disease or hepatitis C virus, possibly to promote fibrosis and inflammation [246].

In a mouse model of chronic CCl_4 and bile duct ligation injury, Sema7a is expressed by the hepatic stellate cells (HSCs), and is upregulated with its receptor Integrin β1 (but not Plexin C1). Sema7a KO mice display less fibrosis and infiltration of F4/80+ macrophages than WT mice after CCl_4 injection, with a down regulation of IL-6 and MCP-1. The authors indicate that these effects could be mediated through the TGFβ -pERK- pAKT pathway [246]. However, they did not examine TGFβ signalling *in vivo*, or if the Sema7a KO mice had less activated HSCs.

In a model of ischemia reperfusion injury, Plexin C1 KO mice had less infiltrating PMNs lower serum ALT, AST, TNFα and IL-6. Rosenberger *et al*. demonstrate this is due to Plexin C1 expression on the immune cells through a bone marrow transfer. The effects are mediated by Sema7a, as blocking the Sema7a – Plexin C1 interaction reduced the measured injury parameters [245]. However, there was very little necrosis in their model, reflected by the mild raise in ALT. The authors did not show where the Sema7a was being expressed, or if the PMNs were Ly6G+ neutrophils as they claimed, other immune cells were not examined.

Other studies from the Rosenberger lab suggest Sema7a promotes pulmonary inflammation, by enabling Plexin C1 expressed by PMNs to bind onto endothelial Sema7a, enabling PMNs to transmigrate into the lungs [211,237]. Sema7a KO mice had less pulmonary inflammation after LPS inhalation [212] and hypoxia [211]. Plexin C1 KO mice, or blocking the Sema7a – Plexin C1 interaction, reduced PMN infiltration into the lungs a high pressure ventilation model [237] and into the peritoneum during zymosan A induced peritonitis [238]. Together these studies show that Sema7a promotes inflammation by facilitating PMN endothelial transmigration.

TGFβ is a critical mediator of bleomycin induced pulmonary fibrosis and is enhanced by Sema7a. To study the underlying mechanism, mice with pulmonary transgenic TGFβ expression (TGFβ+) were used. TGFβ+ mice had a higher expression of Sema7a, Integrin β1 and Plexin C1, than WT mice. Expression of Sema7a enhanced TGFβ induced cell death, myofibroblast accumulation, collagen deposition and ECM secretion, compared to TGFβ+ Sema7a KO mice. TGFβ induced injury was independent of the canonical SMAD2/3 signalling but required pPI3K – pAKT (phosphoinositide 3-kinase (PI3K) – protein kinase B (PKB, AKT)). The authors claimed there was no difference between pulmonary inflammation in Sema7a KO mice and Sema7a WT mice, but this data was not shown [247]. The location of TGFβ induced Sema7a expression in the lung was not depicted. Together, this data shows Sema7a enhances TGFβ induced fibrosis by enhancing cells death and upregulating ECM synthesis.

Overall, Sema7a signalling promotes TGFβ signalling to promote fibrosis in both lung and in the liver. In pulmonary fibrosis, TGFβ -Sema7a signalling did not promote inflammation. However, in chronic liver injury, Sema7a KO mice had less CD45+ cells and F4/80+ cells infiltrating the liver this was associated with less IL-6 and MCP-1

signalling. In other *in vitro* and *in vivo* models, Sema7a promotes inflammation by activation of T cells, neutrophil transmigration, monocyte chemoattraction and macrophage activation. Sema7a may also be part of a positive feedback loop with IL-6 and TNFα. Sema7a also has anti-inflammatory roles, when macrophages bind Sema7a through their Integrin αvβ1 receptor, they produce IL-10.

The APAP mouse model

The APAP mouse model closely mimics APAP overdose in human patients [3]. To study the role of Sema7a during APAP injury and recovery, I used a 350 mg/kg mouse model using 9-12 week old male C57Bl6/J mice, or aged matched Sema7a KO male mice which are also on the C57Bl6/J background [176]. Mice were starved for 12 hours before administering APAP intraperitoneally. This model was chosen for numerous reasons, discussed below.

GSH is an antioxidant crucial for the detoxification of APAP (see Figure 1. 1) [3,4,14]. GSH is readily synthesised from: L-cysteine, L-glutamic acid and glycine obtained from the diet [248]. Starving mice for 12 hours prior to APAP injection normalises hepatocyte stores of GSH to basal levels. This sensitises the mice to APAP and reduces variability.

Female mice are less susceptible to APAP injury. 2 hours after APAP administration, both male and female mice have increased ALT, depleted GSH stores [249,250], protein adduct formation and activation of the JNK pathway [249,251]. However, 4 hours after APAP administration, female mice begin to restore their GSH stores [249,250], leading to lower ALTs and necrosis [249–251] and faster recovery compared to male mice [249,250]. Immature 3 week old mice are also more susceptible to APAP injury, displaying higher ALTs and necrosis compared to 8 – 10 week old sex matched mice [251]. To study APAP injury in adults we used 9- 12 week old male mice.

The Sema7a KO mice obtained from Jackson labs are on a C57BL6/J background [176]. To match this background strain, I used C57BL6/J mice as WT controls. These C57Bl6/J mice have a moderate response to APAP injury. Harrill *et al.* treated 36 different mice strains with 300 mg/kg APAP for 24 hours. Necrosis, ALT and GSH depletion all varied, with necrosis ranging from 0-80% with correlating ALT [252]. The C57Bl6/J strain were median responders with 40% necrosis and around 2000 U/L

ALT [252]. The C57Bl6/J (background) strain is therefore suitable for this moderate APAP study as adverse effects will be limited, and we can investigate the role of Sema7a during APAP injury and recovery.

To study APAP injury and recovery, the dose must give reproducible levels of necrosis, injury and inflammation but low enough to allow recovery. Previously, our lab have used a 350 mg/kg APAP dose in C57Bl6/J mice to study APAP injury [32]. The mice tolerated this dose well with reproducible levels of necrosis. Doses higher than 350 mg/kg may cause too severe an injury in the mice and prevent recovery [147], or be lethal [23,53]. Therefore, I used a 350 mg/kg APAP dose in C57Bl6/J male mice to study APAP injury and recovery.

Summary

The only viable therapy for APAP overdose, NAC, is only effective in the first 12 hours following APAP ingestion. Outside of this window, patients require a liver transplantation. Patients with a moderate overdose can spontaneously recover [3]. Understanding these mechanisms will lead to novel therapies.

The innate immune system is present in both the injury and recovery phases of APAP injury. Initially, the innate immune system promotes APAP injury. During recovery, the macrophages switch to a restorative phenotype which phagocytose cellular debris, secrete anti-inflammatory cytokines such as IL-10, to reduce inflammation, and TNFα and IL-6 to prime the remaining hepatocytes to proliferate [4,35]. Macrophages are also responsible for secreting Wnt and TGFβ, to induce regeneration or senescence respectively [144,150]. Novel therapies may influence the immune system towards a restorative phenotype.

Sema7a has diverse roles in the immune system. It can act as a chemoattractant for dendritic cells, monocytes and macrophages [228–230]; activate T cells and macrophages [225,232,235]; and facilitate PMN endothelial transmigration into the lungs [211,212,237]. During liver fibrosis, Sema7a KO mice have less inflammation compared to WT mice [212,246]. Sema7a can also modulate macrophage secretion, depending on which receptor receives it. When macrophages bind to Sema7a on intestinal epithelial cells through Integrin αvβ1, macrophages secrete IL-10, an anti- inflammatory cytokine [236]. Conversely, when Sema7a expressed on activated T cells binds to Integrin α1β1 on macrophages the proinflammatory cytokines IL-6 and TNFα are secreted [231]. To date, there are more papers indicating Sema7a promotes inflammation than reduces inflammation. I therefore hypothesise Sema7a promotes inflammation during APAP injury.

Sema7a can also enhance TGFβ signalling during liver and lung fibrosis [246,247]. During APAP injury, macrophages secrete TGFβ to induce cell cycle arrest, marked by p21 expression [144]. Furthermore, Sema7a may be able to act as a barrier to APAP induced necrosis through modulation of the cytoskeleton.

Hypothesis and Aims

Hypothesis: Sema7a promotes injury and inflammation during APAP injury

Aims:

1. Examine if Sema7a+ hepatocytes form a boundary to limit the spread of cell death
2. Examine if Sema7a promotes p21 expression in hepatocytes
3. Define if Sema7a delays proliferation during recovery from APAP injury
4. Investigate if Sema7a has a pro- inflammatory effect during APAP injury

Chapter 2 - Materials and Methods

In vivo experiments

Animal models

The animals used in this study are male C57BL6/J or Sema7a KO mice, which were purchased from the Jackson Laboratory and bred on a C57BL6/J background. Animals were housed in a specific pathogen-free environment and kept under standard conditions with a 12 h day/night cycle and access to food and water *ad libitum*. All animal experiments were carried out under procedural guidelines, severity protocols and with ethical permission from the University of Edinburgh Animal Welfare and Ethical Review Body (AWERB) and the Home Office (UK), licence numbers 70/7847 and P231C5F81.

Genotyping

Genotyping was performed by the commercial Transnetyx service. Mice were either homozygous knockouts for Sema7a$^{-/-}$ or homozygous WT (Sema7a$^{WT/WT}$).

For in house genotyping, ear clips were digested overnight with proteinase K in a shaking water bath at 55 °C. After heat inactivation at 95 °C, digests were centrifuged (10 min, 18,000 x g) and the supernatant collected. Genomic PCR was run using OneTaq DNA Polymerase kit (Biolabs) with 0.5 µM primers (Sigma): Common forward primer (GCA CAG CCC TGT AGT GTC TC), WT reverse primer (AGC CTC TTC ACT GCT CCA C), Sema7a KO reverse primer (CCG GGG GAT CCA CTA GTT CT). PCR products were run in a 0.5x TBE 2% agarose gel in with a 1 KB ladder. Bands were detected at: WT 182bp and Sema7a KO 249bp.

APAP experiments

9-12 week old male mice were fasted for 12 hours then intra-peritoneally (i.p.) injected with 350 mg/kg paracetamol (Acetaminophen, APAP (Sigma)) or sterile saline by injection. Mice were kept in a heat box at 28 °C, and closely monitored for the duration of the experiment. To measure proliferation, 100 µL 1 mg/ml 5-bromo-2'-deoxyuridine (BrdU, Sigma) was injected i.p. 1 hour before culling.

Mice were humanely euthanised according to UK Home Office regulations. Blood was collected by cardiac puncture, clotted overnight at 4°C then centrifuged for 10 min, 8,000 x g at 4 °C and serum removed.

Livers were perfused via the inferior vena cava (IVC) with Phosphate Buffered Saline Solution (PBS). Samples of liver were embedded in optimal cutting temperature compound (OCT), or snap frozen, and stored at -80 °C. Liver, kidney, spleen and intestine were collected and fixed in formalin overnight, and paraffin embedded (FFPE). Embedding in paraffin blocks was performed by Shared University Research Facilities (SuRF) Histology, Queen's Medical Research Institute (QMRI), University of Edinburgh.

Serum liver function tests

Serum analysis was performed by Dr Forbes Howie at the QMRI, University of Edinburgh. Serum Albumin, bilirubin, alanine aminotransferase (ALT), aspartate transaminase (AST), alkaline phosphatase (ALP) and glutamate dehydrogenase (GLDH) were measured in non-haemolysed serum samples according to manufacturer instructions (Alpha Laboratories). Kit instruction were adapted for use in the Cobas Fara or Cobas Mira analyser (Roche).

In vivo phagocytosis assay

100 µL PKH26PCL (10 µM in Diluent B; Sigma) or vehicle control was injected intravenously via the tail vein, 4 hours post APAP injection. Mice were sacrificed at 12 h post APAP injection. For the 24 hours in vivo phagocytosis experiments, PKH26PCL was injected at 8 hours post APAP injections, and mice sacrificed at 24 hours post APAP injections. Peripheral and cardiac blood, peritoneal lavage and liver tissue were collected for flow cytometry analysis (see 'Tissue collection and staining for flow cytometry')

Tissue collection and staining for flow cytometry

Peritoneal lavage collection and staining for flow cytometry

The peritoneal cavity was washed with 1 ml PBS. The collected peritoneal lavage was centrifuged for 5 min, 300 x g at 4°C. The supernatant was stored at -80°C. The pellet was resuspended in PBS, filtered, and stained with L/D for 40 min at 4 °C. After blocking for 20 min 4 °C in 10 % mouse serum, samples were then stained for 20 min at 4°C with the '*In vivo* phagocytosis Flow Cytometry Panel for Peritoneal Lavage'. Cells were fixed and lysed with 200 µL 1x BD Phosflow Lyse/ Fix (BD Biosciences) for 15 min at RT. Cells were kept in Fluorescent Activated Cell Sorting (FACS) wash (1%FCS, 2.5 mM Ethylenediaminetetraacetic acid (EDTA) in PBS).

Liver digestion and non-parenchymal cell isolation and staining for flow cytometry

Isolation of hepatic non-parenchymal cells (NPCs), labelling and flow cytometry was performed by Jennifer Cartwright. The liver digestion protocol was based on the protocol previously published by Lynch *et al* [253]. The staining protocol followed Campana's [72] protocol, with minor modifications.

0.5 g of perfused liver from the central lobe was mechanically homogenised with a scalpel, followed by enzymatic digestion: collagenase V (0.8 mg/ml; Sigma-Aldrich), collagenase D (0.625 mg/ml; Roche), dispase (1 mg/ml, Gibco), and DNase (30 µg/ml, Roche) in RPMI 1640, for 20 min at 37 °C in a shaking incubator, with vigorous shaking every 5 min.

Liver digests were filtered through a 100 µm filter, and enzymes inactivated by adding 30 ml cold medium (RPMI,10% FCS, 4 °C). The NPC fraction of the liver was harvested by two centrifugations in 30 ml cold medium at 300 x g for 5 min at 4 °C, discarding the supernatant each time.

NPC suspensions were passed through a 40 µm filter, stained with toluidine blue dye and live cells were counted with a BioRad analyser, then diluted to 7,000,000 cells/ml.

NPCs were washed in PBS and stained with Live/Dead (L/D) for 40 min at RT, then blocked in 10% mouse serum. 1,000,000 cells/sample were stained with the Liver PKH Flow Cytometry Panel (Table 2. 6) for 40 min Room Temperature (RT) followed by two FACS buffer washes.

Red blood cells were lysed, and NPCs were fixed with 1x BD Phosflow Lyse/ Fix (BD Biosciences) for 10 min at 4 °C. The NPC suspension was washed and kept in FACS buffer.

Calculating the absolute number of NPCs per gram of liver

The total number of live cells in the whole liver digest volume was calculated and divided by the weight of the liver lobe before digestion, providing the number of live cells per gram of liver. The specific NPC population count (selected in Figure 2. 10) was made into a percentage of the live cells count, as analysed by the BD LSR Fortessa SORP FACS. This was multiplied by the number of live cells per gram of liver, giving the absolute number of a specific NPC population per gram of liver.

Peripheral blood collection and staining for flow cytometry

Peripheral blood was collected into anticoagulating EDTA tubes from untreated WT or Sema7a KO mice through a tail nick. Or from the IVC. of mice which had been starved for 12 hours prior to i.p. injection of saline, then left for 12 h before culling, to mimic an APAP experiment. 25 µL blood was stained for 20 min at RT in the required antibody cocktail (see 'Flow cytometry on peripheral blood').

Cells were washed with PBS and stained with 1:1,000 Live/ Dead (L/D) e780 (L10120, Life technologies) for 40 min, followed by fixation and lysis with 200 µL BD Phosflow Lyse/ Fix (BD Biosciences) for 15 min RT. Cells were kept in FACS wash.

Bone Marrow Derived Macrophage *in vitro* experiments

Bone marrow derived macrophage (BMDM) isolation

The femurs of 10-12 week old C57BL6/J males were flushed with BMDM medium (DMEM/F12 (gibco), 10% FCS, 1% L-Glut, 1% Penicillin/streptomycin (P/S) and 50 ng/ml Macrophage colony stimulating factor-1 (M-CSF, Miltenyi Biotec)), to collect the bone marrow, which was cultured at a single cell suspension in Ultralow attachment flasks (Corning). BMDMs were kept for a week in BMDM medium.

Apoptotic thymocytes (ApopTs)

Thymi were isolated from 6 week old mice, pushed through a 100 µm filter, and then filtered through a 40 µm filter. Thymocytes were cultured at a single cell suspension in 10% FBS, 1:100 P/S, RPMI (gibco) for 2 h before adding 10 µg/ml hydrocortisone (Sigma) for 16 h, to make them apoptotic.

BMDM staining for flow cytometry

BMDMs were stained with 1:1,000 L/D, then blocked in 10% FCS, PBS for 30 min, followed by a 20 min stain with the required antibody cocktail.

Flow cytometry on BMDMs

Compensation for all experiments was set up using eBioscience Ultracomp eBeads.

BMDM phagocytosis assay

ApopTs pre-stained with CMTMR (Life technologies) were cultured with BMDMs in BMDM medium for 1 or 2 hours. BMDMs were stained with 1:1,000 L/D, and CD11b BV650 (Biolegend). The experiment was run in triplicate. Phagocytosis was assessed on the ACEA Biosciences Novocyte and analysed (Figure 2. 1) using NovoExpress 1.2.4 (ACEA Biosciences).

Sema7a receptor expression on BMDMs

BMDMs were incubated overnight with rmSema7a and integrin staining assessed by flow cytometry (Table 2. 1) and assessed using a BD LSR Fortessa SORP FACS. Results were analysed using FlowJo v10.0.07.2. For gating see Figure 2. 2.

Table 2. 1 Sema7a receptor panel on BMDMs

Marker	Fluorophore	Clone	Channel	Manufacturer	Staining Conc.
CD11b	BV650	M1/70	V675/30	Biolegend	1:100
Integrin α1	APC	HMα1	R675/30	Biolegend	1:100
Integrin αυ	PE	RMV-7	B572/28	Biolegend	1:100
L/D	e780		R780/60	Life technologies	1:1,000

Figure 2. 1 Gating strategy to analyse BMDM phagocytosis

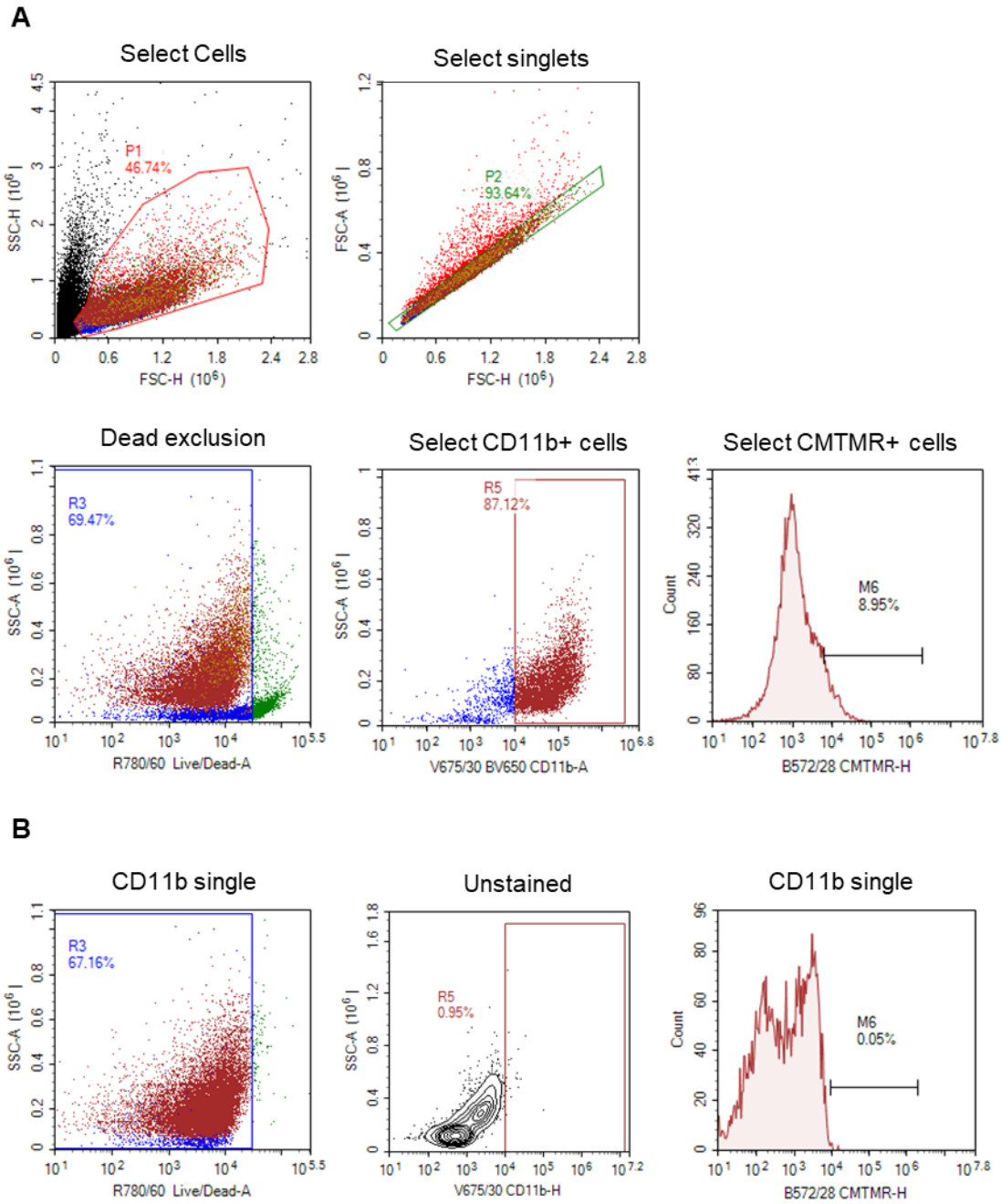

Figure 2. 1

BMDMs were isolated from healthy 10-12 week old WT and Sema7a KO mice. BMDMs were fed apoptotic thymocytes, pre-labelled with CMTMR, for 1 or 2 hours. BMDMs which have phagocytosed apoptotic T cells will be CD11b+ CMTMR+

The gating strategy to detect CD11b+ CMTMR+ BMDMs is as follows:

A) Cells were gated for size, singlets, L/D -, and CD11b+. This CD11b positive population was assessed for CMTMR

B) Gates were set using single colour controls, or unstained sample for CD11b.

Figure 2. 2 Gating strategy to analyse Sema7a receptors on BMDMs

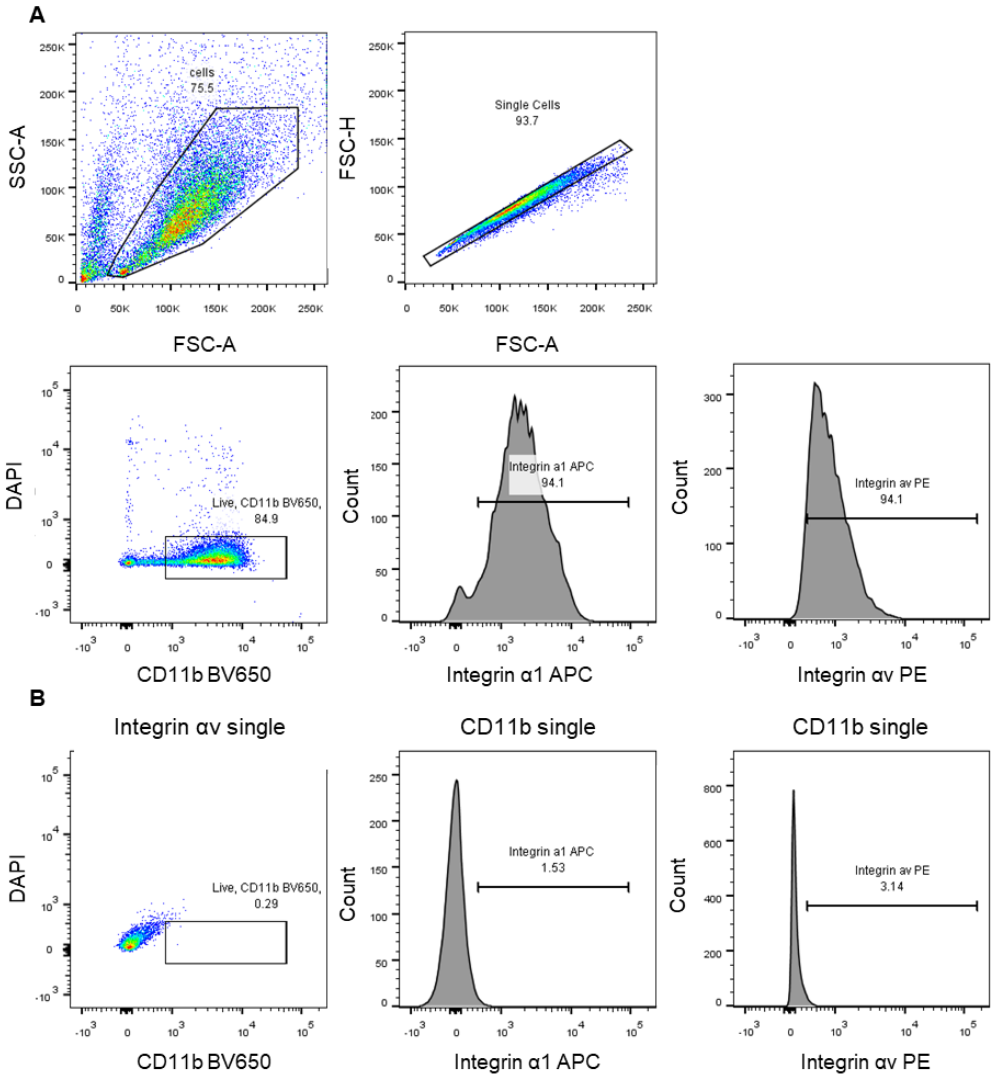

Figure 2. 2

BMDMs were isolated from healthy 10-12 week old WT and Sema7a KO mice, and assessed for the expression of: Integrin α1 and αv, the Sema7a receptors. To examine rector expression, the following gating strategy was used:

A) BMDMs were gated for size, singlets, DAPI negative (live), and CD11b+. This CD11b+ population was assessed for Integrin α1 and αυ expression.

B) Gates in (A) were set using single colour controls, as indicated.

Flow cytometry on peripheral blood

Peripheral blood was prepared as previously described ('Peripheral blood collection and staining for flow cytometry'). Cells were gated on size, singlets, live, CD45+, and Lineage- (B and T cell exclusion). For this initial gating see Figure 2. 3.

Figure 2. 3 Selecting live, CD45+, lineage- cells in peripheral blood

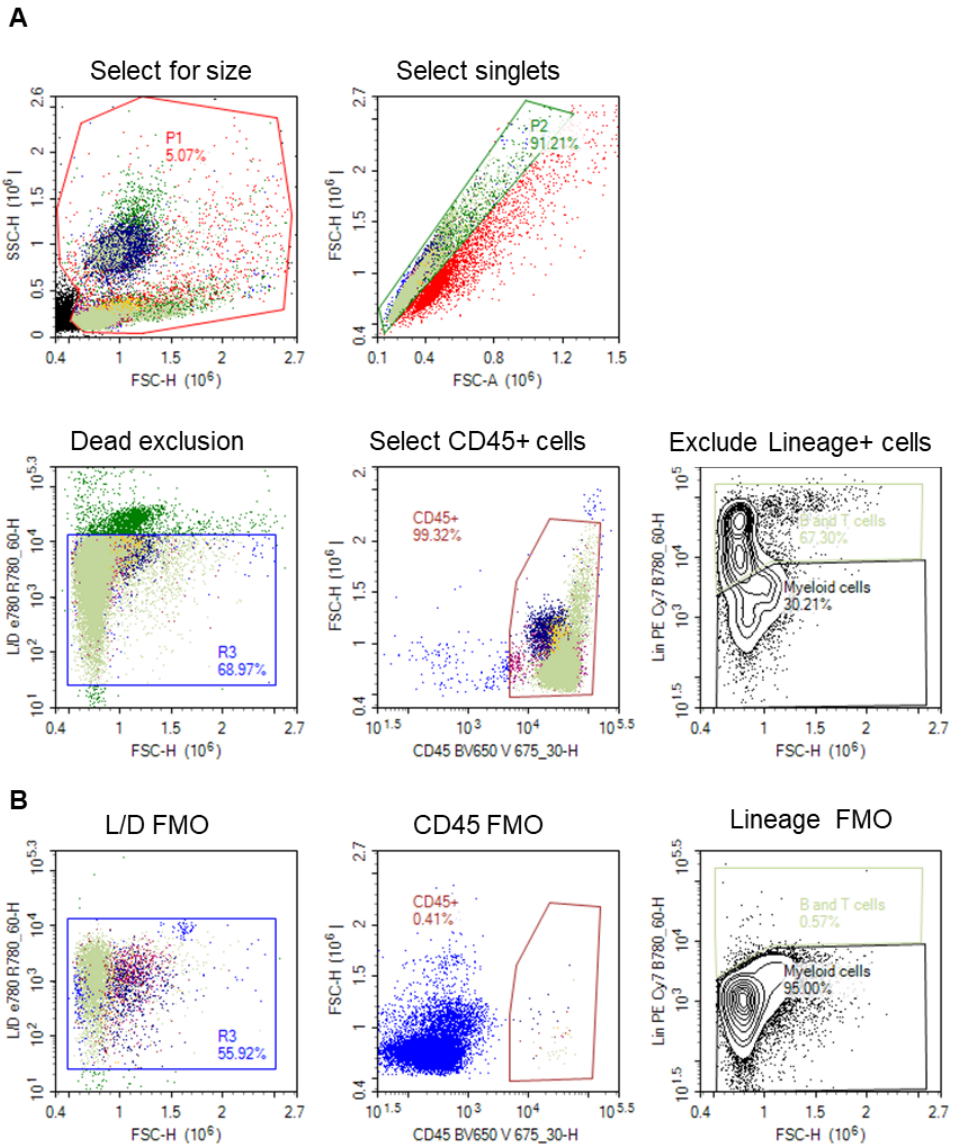

Figure 2. 3

Mouse blood was collected from healthy, and APAP injured, WT and Sema7a KO mice. CD45+ leukocytes were selected as follows:

A) Cells in peripheral blood were gated for size, singlets, live (L/D-), CD45+, and Lineage- (B and T cell exclusion).
B) FMOs were used to set the gates for L/D, CD45 and Lineage, as indicated.

Sema7a receptor expression on neutrophils

Peripheral blood was stained for the 'Sema7a receptor panel on peripheral blood'(see Table 2. 2) and analysed on the Novocyte with NovoExpress 1.2.4 software (ACEA Biosciences). Cells were gated for size, singlets, L/D-, CD45+, and Ly6G+. The expression of the Sema7a receptors: Integrinα1 and Integrinαυ, Plexin C1 were analysed on both the CD45+ population and the CD45+ Ly6G+ population (see Figure 2. 4).

Table 2. 2 Sema7a receptor panel on peripheral blood

Marker	Fluorophore	Clone	Channel	Manufacturer	Staining Conc.
CD11b	BV650	M1/70	V675/30	Biolegend	1:100
Integrin α1	APC	HMα1	R675/30	Biolegend	1:100
Integrin αυ	PE	RMV-7	B572/28	Biolegend	1:100
Plexin C1	Alexa 488	-	B530/30	R&D	1:50
Ly6G	Pacific Blue	1A8	V445/45	Biolegend	1:100
Lineage (CD3, CD19,)	PE Cy7	CD3: 145-2C11 CD19: 6D5	B780/60	Biolegend Biolegend	1:200
L/D	e780		R780/60	Life technologies	1:1,000

Figure 2. 4 Gating for the Sema7a receptors on neutrophils

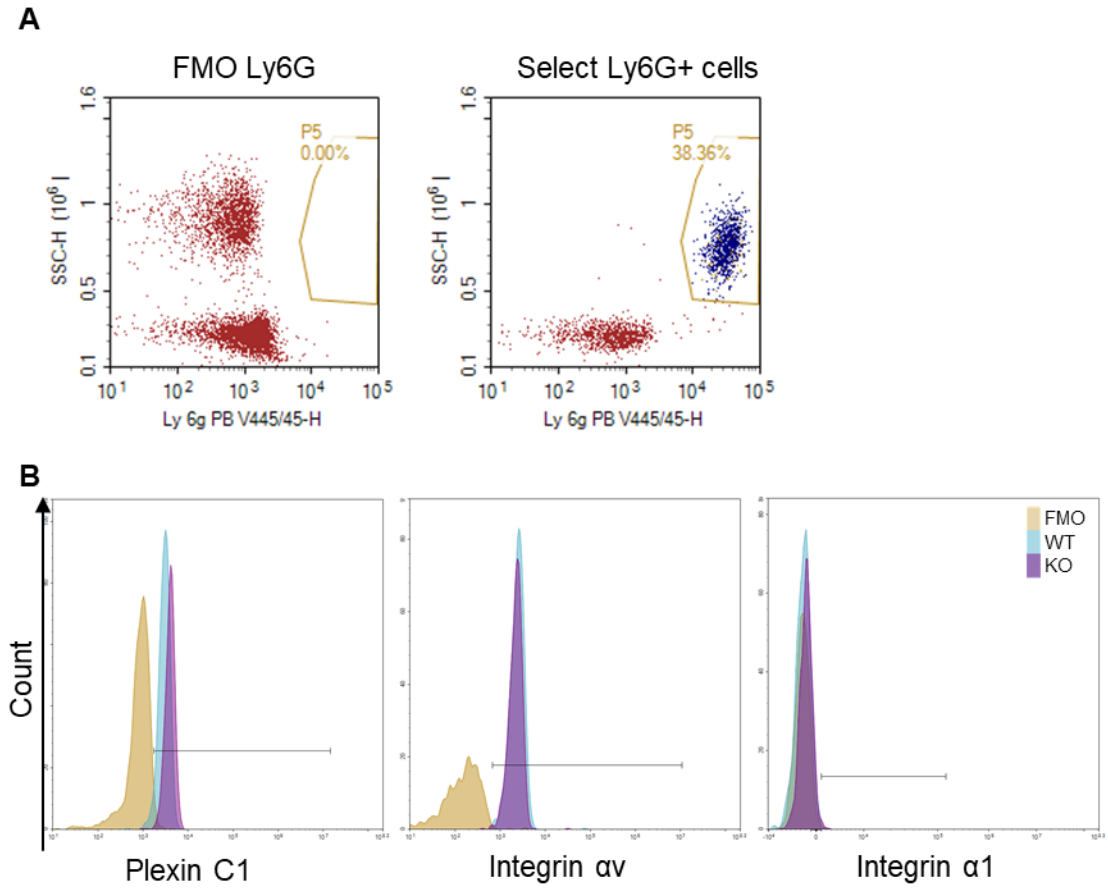

Figure 2. 4

Peripheral blood was isolated from healthy adult male WT and Sema7a KO mice. single, live, Lineage-, CD45+ leukocytes were selected as in Figure 2. 3.

A) Ly6G+ cells were selected (right) from the CD45+ population. The gate was set using the FMO (left)

B) To analyse expression of the Sema7a receptors on neutrophils, gates were set using the FMO (yellow). WT blood (cyan), Sema7a KO blood (magenta).

Numbers of neutrophils and monocytes in peripheral blood

Peripheral blood was stained with the panel in Table 2. 3, and analysed on the Novocyte, (ACEA Biosciences), which can give the absolute count of cell populations. Data was quantified using NovoExpress 1.2.4 software (ACEA Biosciences). Cells were pre-gated as in Figure 2. 3, then neutrophils and monocytes were selected (see Figure 2. 5).

Table 2. 3 Neutrophil and monocyte panel for peripheral blood

Marker	Fluorophore	Clone	Channel	Manufacturer	Staining Conc.
CD45	BV650	30-F11	V675/30	Biolegend	1:100
CD11b	Alexa Flour 488	M1/70	B530/30	eBioscience	1:100
CD115	APC	AFS98	R675/30	Biolegend	1:100
Ly6G	PE	1A8	B572/28	Biolegend	1:100
Ly6C	PB	HK1.4	V445/45	Biolegend	1:100
Lineage (CD3, CD19,)	PE Cy7	CD3: 145-2C11 CD19: 6D5	B780/60	Biolegend Biolegend	1:200
L/D	e780		R780/60	Life technologies	1:1,000

Figure 2. 5 Gating strategy to examine the presence of neutrophils and monocytes in blood

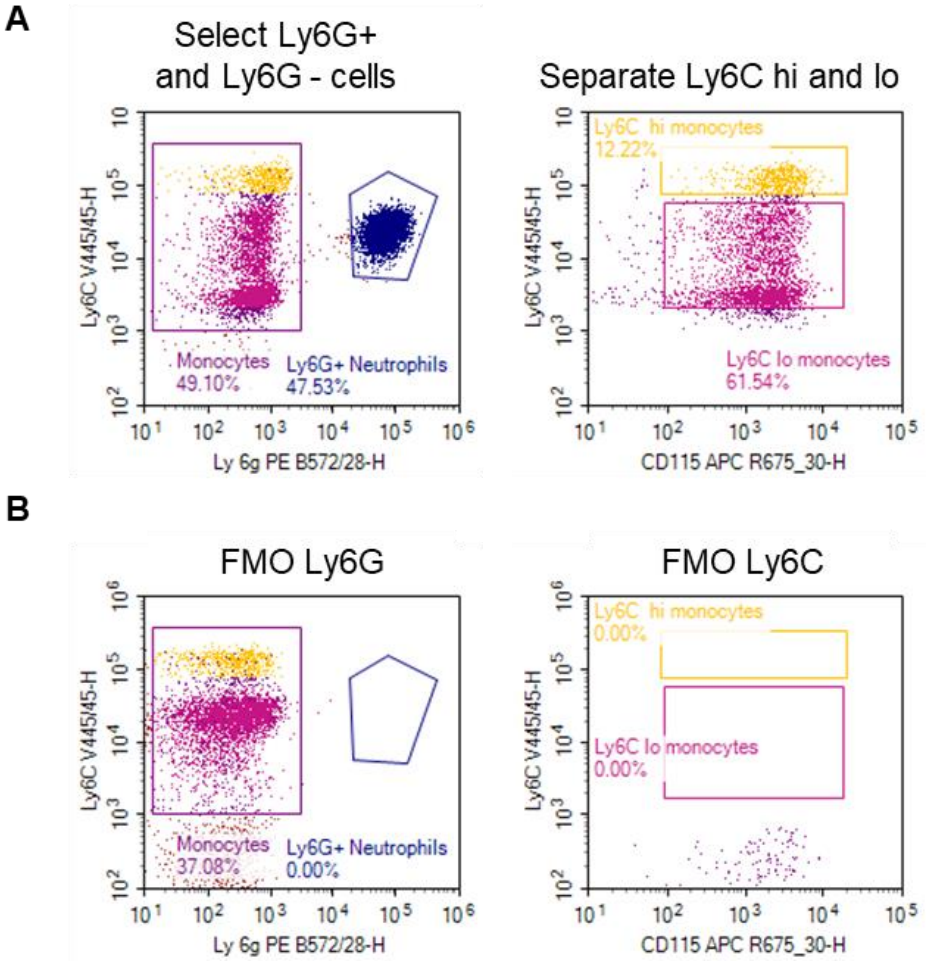

Figure 2. 5

Peripheral blood was isolated from 10-12 week old male WT and Sema7a KO mice. the neutrophil and monocyte population sin the blood was then examined using the following gating strategy.

A) Cells were pre gated on: size, singlets, live, CD45+, and Lineage-**.** Ly6G+ neutrophils and Ly6G- monocytes were selected (left). Monocytes were further subdivided in to Ly6C^{hi} and Ly6C ^{lo} (right).
B) Gates were set using FMOs for Ly6G (left) and Ly6C (right).

Flow cytometry analysis for *in vivo* phagocytosis

Peripheral blood, peritoneal lavage and liver was taken and stained as above. All tissues were analysed on the BD LSR Fortessa SORP FACS. Results were analysed using FlowJo v10.0.07.2 (Tree Star).

Peripheral Blood

30 µL blood was stained with the 'PKH Blood Flow Cytometry Panel' (see Table 2. 4), or FMO equivalent. Neutrophils and monocytes were selected as in Figure 2. 5. Phagocytosis (PKH+) was analysed using the gating strategy in Figure 2. 6.

Table 2. 4 *In vivo* phagocytosis flow cytometry panel for blood

Marker	Fluorophore	Clone	Channel	Manufacturer	Staining Conc.
CD45	BV650	30-F11	V660/20	Biolegend	1:100
CD11b	Alexa Flour 488	M1/70	B530/30	eBioscience	1:100
CD115	APC	AFS98	R670/14	Biolegend	1:100
Ly6G	PB	1A8	V450/50	Biolegend	1:100
Ly6C	PerCyP/Cy5.5	HK1.4	B710/50	Biolegend	1:100
Lineage (CD3, CD19,)	PE Cy7	CD3: 145-2C11 CD19: 6D5	Y/G 780/60	Biolegend Biolegend	1:200
L/D	e780		R780/60	Life technologies	1:1,000
PKH	Fluoresces in the PE channel		Y/G 586/15	Sigma	

Figure 2. 6 Gating strategy to analyse phagocytosis in the blood

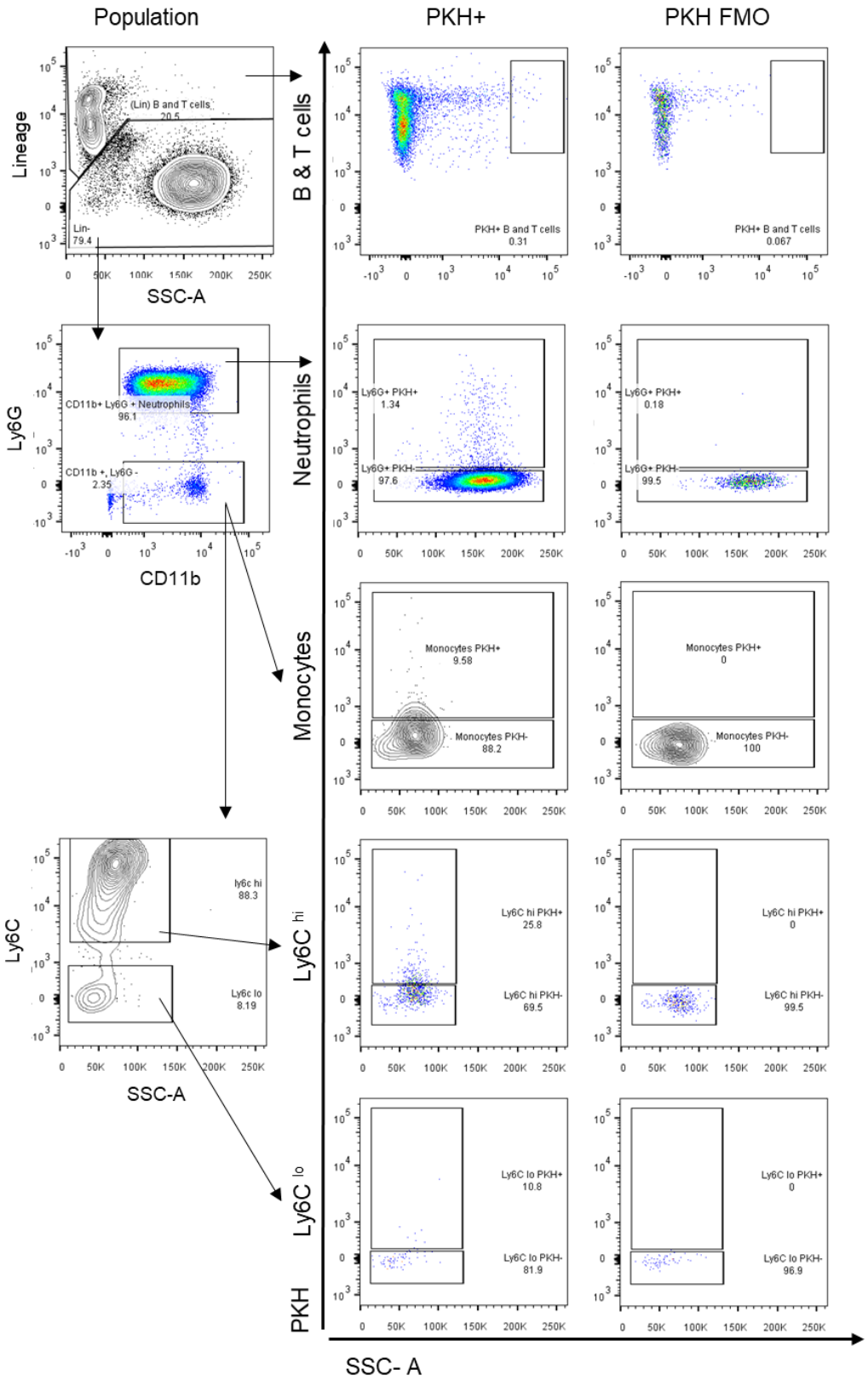

Figure 2. 6

10-12 week old WT and Sema7a KO mice were starved for 12 hours and injected with 350 mg/kg APAP. Mice were then administered PKH, a phagocytic dye. At either 12 or 24 hours post APAP injection, blood was collected from mice through a cardiac puncture. Single, live, CD45+, Lineage-, cells were selected as in Figure 2. 3.

Ly6G+ neutrophils and Ly6G- monocytes were selected from the CD45+ Lineage- population. The Ly6G- monocytes were separated into Ly6C^{hi} and Ly6C^{lo}. Neutrophils and monocytes were subsequently (left column) analysed for frequency of phagocytosis (%PKH+; central column). These gated were set using an FMO (right column).

Peritoneal lavage

The peritoneal lavage was stained with the panel in Table 2. 5 and was based on the staining panel described by Bain *et al*. [70]. The neutrophil and macrophage compartments of the peritoneum were selected using the gating strategy in Figure 2. 7. FMOs were used to set the gates for the different populations (Figure 2. 8). Phagocytosis of each population was analysed using a PKH FMO (Figure 2. 9).

Correction: Bain *et al*. [70] used a lineage negative marker to remove B and T cells. This was not included in this analysis. Consequently, the 'Ly6C monocyte' gate includes B cells, T cells, monocytes and macrophages, and is therefore labelled incorrectly.

To analyse the peritoneal macrophages, dendritic cells, B1 cells, T cells and neutrophils should have been excluded. This was not performed. Therefore, the MHC II + F4/80- gate will include dendritic cells and B1 cells [70,254]. The MHC II + F4/80- gate will include T cells, monocytes and neutrophils. F4/80 can still be used to select mature peritoneal macrophages.

These populations: Ly6C monocytes, Ly6C^{hi} monocytes, MHC II + F4/80- and MHC II + F4/80- have been excluded from the analysis but are still shown on the flow cytometry plots.

Table 2. 5 *In vivo* phagocytosis flow cytometry panel for peritoneal lavage

Marker	Fluorophore	Clone	Channel	Manufacturer	Staining Conc.
CD11b	Alexa Flour 488	M1/70	B530/30	eBioscience	1:100
Ly6G	PE Cy7	IA8	Y/G 780/60	Biolegend	1:200
Ly6C	PB	HK1.4	V450/50	Biolegend	1:100
F4/80	APC	BM8	R670/14	eBioscience	1:100
MHCII (I-Ab)	PerCP/Cy5.5	AF6-120.1	B710/50	Biolegend	1:200
L/D	e780		R780/60	Life technologies	1:1,000
PKH	Fluoresces in the PE channel		Y/G586/15	Sigma	

Figure 2. 7 Gating strategy for the peritoneal lavage in the *in vivo* phagocytosis assay

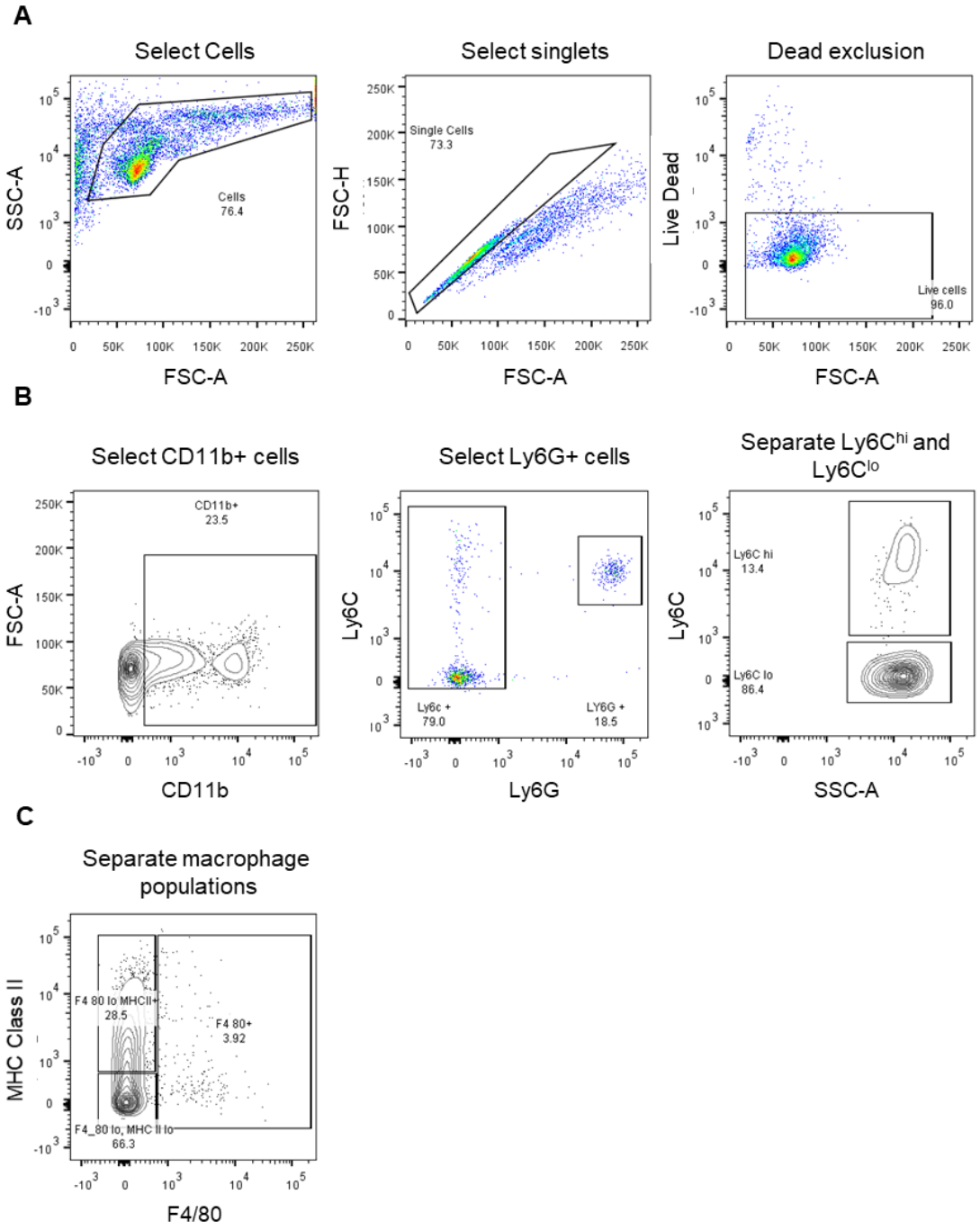

Figure 2. 7

1ml peritoneal lavage was collected from adult WT and Sema7a KO mice at 12 or 24 hours post APAP injury. Peritoneal exudate cells were analysed by flow cytometry as follows:

A) Cells were gated for size, singlets, live (L/D-).
B) After the gating in (A), the CD11b+ population was selected and divided into Ly6G+ neutrophils and Ly6G- cells. Ly6C^{hi} monocytes were selected from Ly6G- cells.
C) Peritoneal macrophages were separated from the live single cell population in (A), using F4/80.

Gates were set using FMOs, as demonstrated in Figure 2. 8.

Figure 2. 8 FMOs used to gate the *Table 2.* 5 In vivo phagocytosis flow cytometry panel for peritoneal lavage

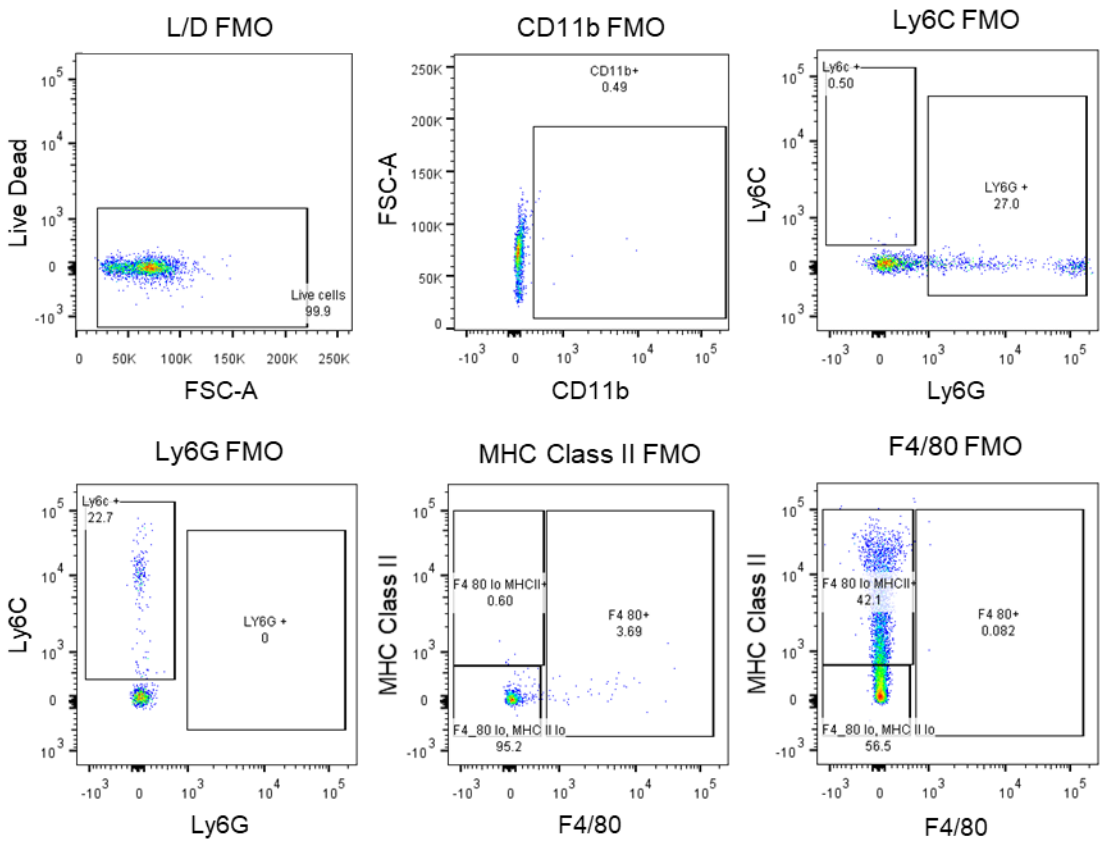

Figure 2. 8

Populations of neutrophils, monocytes and macrophages in the peritoneal exudate, were analysed in WT mice at 12 and 24 hours post 350m/kg APAP. Gates were set using FMOS as shown.

Figure 2. 9 Gating strategy to analyse phagocytosis in the peritoneal lavage

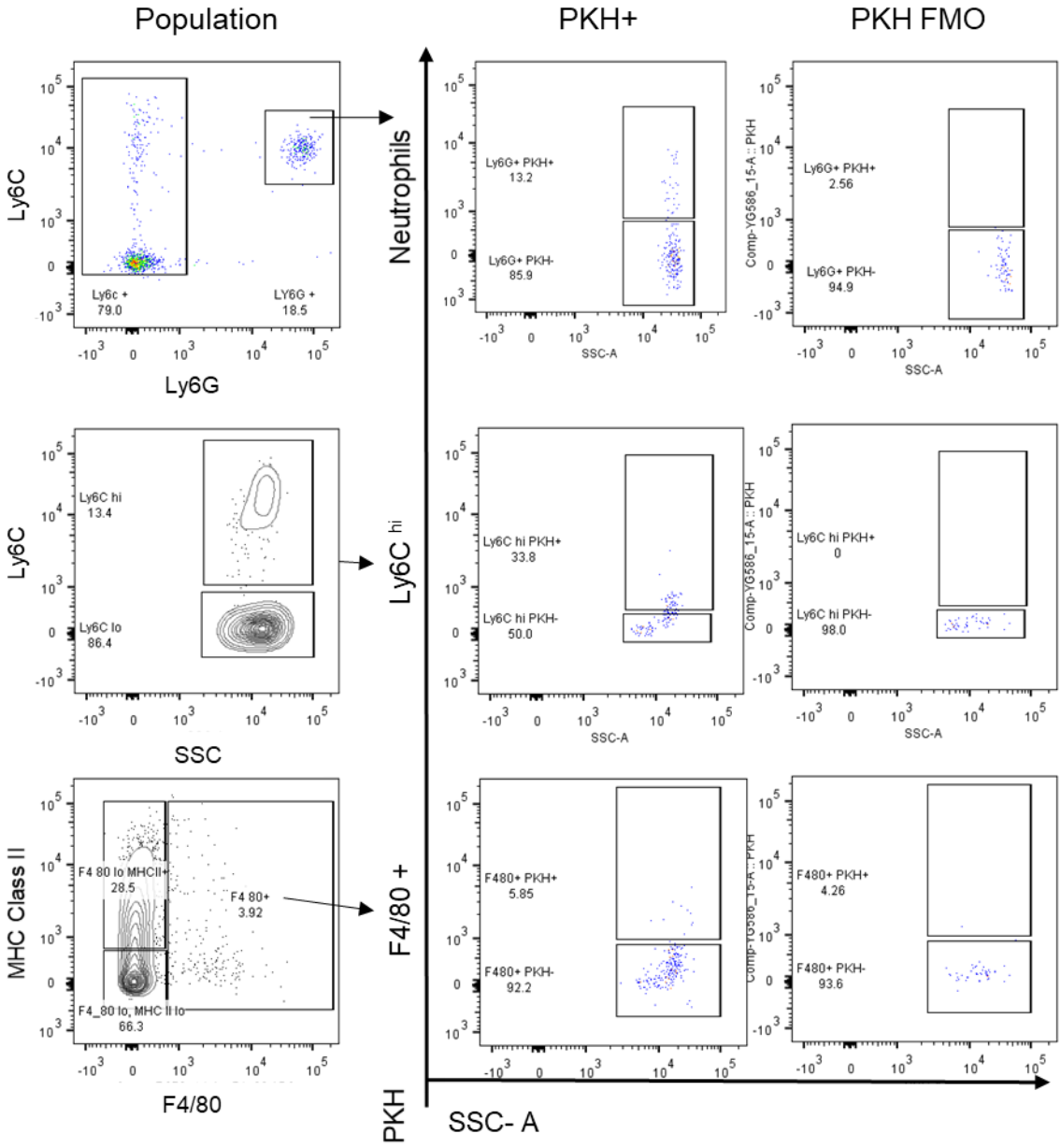

Figure 2. 9

Peritoneal exudate cells were collected from WT and Sema7a KO mice at 12 or 24 hours post APAP injury. Mice were injected with PKH, a phagocytic dye, at 4 or 8 hours APAP respectively, or Diluent B as a control. Neutrophils, Ly6C^{hi} monocytes and macrophages were identified (left column, gating strategy Figure 2. 7). Each population was analysed for frequency of phagocytosis (PKH+, centre column). Gates to measure the frequency of phagocytosis were set using the mouse which had been injected with Diluent B, and therefore acted as an FMO (right column).

Liver

The NPC fraction of the liver was stained with the 'Liver PKH Flow Cytometry Panel' (Table 2. 6) and gated as show in Figure 2. 10. Gates were set using FMOs, as shown in Figure 2. 12. Each NPC population was analysed for phagocytosis (PKH positivity), as shown in Figure 2. 13. To assess viability, NPC populations were selected as in Figure 2. 10, without the first Live/ Dead (L/D) gate. The NPC populations were assessed for viability by gating for L/D, on the individual populations. This viability gate was set using the respective NPC population, which had previously been gated for L/D as normal.

Table 2. 6 *In vivo* phagocytosis flow cytometry panel for NPCs

Marker	Fluorophore	Clone	Channel	Manufacturer	Staining Conc.
CD45	AF700	30-F11	R730/45	Biolegend	1:100
CD11b	BV650	M1/70	V670/30	eBioscience	1:100
Ly6G	PB	1A8	V450/50	BD Pharmingen	1:100
CD62L	FITC		B530/30		1:200
F4/80	APC	BM8	R670/30	Biolegend	1:100
Ly6C	PerCP/Cy5.5	HK1.4	B695/40	Biolegend	1:100
DUMP (CD3, CD19, NK1.1)	PE/Cy7	CD3=145-2C11, CD19=6D5	Y/G 780/60	Biolegend	1:200
L/D	e780		R780/60	Life technologies	1:1,000
PKH	Fluoresces in the PE channel		Y/G 582/15	Sigma	

Figure 2. 10 Gating strategy for NPCs of the liver at 24 hours post APAP injection

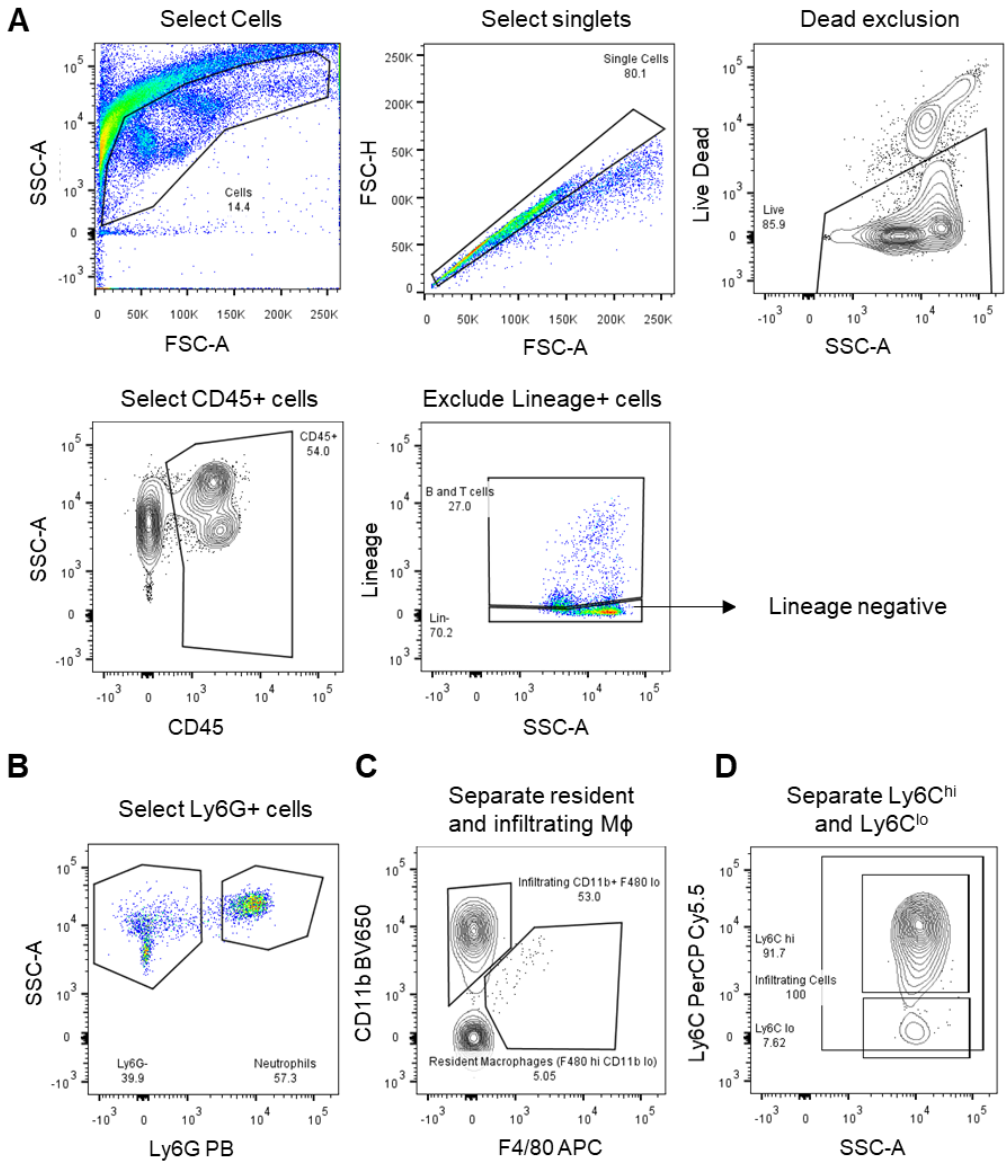

Figure 2. 10

WT and Sema7a KO adult mice were treated with 12 or 24 hours 350mg/kg APAP. The NPC fraction was isolated from the liver. Neutrophils, monocytes and macrophages were identified as follows:

A) The NPC fraction was gated for cells, singlets, live (L/D-), CD45+, and Lineage–
B) The lineage negative population was gated for Ly6G+ (neutrophils), and Ly6G- cells
C) The Ly6G- cells were separated in to liver resident macrophages (Mϕ) (CD11b^{lo}, F4/80^{hi}), and infiltrating Mϕ (CD11b+, F4/80^{lo}).
D) The infiltrating Mϕ were further subdivided to Ly6C^{hi} and Ly6C^{lo}

Figure 2. 11 Gating strategy for NPCs of the liver at 12 hours post APAP injection

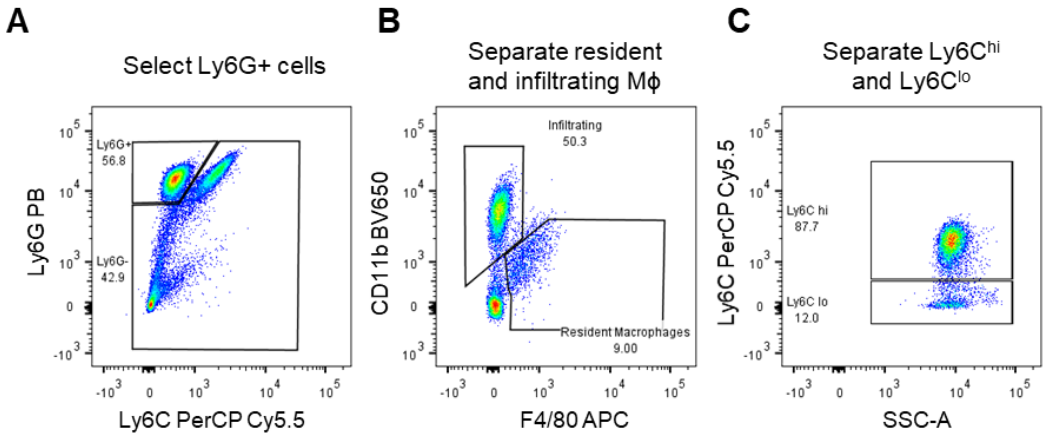

Figure 2. 11

In the 12 hours post APAP injection *in vivo* phagocytosis experiment, Ly6G PB and Ly6C PB antibodies were accidentally used in the same antibody cocktail, which was used for all samples. Fortunately, the Ly6C PerCP Cy5.5 antibody was also included, so the Ly6G+ and Ly6G- populations could still be separated. Gates were set using an FMO.

Single, live (L/D-), CD45+, and Lineage – ells were selected as in Figure 2. 10.

A) The lineage negative population was gated for Ly6G+ (neutrophils), and Ly6G- cells
B) The Ly6G- cells were separated in to liver resident Mϕ ($CD11b^{lo}$, $F4/80^{hi}$), and infiltrating Mϕ (CD11b+, $F4/80^{lo}$).
C) The infiltrating Mϕ were further subdivided to $Ly6C^{hi}$ and $Ly6C^{lo}$

Figure 2. 12 FMOs for the *In vivo* phagocytosis flow cytometry panel for NPCs

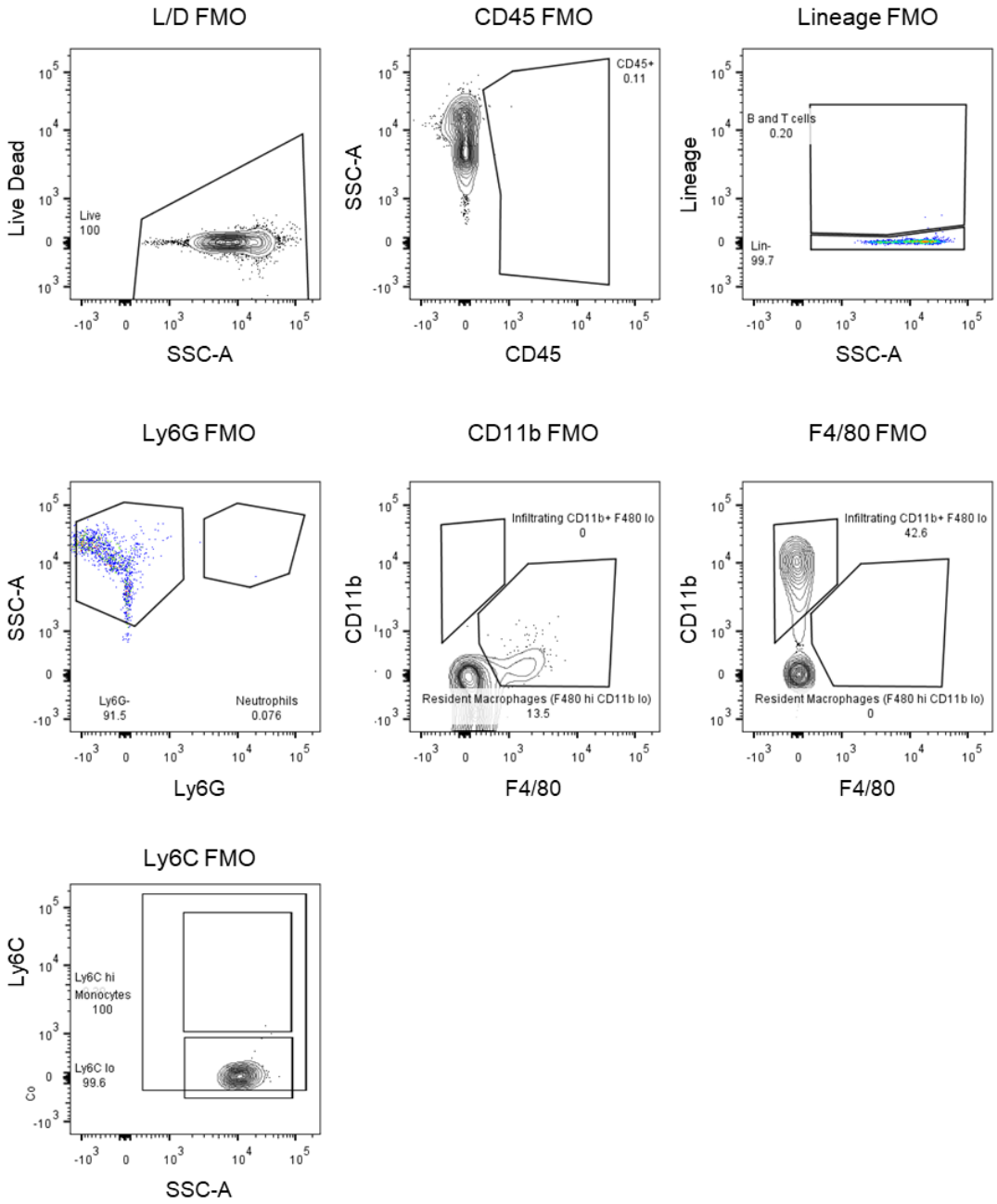

Figure 2. 12

To select neutrophils, monocytes and macrophages in the mouse NPC fraction of the liver in Figure 2. 10 and Figure 2. 11, FMOs were used, as indicated by their individual titles.

Figure 2. 13 Gating strategy to identify phagocytic NPCs in the liver.

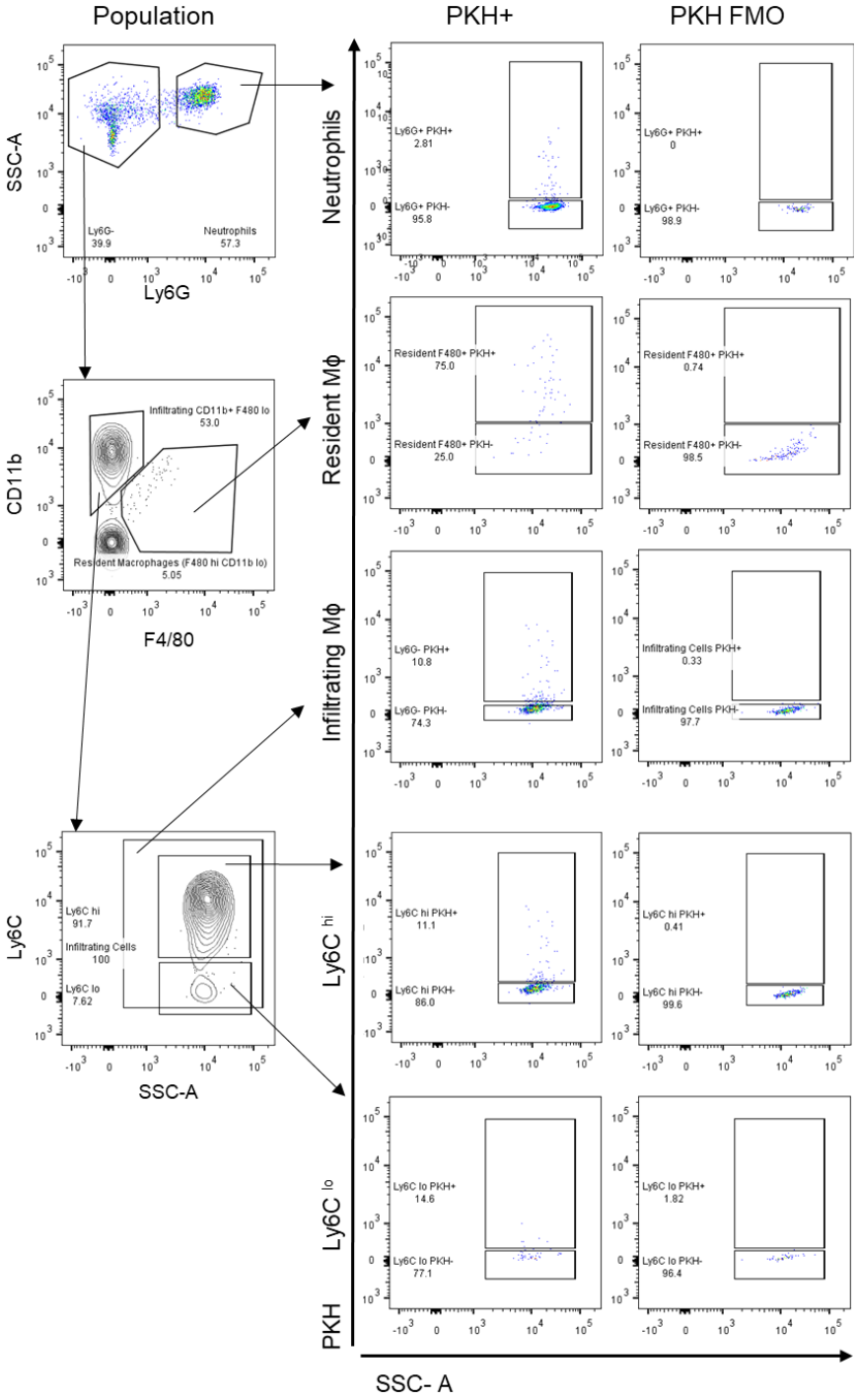

Figure 2. 13

WT and Sema7a KO adult mice were treated with 12 or 24 hours 350mg/kg APAP. At 4 or 8 hours APAP respectively, mice were injected with PKH, a phagocytic dye. The NPC fraction was isolated from the liver. Neutrophils, monocytes and macrophages were identified as in Figure 2. 10. Each NPC population (left) was analysed for phagocytosis (PKH+, centre). Gets were set using an FMO (right).

Immunohistochemistry

4 µm-thick FFPE sections were dewaxed and rehydrated before 15 min heat mediated antigen retrieval in Sodium Citrate pH 6 or Tris-EDTA pH 8, depending on the antibody used (see Table 2. 7). Sections were permeabilised in PBS 0.1% Tween 20 (PBST) for 5 min, washed in PBS, and treated with Protein Block (Spring Bio) for 30 min at RT, and stained with the primary antibody overnight at 4 °C. Frozen sections were fixed for 20 min in ice cold Methanol: Acetone (1:1) before a 30 min Protein Block at RT, followed by overnight incubation with the primary antibody at 4 °C. Secondary antibodies were applied for 1 h RT. Sections were stained with DAPI (1:1,000) and mounted with fluromount (Southern Biotech). All primary antibodies used in the current study are provided together with method of antigen retrieval and working dilution in Table 2. 7. Fluorescent secondary antibodies are detailed in Table 2. 8. Isotype controls were used for all stains, see Figure 2. 14.

For 3,3'-diaminobenzidine (DAB) stains, slides were sequentially blocked with Bloxall (Vector) for 15 min, then Avidin and Biotin (Invitrogen) for 10 min each, followed by 30 min Protein Block at RT. Sections were stained overnight at 4 °C with the primary antibody, followed by the secondary antibody for 1 h at RT (see Table 2. 8). Slides were blocked with R.T.U. VECTASTAIN Elite ABC reagent (Vector) for 30 min, before detection with DAB (DAKO). Slides were counterstained with haematoxylin before dehydration and mounting. Isotype controls were used for all DAB stains (Figure 2. 15).

Haematoxylin and Eosin (H&E) staining and block processing was performed by SuRF Histology at the QMRI, University of Edinburgh.

Table 2. 7 Primary antibodies used for immunohistochemistry and immunofluorescence

Antibody	Dilution from stock	Fixation	Heat Mediated Antigen retrieval	Manufacturer	Cat. Number	Host
BrdU	1:200	Formalin	15min TE	Abcam	ab6640	Rt
Active Caspase 3	1:200	Formalin	15min Sodium Citrate	BD Pharmingen	BD559565	Rb
CD45	1:50	Methanol: Acetone	N/A	TONBO bioscience	700451-V100	Rt
CD45	1:200	Formalin	15min TE	R&D	MAB114	Rt
Cyp2e1	1:500	Formalin	15min Sodium Citrate	Atlas antibodies	HPA009128	Rb
F4/80	1:200	Methanol: Acetone	N/A	Abcam	ab6640	Rt
HMGB1	1:500	Formalin	15min Sodium Citrate	Abcam	ab18256	Rb
Hnf4a	1:200	Formalin	15min TE	Perseus Proteomics Inc.	PP-H1415-00	Ms
ICAM-1	1:200	Methanol: Acetone	N/A	Abcam	ab119871	Rt
Integrin β1	1:200	Methanol: Acetone	N/A	Millipore	MAB1997	Rt
K19	1:200	Formalin	15min TE	DSHB	Troma III	Rt
Ly6G	1:500	Formalin	15min TE	Biolegend	127601	Rt
p21	1:200	Formalin	15min TE	Abcam	ab188224	Rb
Plexin C1	1:150	Formalin	15min TE	R&D Systems	AF5375	Shp
Sema7a	1:100	Formalin	15min TE	Abcam	ab23578	Rb
Vimentin	1:500	Formalin	15min TE	Abcam	ab92547	Rb

TE, Tris ETDA pH 8; Ms, Mouse; Rb, Rabbit; Rt, Rat; Shp, Sheep.

Table 2. 8 Secondary antibodies used for immunohistochemistry and immunofluorescence

Target species	Conjugate	Fluorophore	Dilution from stock	Manufacturer	Cat. Number	Host
Mouse	Fluorescent	Alexa 488	1:200	Invitrogen	A21202	Donkey
Rabbit	Biotinylated	-	1:200	Vector	BA-1000	Goat
Rabbit	Fluorescent	Alexa 555	1:200	Invitrogen	A31572	Donkey
Rat	Biotinylated	-	1:200	Vector	BA-9400	Goat
Rat	Fluorescent	Alexa 488	1:200	Invitrogen	A21208	Donkey
Sheep	Biotinylated	-	1:200	Vector	BA-6000	Rabbit
Sheep	Fluorescent	Alexa 555	1:200	Invitrogen	A21436	Donkey
Sheep	Fluorescent	Alexa 488	1:200	Invitrogen	A11015	Donkey

Figure 2. 14 Controls for immunofluorescent stains

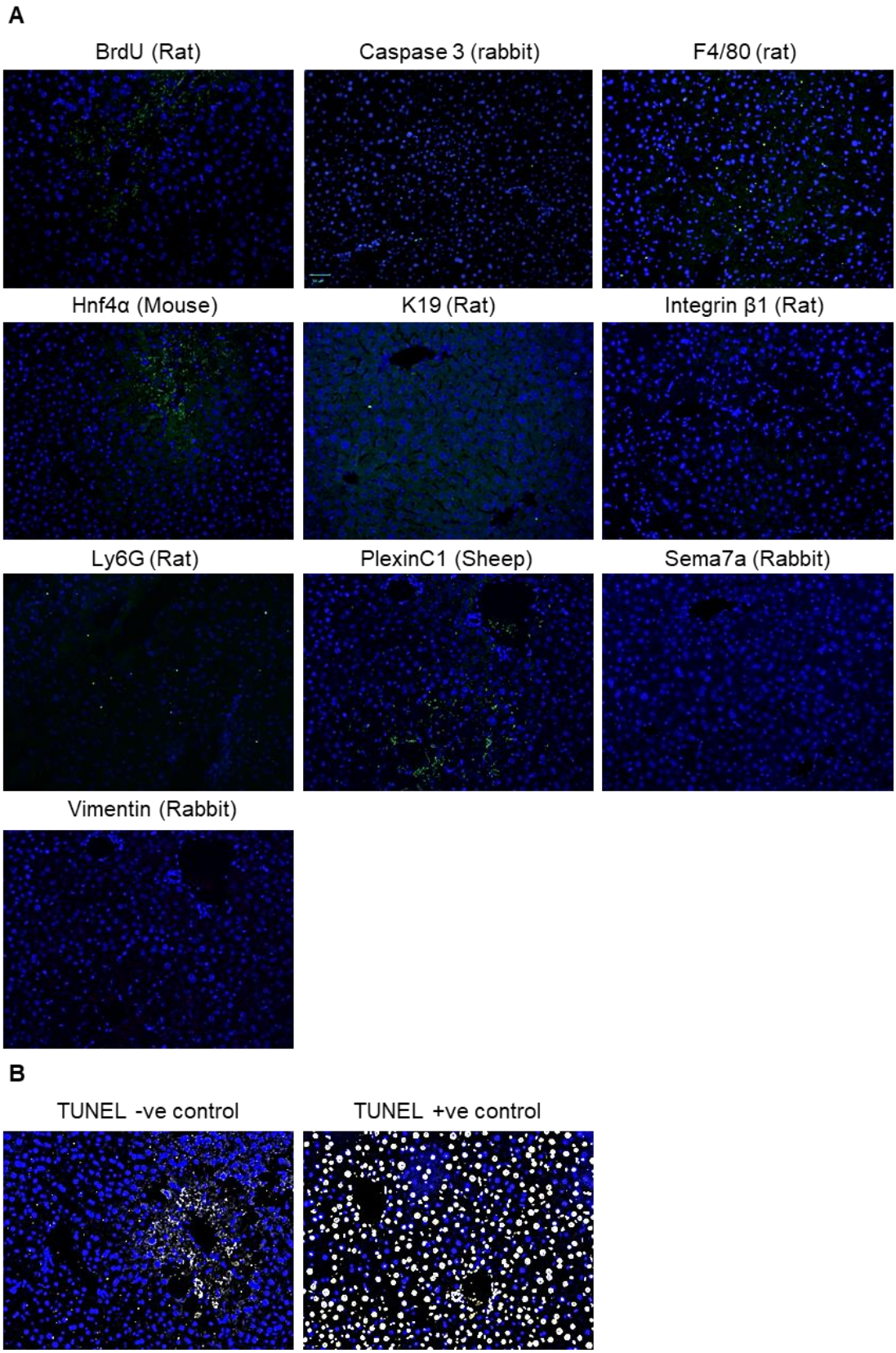

Figure 2. 14

A) Immunofluorescent isotype control images. Image labels indicate which immunostain the isotype control corresponds too. DNA is stained with DAPI, in these images the fluorescent signal has been coloured green. 20x magnification

B) Negative (left) and positive (right) controls for the TUNEL assay. The negative control used a 24h APAP injured tissue section, but without the enzyme required to label double stranded DNA breaks. Positive control used a healthy mouse, which was treated with DNAse I, as per manufacturer's instructions.

Figure 2. 15 Isotype controls for DAB stains

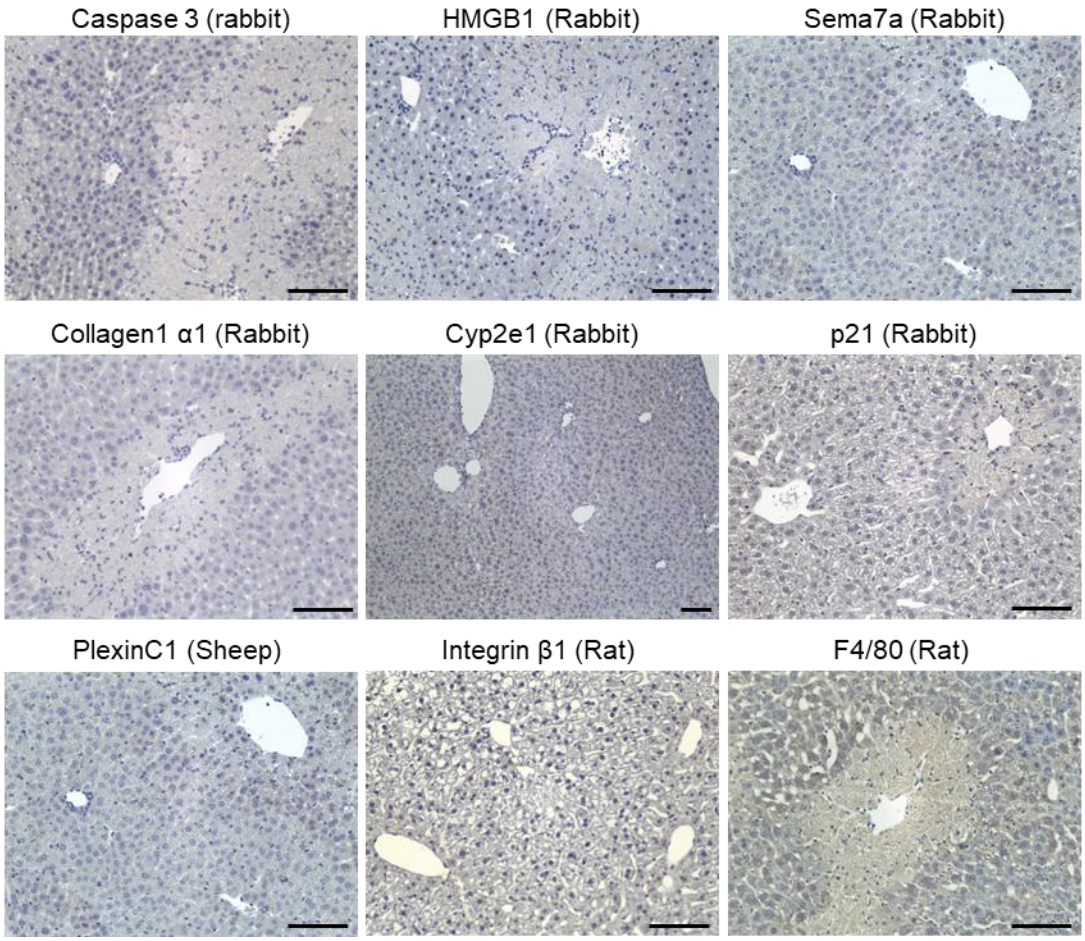

Figure 2. 15

Brightfield images of isotype controls for DAB stains. Image labels indicate which immunostain the isotype control corresponds too. DNA is stained with haematoxylin. Scale bars 100 μm

Microscopy and Image Analysis

Fluorescent and brightfield images were acquired using a Nikon Eclipse e600 microscope fitted with a Retiga 2000R camera (Q-Imaging, Image Pro premier software). Images were contrasted and analysed using Fiji ImageJ on 6 random non-overlapping fields per mouse. (ImageJ version 1.52e software for Windows (ImageJ Software, National Institutes of Health, USA, available at: http://rsb.info.nih.gov/ij/).

Confocal microscopy was performed with an inverted Leica TCS SP8 Confocal microscope with 3 detectors. High magnification images used the Nyquist criterion to give the maximum resolution using 60x objective lens. Images were converted from Z- stacks to Maximum Intensity Projections, and contrast adjusted using Fiji ImageJ

In immunofluorescence studies, necrotic areas were identified by background auto-fluorescence, and a lack of intact hepatocyte nuclei. On DAB stains, necrotic areas were identified through a lack of intact hepatocyte nuclei, hepatocyte ballooning, disrupted tissue architecture and background DAB staining.

Numbers of different single cell populations were counted manually; Jennifer Cartwright counted the number of Ly6G+ in necrotic areas. Pixel density, and the number of F4/80+ cells per 20x field of view during the APAP time course, was quantified using a macroinstruction.

The number of F4/80+ cells per area was calculated by categorising the input image into three zones: healthy, central and out necrotic (Figure 2. 16). The number of F4/80+ macrophages was counted in each zone and divided by the area.

Figure 2. 16 Quantification of the number of F4/80+ cells per area

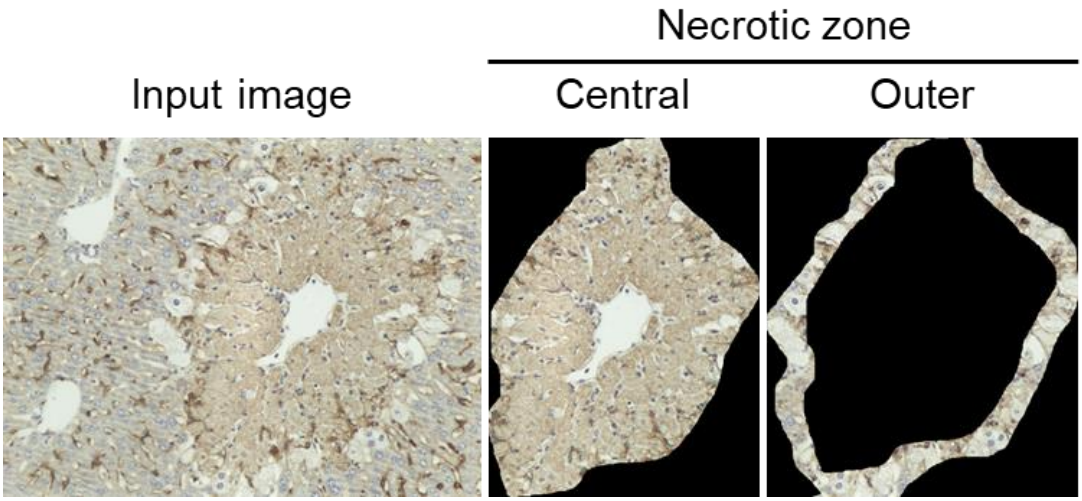

Figure 2. 16

Tissue sections from WT and Sema7a KO mice were stained for F4/80 and imaged using a 20x lens.
The central necrotic zone was selected using Fiji ImageJ and removed from the input image. The out necrotic zone was then selected. F4/80+ macrophages were counted in the healthy parenchyma, central and outer necrotic zone and dived by the area (pixels ^{2}), to five number of F4/80+ macrophages per area.

Necrotic areas on H&E stains were quantified using the inForm 2.4 (Perkin Elmer) software. H&E stained sections were scanned using the Polaris multispectral slide scanner. The Polaris uses a brightfield scan to identify the tissue, then eight 10x fields, at 1 μm resolution, were selected per mouse. Selected fields underwent multispectral imaging (MSI) by the Polaris. The resulting images were segmented and analysed with the inForm trainable tissue segmentation software, to identify necrotic areas (see Figure 2. 17). Polaris and inForm software were also used to count numbers of Ly6G+ cells in liver tissue. For this analysis, 8 20x fields are selected for MSI by the Polaris. The inForm software segmented the tissue into single cells. Haematoxylin was used to identify nuclei, then DAB positive cells (Ly6G+) were identified by setting a threshold, which remained constant in each experiment.

Fluorescent stains were imaged and quantified using the Perkin Elmer Operetta high content imaging system. Images were acquired using a 20x objective lens. Images were analysed using Columbus software. All parameters and variables remained constant in each experiment. Background fluorescence in 488 and 546 channels was reduced using the sliding parabola module, with a defined curvature. DAPI positive nuclei were detected using method ‘C’. The DAPI intensity, morphology and size of these nuclei were used to exclude any artefacts (see Figure 2. 18). Selected nuclei were then assigned as positive or negative based on the pixel intensity in the normalised 488 or 546 channels. Depending on the experiment, positivity was detected in either the nucleus (e.g. BrdU, TUNEL, Hnf4a) or in the cytoplasm using a 15-pixel ring surrounding the nuclei (e.g. F4/80, CD45, Sema7a). For each experiment, identical thresholds were set to assign nuclei to their respective population. For an example analysis pipeline see Figure 2. 18.

Figure 2. 17 Necrosis analysis using the inForm software

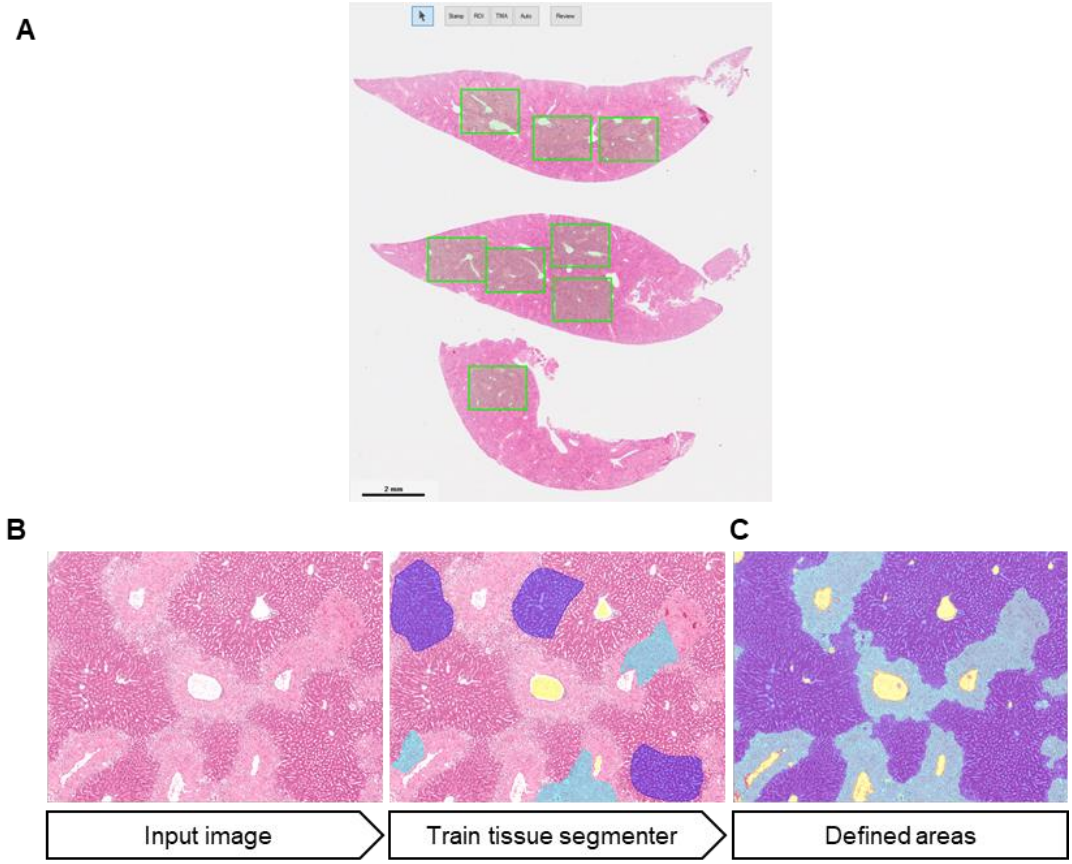

Figure 2. 17

Example pipeline to analyse necrosis using the Polaris and the inForm software
A) 8 10x fields of HnE stained tissue are selected to be multispectral imaged by the Polaris. Scale bar 2 mm.
B) The inForm software was trained to identify: necrosis (cyan), healthy parenchyma (purple), vessels (yellow) and red blood cells (RBCs, red).
C) After training, the inForm software can reliably segment tissue into the defined areas, which can then be used to calculate %necrosis.

Figure 2. 18 Single cell analysis pipeline using Colombus software

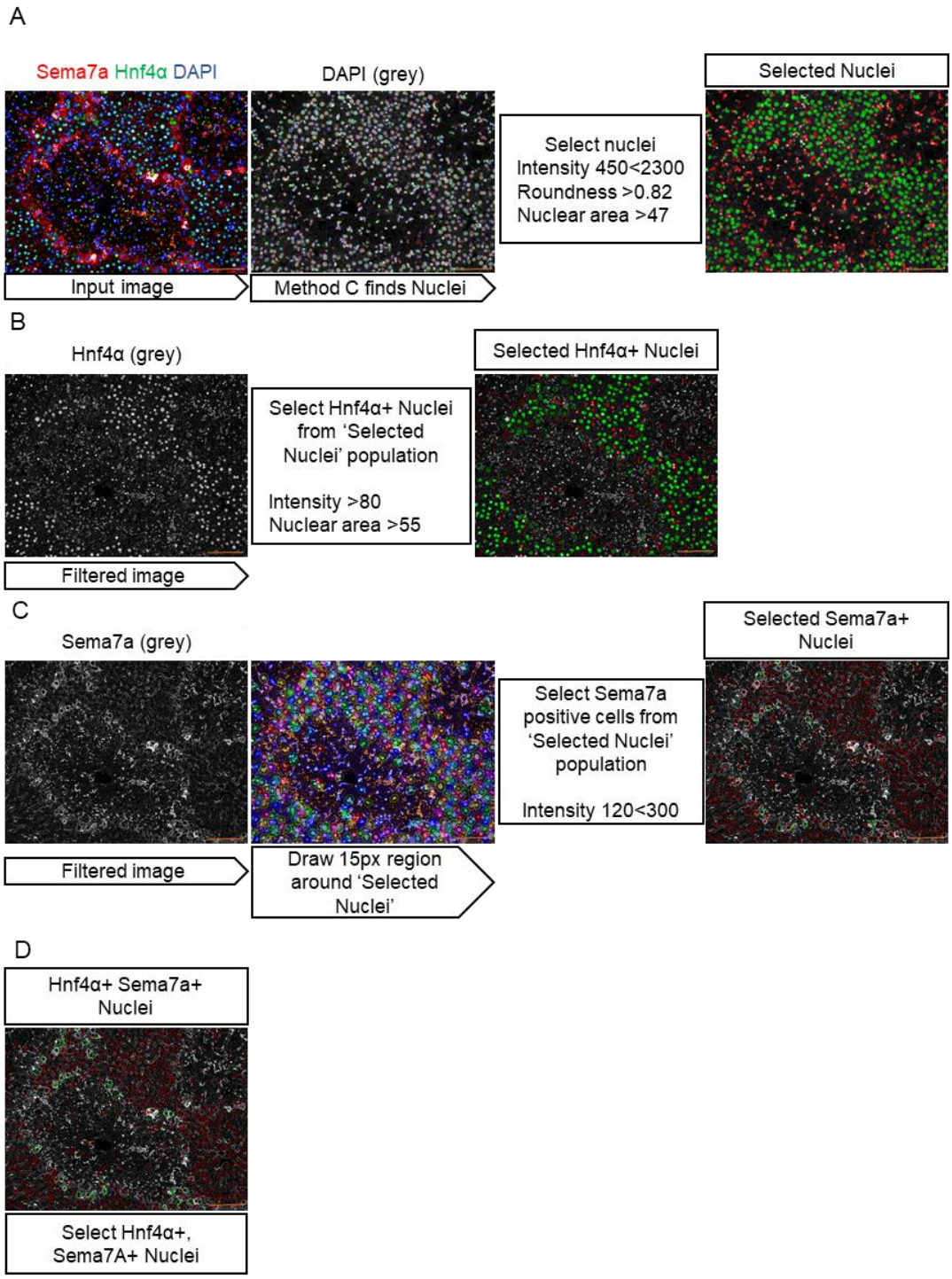

Figure 2. 18
Example pipeline to identify Hnf4α+, Sema7a+ hepatocytes in liver sections from WT mice at 24 hours post APAP injury.

A) DAPI+ nuclei are identified with 'Method C', a built in algorithm in the Columbus software. Artefacts are excluded based on morphology and intensity of the nuclei, to give the 'selected nuclei' population.
B) The image is filtered using the sliding parabola algorithm, which removes background fluorescence. Hnf4α expression is then examined in the selected nuclei' population
C) A 15 pixel ring is drawn around the selected nuclei and tested for Sema7a expression.
D) Dual positive Sema7a+ Hnf4α cells are identified.

Scale bars 100 um

TUNEL assay

4 µm FFPE tissue was dewaxed, rehydrated and permeabilised for 5 min in Sodium citrate. DNA fragments and breaks were labelled using the Terminal deoxynucleotidyl transferase–mediated biotinylated deoxy-uridine triphosphate nickend labelling (TUNEL) assay, according to manufacturer instructions (*In Situ* Cell Death Detection Kit, TMR Red, Roche). TUNEL+ nuclei were quantified using the Perkin Elmer Operetta high content imaging system.

Protein quantification

Protein extraction

60 mg liver tissue was homogenised with a Tissue Tearor (Biospec Products) in cold Meso Scale Diagnostics (MSD) lysis buffer (150mM NaCl, 20mM Tris pH7.5, 1 mM EGTA, 1mM EDTA, 1% Triton X-100, 1X Halt Protease inhibitor Cocktail (Thermo Scientific)). Homogenates were slowly mixed for 30 min, then centrifuged for 10 min 20,000 x g at 4 °C. The aqueous supernatant was removed, and the protein concentration was determined using a Pierce BCA Protein Assay Kit (Thermo Scientific).

Quantification of cytokines in mouse serum and liver

10 pro-inflammatory cytokines were multiplexed (IFN-γ, IL-10, IL-12p70, IL-1β, IL-2, IL-4, IL-5, IL-6, CXCL1, TNF-α) in mouse serum and liver using the V-PLEX Pro-inflammatory Panel 1' mouse plate (MSD), following the manufacturer instructions.

100 µg of liver homogenate, or 25 µL serum, were assayed in single wells in a 96 well V-PLEX plate. The provided standards were run in duplicate. Each well was made to 50 µL in diluent 41 and placed in a shaking incubator (600rpm) for 2 hours at RT. Wells were washed in PBST then incubated with 'Detection Antibody Solution' for 2 hours in a shaking incubator. After washing in PBST, 2x 'Read Buffer' was added. The plate was read on the QuickPlex SQ 120 analyser (MSD). Concentrations of each cytokine was quantified using the standard curve for the respective cytokine.

Sema7a enzyme-linked immunosorbent assay (ELISA)

Mouse liver protein homogenate was diluted to 0.5 mg/ml and mouse serum was diluted 1:5 in sample diluent. Samples were assayed in duplicate using the Mouse LS Bio sandwich ELISA kit according to manufacturer instructions (Manufacturer; LS-F6958)

Healthy human serum was collected by Fiona Chapman and Dan Pugh. Participants provided written consent according to the NRS BioResource generic consent form. Human serum from was taken from APAP overdose patients on day 1 of admission. Ethical approval from the Scotland 'A' Research and Ethics Committee had been previously gained for a previous study [255]. Serum was diluted 1:1 in sample diluent from the LS Bio sandwich ELISA kit (LS-F21047), and run in duplicate, following the kit instructions.

Quantitative reverse transcriptase PCR (qRT-PCR)

40 mg of liver tissue was homogenised in 500 µL Qiazol (Qiagen). Homogenates were mixed with 100 µL chloroform, incubated at RT for 3 min, and then centrifuged at 4 °C 1,200 x g, for 15 min. The aqueous supernatant was removed and mixed in an equal volume of 70% ethanol. BMDMs were lysed in Buffer RLT. RNA was extracted using an RNAeasy Kit according to manufacturer instructions (Qiagen). Reverse Transcription and Real Time-qPCR was performed using Qiagen Quantitect and

Quantifast reagents on a LightCycler 480 II (Roche). Commercial primers from Qiagen's Quantitect range were used. Gene expression was normalised to the housekeeping gene *peptidylprolyl isomerase A (PPIA)*. Samples were run in triplicate. Primers: *AKT1*, QT00114401; *CCL2*, QT00167832; *CXCL1*, QT00115647; *IL-1β*, QT01048355; *IL-6*, QT00098875; *ITGα1*, QT01559138; *ITGB1*, QT00155855; *MAPK1*, QT00133840; *Plxnc1*, QT00145418; *PPIA*, QT00247709; *PTK2*, QT01059891; *Sema7a*, QT00173488; *TGFB1*, QT00145250; *TGFBR1*, QT00135828; *TGFRB2*, QT00135646;

Statistics

GraphPad Prism 8 Software was used for all statistical analysis. Data are presented as mean ± s.e.m. n refers to biological replicates. A Shapiro-Wilk test was used to determine whether data fitted a normal distribution. Anomalies were only removed if they were identified using a Grubbs test (alpha=0.05). Each dot represents a mouse.

A two-tailed unpaired t-test, with a Welch correction applied if required, or Mann Whitney test was used to compare two sample parametric or non-parametric data respectively. A one-way ANOVA with Tukey's multiple comparison test or a Kruskal-Wallis test with Dunn's Multiple Comparison Test was used for multi-sample parametric or non-parametric data respectively.

Two-way ANOVA with Sidak's multiple comparison test was used to analyse parametric data with two independent variables.

Chapter 3 - Sema7a is expressed by peri-necrotic hepatocytes during APAP injury

Introduction

APAP overdose causes 46% of acute liver failure in the UK and the USA, with 200 deaths annually in the UK [1,2]. The only therapy for APAP overdose, NAC, is effective in the first 12 hours following APAP ingestion. After this timepoint, 22% of patients require a liver transplant, which are often not found in time [3]. Research is needed to find a suitable therapy to prevent liver failure and promote recovery after the initial 12 hour time window. One potential therapeutic avenue could be to manipulate the innate immune system to promote recovery and avoid multi-organ failure.

The innate immune system is present in both the injury and recovery phases of APAP injury. Dying hepatocytes release danger-associated-molecular patterns (DAMPs), which are detected by and activate Kupffer cells, the liver resident macrophage [4]. Activated Kupffer cells secrete a plethora of cytokines including: TNFα, IL-6, CXCL1, IL-1β and IL-18 to trigger and recruit the innate immune system [4,44]. During the initial stages of APAP injury, inflammation enhances injury. For example, secreted TNFα primes hepatocytes to apoptose, enhancing hepatocyte loss [4,35].

During recovery, the innate immune system is beneficial as macrophages and neutrophils remove cellular debris through phagocytosis [35]. Phagocytosis causes macrophages to switch from a pro-inflammatory to an anti-inflammatory phenotype [72,256]. The restorative macrophages secrete anti-inflammatory cytokines such as IL-10 to reduce inflammation [256], and TNFα and IL-6 to stimulate the remaining hepatocytes to proliferate [17]. Novel therapies may influence the immune system towards a restorative phenotype.

Semaphorin 7a (Sema7a) has diverse roles in the immune system. It promotes monocytes to release pro-inflammatory cytokines [231], and can act as a chemoattractant for dendritic cells monocytes and macrophages [228–230], or induce the transmigration of neutrophils into hypoxic tissue [211]. Sema7a can also modulate macrophage secretion of pro- or anti- inflammatory cytokines, depending on which receptor receives it. For example, when Sema7a on activated T cells is received by Integrin α1β1 on macrophages, pro-inflammatory cytokine production is induced [231]. Conversely, when macrophages receive Sema7a from intestinal epithelial cells through αvβ1 integrin, anti-inflammatory cytokines are secreted [236].

In chronic liver and lung injury, Sema7a forms a positive feedback loop with the TGFβ to promote fibrosis [246,247]. In the liver, Sema7a KO mice injured with chronic CCl_4 administration, or bile duct ligation, display less infiltrating CD45+ leukocytes and F4/80+ macrophages, lower transcription of *IL-6* and *MCP-1* [246], a key chemoattractant for monocytes [63]. In APAP injury, infiltrating macrophages secrete TGFβ to induce hepatocyte senescence, marked by p21 expression. This senescence prevents hepatocyte proliferation and recovery, and patients are more likely to undergo liver failure [144]. In acute APAP injury, Sema7a may have a role in inflammation, which is key during both injury and recovery from APAP injury.

This chapter aims to characterise the expression of Sema7a and its receptors Plexin C1 and Integrin β1, in healthy mice and during APAP injury. I will also examine if Sema7a is simply a marker for cells about to undergo cell death, senescence, or if Sema7a has a direct role in promoting recovery from APAP injury. Finally, I will examine the relationship of Sema7a expressing cells and macrophages during APAP injury.

Results

Sema7a is expressed on peri-necrotic cells at peak APAP injury

To investigate if Sema7a expression is regulated in APAP injury or recovery, Sema7a protein expression was assessed during a time course of APAP overdose (Figure 3. 1A). In this model, centrilobular necrosis and inflammation begins to develop by 4 hours post-APAP administration. Necrosis spreads into the parenchyma as the injury develops, until 24 hours post APAP. From 36 hours post APAP overdose, necrosis resolves, and the mice recover from APAP injury (Figure 3. 1B & C).

Sema7a expression is absent in healthy mice and the early stages of APAP injury (4-8 hours). As necrosis and inflammation continues from 12 to 24 hours post APAP injury, Sema7a expression is induced in cells surrounding the necrotic areas, peaking at 24 hours. During the recovery phase (36 - 60 hours post APAP) Sema7a expression diminishes as necrosis resolves (Figure 3. 1B & D). Since peak injury and Sema7a expression coincide at 24 hours APAP, further studies were focussed on this time point.

Figure 3. 1

A) Schematic overview of the APAP injury time course experiment (performed by Philip Starkey Lewis).
B) Sema7a expression during a time course of 350 mg/kg APAP. Scale bars 100 µm. Black dashes outline necrotic areas. Yellow dashes outline Sema7a positive peri-necrotic cells.
C) Polaris analysis of necrotic area during APAP injury (performed by Philip Starkey Lewis).
D) Percentage area of Sema7a positivity.

Scale bars 100 µm. CV, central vein; PT, Portal tract. The APAP injury mouse experiment was performed once.

Each dot represents an individual mouse. Data was checked for normality and equal variance. This applies to every figure henceforth.

Figure 3. 1 Peri-necrotic cells express Sema7a during APAP injury

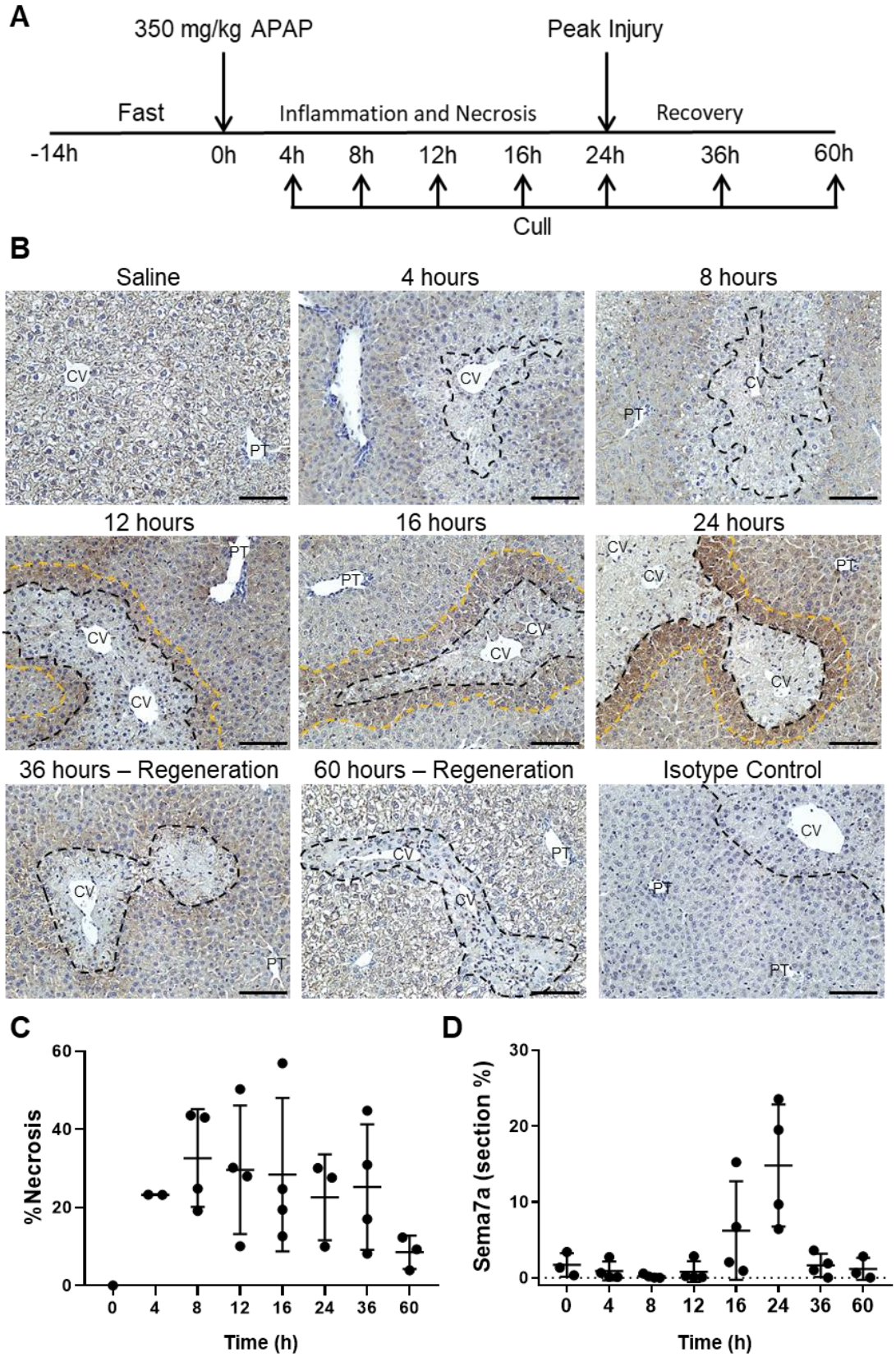

Sema7a cells are viable, and surround the necrosis

At 24 hours post APAP there is ongoing necrosis, the predominant mode of hepatocyte death during APAP injury [17,27,257]. Since Sema7a is expressed by cells adjacent to the necrotic area during APAP injury, I undertook studies to determine whether Sema7a identifies cells about to undergo necrosis, or if Sema7a+ cells form a boundary around the necrosis.

A Terminal deoxynucleotidyl transferase dUTP nick end labelling (TUNEL) assay was performed to label dying cells (Figure 3. 2A). Healthy mice were TUNEL-negative. At 24 hours APAP, the characteristic necrotic (TUNEL+) pattern is seen. Comparing Sema7a stained serial section indicates the Sema7a+ hepatocytes lie outside the TUNEL+ area, with three cells on average being dual positive for Sema7a and TUNEL (Figure 3. 2B).

To ensure Sema7a cells were not undergoing apoptosis, serial sections were stained for active Caspase 3, an apoptosis marker, and Sema7a (Figure 3. 2C). In healthy mice, Caspase 3+ cells were absent. At 24 hours APAP, an average of 29 Caspase 3+ cells are observed at the edge of necrotic areas. Comparing the Caspase 3 and Sema7a stains shows that the Sema7a+ hepatocytes lie adjacent to Caspase 3+ cells (Figure 3. 2C), with an average of two Caspase 3+ cells being dual positive for Sema7a per field (Figure 3. 2D).

Therefore, Sema7a is expressed by viable cells, and is not a marker for cell death. Due to the position of Sema7a+ cells, they may act as a boundary to necrosis, which will be investigated in Chapter 4.

Figure 3. 2 Sema7a+ cells are viable

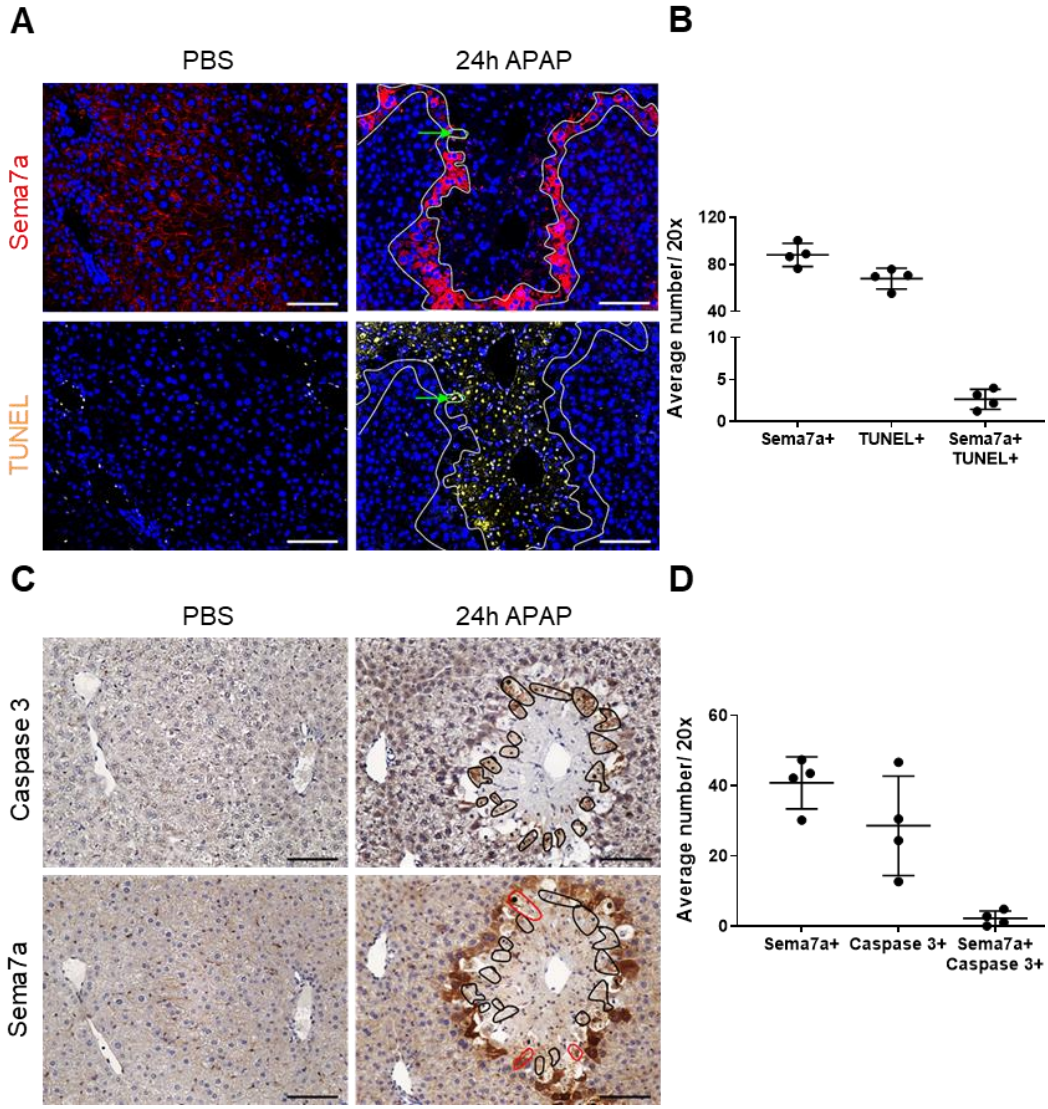

Figure 3. 2

A) Serial staining of Sema7a (top) and TUNEL (bottom) in mice treated with saline (left) or 24 hours 350 mg/kg APAP (right). The identified Sema7a+ region is encircled in white; this region was overlaid on the TUNEL serial image. Green arrows indicate cells dual positive for TUNEL and Sema7a (Sema7a+ TUNEL+).

B) Average number of Sema7a+, TUNEL+ or dual + cells, in mice treated with 24 hours 350 mg/kg APAP.

C) Serial staining of active Caspase 3 (top) and Sema7a (bottom) in mice treated with saline (left) or 24 hours 350 mg/kg APAP (right). Identified active Caspase 3+ nuclei are labelled in black; these labels were overlaid on the Sema7a serial image. Cells dual positive for active Caspase 3 and Sema7a (Sema7a+ Caspase 3+) are highlighted in red.

D) Average number of Sema7a+, Caspase 3+ or dual + cells, in mice treated with 24 hours 350 mg/kg APAP.

Scale bars 100 µm. The APAP injury mouse experiment was performed once.

Sema7a is expressed by hepatocytes

To define which cells express Sema7a, dual immunohistochemistry (IHC) was performed with markers for the main liver cell types including: Hnf4α for mature hepatocytes [258], CK19 for ductular cells [259] and ICAM-1 for endothelial cells [260]. Dual staining of Sema7a with Hnf4α reveals that during APAP injury, Sema7a becomes expressed on peri- necrotic hepatocytes, from here on referred to as Sema7a+ hepatocytes (Figure 3. 3A).

Sema7a expression during APAP injury was further examined in whole liver. Quantitative reverse transcription PCR (qRT-PCR) revealed a 9.5 fold increase of *Sema7a* mRNA in the whole liver at 24 hours post-APAP injection, compared to healthy controls (Figure 3. 3B). This was not reflected by an increase in Sema7a protein levels in the whole liver, as measured by an ELISA (Figure 3. 2C). However, Sema7a was significantly elevated in mouse serum at 12 and 24 hours post APAP injection (P=0.0127 & P=0.007, respectively) (Figure 3. 3D). This increase of Sema7a in the serum correlates (Pearson coefficient (r) = 0.728) with an increase in ALT, a serum biomarker used clinically to detect hepatocellular damage [261].

As serum Sema7a correlated with ALT in our murine APAP injury model, we investigated if Sema7a could be used as a serum marker to indicate the degree of hepatocellular injury in human paracetamol overdose (POD) patients. To assess correlation sera with a range of ALT levels, from a previous POD study [255], was selected and separated into a Mid ALT (1000 < 4600 u/L) or high ALT (>5,000 u/L) group. The levels of Sema7a in this POD sera and sera from healthy patients was measured using an ELISA. In human POD, Sema7a does not correlate with ALT and therefore injury (Pearson r = -0.0571) (Figure 3. 3F&G).

Figure 3. 3 Sema7a is expressed by hepatocytes during APAP injury

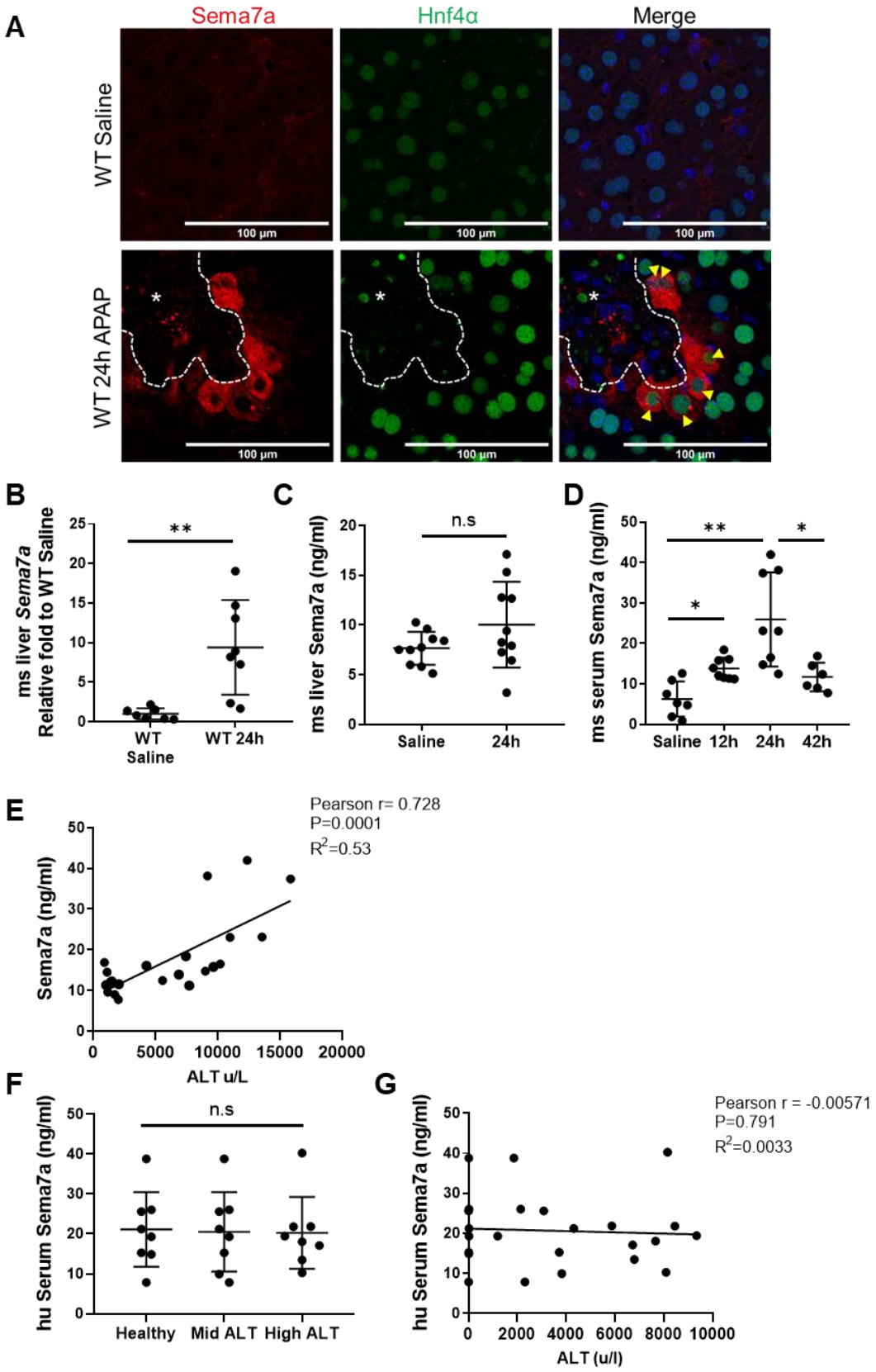

Figure 3. 3

A) Confocal images of Hnf4a (green) and Sema7a (red), merged (right), in WT mice treated with 24 hours saline (top), or 24 hours 350 mg/kg APAP (bottom). Yellow arrows indicate Sema7a+ Hnf4a+ hepatocytes. Scale bars 100 µm.
B) Sema7a expression in whole liver lysate measured by qRT-PCR, Unpaired t-test with Welch's correction.
C) ELISA for Sema7a in whole liver lysate from mice treated with saline or 24 hours 350mg/kg APAP. Unpaired t-test with Welch's correction.
D) ELISA for Sema7a in serum from healthy mice or mice treated with 12, 24 or 42 hours 350mg/kg APAP. Brown-Forsythe ANOVA test, with Games-Howell's multiple comparisons test.
E) Linear regression of Sema7a and ALT in mouse serum.
F) ELISA for human Sema7a in serum from healthy or paracetamol overdose patients. Mid ALT, 1000 < 4600 u/L; High ALT, >5000 u/L. One-way ANOVA.
G) Linear regression of Sema7a and ALT in human serum.

* $p<0.05$, ** $p<0.01$. ms, mouse; hu, human. The APAP injury mouse experiment was performed three times.

Sema7a is not expressed by other liver cells

To examine if Sema7a is expressed by the other main cell types of the liver, dual IHC of Sema7a was performed with the CK19 and the endothelial cell marker ICAM-1. This IHC shows Sema7a is not expressed on ductular cells (Figure 3. 4) or endothelial cells (Figure 3. 5). Hepatic stellate cells (HSCs) were also negative for Sema7a (inferred from Figure 3. 7 & Figure 3. 9). Therefore, Sema7a is expressed by hepatocytes during APAP injury.

Figure 3. 4 Sema7a is not expressed on ductular cells

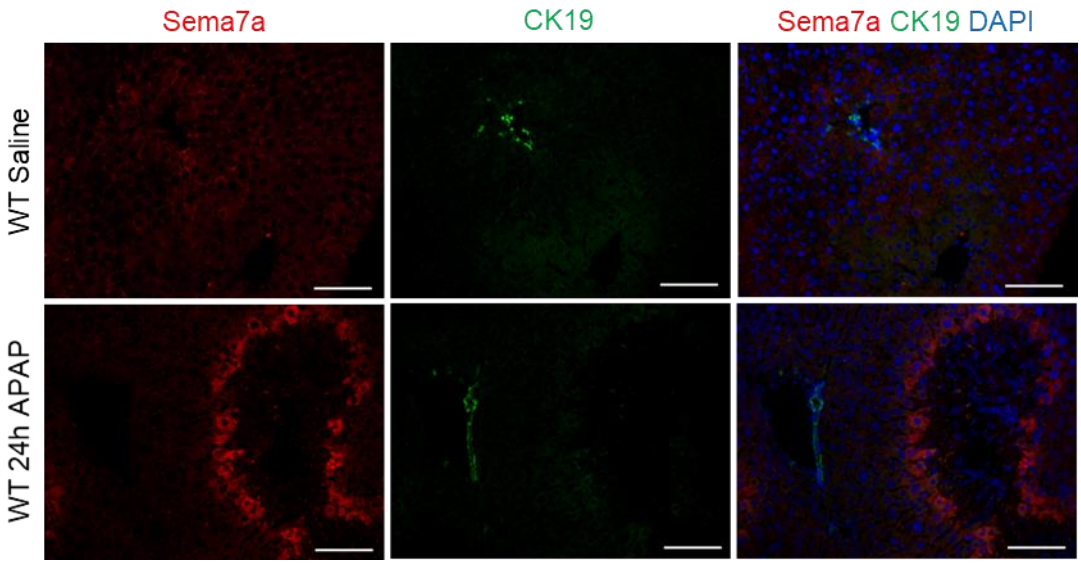

Figure 3. 4

Sema7a (red) is not expressed by ductular cells (K19, green) in WT mice treated with saline (top, n=4) or 24 hours 350mg/kg APAP (bottom, n=5).
Nuclear stain DAPI (blue). Scale bars 100 µm. The APAP injury mouse experiment was performed twice.

Figure 3. 5 Sema7a is not expressed on endothelial cells

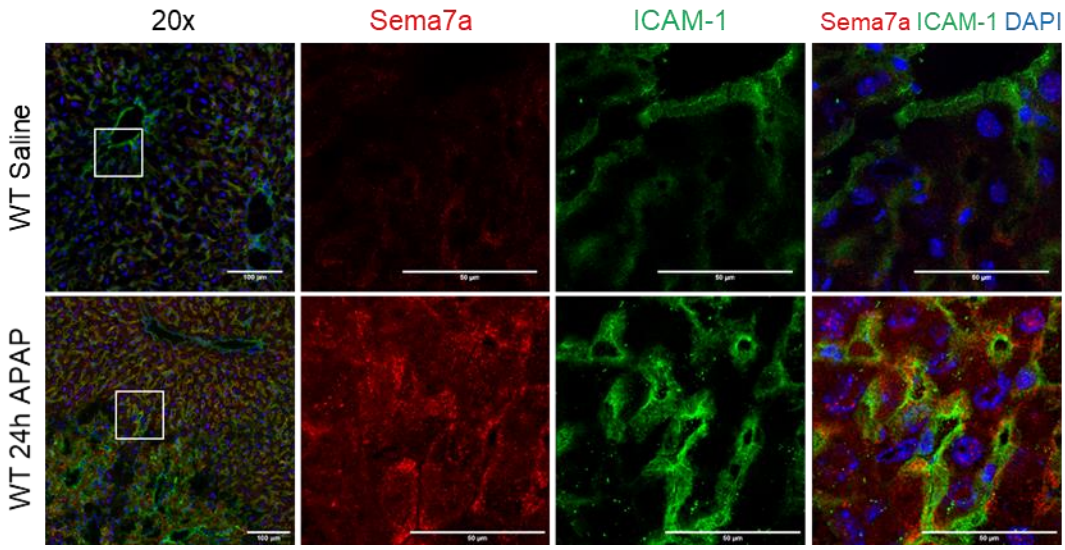

Figure 3. 5

Sema7a (red) is not expressed on ICAM-1+ (green) endothelial cells in mice treated with 24 hours saline (top), or 24 hours 350 mg/kg APAP (bottom). Nuclear stain DAPI (blue). Scale bars: 20x, 100 µm; 60x, 50 µm

The Sema7a receptors Plexin C1 and Integrinβ1 are stable during APAP injury

Plexin C1 and Integrin β1 are the Sema7a receptors [231,262]. To examine if they are affected by APAP injury, their expression was assessed. *Plexin C1* expression remained constant during APAP injury, but *Integrin β1* was more highly expressed at 24 hours APAP (P=0.0344) (Figure 3. 6A & B). In healthy mice, Plexin C1 and Integrin β1 have similar expression patterns. Proteins levels of Integrin β1 are unaltered by APAP injury, but Plexin C1 is more widely expressed covering an average of 10% of each 20x field, compared to 7.7% in healthy mice (P=0.0208) (Figure 3. 6C & D).

Dual immunofluorescence and confocal imaging was utilised to determine the extent of co-localisation between Sema7a and Plexin C1. At 24 hours APAP injury, Plexin C1 was expressed on cells lying between the Sema7a+ hepatocytes, and on cells dispersed across the healthy parenchyma (Figure 3. 7A). These cells are not Hnf4a+ hepatocytes (Figure 3. 7B), or CK19+ ductular cells (Figure 3. 8). In the liver, vimentin labels the type III intermediate filaments contained in HSCs and the smooth muscle cells of arterioles and veins [263,264]. Plexin C1 was exclusively expressed by a subset of vimentin+ HSCs, but not vimentin+ arterioles or venules (Figure 3. 9).

Figure 3. 6 Plexin C1 and Integrin β1 expression during APAP injury

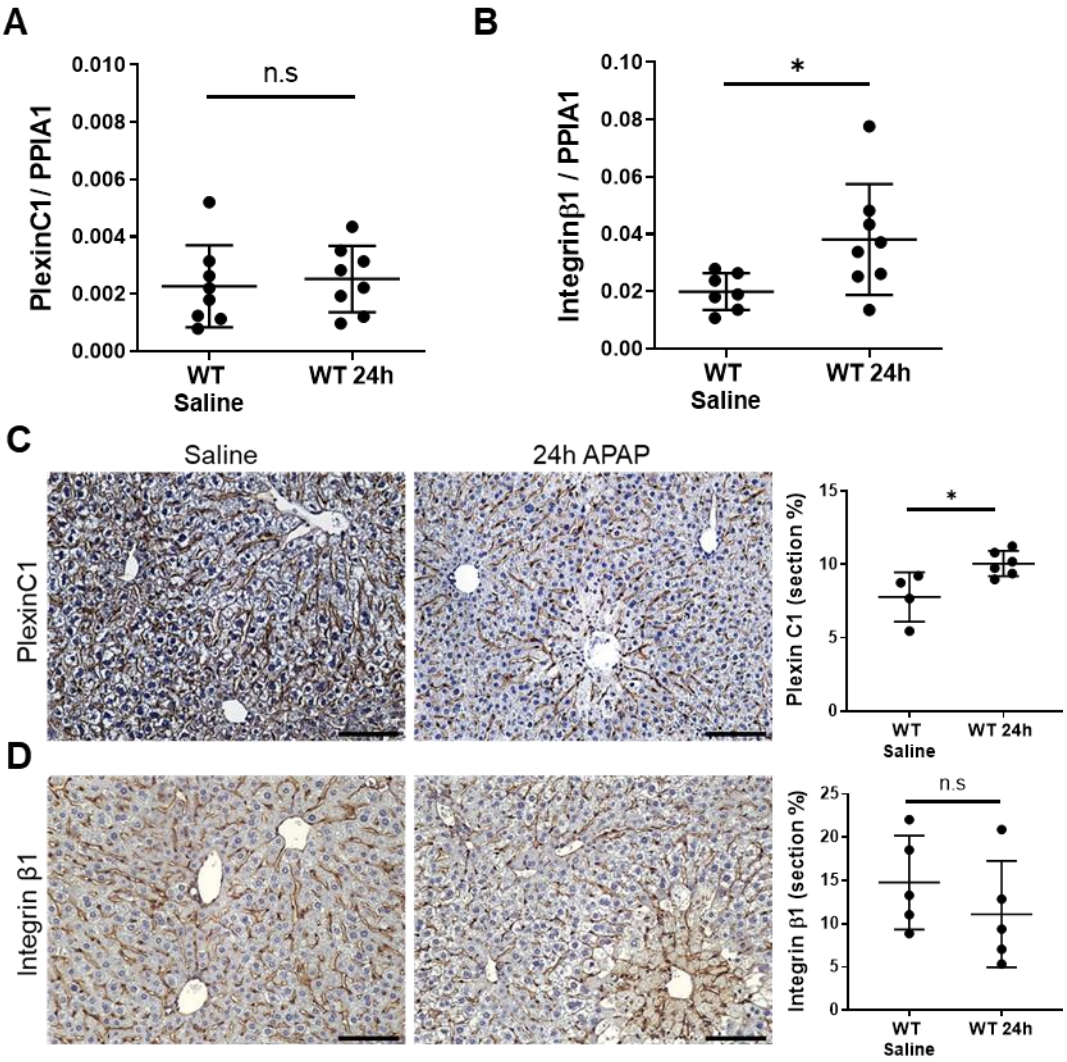

Figure 3. 6

Expression of the Sema7a receptors, Plexin C1 and Integrin β1 were examined in WT mice which were treated with saline (left), or 24 hours 350 mg/kg APAP (right).

A) *PlexinC1* mRNA expression, relative to *PPIA1* in whole liver lysate.
B) *Integrin β1* mRNA expression, relative to *PPIA1* in whole liver lysate (Welch's correction applied).
C) Protein expression of Plexin C1 in the liver. Area of Plexin C1 positivity is quantified (right)
D) Protein expression of Integrin β1 in the liver. Area of Integrin β1 positivity is quantified (right)

Scale bars 100 µm. *p<0.05; Unpaired t-test. Data is shown from three APAP mouse experiments.

Figure 3. 7 Plexin C1 is not expressed by hepatocytes

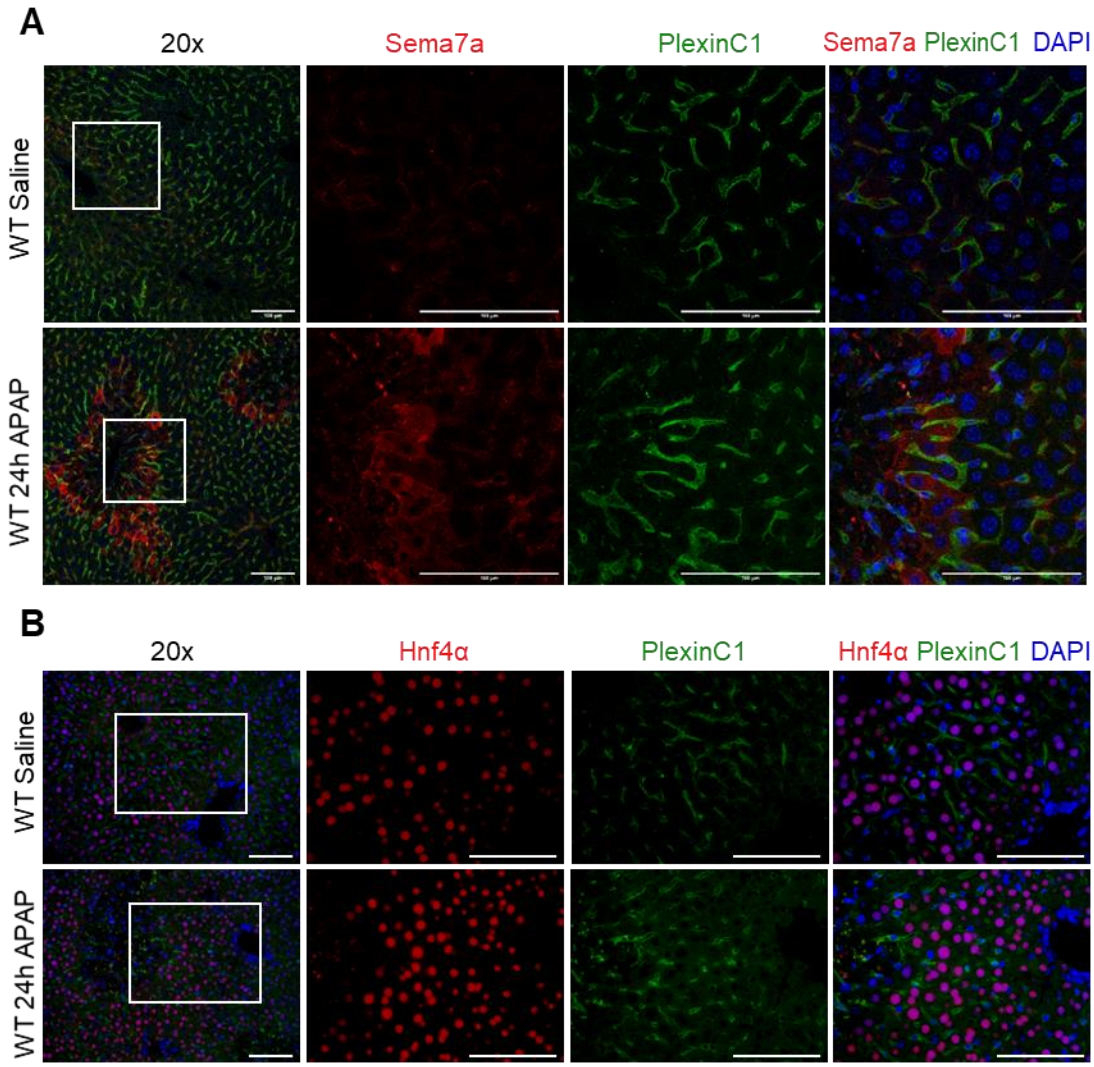

Figure 3. 7

A) Confocal images of Sema7a (red), and its receptor Plexin C1 (green) with DAPI (blue) in the liver of WT mice treated with saline (top) or 24 hours 350 mg/kg APAP (bottom).

B) Plexin C1 (green) expression with Hnf4α (red) and DAPI (blue) in the liver of WT mice treated with saline (top) or 24 hours 350 mg/kg APAP (bottom).

20 x image (left). White inset indicates areas examined at a higher magnification. Scale bars 100 µm. Representative images are shown.

Figure 3. 8 Plexin C1 is not expressed by ductular cells

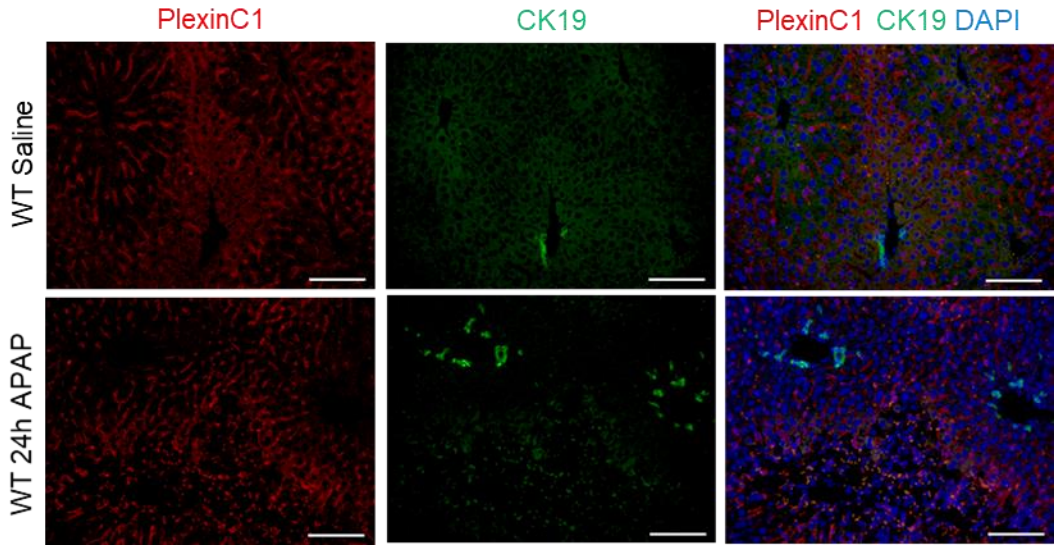

Figure 3. 8

Expression of Plexin C1 (red) and K19 (ductular marker, green) and DAPI (blue) in WT mice treated with saline (top, n=3) or 24 hours post APAP injection (bottom, n=4). Representative images are shown. Scale bars 100 µm

Figure 3. 9 Plexin C1 is expressed by Hepatic Stellate Cells

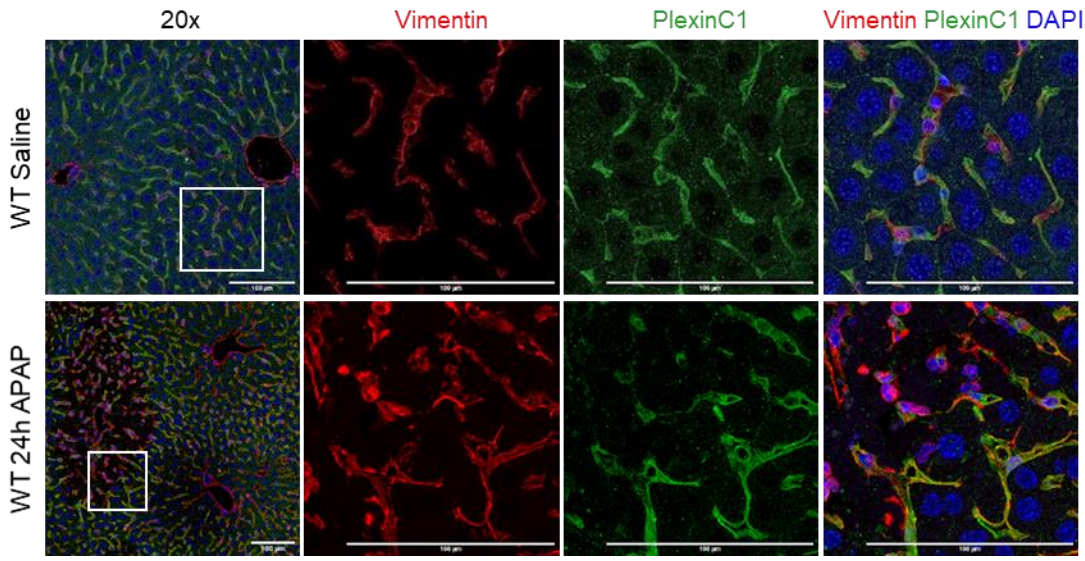

Figure 3. 9

Plexin C1 (green) is expressed by hepatic stellate cells (vimentin, red), dual expression in yellow, with DAPI (blue). Mice were treated with saline (top) (n=5) or 24 hours 350 mg/kg APAP (bottom) (n=5). Inset on 20x images (left) shows location of 60x images. Scale bars 100 µm. Data is shown from two APAP mouse experiments.

Integrin β1 is widely expressed in the liver

To define where Integrin β1 is expressed in the liver, in relation to the Sema7a+ hepatocytes, dual IHC was utilised. Integrin β1 outlines the Sema7a+ hepatocytes and appears to be expressed by cells lying between the Sema7a+ hepatocytes (Figure 3. 10A). This was confirmed with a dual stain of Integrin β1 and Hnf4α, where Integrin β1 is seen outlining the hepatocytes, as indicated by the white arrows in (Figure 3. 10B). Integrin β1 is also expressed by vimentin+ HSCs (Figure 3. 11), which interject between the Sema7a+ hepatocytes. Unlike Plexin C1, Integrin β1 is also expressed by the vimentin+ smooth muscle cells of the arterioles and veins, and the vimentin negative bile ducts (Figure 3. 11). Together, these IHC images show Integrin β1 is widely expressed in the liver, as previously reported [265]. As HSCs express both Plexin C1 and Integrin β1, and lie between the Sema7a+ hepatocytes, they are most likely to receive Sema7a signalling. Due to the ubiquitous expression of Integrin β1, Sema7a could interact with Integrin β1 expressed by many cell types, including other hepatocytes or immune cells.

Figure 3. 10 Integrin β1 is expressed by hepatocytes

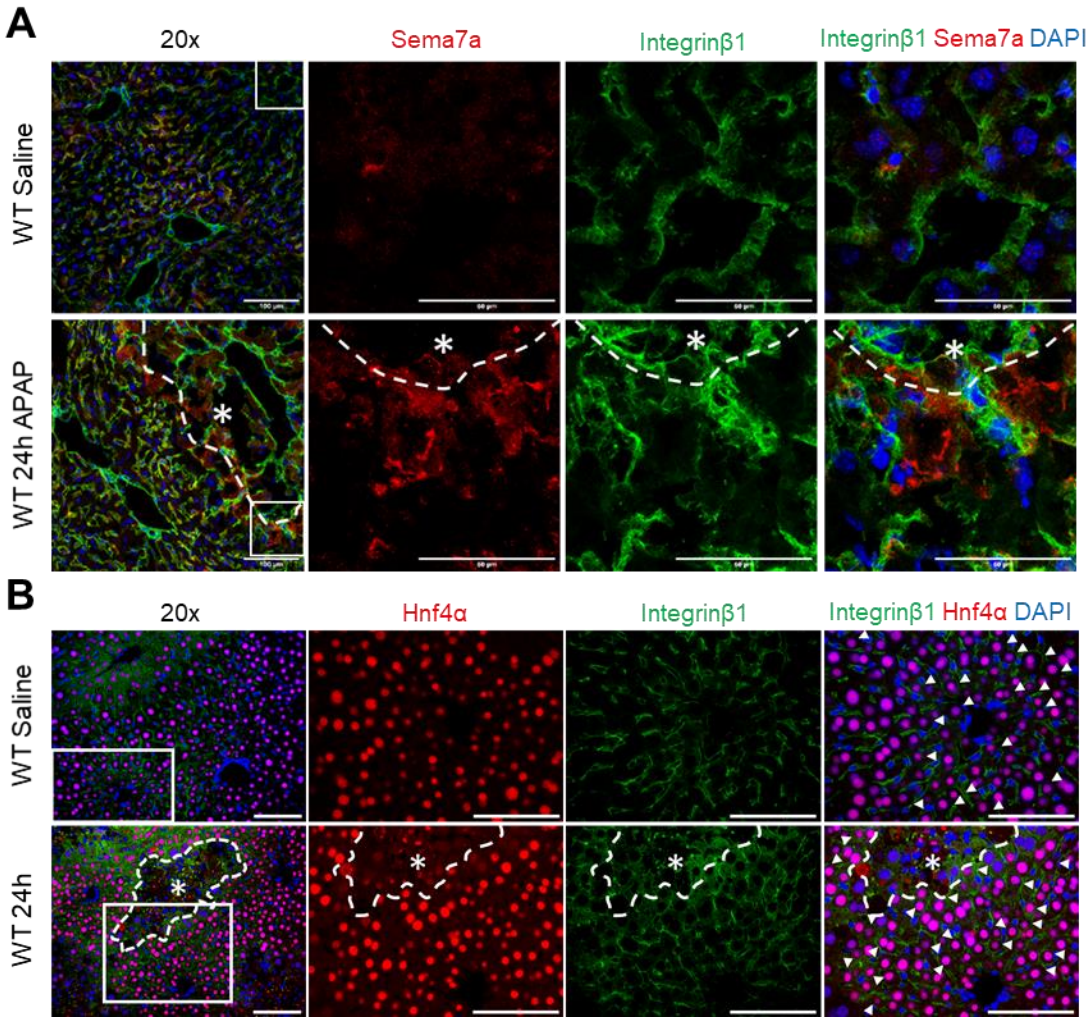

Figure 3. 10

A) Confocal images of Integrin β1 (green) and Sema7a (red) with DAPI (blue) in mice treated with saline (top) or 24 hours 350 mg/kg APAP (bottom). Scale bars 100 µm, or 50 µm on 60x inset images.
B) Integrin β1 (green) and Hnf4α (red) expression with DAPI (blue), dual Hnf4α and DAPI (magenta) in mice treated with saline (top) or 24 hours 350 mg/kg APAP (bottom). White arrows indicate Integrin β1 and Hnf4α positive cells. Scale bars 100 µm.

White dashes and asterix indicate necrotic areas.

Figure 3. 11 Integrinβ1 is expressed by hepatic stellate cells

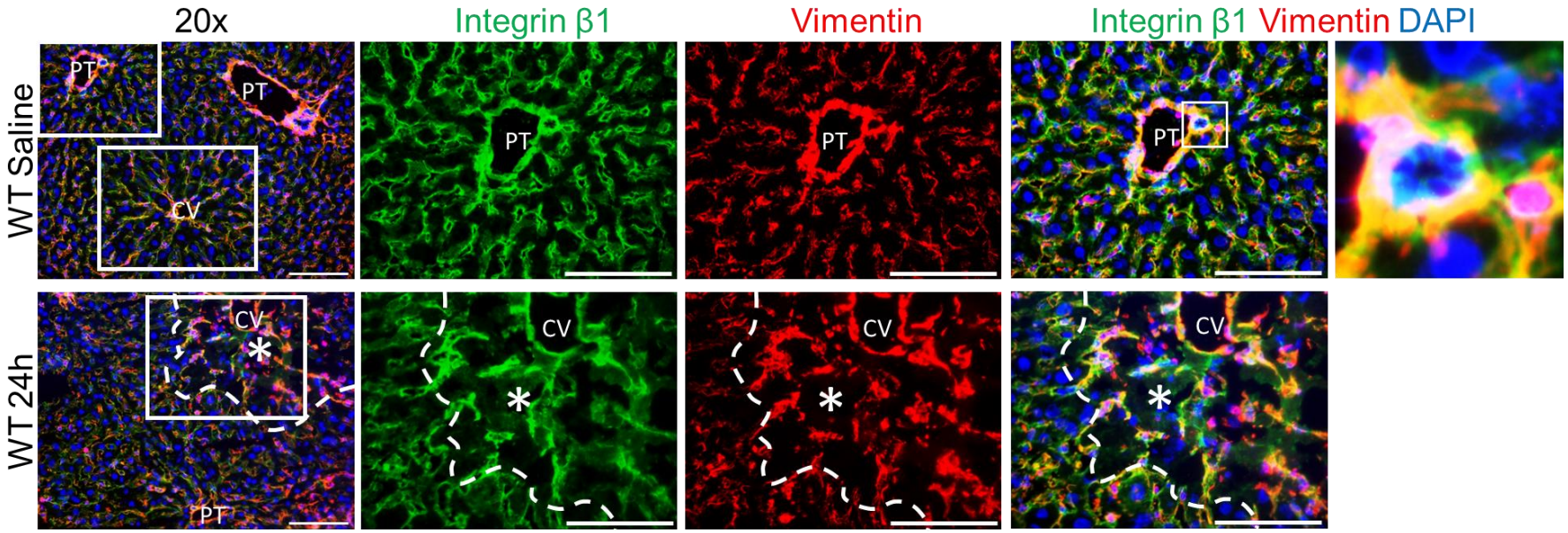

Figure 3. 11

Expression of Integrin β1 (green), vimentin (red), dual expression yellow, with DAPI (blue) in WT mice treated with saline (top) or 24 hours 350 mg/kg APAP (bottom row). Inset on 20x images indicate areas taken for 40x images. Inset on 40x images shows Integrin β1 expression at the portal triad (green surrounding the duct nuclei), independent of vimentin.
Representative images from n= 5 mice (two APAP experiments). White dashes and asterix indicate necrotic areas. Scale bars 100 µm. PT, portal triad; CV, central vein.

Sema7a does not mark proliferating cells in APAP injury

One of my aims is to investigate if Sema7a promotes hepatocyte proliferation, and therefore promotes recovery from APAP injury. As Sema7a expression reduces during recovery (36 – 60 hours APAP, Figure 3. 1), it is unlikely to be directly involved in proliferation. To test this theory, proliferative cells were labelled with BrdU. At 42h post APAP overdose 5% of all nuclei are BrdU+ (Figure 3. 12C), with less than 1% of BrdU+ cells expressing Sema7a (Figure 3. 12B &E).

To confirm that Sema7a is not involved proliferation, Sema7a expression was examined in a highly proliferative model - partial hepatectomy (PHx). 70% of the liver mass is removed surgically, and the remaining liver mass enters hyperplasia to replaced lost tissue. Peak proliferation occurs at 48 hours, and mice recover their liver mass by 1 week post-surgery. Both sham (control) and PHx surgeries were performed by Sofia Ferreira-Gonzalez.

At 48 hours post 70% PHx, 7.8% of all nuclei are positive for Ki67, a proliferation marker, compared to 0.6% of sham operated mice, as expected (P=0.004) (Figure 3. 13A & B). However, Sema7a was not expressed in these mice, suggesting it is not involved in proliferation (Figure 3. 13C). To conclusively prove Sema7a has no direct role in hepatocyte proliferation, Sema7a KO mice could undergo 70% PHx and compared to WT mice. However, this was outside the scope of my project.

Figure 3. 12 Sema7a hepatocytes are not proliferative

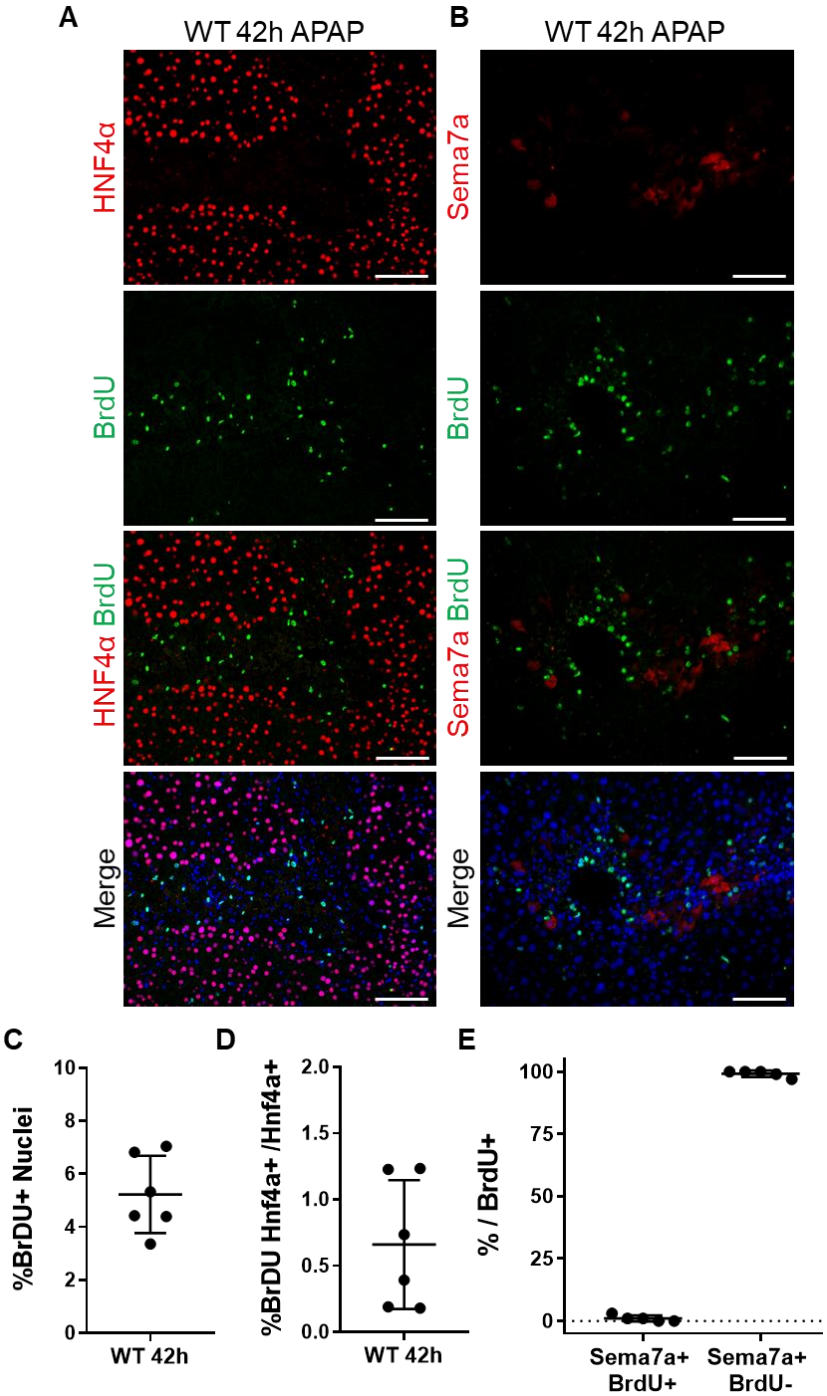

Figure 3. 12

A) Representative images of Hnf4α (red) (n=6), or B) Sema7a (red) (n=5), with BrdU (green) and DAPI (blue), in mice recovering from 350 mg/kg APAP injury at 42 hours. Scale bars 100 µm.

C) Quantification of BrdU expression at 42 hours APAP

D) Quantification of proliferating hepatocytes at 42 hours APAP

E) Quantification of proliferating Sema7a+ cells at 42 hours APAP

Data is shown from three APAP mouse experiments.

Figure 3. 13 Sema7a is not expressed during liver regeneration after a partial hepatectomy

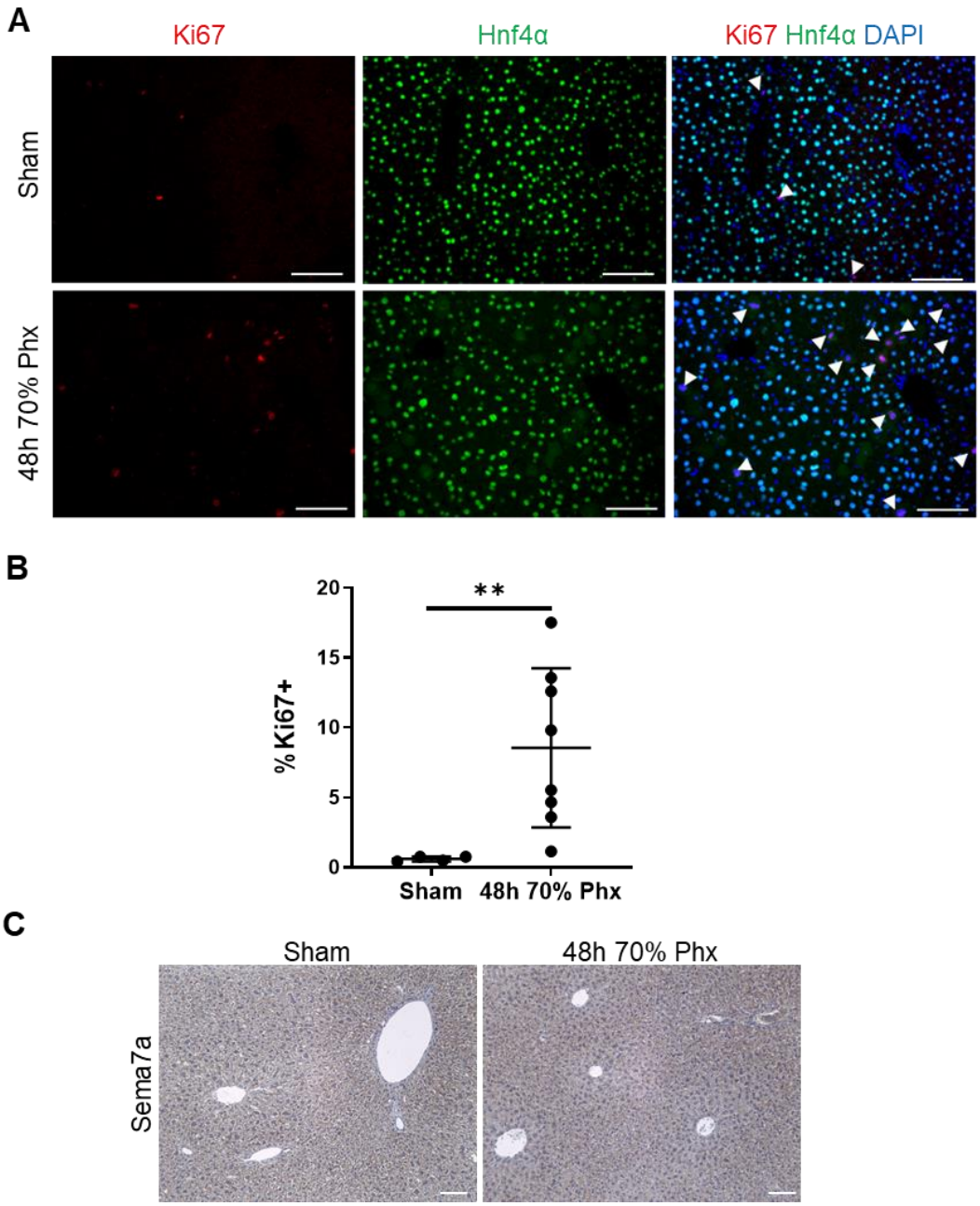

Figure 3. 13

A) Ki67 (red) and Hnf4α (green) with DAPI (blue) in mice with a sham surgery (control) or 48h post 70% PHx (right). White arrow heads indicate proliferating nuclei. Images are representative of n=8 PHx or n=4 sham mice. Experiment was performed once.
B) The percentage of Ki67+ proliferating nuclei is raised at 48 hours post 70% PHx. Mann Whitney test **p<0.01.
C) Sema7a is not expressed during proliferation. Sham (left) or 48 hours post 70% PHx (right). Images are representative of n=5 PHx or n=2 Sham mice.

Representative images are shown. Scale bars 100 µm. Both the partial hepatectomy (PHx) and sham surgeries were performed by Sofia Ferreira-Gonzalez.

A proportion of Sema7a+ cells are in cell cycle arrest

Senescence is induced in times of cellular stress. It is detected by the lack of proliferation and the presence of key markers such as p21. As Sema7a is absent from proliferating cells, and p21+ hepatocytes can be found surrounding the necrotic region, during APAP injury [144], in a similar location to the Sema7a positive hepatocytes, I investigated whether the Sema7a+ hepatocytes were undergoing senescence.

Serial sections were stained for Sema7a and p21 (Figure 3. 14A). In healthy mice, p21 expression is negligible, as expected. At 16 hours APAP an average of five p21 positive hepatocytes could be detected in the parenchyma and the peri- necrotic hepatocytes. At 24 hours post APAP overdose, an average of 16 p21+ hepatocytes could be detected per field of view, as injury progressed from 16 to 24 hours APAP post overdose (Figure 3. 14B, Saline vs 24 hours P=0.0002. 16 vs 24 hours P=0.0041).

Comparing p21 and Sema7a serial IHC, shows that the number hepatocytes dual positive for both p21 and Sema7a (Sema7a+ p21+) increase from two on average per field at 16 hours to eight at 24 hours post APAP overdose (Figure 3. 14C, Saline vs 24 hours P=0.0004. 16 vs 24 hours P=0.0051). At 24 hours APAP 18% of the Sema7a+ also express p21 (P=0.0059, Figure 3. 14D). These results demonstrate that a fifth of the Sema7a positive hepatocytes are in cell cycle arrest. Bona fide senescence should be confirmed using other senescence markers such as p16 and DCR2. In Chapter 4, I will investigate if a lack of Sema7a influences p21 expression.

Figure 3. 14 p21 increases with injury and is expressed by Sema7a+ cells

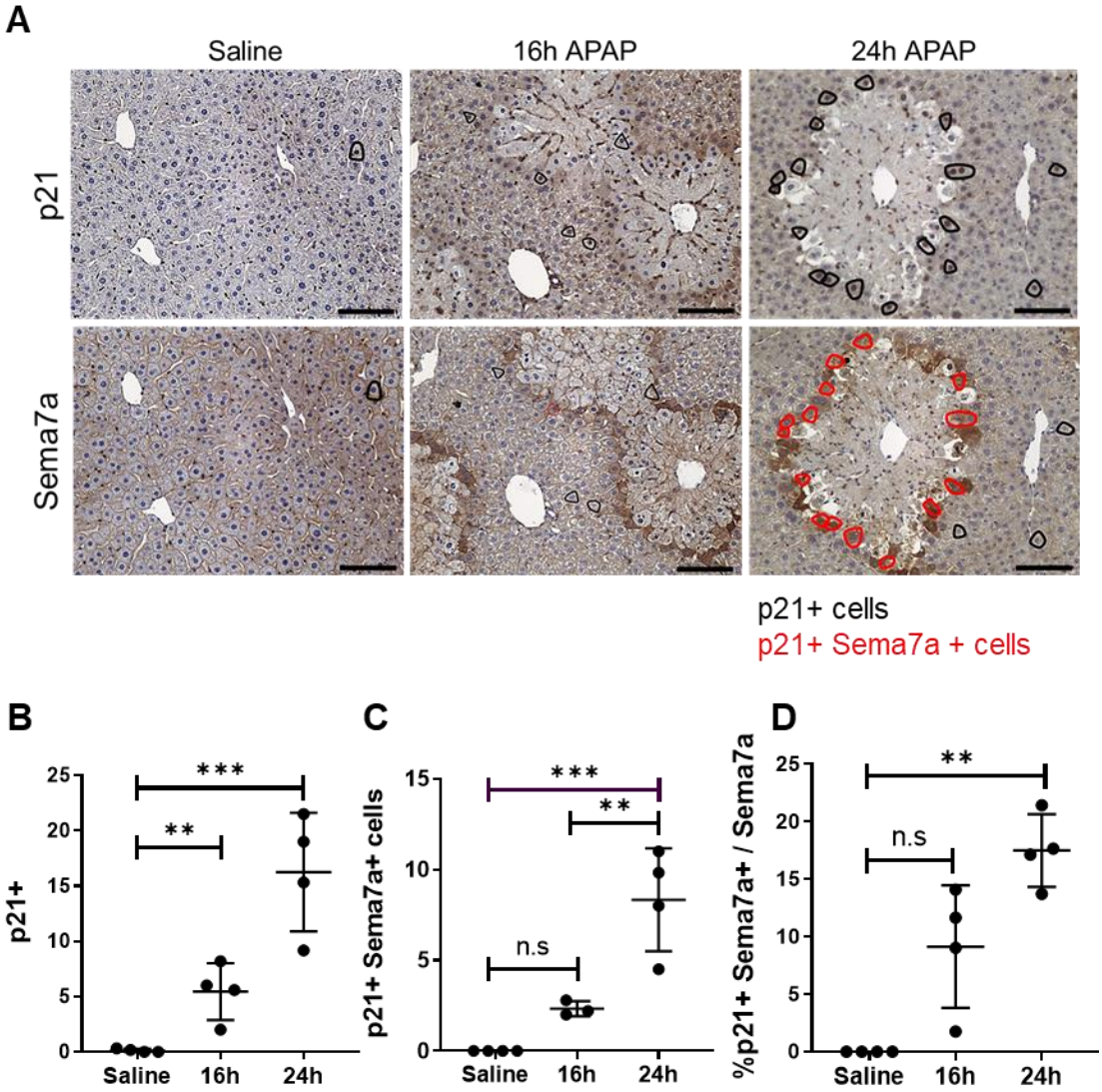

Figure 3. 14

A) Serial staining of p21 (top) and Sema7a expression (bottom) in saline (left), or 16 (centre) and 24 hours (right) 350mg/kg APAP. Black encircles cells with p21+ nuclei. Red, indicates p21+ Sema7a+ cells.
B) Number of p21+ cells. One-way ANOVA. Tukey's multiple comparisons test.
C) Number of p21+ Sema7a+. One-way ANOVA. Tukey's multiple comparisons test.
D) Percentage p21+Sema7a+ cells in Sema7a+ cells. Kruskal-Wallis test, Dunn's multiple comparisons test.

Data is shown from two APAP mouse experiments. Scale bars 100 µm. *p<0.05, **p<0.01, ***p<0.001.

The relationship between Sema7a+ hepatocytes and immune cells

The innate immune system is essential during APAP injury and recovery, and is recruited by DAMPs and cytokines released by activated Kupffer cells and dying hepatocytes [44]. Sema7a has been reported to regulate the expression of the pro-inflammatory factors MCP-1, TGFβ, IL-6 and IL-1β [212,246,247]. The expression of these factors was examined using qRT-PCR at 24 hours when Sema7a expression is highest. *MCP-1* was upregulated 18 fold, and *TGFβ1* was upregulated two fold higher than healthy mice (p=0.0061, P=0.0295, respectively), but the expression of the TGFβ receptors remained constant (Figure 3. 15). The possibility that Sema7a signalling could influence these genes will be investigated in Chapter 5.

To examine the localisation of the CD45+ immune cells, in relation to Sema7a+ hepatocytes, confocal imaging was performed. CD45+ cells are predominantly located within the necrotic area during APAP injury. Some CD45+ cells are closely associated with the Sema7a+ hepatocytes (Figure 3. 16A). For an interaction to occur, CD45+ cells must express the Sema7a receptors Plexin C1 or Integrin β1, in a dimer with either Integrin α1 or αv. This was examined with flow cytometry (Figure 3. 16B). 20-30% of CD45+ cells express Plexin C1, Integrin β1 and αv, but only 2.3% of CD45+ cells expressed Integrin α1 (Figure 3. 16C). Suggesting that immune cells bind to Sema7a through either Plexin C1 or the Integrin β1- αv dimer.

Figure 3. 15 mRNA expression of pro-inflammatory factors

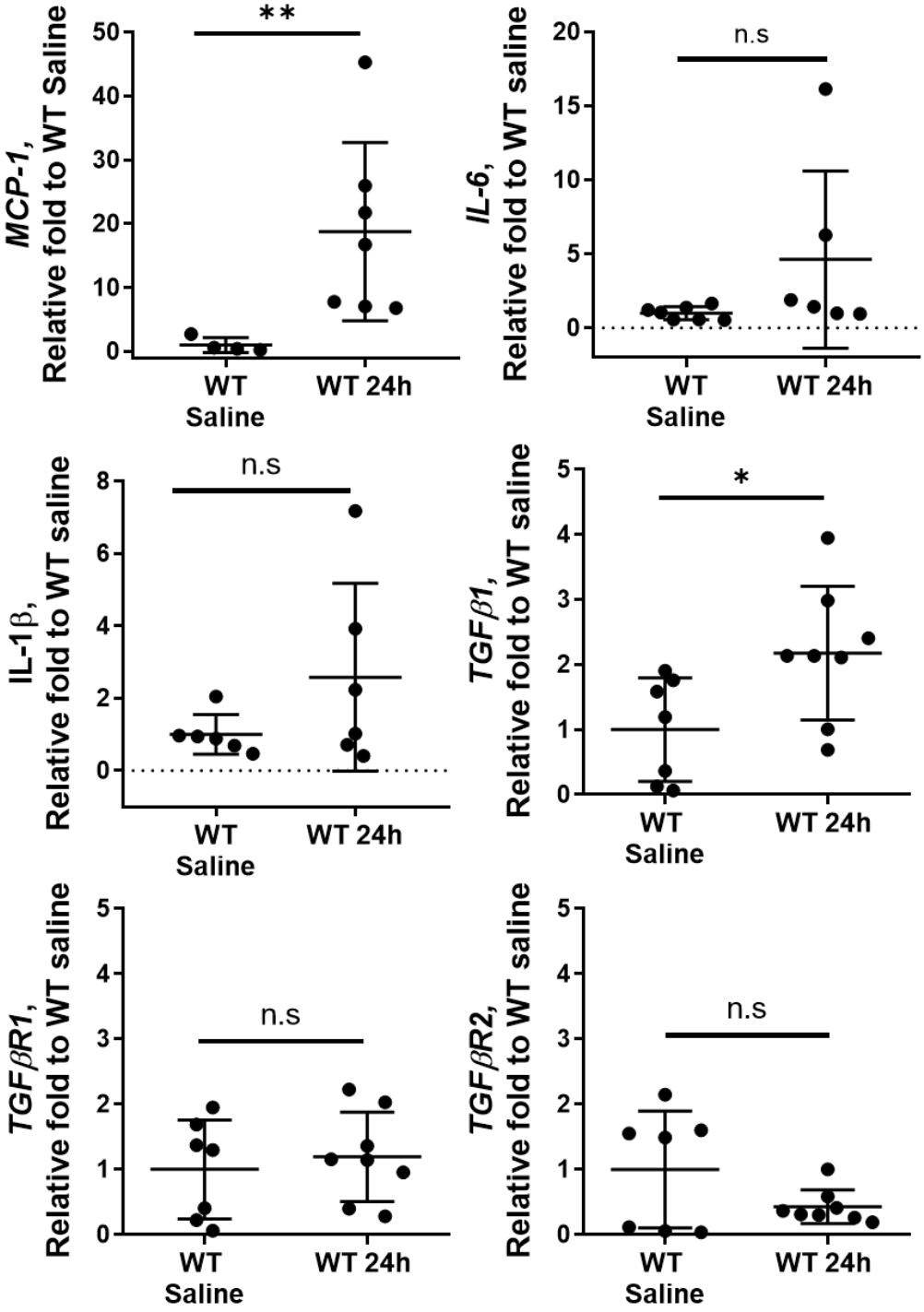

Figure 3. 15

mRNA expression of the indicated genes in whole liver lysate from WT mice treated with saline or 24 hours 350 mg/kg APAP, relative to saline treated mice.

Unpaired t-test except for: *MCP-1*, *IL-6*; *TGFβR2*, which required a Mann Whitney test. *p<0.05, **p<0.01. Data is shown from three APAP mouse experiments.

Figure 3. 16 Circulating CD45 + Cells express the Sema7a Receptors

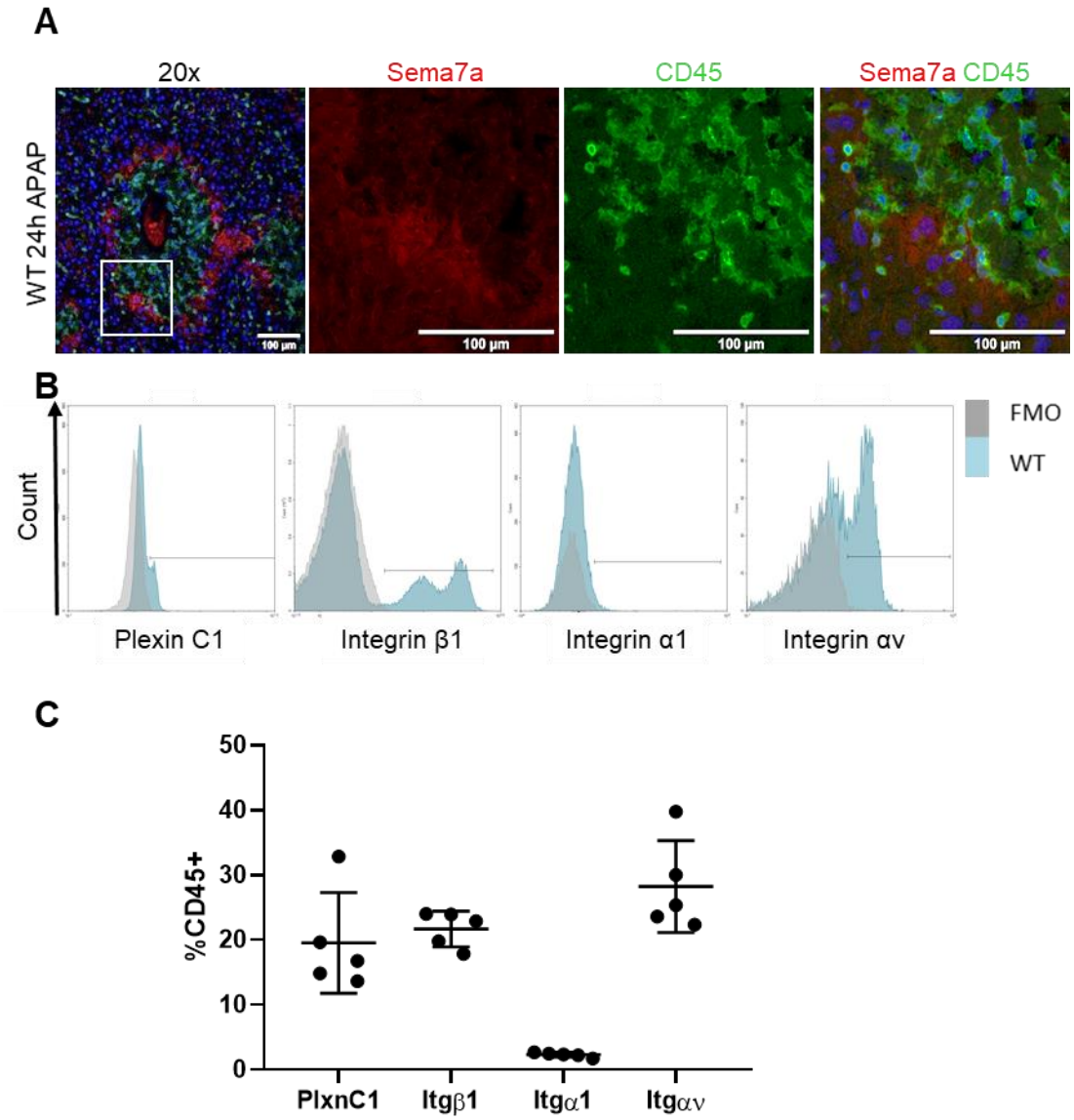

Figure 3. 16

A) Confocal images of CD45+ cells (green) and Sema7a cells (red), with DAPI (blue) at 24 hours 350 mg/kg APAP. Scale bars 100 µm.
B) Expression of Sema7a receptors (blue) on single, live, CD45+ cells isolated from peripheral blood of healthy mice. Gates were set using the relative FMO (grey)
C) Quantification of (B)

Plexin, Plxn; Integrin, Itg. Flow cytometry experiment was performed once.

A proportion of the CD45+ sitting close to the Sema7a+ hepatocytes are F4/80+ macrophages, as shown by confocal imaging in Figure 3. 17A. The F4/80+ macrophages did not appear to express Sema7a, ideally this should be confirmed by flow cytometry, but at the time of analysis there wasn't a suitable antibody available. However, isolated bone marrow derived macrophages (BMDMs) had negligible levels of *Sema7a* relative to the housekeeper, *PPIA-1*, suggesting macrophages do not express Sema7a (Figure 3. 17B).

To assess if macrophages could receive Sema7a, expression of the Sema7a receptors was examined. mRNA expression of *PlexinC1, Integrin β1, α1* and *αv* was detected in BMDMs (Figure 3. 17B) and at the protein level by IHC for Integrin β1 (Figure 3. 17C), and flow cytometry for Integrin α1 and αv (Figure 3. 17D & E).

Together, during APAP injury, pro-inflammatory cytokines including *MCP-1* are synthesised in the liver to activate the innate immune system. F4/80+ macrophages and other CD45+ leukocytes are attracted to the necrotic area. Some of these cells become marginalised to the edge of necrosis, in close association with the Sema7a+ hepatocytes. As macrophages express the Sema7a receptors there may be a signalling interaction occurring during APAP injury. The relationship between Sema7a and the immune system will be examined in more detail in Chapter 5.

Figure 3. 17 F4/80+ Macrophages are adjacent to Sema7a+ hepatocytes

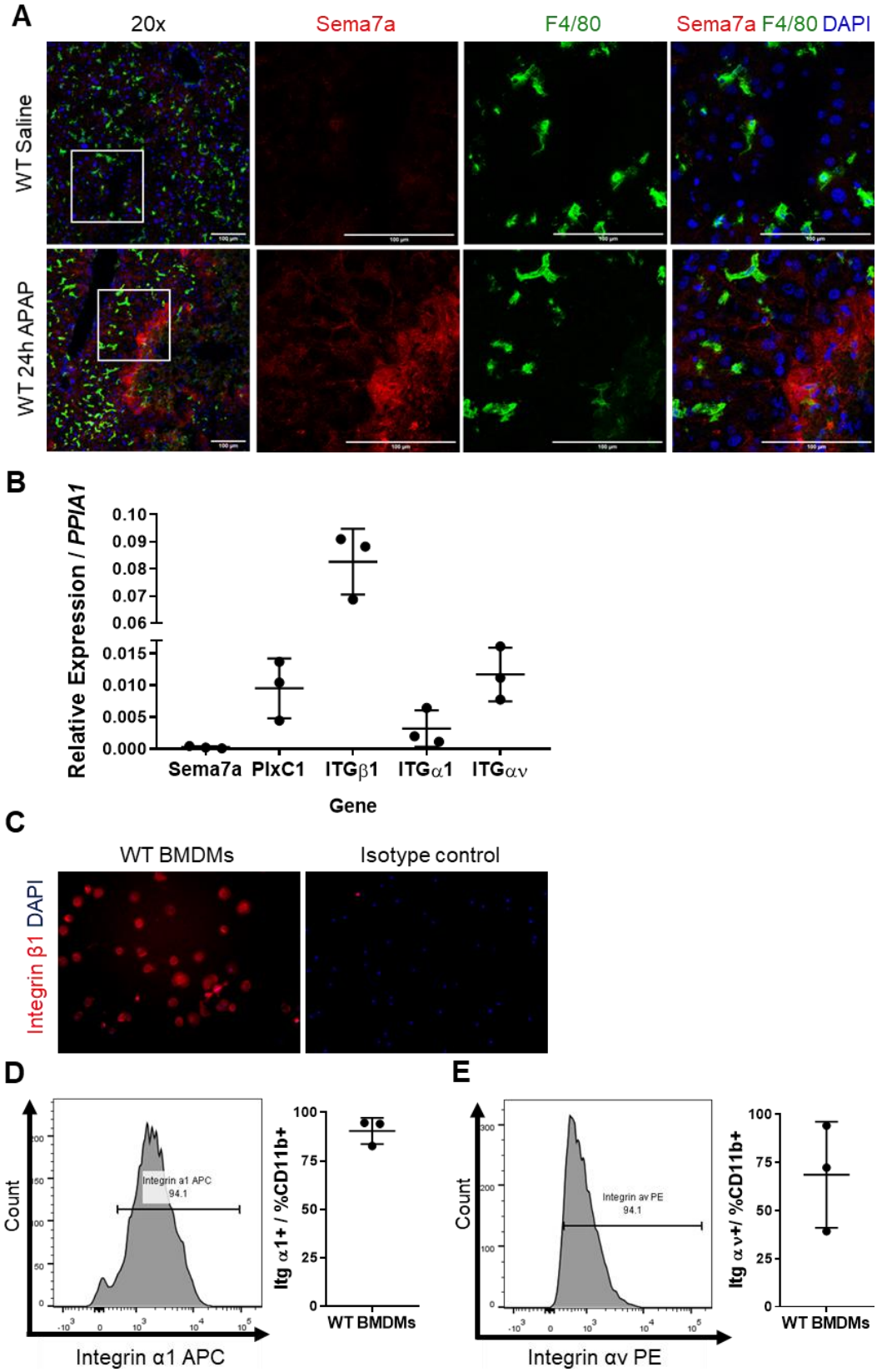

Figure 3. 17

A) Confocal images of F4/80+ macrophages (green) and Sema7a (red), in mice treated with 24 hours saline solution (top), or 24 hours 350 mg/kg APAP (bottom). Scale bars 100 µm.
B) mRNA expression of Sema7a and its receptors: Plexin C1 (PlxC1), Integrin (ITG) β1, α1 and αv in BMDMs
C) Integrin β1 (red) is expressed by bone marrow derived macrophages (BMDMs) (left), right shows the isotype control
D) Frequency of Live, CD11b+ BMDMs which express Integrin α1, measured by flow cytometry.
E) Frequency of Live, CD11b+ BMDMs which express Integrin αv, measured by flow cytometry.

Each dot represents a single BMDM experiment.

Discussion

Novel treatments for APAP injury may promote the pro-restorative arm of the innate immune system. Sema7a has been previously reported as an important immunomodulator, it can act as a chemoattractant for both monocytes and dendritic cells [151], and stimulate the production of both pro- [231] and anti- inflammatory[236] cytokines from macrophages. Furthermore, Sema7a KO mice have less inflammation in both liver [246] and lung [212] injuries. I questioned if Sema7a had a role during APAP injury or recovery.

At 12- 24 hours post APAP administration, Sema7a becomes expressed in peri - necrotic Hnf4α+ hepatocytes. These Sema7a+ hepatocytes are viable and encircle the Caspase 3+ and TUNEL+ cells. Sema7a+ hepatocytes may act as a physical boundary to prevent the spread of necrosis and may further prevent injury by acting as a barrier between the necrosis and the healthy parenchyma. In Chapter 4 I will investigate this in more detail using Sema7a KO mice.

At 24 hours post APAP administration, Sema7a expression is increased at the transcript, but not the protein level. The elevated *Sema7a* may replace Sema7a detected in the serum, which was significantly increased at 12 and 24 hours APAP, and correlated with the hepatocellular injury marker ALT.

Sema7a may be cleaved or secreted during APAP injury to promote inflammation. In rheumatoid arthritis, ADAM17 cleaves Sema7a from T cells and monocytes in the synovial fluid. This shed Sema7a binds to Integrin β1 on monocytes and macrophages causing them to secrete IL-6 and TNFα, promoting inflammation in the arthritic joint [232]. In human blood, Sema7a is expressed on human platelets [233] and erythrocytes where it carries John Milton Hagen (JMH) group antigens [234]. *In vitro* studies suggest the JMH antigens activate T cell proliferation and secretion of the pro-inflammatory cytokines IL-8 and IFN-γ [235]. In contrast to the mouse data, POD patients did not express Sema7a more highly in the serum during injury. This may reflect a difference in species, or when the time the blood samples were taken. Serum samples were taken on day one of hospital admission, but the time between overdose and admission will vary hugely, unlike our time-controlled mouse experiments. To confirm clinical relevance Sema7a expression in human POD liver should be examined, unfortunately, I could not find a working antibody for Sema7a in human liver.

In both humans and mice, peri-necrotic p21 expression correlates with the degree of APAP injury [144]. p21 is a key cell cycle arrest marker, which can be induced by TGFβ signalling in times of cellar stress [143,144]. As Sema7a has previously been shown to promote TGFβ signalling [246,247], and Sema7a hepatocytes are also located in the peri-necrotic area I investigated if the Sema7a hepatocytes express p21. 18% of the Sema7a+ hepatocytes expressed p21, suggesting that some of the Sema7a+ hepatocytes are in cell cycle arrest. The possibility that Sema7a is involved with p21 expression will be investigated using Sema7a KO mice in Chapter 4.

APAP injury is both enhanced and resolved by the innate immune system [35]. A multitude of DAMPs released by dying hepatocytes, and cytokines released by activated Kupffer cells, recruit leukocytes to the liver during APAP injury [44]. At 24 hours post APAP administration, these CD45+ cells can be seen infiltrating to the necrotic area. A portion of these cells are F4/80+ macrophages, which were closely associated with Sema7a+ hepatocytes. BMDMs express the Sema7a receptors. Therefore, Sema7a+ hepatocytes may modulate macrophage behaviour or localisation during APAP injury. Previously, Sema7a been shown to stimulate macrophages to produce both pro [231]- and anti- [236] inflammatory cytokines via Integrin β1. The effects of Sema7a on macrophages during APAP injury will be explored in Chapter 5.

The Sema7a receptors Plexin C1 and Integrin β1 are both expressed by HSCs. Integrin β1 is also expressed by most cell types of the liver, as shown here and previously reported [265]. HSCs secrete cytokines and growth factors which are protective against APAP induced necrosis [266,267]. However, later timepoints from APAP overdose were not examined in these mice to ensure resolution of necrosis, and an absence of inflammation and activation of native HSCs.

At 24 hours post APAP overdose, Plexin C1 expression was increased. As this is the timepoint for peak Sema7a expression, it may promote the expression of Plexin C1. In melanocytes, Sema7a promotes Plexin C1 [217] to induce melanocyte spreading *in vitro* [216,217]. However, *PlexinC1* was reduced in HSCs isolated from mice treated with chronic CCl_4 and bile duct ligation [246]. If Sema7a promotes Plexin C1 in our acute APAP model, I expect Plexin C1 expression to decrease in Sema7a KO mice during APAP injury. This will be examined in Chapter 4.

After APAP injury, the hepatocytes must proliferate to replace lost cells. To see if Sema7a has a role in recovery, its expression from 36h – 60h post APAP administration was examined. During this recovery period, the expression of Sema7a reduces. Proliferative BrdU+ cells were also negative for Sema7a. Together, these results indicate that Sema7a has no direct role in proliferation after APAP injury. This was confirmed in the PHx model, at peak proliferation there was an absence of Sema7a+ hepatocytes. However, Sema7a may have an indirect role in promoting recovery from APAP injury. By preventing the spread of necrosis, Sema7a may indirectly promote regeneration by allowing healthy cells to proliferate. This will be investigated in Chapter 4.

To conclude, Sema7a becomes expressed on peri-necrotic hepatocytes during APAP injury. These hepatocytes are viable, non-proliferative and may form a boundary between the necrosis and the remaining healthy cells. The Sema7a+ hepatocytes may also interact with macrophages or other immune cells during APAP injury. Using Sema7a KO mice I will confirm if Sema7a+ hepatocytes are required as a barrier to prevent the spread of necrosis, which may indirectly aid recovery. I will also explore if Sema7a promotes inflammation during APAP injury.

Chapter 4 - Sema7a prevents the spread of necrosis into the parenchyma during APAP injury

Introduction

In Chapter 3, viable Sema7a+ hepatocytes were discovered encircling the necrosis at peak APAP injury. HSCs lie in between the Sema7a+ hepatocytes and express the Sema7a receptors Plexin C1 and Integrin β1. This chapter aims to investigate if Sema7a+ hepatocytes act as a barrier, to prevent the spread of necrosis.

Cell cycle arrest or senescence is induced during times of oxidative stress or DNA damage to prevent damaged cells from replicating. Senescent cells also secrete factors to recruit the immune system and reinforce senescence [143,268]. It can be beneficial to prevent the spread of damage and mass cell death during tissue insult [145], or detrimental if senescence persists and prevents tissue regeneration [143,144,146].

During APAP injury, TGFβ signalling is upregulated [144,269] and induces cell cycle arrest in peri-necrotic hepatocytes, and prevents hepatocyte proliferation required for APAP recovery [144]. In chronic liver and lung injury models, Sema7a forms a positive feedback loop with TGFβ, independent of SMAD 2/3, to promote noncanonical TGFβ signalling [246,247]. In Chapter 3, *TGFβ1* mRNA expression was significantly upregulated at 24 hours post APAP administration, at the same time point of peak Sema7a expression.

As Sema7a can promote TGFβ signalling, and modulate the immune system, Sema7a may be part of a stress response with p21 to recruit the immune system and limit the spread of damage. Moreover, Sema3a is now recognised as a senescence marker [145]. To be in cell cycle arrest, cells must be non-proliferative and express several cell cycle arrest markers. In Chapter 3, none of the Sema7a+ hepatocytes expressed the proliferation marker BrdU. Furthermore, a fifth of the Sema7a+ hepatocytes express the cell cycle arrest marker p21.

To investigate the role of Sema7a during APAP injury and recovery in more detail, mice with Sema7a constitutively deleted [176] (Sema7a knock out (KO) mice) were treated with 350 mg/kg APAP, and compared to WT mice of the same genetic background. This chapter characterises the Sema7a KO mice during homeostasis, APAP injury and recovery. Specifically, I examine the following: firstly, if Sema7a+ hepatocytes prevent APAP injury by acting as a barrier to contain the spread of necrosis. Secondly, whether Sema7a promotes the expression of its receptors, Integrin β1 and Plexin C1. Thirdly, I investigate if Sema7a promotes expression of the

cell cycle arrest marker p21. Lastly, I explore if Sema7a promotes hepatocyte proliferation after APAP injury. The effects of Sema7a on inflammation during APAP injury will explored in detail in Chapter 5.

All data presented was assessed for normality. If required, a Welch test was applied to correct for unequal variances between samples. Each dot represents an individual mouse.

Results

Sema7a is absent in Sema7a KO mice

To ensure the Sema7a KO mice were deficient for Sema7a, I assessed their expression of Sema7a at the genomic, mRNA and protein level (Figure 4. 1). Sema7a was absent at all levels, confirming Sema7a KO mice are deficient for Sema7a. In comparison, mRNA expression in WT mice was significantly upregulated (P= <0.0001) at 24 hours post APAP administration, compared to healthy WT and Sema7a KO mice, or Sema7a KO mice at 24 hours post APAP administration.

Figure 4. 1 Sema7a is absent in Sema7a KO mice

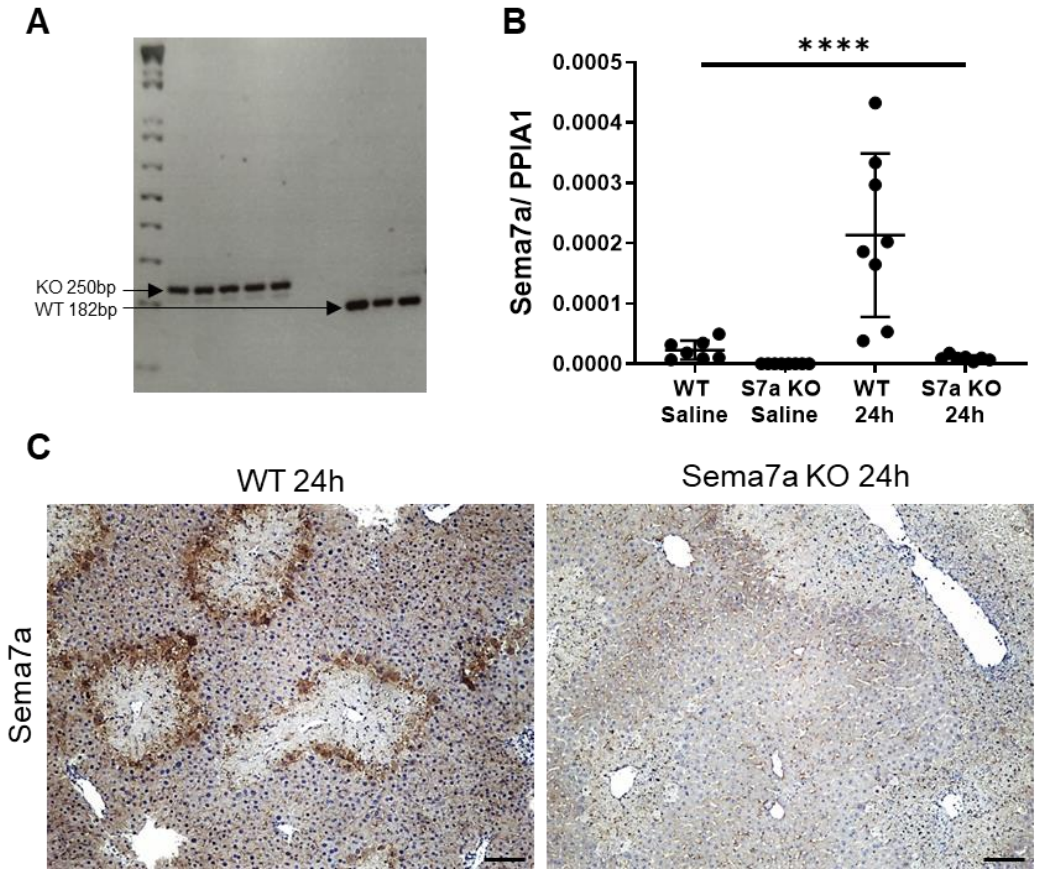

Figure 4. 1

Sema7a is absent in Sema7a KO mice, as confirmed by:

A) Genomic DNA PCR. The WT band for Sema7a is detected at 182bp, and the Sema7a KO band at 250bp. 1KB ladder on a 2% agarose gel.
B) mRNA expression of Sema7a in whole liver lysate, relative to the housekeeper *PPIA1*. N=8. One-way ANOVA**.** WT mice have significantly upregulated *Sema7a* at 24 hours post APAP injury, compared to healthy WT mice and Sema7a KO mice, and Sema7a KO mice treated with 24 hours APAP. ****p<0.0001.
C) Sema7a protein expression at 24 hours 350 mg/kg APAP. Scale bars 100 µm.

Data is shown from three APAP mouse experiments.

Each dot represents an individual mouse. Data was checked for normality and equal variance. This applies to every figure henceforth.

Sema7a KO mice do not have a baseline phenotype

Before treating the Sema7a KO mice with APAP, I ensured healthy mice did not have a baseline phenotype which could alter their response to APAP treatment. Histologically, the livers of Sema7a KO mice appear normal (Figure 4. 4B).

To examine liver function, liver function tests (LFTs) were performed. LFTs measures a panel of serum biomarkers associated with liver function: alanine transaminase (ALT), alkaline phosphatase (ALP), aspartate transaminase (AST), bilirubin and albumin. In the clinic raised LFTs indicate disease aetiology. For details on each LFT biomarker, please see Table 4. 1. There was no significant difference between any of the biomarkers between the healthy WT and Sema7a KO mice, suggesting that liver function is unaltered by a deficiency of Sema7a (Figure 4. 2).

To ensure APAP metabolism is unaffected in the Sema7a KO mice, Cyp2e1 expression was examined. Cyp2e1 is restricted to zone 3 (Figure 4. 3), and converts APAP into the hepatotoxic metabolite NAPQI, giving APAP injury its characteristic centrilobular necrosis pattern. In the Sema7a KO mice, Cyp2e1 is still restricted to zone 3 and the area of expression is not significantly different to the healthy WT mice (Figure 4. 3).

As the serum liver function tests, histology and Cyp2e1 expression are equivalent between the healthy WT and Sema7a KO mice, any differences seen during APAP injury will be due to a lack of Sema7a expression.

Table 4. 1 Serum biomarkers used to assess liver function

Biomarker	Function	Indications
ALT	ALT is a cytoplasmic enzyme found in high concentrations of the liver. In gluconeogenesis ALT catalyses the transfer of amino groups from alanine to ketoglutaric acid to produce pyruvic acid	Released into the serum specifically during hepatocellular damage. Extremely high levels are seen during: Hepatitis, APAP injury, ischemia reperfusion injury
AST	AST is located in the mitochondria and cytoplasm of: liver, cardiac and skeletal muscle, kidneys, brain and pancreas. In gluconeogenesis AST catalyses the transfer of amino groups from aspartic acid to ketoglutaric acid to produce oxaloacetic acid	Released into the serum upon cellular injury. Not specific to the liver High levels: liver necrosis, cirrhosis or myocardial infarction
ALP	ALP is concentrated to the bile canaliculus. ALP can also be detected in bones and the intestines ALP is a zinc metalloenzyme which perform lipid transportation.	Increased levels: Biliary disease or injury, hepatitis or bone disease
Bilirubin	Bilirubin is a breakdown product of erythrocytes, a liver specific process. Unconjugated bilirubin is insoluble. Conjugating bilirubin to albumin makes it water soluble	Inability of hepatocytes to clear bilirubin High levels indicate: jaundice, hepatitis, hepatocellular damage Moderate levels: biliary obstruction
Albumin	Albumin is a globular protein synthesised in the liver It regulates the oncotic pressure of the blood and can act as a carrier protein	Synthetic function test predominantly used to detect chronic liver disease. Low levels: decreased synthesis in the liver High levels: during APAP injury may indicate dehydration

Information was gathered from: [270,271]

Figure 4. 2 Liver function is unaltered in healthy Sema7a KO mice

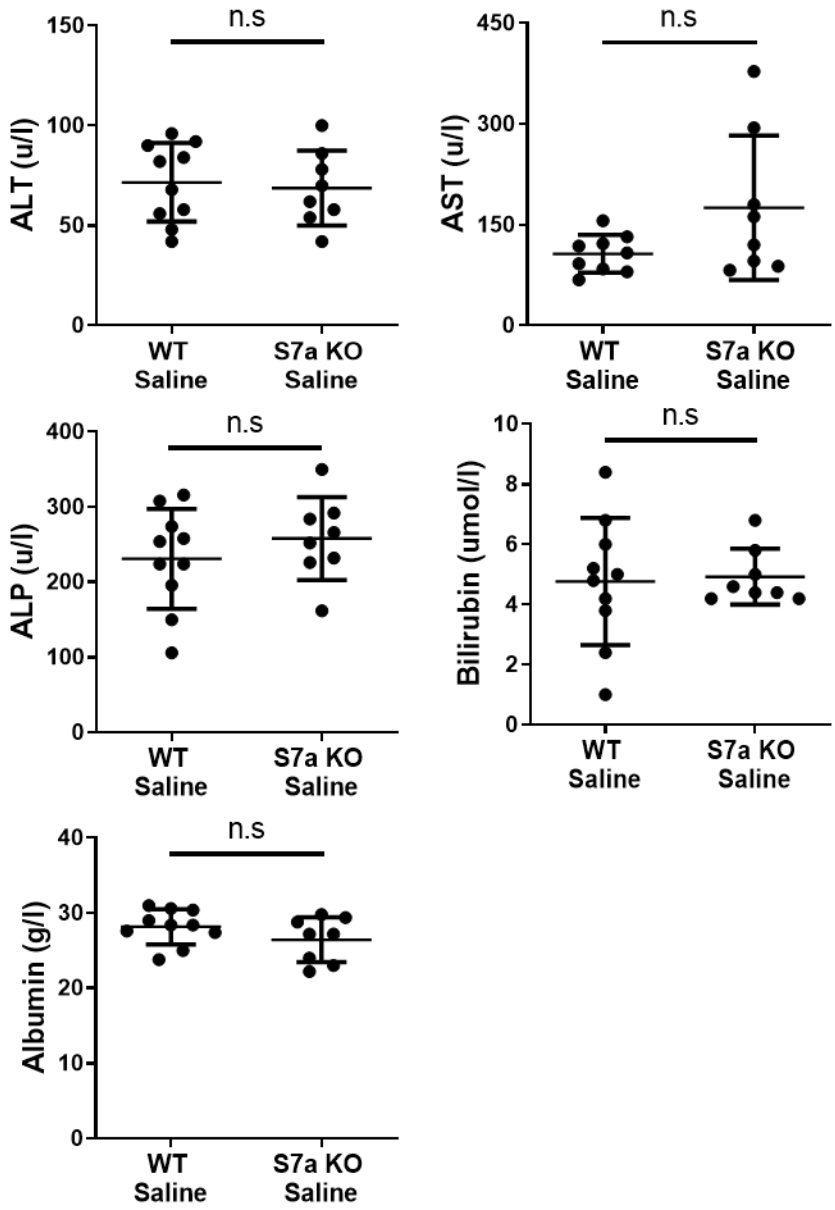

Figure 4. 2

To assess baseline function of the liver in Sema7a KO mice, serum biomarkers which indicate liver function were examined in saline treated WT and Sema7a KO mice. Alanine transaminase (ALT), aspartate transaminase (AST), alkaline phosphatase (ALP), bilirubin and albumin.
Unpaired t-test. Data from three APAP mouse experiments is shown.

Figure 4. 3 Cyp2e1 areas are the same in WT and Sema7a KO mice

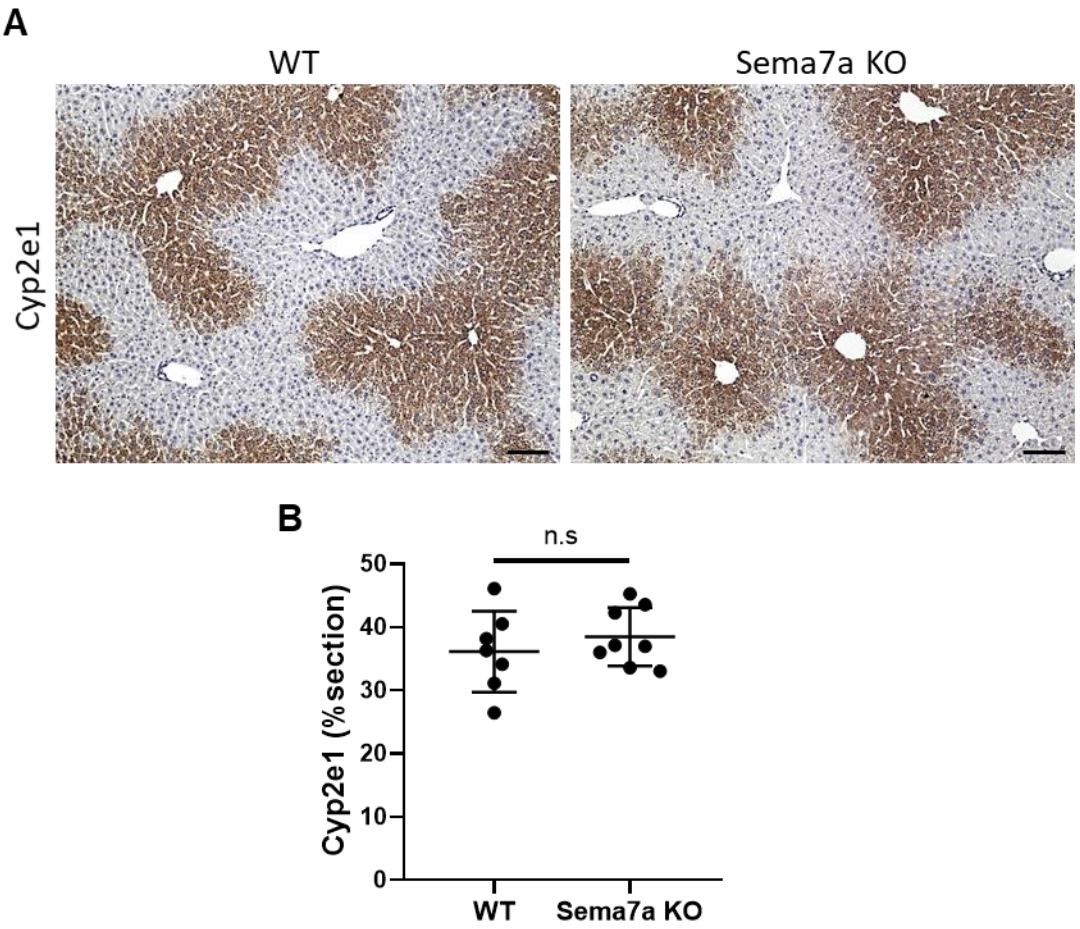

Figure 4. 3

A) Cyp2e1 DAB staining in healthy WT and Sema7a KO mice, representative images shown. 10x magnification. Scale bars 100 µm.
B) Average percentage area of Cyp2e1 positivity in healthy WT and Sema7a KO mice.

Data from three APAP mouse experiments is shown.

Sema7a KO mice are more susceptible to APAP injury

To investigate the role of Sema7a during APAP injury, WT and Sema7a KO mice were treated with 350mg/kg APAP at the following time points: i) 12 hours, when hepatocyte Sema7a expression is first detected, with ongoing inflammation and necrosis; ii) 24 hours, the time point of peak injury and Sema7a expression; iii) 42 hours, to compare recovery of the Sema7a KO and WT mice. For a schematic of the experiment see Figure 4. 4A.

The histology of WT and Sema7a KO mice was compared using H & E staining. Healthy WT and Sema7a KO mice have similar histology. At 12 hours post APAP injection, both WT and Sema7a KO mice have centrilobular necrosis with a faint boundary between the centrilobular necrosis and healthy tissue. Tissue necrosis was quantified using the Polaris and trainable inForm software. At 12 hours post APAP injury the Sema7a KO mice have significantly more necrosis (P= 0.0391) than WT mice. At 24 hours APAP, the boundary between the centrilobular necrosis and healthy tissue becomes defined in the WT mice, but not the Sema7a KO mice. The Sema7a KO mice also appear to have more infiltrating small mononucleated cells (identified by the presence of small blue nuclei) in the necrotic area (Figure 4. 4B). At 42 hours APAP the WT and Sema7a KO mice are histologically similar and are recovering from APAP injury seen by the reduced necrosis (Figure 4. 4C).

Figure 4. 4 Sema7a KO mice have more necrosis than WT mice

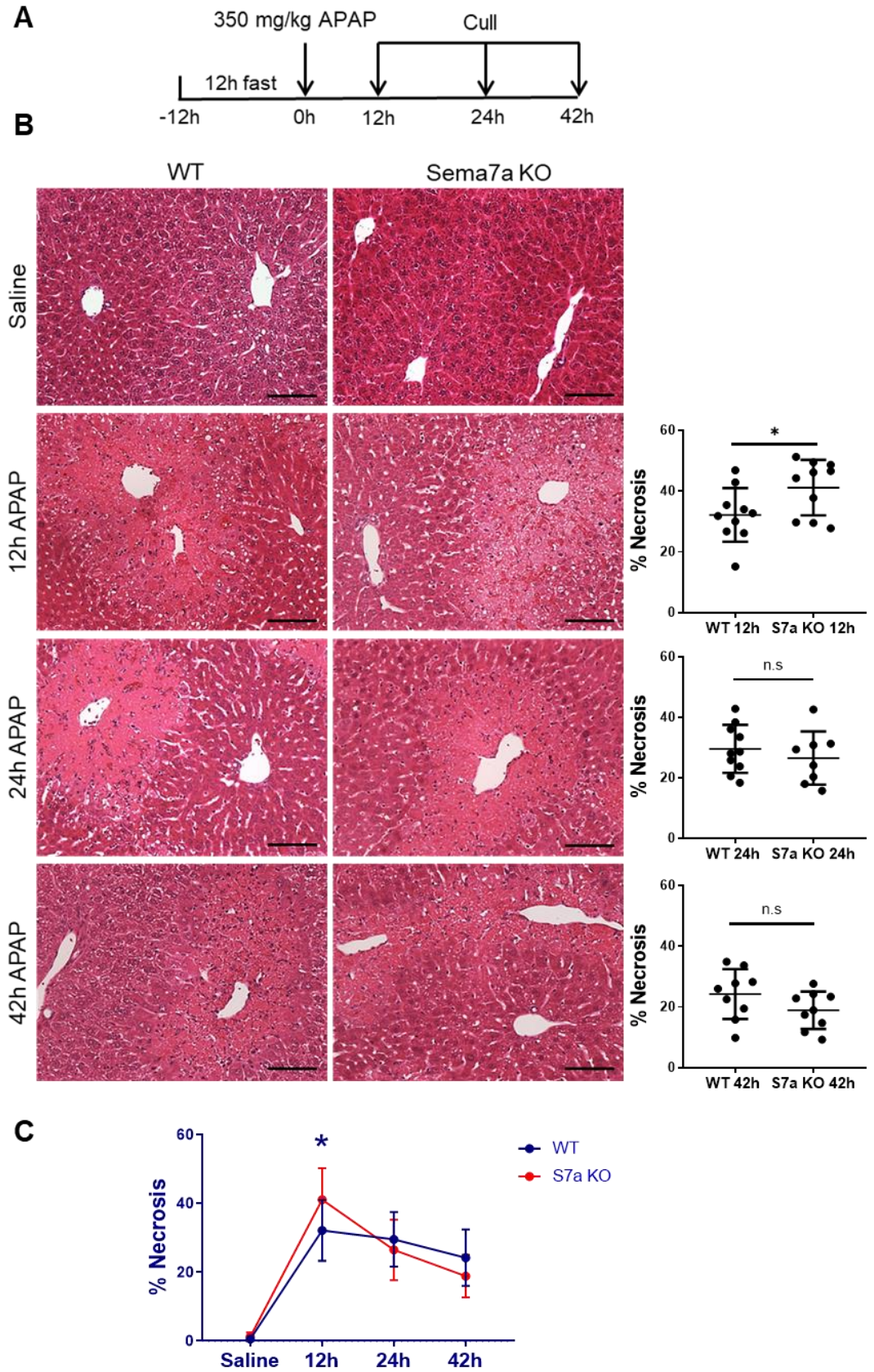

Figure 4. 4

A) Schematic of the APAP injury time course experiment
B) H&Es of WT (left) or Sema7a KO mice (centre) treated with saline (top row), 12 hours (second row), 24 hours (third row), or 42 hours (bottom row) 350mg/kg APAP. Area of necrosis (right) was quantified using the Polaris. Unpaired t-test.
C) Area of necrosis over the time course of APAP injury. Two-way ANOVA with Sidak's multiple comparisons test. WT, blue; Sema7a KO, red.

Data from eight APAP mouse experiments is shown.*$p<0.05$. Scale bars 100 µm.

To further assess the extent of APAP injury in the WT and Sema7a KO mice, LFTs were performed. The increased necrosis at 12 hours APAP in the Sema7a KO mice is accompanied by raised ALT (P=0.0095), AST (P= 0.0107) and albumin (P= 0.0212), confirming increased hepatocellular damage. Elevated albumin during acute liver injury may be due to dehydration, mice are less likely to eat or drink with a sore abdomen (Figure 4. 5). Necrosis at 24 hours and 42 hours post APAP injection was not significantly different in the WT and Sema7a KO mice. However, the Sema7a KO mice still had more ongoing damage as they had higher bilirubin (P= 0.0109) at 24 hours APAP (Figure 4. 6) and higher ALP (P= 0.0306) at 42 hours APAP (Figure 4. 7). These result show that throughout the APAP time course, Sema7a KO mice are more injured than WT mice.

During all the APAP experiments, the mice were watched closely and culled if they approached the moderate severity threshold. Figure 4. 8 shows the numbers of WT and Sema7a KO mice which were humanely culled during the APAP experiments. Although not significant, the Sema7a KO mice reached the severity limit more often than WT mice. Indicating that Sema7a KO mice succumb to APAP injury more easily than WT mice. To confirm this, a survival experiment should be performed. This was not practically possible due to a lack of Sema7a KO mice.

Figure 4. 5 Sema7a KO mice have elevated serum transaminases at 12 hours post APAP injury

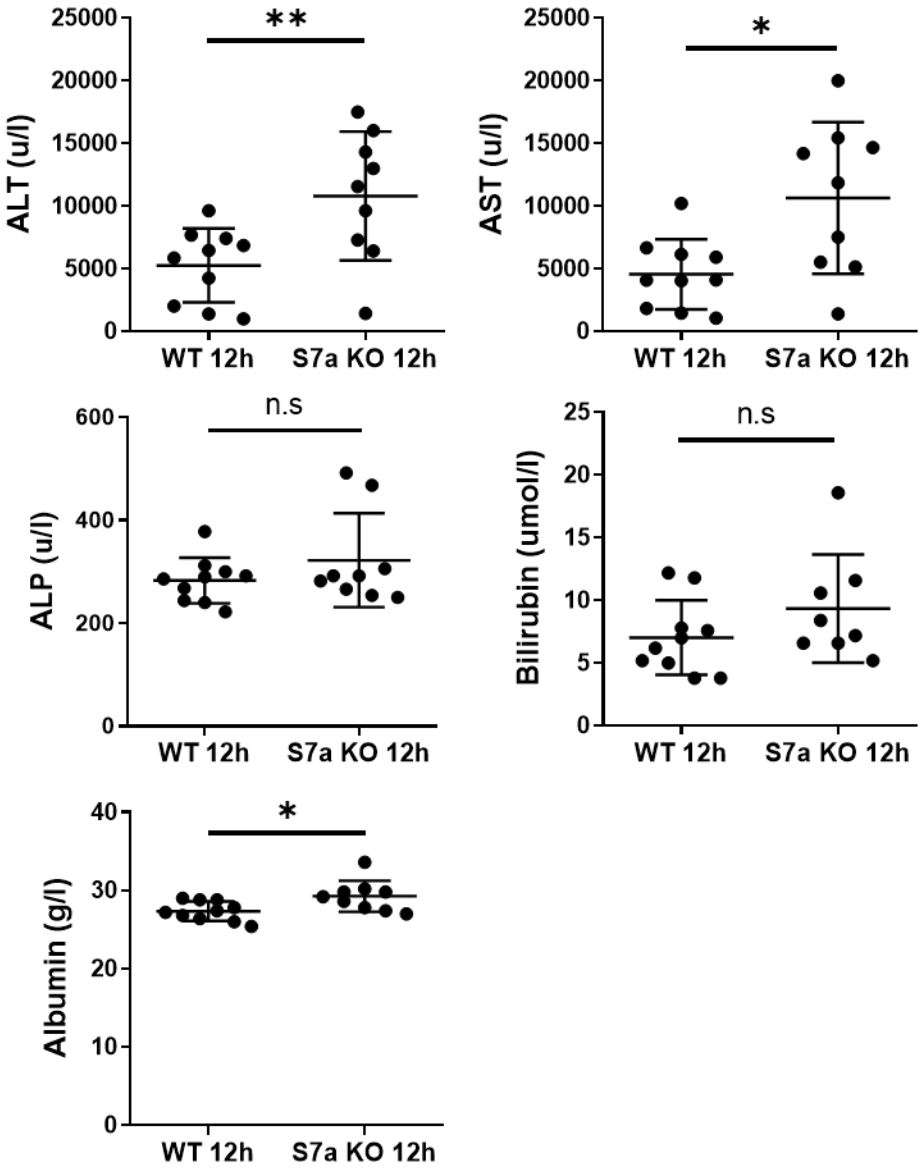

Figure 4. 5

Serum biochemical markers for liver function in WT and Sema7a KO mice treated with 350mg/kg APAP for 12 hours.

Alanine transaminase (ALT), aspartate transaminase (AST), alkaline phosphatase (ALP), bilirubin and albumin.

Data from three APAP mouse experiments is shown. Unpaired t-test. *p<0.05, p<0.01**

Figure 4. 6 Sema7a KO mice have raised bilirubin at 24 hours post APAP injury

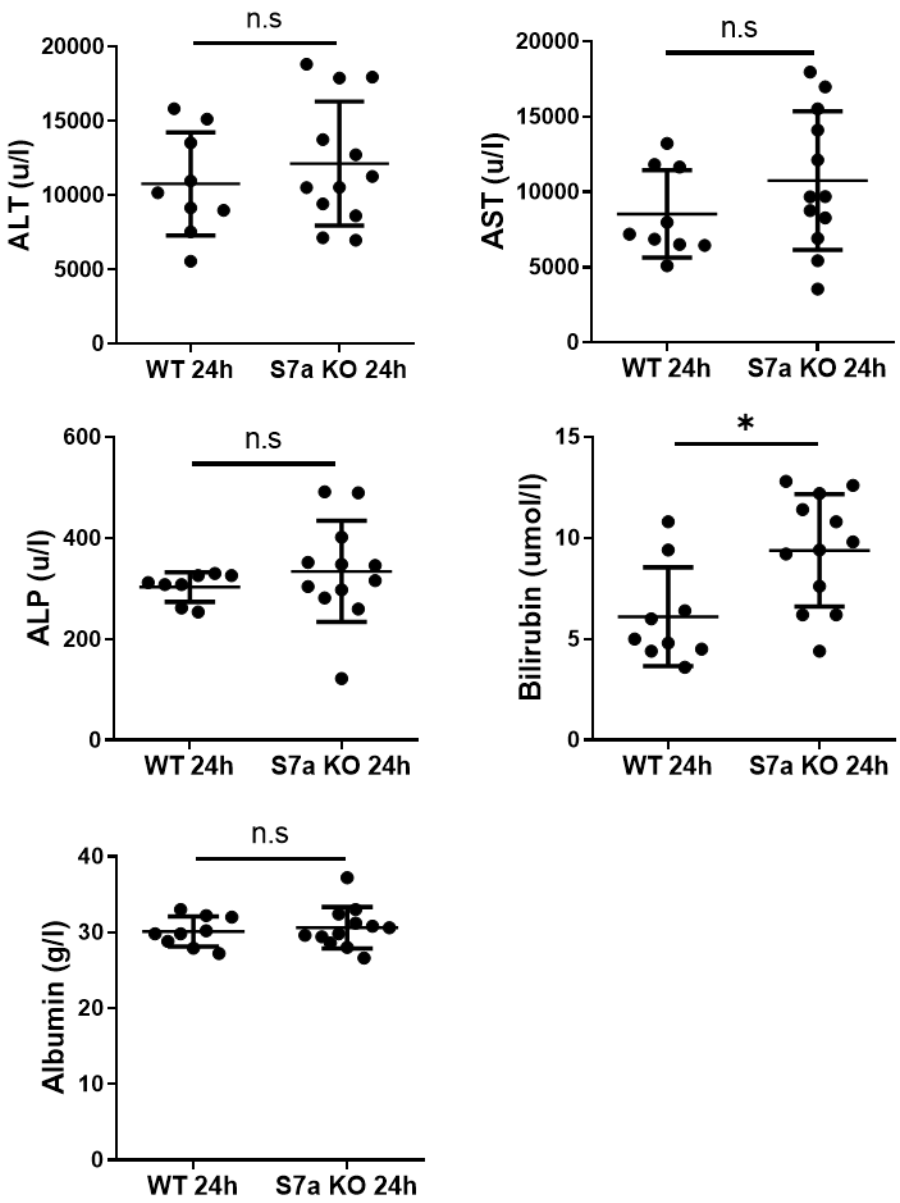

Figure 4. 6

Serum biochemical markers for liver function in WT and Sema7a KO mice treated with 350mg/kg APAP for 24 hours

Alanine transaminase (ALT), aspartate transaminase (AST), alkaline phosphatase (ALP), bilirubin and albumin.

Unpaired t-test. p*<0.05. Data from three APAP mouse experiments is shown.

Figure 4. 7 Sema7a KO mice have raised ALP levels at 42 hours post APAP injury

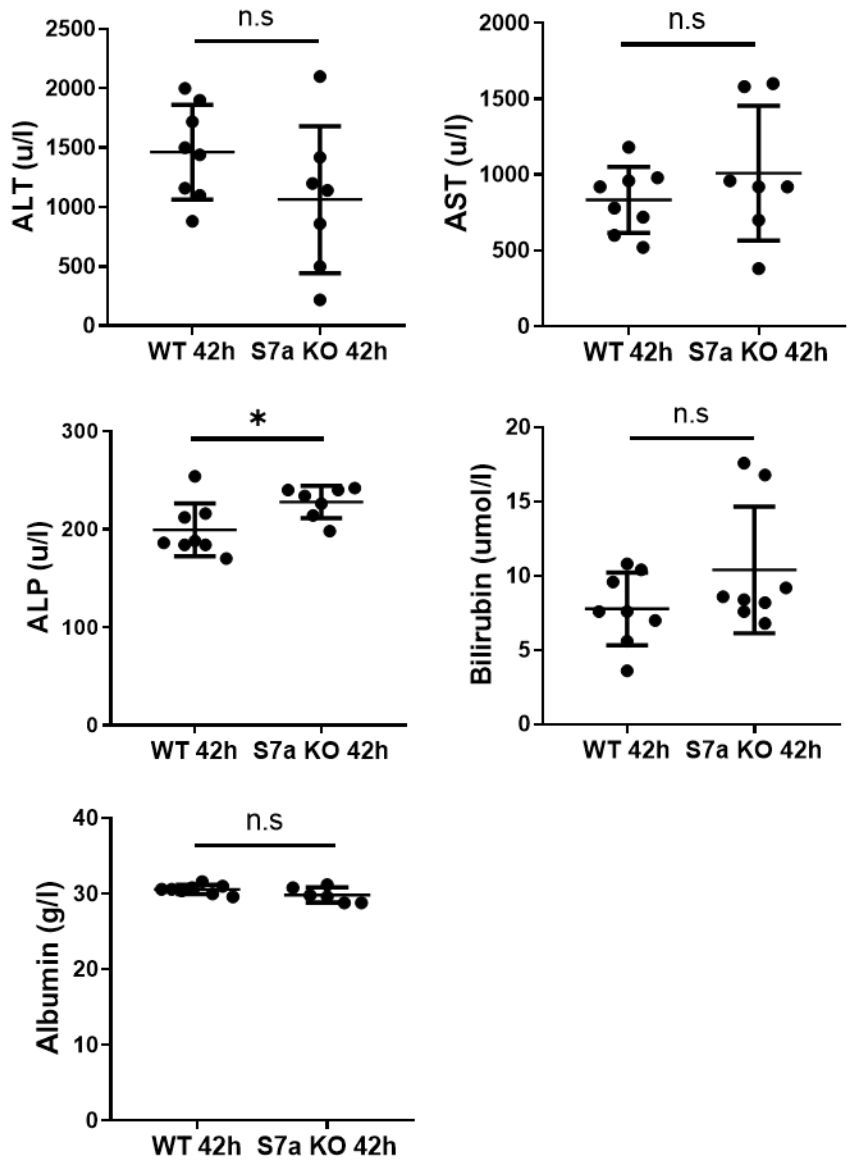

Figure 4. 7

Serum biochemical markers for liver function in WT and Sema7a KO mice treated with 350mg/kg APAP for 42 hours
Alanine transaminase (ALT), aspartate transaminase (AST), alkaline phosphatase (ALP), bilirubin and albumin.
Unpaired t-test. Data from three APAP mouse experiments is shown.

Figure 4. 8 Sema7a KO mice are more sensitive to APAP injury

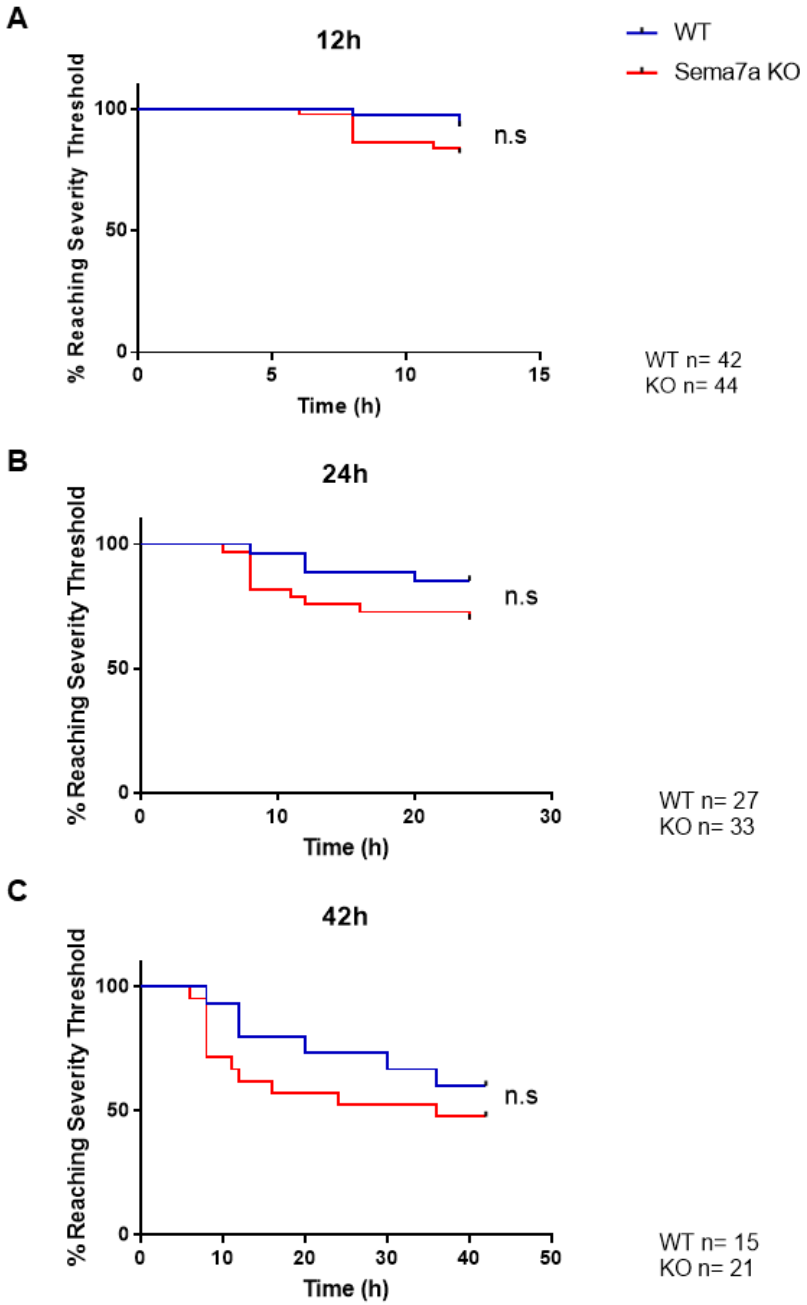

Figure 4. 8

Percentage of WT (blue) and Sema7a KO (red) mice reaching the severity threshold during 350mg/kg APAP experiments. Please not the x axis scale is different on the three graphs.

A) All mice to from all experiments to 12 hours APAP
B) Only mice taken to 24 hours and beyond, plus those humanely culled during the 12 hours APAP experiments
C) Only mice taken to 42 hours APAP, plus those humanely culled in the 12 hours and 24 hours APAP experiments.

Data from eight APAP mouse experiments is shown.

ICAM-1+ expression is unaltered with APAP injury

Microvasculature damage during APAP overdose further enhances injury [272,273]. APAP toxicity directly targets the LSECs, causing them to swell, with gaps in the sinusoidal wall being detected from two hours post APAP overdose [18,19]. This results in microvascular permeability, and extravagation of erythrocytes [20,21]. These changes can be detected before a rise serum ALTs and hepatocyte necrosis [18,272]. The breakdown and congestion of the centrilobular microvasculature causes ischemic injury and enhances oxidant stress in the liver [19].

In our APAP experiments, the Sema7a KO mice's livers are harder to perfuse. To assess if the increased susceptibility of the Sema7a KO mice to APAP injury was due to increased vascular damage, ICAM-1 expression was assessed. There was no significant difference in the number of ICAM-1+ cells between healthy WT and Sema7a KO mice or at 24 hours APAP injury. ICAM-1+ expression is upregulated by pro-inflammatory cytokines during injury to aid neutrophil and monocyte recruitment [260,274]. However, the number of ICAM-1+ cells remained constant between the WT and Sema7a KO saline and APAP treated mice (Figure 4. 9).

To assess if ICAM-1 expression is being upregulated during APAP injury, a quantitative test should be used. IHC is used to describe the location of protein expression with in a tissue, and the number of cells which express the protein of interest. However, fluorescence intensity does not directly correlate with the number of proteins expressed by a cell. Fluorescence can vary within a tissue and within a staining batch. Sources of variation within IHC include: tissue perfusion, the extent of injury (necrotic areas are always more auto-fluorescent), tissue fixation, antigen retrieval and edge effects. To quantify an upregulation in ICAM-1 expression, a quantitative analysis i.e. an ELISA for ICAM-1 should be performed. However, it will not directly answer the question of: Do Sema7a KO mice have increased vascular damage? As a loss or gain of ICAM-1+ could be contributed to a loss of ICAM-1+ LSECs, or a change in expression of ICAM-1 to recruit immune cells. Alternative methods to assess vessel permeability are the Evans blue assay, which detects extravagated albumin, or electron microscopy to assess the damage to the sinusoidal wall.

Figure 4. 9 ICAM-1 is unaffected by APAP injury or Sema7a deficiency.

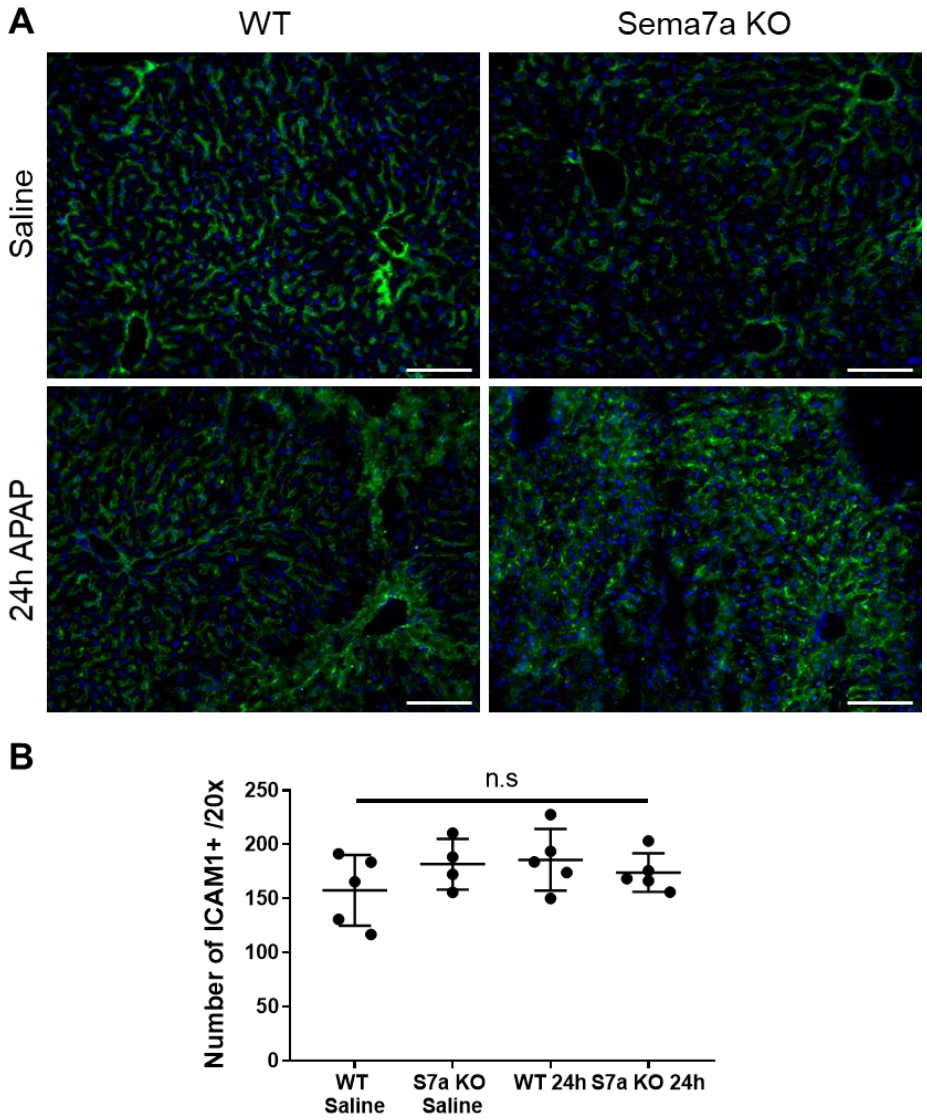

Figure 4. 9

A) ICAM-1 (green) expression on cryosections in WT (left) and Sema7a KO mice (right) treated with saline (top) and 24 hours APAP 350mg/kg treated mice (bottom). 20x images. Scale bars 100µm.

B) Number of DAPI+ ICAM-1+ cells were counted using the Perkin Elmer Operetta. Each dot represents the average number of ICAM-1+ cells per 20x field of view, per individual mouse. One-way ANOVA. No significance was detected between any of the samples.

Sema7a acts as a physical barrier during APAP injury

In the above section, I demonstrated that Sema7a deficiency resulted in increased APAP injury. In WT mice, Sema7a+ hepatocytes surround the necrosis, which suggests Sema7a acts as a barrier against the spread of necrosis. To test this, a TUNEL assay was performed to identify the localisation of necrotic and apoptotic cells.

TUNEL assays were performed on WT and Sema7a KO at 24 hours post APAP administration, when Sema7a expression is highest. Sections were scanned using the Perkin Elma Operetta. DAPI+ nuclei were identified using the Colombus software. Necrotic TUNEL+ nuclei were identified in this DAPI+ population to avoid auto-fluorescent false positives. The percentage of TUNEL+ nuclei in the DAPI+ population was then calculated.

WT and Sema7a KO mice had the same percentage of TUNEL+ nuclei, confirming the necrosis H&E analysis in Figure 4. 4. In WT mice, TUNEL+ nuclei are confined to the necrotic area. However, Sema7a KO mice had TUNEL+ nuclei in the surrounding healthy parenchyma (P= 0.0151). This data supports that peri-necrotic Sema7a+ hepatocytes act as a barrier to limit the spread of necrosis (Figure 4. 10C).

Cellular damage or stress can induce senescence. In Chapter 3, a fifth of Sema7a+ hepatocytes expressed the senescence marker p21. To test if Sema7a promotes p21 expression, or if a lack of Sema7a causes more stress induced cell cycle arrest, p21 expression was examined in WT and Sema7a KO mice. At 24 hours post APAP administration, there was no difference in the number of p21+ nuclei (Figure 4. 11A).

To assess if a lack of Sema7a+ hepatocytes causes more cell stress in the parenchyma, the frequency of p21+ nuclei in the peri-necrotic hepatocytes and healthy parenchyma was assessed. Again, there was no significant difference between the WT and Sema7a KO mice (Figure 4. 11C & D). These results demonstrate that during APAP injury, Sema7a has no influence on p21 expression, and if Sema7a is induced as part of a stress response, it is independent from p21 signalling. These results do not rule out that Sema7a influences p21 expression at another time point. Bird *et al.* performed most of their experiments at 48 hours post APAP injection [144]. In our model, Sema7a expression decreases after 24 hours post APAP administration, so it is unlikely to play a role in p21 expression at later time points.

Figure 4. 10 Sema7a limits the spread of necrosis

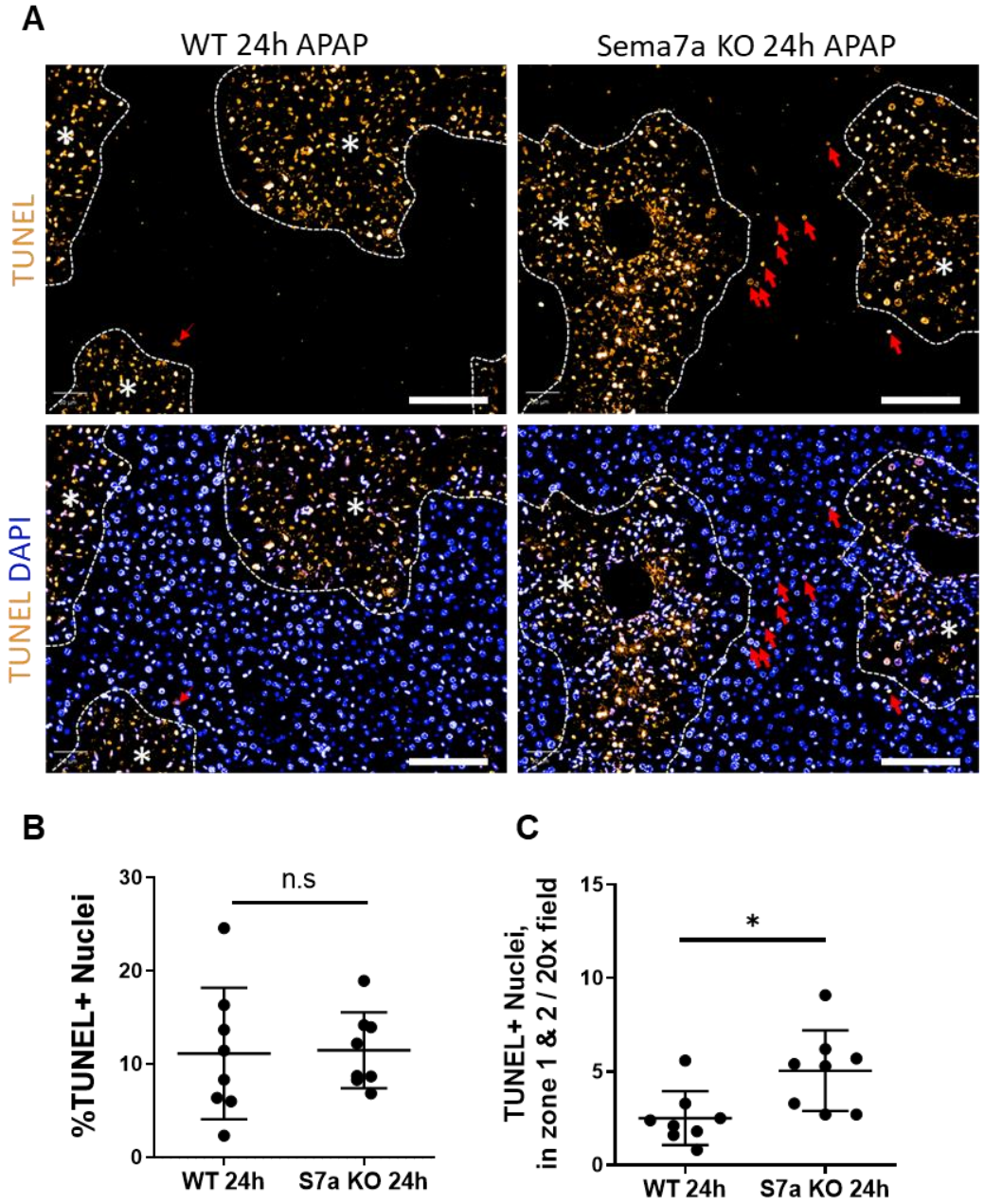

Figure 4. 10

A) TUNEL assay for necrosis (top, yellow), in WT (left) and Sema7a KO (right) mice at 24 hours 350 mg/kg APAP. Lower panels show the merged TUNEL and DAPI (blue) images. Dotted lines indicate the edge of necrosis. * label areas of necrosis. Red arrows indicate TUNEL+ nuclei outside the necrotic area. Scale bars 100 µm

B) Percentage of TUNEL+ nuclei in WT and Sema7a KO mice. N=8 for each group

C) Average number of TUNEL+ nuclei outside the necrotic area, per 10 x20 fields of view. N=8 for each group. p*<0.05

Data from three APAP mouse experiments is shown.

Figure 4. 11 Sema7a does not influence p21 expression during APAP injury

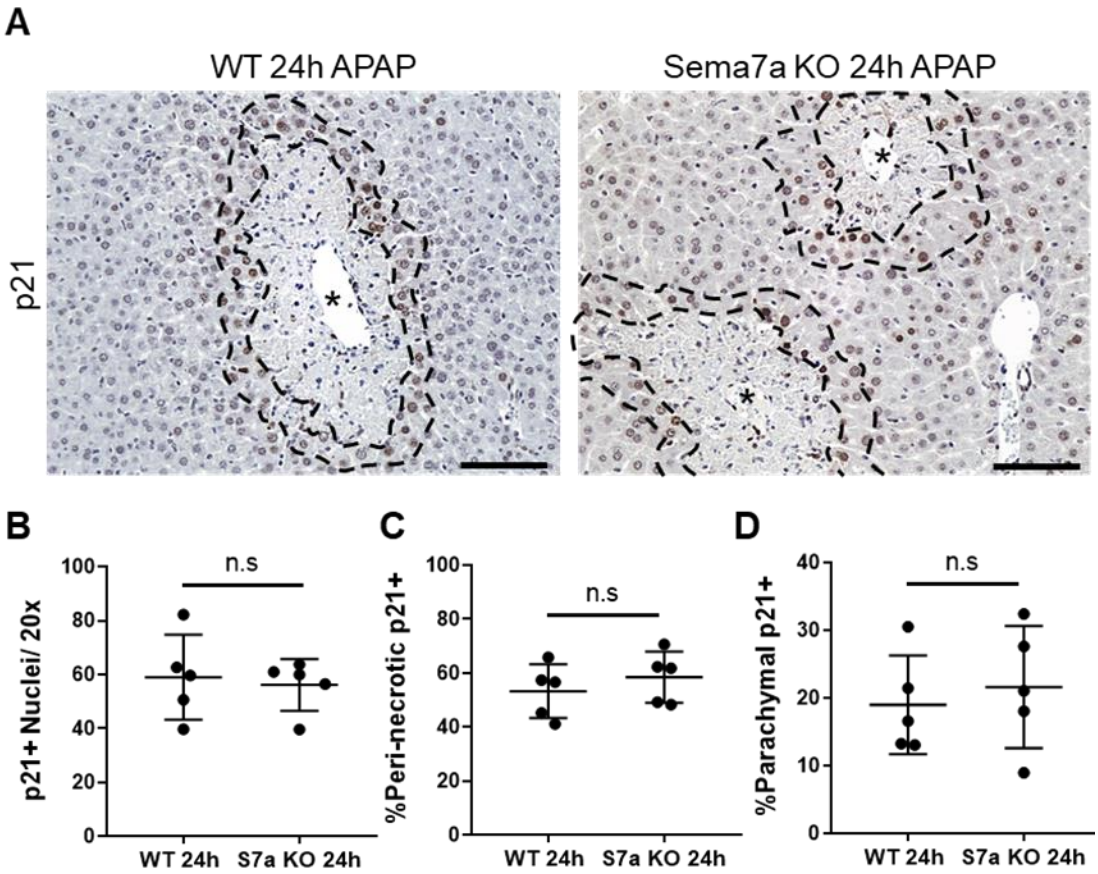

Figure 4. 11

A) p21 expression in WT (left) and Sema7a KO mice (right) at 24h 350mg/kg APAP.
B) Average number of p21 nuclei. Unpaired t test.
C) Average percentage of p21+ cells found in the peri-necrotic area (outlined in black dashes). Mann Whitney test.
D) Average percentage of p21+ cells detected outside the necrotic and peri-necrotic area. Mann Whitney test.

Percentages are of the total p21+ nuclei population, averaged from six 20x fields of view. Peri-necrotic area outlined with black dashes. * indicates necrotic area. Scale bars 100μm. Data from two APAP overdose experiments is shown.

High Mobility Group Box 1 (HMGB1) is a highly conserved protein and known DAMP. In the steady state, HMGB1 is retained in the nucleus, where it acts as a DNA chaperone to facilitate DNA transcription and binding. A lack of nuclear HMGB1 is a sign of cell stress. During injury, HMGB1 is passively released upon necrotic, but not apoptotic, cell death. In this setting HMGB1 acts as a DAMP to recruit more inflammatory cells. HMGB1 function is modulated by several post-translational modifications. Acetylated HMGB1 is actively secreted by macrophages as a cytokine, contributing to the recruitment of macrophages and dendritic cells to the site of injury [275–277]. In APAP injury, HMGB1 is released from necrotic cells as a DAMP, with serum levels of HMGB1 correlating with severity of APAP injury [278]. Neutralizing HMGB1 with an antibody or deleting hepatic HMGB1, reduces APAP induced necrosis and inflammation [53,279].

As Sema7a KO mice have more injury, and appear to have more infiltrating mononuclear cells, I questioned if HMGB1 was being released from the nucleus to promote inflammation. At 24 hours post APAP overdose, HMGB1 remains in the nuclei of hepatocytes in WT mice. In the Sema7a KO mice, the peri-necrotic hepatocytes which would express Sema7a consist of significantly more HMGB1 negative nuclei (P= 0.0058) (Figure 4. 12). This suggests without Sema7a, the peri-necrotic hepatocytes are more stressed or injured, and possibly secrete HMGB1 to promote inflammation.

Further work is needed to define the role of HMGB1 in this setting. For example, serum levels of HMGB1 could be measured in the WT and Sema7a KO mice during APAP injury. Oxidation and acetylation states of HMGB1 in the liver could be examined using mass spectrometry. *In vitro*, hepatocytes could be isolated from WT and Sema7a KO mice, and treated with APAP and the media analysed for HMGB1 secretion. The effects of this conditioned media on macrophages could then be explored. *In vivo*, mice with a hepatic deletion for HMGB1 could be bred with the Sema7a KO mice to see if the non-nuclear HMGB1 promotes inflammation. However, these experiments are outside the scope of my project.

Figure 4. 12 HMGB1 becomes cytoplasmic in peri-necrotic hepatocytes in Sema7a KO mice

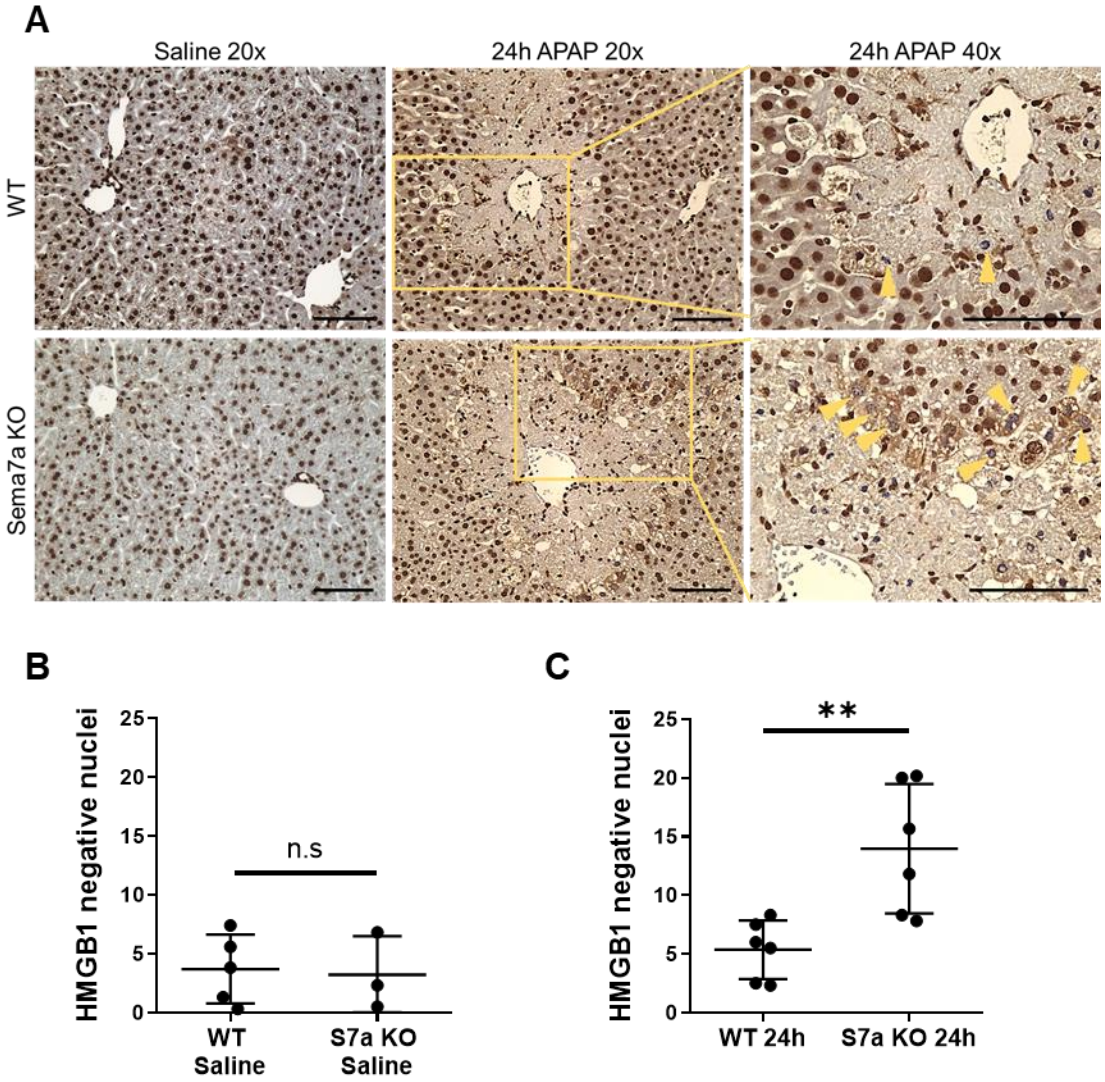

Figure 4. 12

A) HMGB1 staining in saline (left, 20x) or 24 hours APAP (right, 20x and 40x) treated WT (top) and Sema7a KO (bottom) mice. 40x images taken from inset yellow boxes. Yellow arrows indicate HMGB1 negative nuclei.

Representative images shown.

B) Average number of HMGB1 negative nuclei in saline treated mice.

C) Average number of HMGB1 negative nuclei in WT and Sema7a KO mice at 24 hours post APAP administration.

Scale bars 100 µm. Unpaired t-test. *p<0.05. **p<0.01. Data from two APAP overdose experiments is shown.

Sema7a receptor expression in Sema7a KO mice

To examine if Sema7a expression on hepatocytes regulates receptor expression, the expression of Integrin β1 and Plexin C1 was assessed in the liver. *Integrin β1* mRNA expression was not significantly different between WT and Sema7a KO mice treated with saline or at 24 hours post APAP injury. However, *Integrinβ1* was elevated in Sema7a KO mice at 24 hours APAP injury compared to their healthy counterparts (P=0.0427), suggesting a slightly increased *Integrin β1* transcription at 24 hours post APAP injection compared to healthy Sema7a KO mice (Figure 4. 13A). At the protein level, WT and Sema7a KO had the same ubiquitous Integrin β1 expression pattern, and the same area of Integrin β1 positivity in both healthy mice and at 24 hours post APAP administration (Figure 4. 13).

Plexin C1 is expressed at comparable levels in the WT and Sema7a KO mice, in healthy mice and 24 hours post APAP injury. At the protein level, Plexin C1 has the same morphological pattern, and area of Plexin C1 positivity in saline, 12 hours and 42 hours APAP treated WT and Sema7a KO mice. At 24 hours post APAP overdose, there is significantly less Plexin C1 in Sema7a KO mice (P= 0.0208, Figure 4. 14). This data implies that Sema7a promotes PlexinC1 expression in HSCs at 24 hours post APAP administration.

In Chapter 3, I showed that Plexin C1 is expressed on vimentin+ HSCs. To ensure the reduction in Plexin C1 expression is not due to a reduction in HSCs, I compared vimentin expression in WT and Sema7a KO mice. In healthy mice and at 24 hours post APAP overdose, the area of vimentin expression is the same in WT and Sema7a KO mice (Figure 4. 15). Therefore, the reduction in Plexin C1 expression is due to a deficiency of Sema7a. This should be confirmed with a quantitative assay.

During this analysis, I observed that mice with less necrosis at 42 hours post APAP administration had visibly more intact elongated Plexin C1+ HSCs in the remaining necrotic area. This should be quantified by analysing the morphology of vimentin+ HSCs at 42 hours post APAP overdose and correlating it with necrosis. Potentially, these elongated HSCs are secreting ECM factors to aid tissue regeneration. Additional analysis could compare the production of ECM factors. Sema7a has been shown to promote collagen deposition and during chronic liver and lung injury [246,247]. It would be interesting to see if ECM remodelling that is required for tissue regeneration is altered in the Sema7a KO mice.

Figure 4. 13 Integrin β1 expression is unaffected in Sema7a KO mice

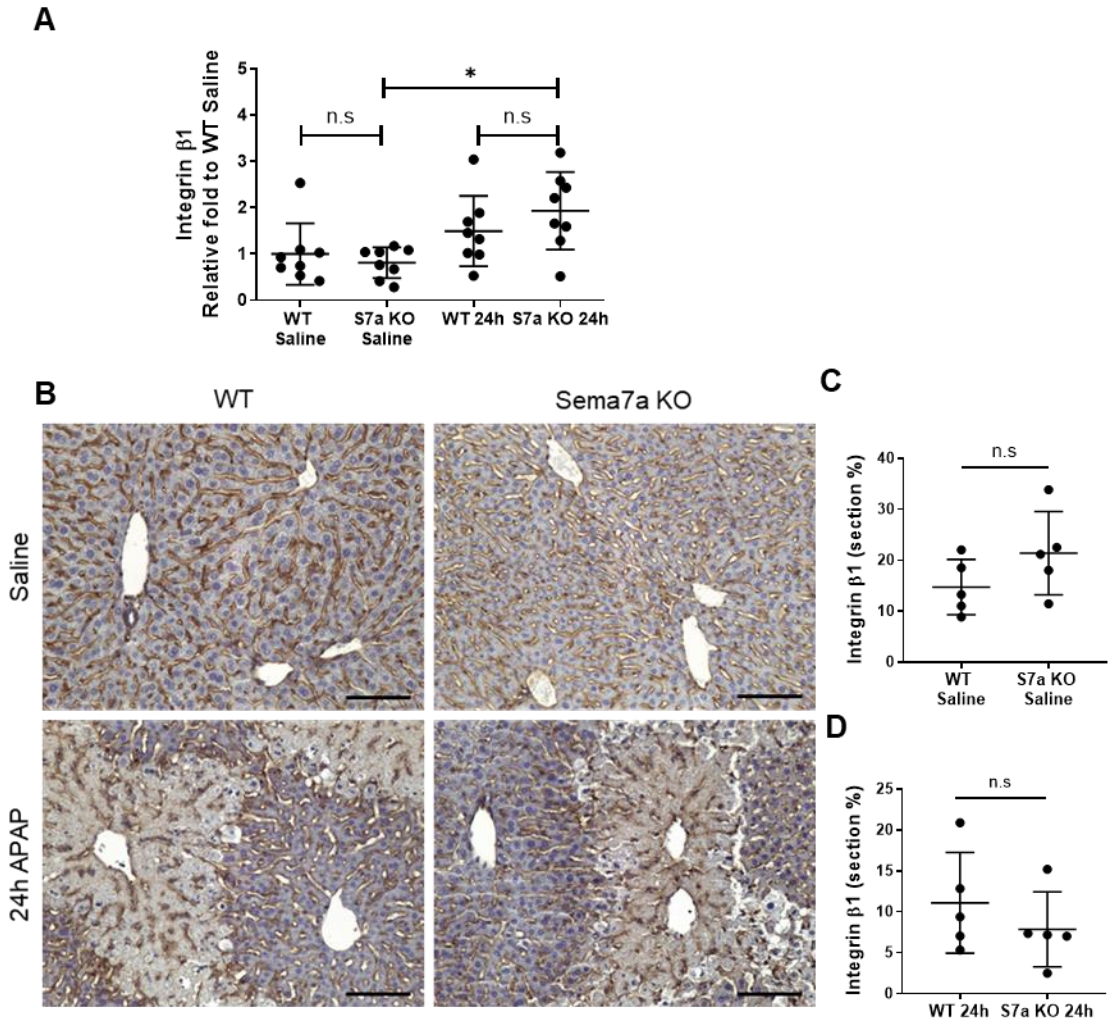

Figure 4. 13

A) mRNA expression of *Integrin β1* in WT and Sema7a KO in whole liver lysate, treated with saline or at 24 hours post APAP administration, relative to WT saline treated mice. Kruskal-Wallis test, Dunn's multiple comparison test. Sema7a KO saline vs, Sema7a KO 24 hours post APAP P=0.0427
B) Integrin β1 staining in saline treated (top) and at 24 hours post APAP administration (bottom) treated WT (left) and Sema7a KO (right) mice. Representative images shown.
C) Average area of Integrin β1 positivity in saline treated mice.
D) Average area of Integrin β1 positivity in WT and Sema7a KO mice at 24 hours post APAP administration

Scale bars 100 µm. Data from three APAP overdose experiments is shown Unpaired t-test, unless otherwise stated. *p<0.05

Figure 4. 14 Plexin C1 expression is reduced in Sema7a KO mice at 24 hours post APAP overdose

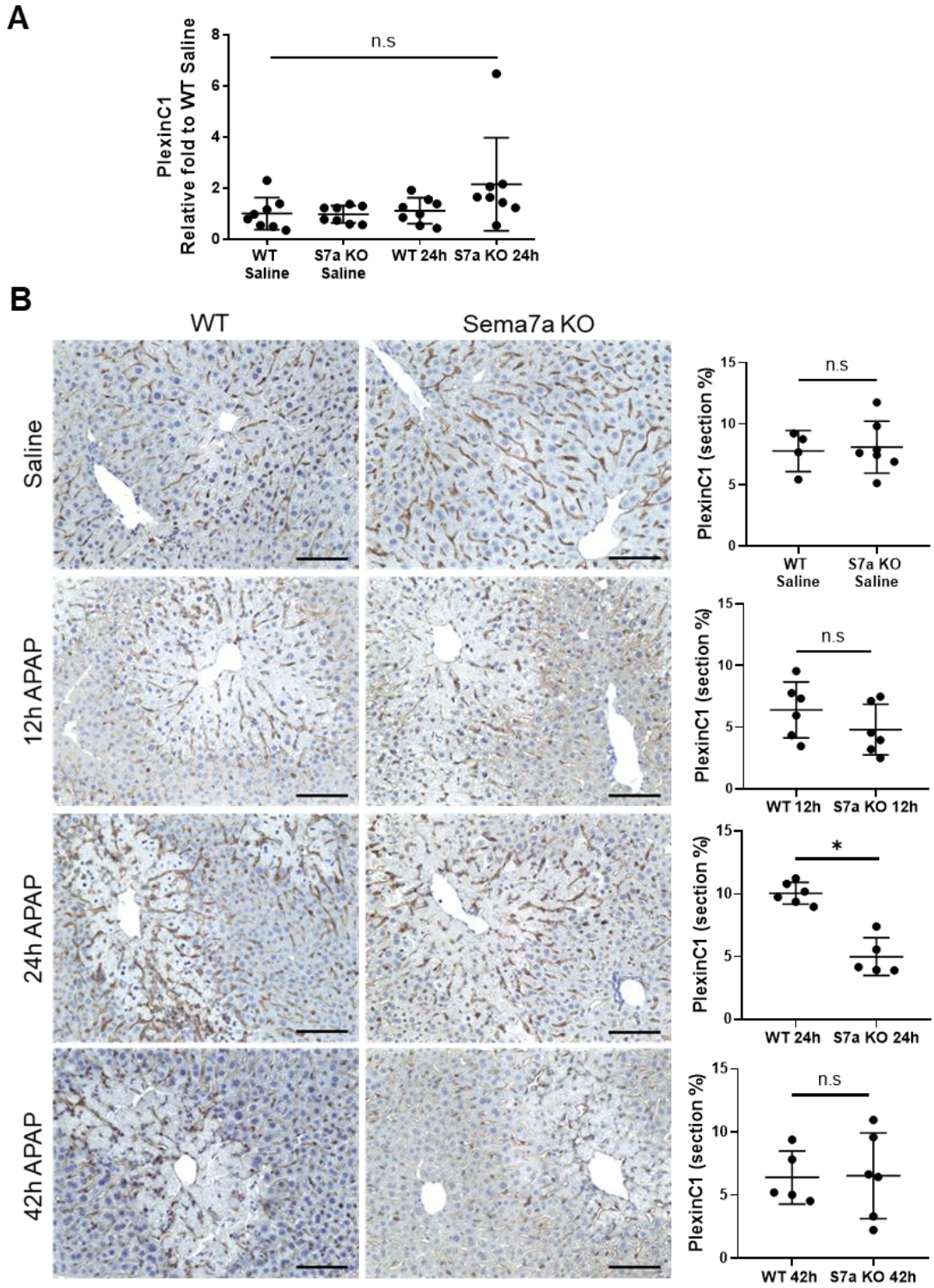

Figure 4. 14

A) *PlexinC1* mRNA expression in whole liver lysate from WT and Sema7a KO mice treated with saline or at 24 hours post APAP overdose. Kruskal-Wallis test.
B) Plexin C1 expression in WT (left) or Sema7a KO mice (centre) treated with saline (top row), 12 hours (second row), 24 hours (third row), or 42 hours (bottom row) post APAP injection.

Scale bars 100 µm. Data from eight APAP experiments is shown. Unpaired t-test, unless otherwise stated. *p<0.05

Figure 4. 15 Vimentin expression is unchanged in Sema7a KO mice

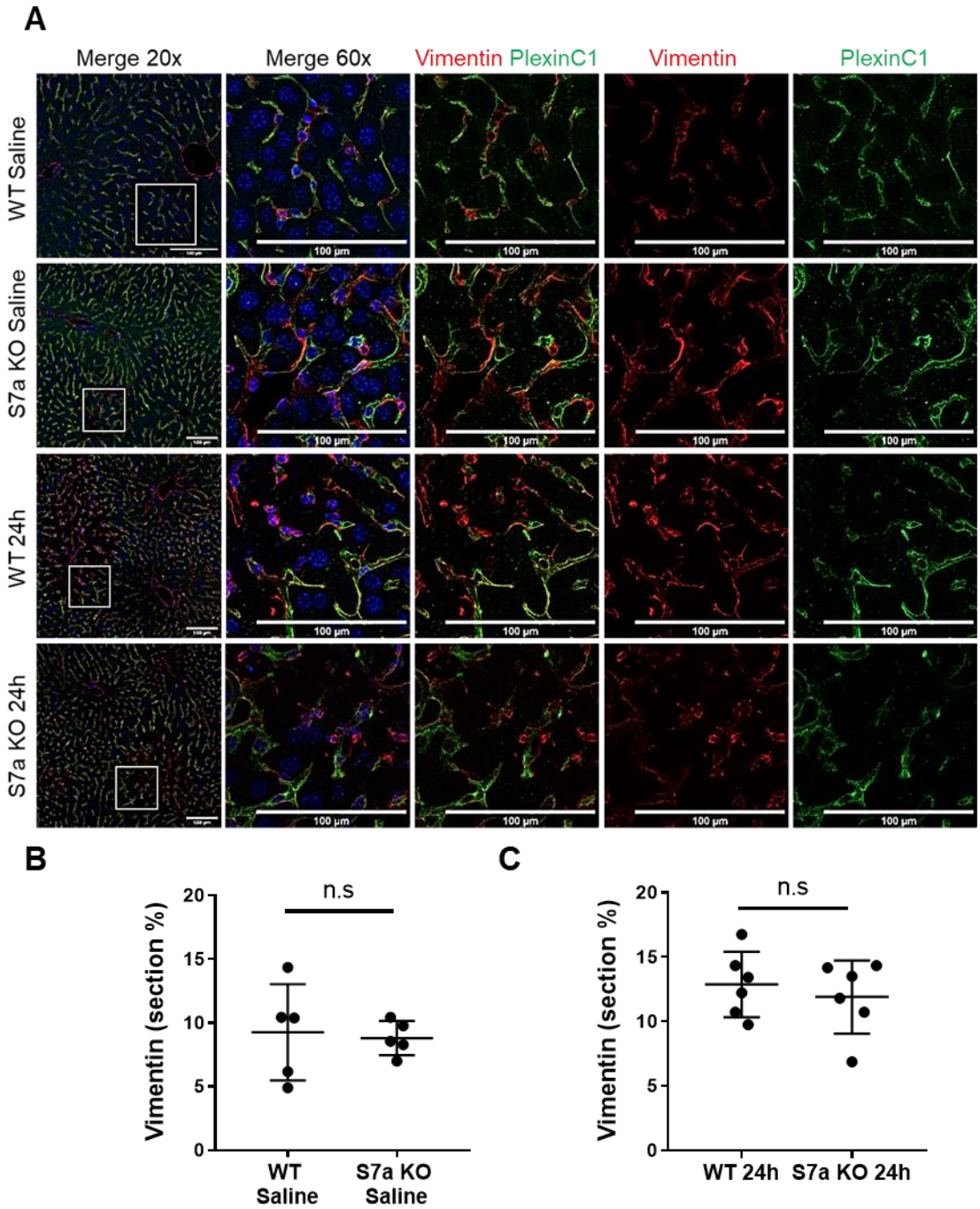

Figure 4. 15

A) Confocal images of Vimentin (red, HSC marker), and Plexin C1 (green) expression with DAPI (blue) in WT and Sema7a KO mice treated with saline (top two rows) or 24 hours APAP (bottom two rows). Left column shows a representative 20x image. White boxes indicate where the 60x images on the right were taken from. Scale bars 100 µm.

B) Average percentage area of vimentin expression in saline treated mice

C) Average percentage area of vimentin expression in WT and Sema7a KO mice treated at 24 hours post APAP administration

Unpaired t-test. Data from two APAP experiments is shown.

Sema7a signalling pathways are not upregulated

Sema7a signalling is predominantly mediated by the p-FAK, p-AKT and p-ERK pathway [209,217,218,246]. In a model of rheumatoid arthritis, ADAM-17 cleaves Sema7a to promote the secretion of pro-inflammatory cytokines from macrophages [232]. Sema7a can also promote TGFβ signalling and expression through a SMAD2/3 independent pathway [246,247]. I questioned if a lack of Sema7a and the subsequent downregulation of Plexin C1 in HSCs was accompanied by a reduction in downstream Sema7a signalling in Sema7a KO mice. These signalling factors were examined in whole liver lysate at 24 hours APAP post overdose with qRT-PCR, but no significant difference was detected between the WT and Sema7a KO mice (Figure 4. 16).

Ideally protein expression of TGFβ and TGFβR1 and protein phosphorylation states of FAK, AKT and ERK should be examined by a western blot to compare the activation of signalling pathways in the WT and Sema7a KO mice. However, due to the technical challenges in detecting temporary phosphorylation states of proteins at a low concentration in the whole liver lysate, I was unable to obtain a clean western blot. I tried to detect both TGFβ and TGFβR1 by IHC. Unfortunately, there is not a working antibody for TGFβ, and I could not optimise the TGFβR1 stain on my sections.

Figure 4. 16 Sema7a signalling genes are unaffected in Sema7a KO mice.

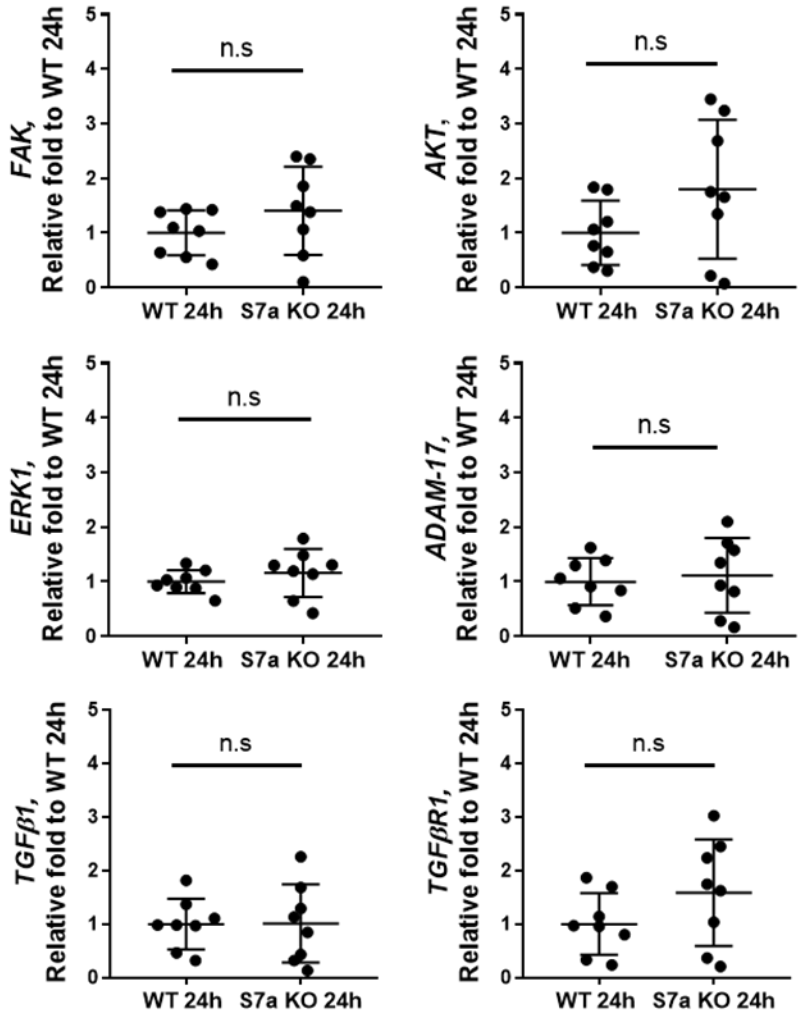

Figure 4. 16
mRNA expression of the indicated genes in whole liver lysate from WT and Sema7a KO mice at 24 hours post 350 mg/kg APAP administration, relative to WT mice. Data from three APAP experiments is shown. Unpaired t-test.

Sema7a does not directly promote proliferation

To recover from APAP injury, the remaining hepatocytes must proliferate to restore the parenchyma. To see if Sema7a had a role in recovery from APAP injury, proliferating cells were labelled with BrdU. At 42 hours post APAP overdose, Sema7a KO mice had the same levels of proliferation as the WT mice (Figure 4. 17) and area of necrosis (Figure 4. 4), indicating that hepatocyte proliferation from APAP injury is not affected by a Sema7a deficiency.

In Chapter 3, I assessed Sema7a expression in the highly proliferative partial hepatectomy (PHx) model. In this model 70% of the liver is surgically removed. The remaining liver mass enters hyperplasia, so that by one week post PHx, the liver mass is restored [146]. Sema7a was not detected in this model, confirming Sema7a is not required for hepatocyte proliferation. Sema7a may indirectly promote liver regeneration after APAP injury by preventing the spread of damage, or by influencing immune cells to phagocytose or to release anti-inflammatory cytokines, which promote recovery.

To be completely certain that Sema7a does not have a role in recovery from APAP injury, necrosis and inflammation in Sema7a KO mice should be assessed at 72 hours and at one week post APAP injection, in comparison to WT mice. By one week post APAP overdose, WT mice will have recovered from APAP injury. Any lingering necrosis or inflammation will indicate that Sema7a KO mice have not recovered, and Sema7a is therefore required for the resolution of APAP injury. These experiments were not possible due to lack of mice.

Figure 4. 17 WT and Sema7a KO mice have the same frequency of proliferation

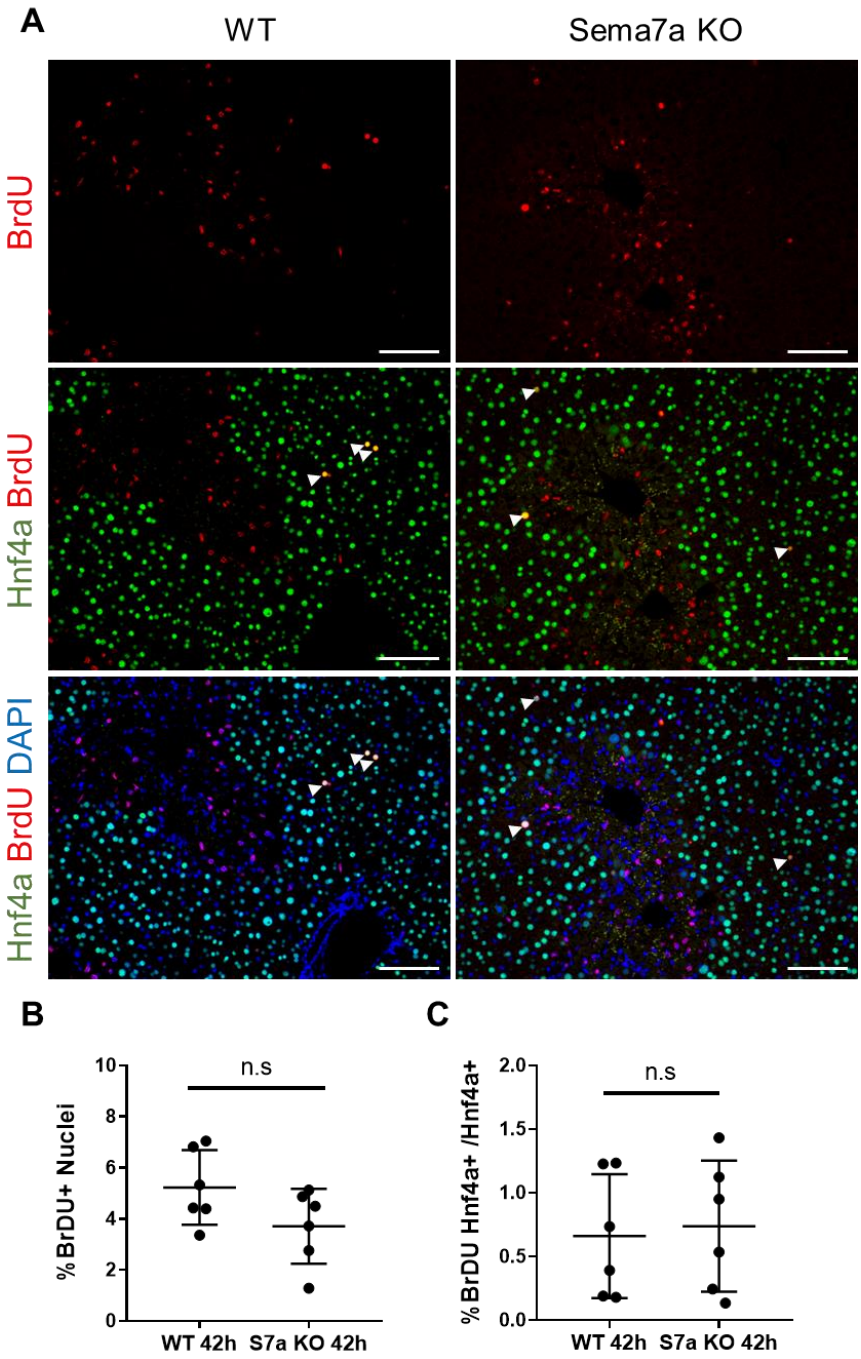

Figure 4. 17

A) Dual stain for BrdU (red) and Hnf4a (green), dual positive yellow, in WT (left) and Sema7a KO (right) mice at 42 hours post APAP injection
B) Percentage of BrdU+ nuclei in WT and Sema7a KO mice
C) Percentage of dual positive Hnf4α and BrdU hepatocytes

Images were quantified using the Columbus software. Scale bars 100μm. Data from three APAP experiments is shown.

Discussion

Centrilobular necrosis is a hallmark for APAP injury. In severe APAP injury, the necrosis spreads across the liver and results in acute liver failure. In our moderate APAP injury model, Sema7a is expressed on peri-necrotic hepatocytes, which contain TUNEL+ nuclei to the centrilobular necrotic area. In Sema7a KO mice TUNEL+ nuclei were detected in the healthy parenchyma. This demonstrates Sema7a+ hepatocytes act to limit the spread of necrosis.

The Sema7a KO mice had more necrosis at 12 hours post APAP injection, elevated LFTs throughout the APAP time course and were more susceptible to APAP injury, compared to WT mice. In addition, Sema7a KO mice had peri-necrotic hepatocytes with non-nuclear HMGB1 expression, indicative of increased cellular stress at 24 hours post APAP injury. Together, this data shows that Sema7a acts to prevent the spread of necrosis and reduces APAP injury.

To the best of our knowledge, this is the first study investigating the role of Sema7a during APAP injury. To ensure the mice with Sema7a constitutively removed did not have an underlying defect, which would affect their response to APAP, I compared healthy WT and Sema7a KO mice. Histology and liver function were similar. In addition, expression of: Cyp2e1, vimentin, HMGB1, ICAM-1 and the Sema7a receptors Plexin C1 and Integrin β1 were the same in healthy Sema7a KO and WT mice. Therefore, any differences between the WT and Sema7a KO mice during APAP injury are due to a lack of Sema7a+ hepatocytes, or possibly Sema7a on infiltrating immune cells, as Sema7a is constitutively removed [176].

TUNEL+ cells were detected in the healthy parenchyma of Sema7a KO mice. The exact mechanism of how this occurs requires further investigation. One possible reason is that Sema7a on hepatocytes binds to Plexin C1 and Integrin β1 on the HSCs to form a physical barrier against the spread of ROS. Without this barrier the integrity is compromised allowing toxic solutes and ROS to spread into the surrounding parenchyma. To test this theory, I tried to compare the location and spread of oxidative stress in the WT and Sema7a KO mice. Due to the instability of ROS, it is difficult to assess their exact location in tissue using IHC. Nitric oxide formed during APAP injury reacts with superoxide to form peroxynitrite, which nitrates tyrosines found in proteins, DNA and lipids to form 3-nitrotyrosine (3-NT) [16]. 3-NT can therefore be used to assess oxidative stress during injury. I attempted to assess the localisation

of 3-NT in Sema7a KO mice, compared to WT mice. Unfortunately, I could not get a successful 3-NT IHC stain.

APAP toxicity has also been suggested to spread through decreased tight junctions or gap junctions. Integrin β1 forms tight junctions with collagen on the ECM and controls epithelial polarity [280]. During APAP injury these tight junctions become disrupted in a dose dependant manner [127,128]. Although the authors did not demonstrate if this could lead to enhanced APAP injury or the spreading of toxicity.

Connexions (Cx) form gap junctions which allow the passage of solutes between cells. In the liver the main Cx is Cx32 [136]. During APAP injury, Cx32 can transmit toxic APAP solutes between cells, increasing liver injury in mice. Genetic deletion or using a the 2-ABP small inhibitor of Cx32 prevents the spread of APAP induced necrosis [137]. *In vitro*, deletion of the Cx32, Cx26 gap junction in coupled hepatocytes prevented synchronised necrotic cell death. Furthermore, coupling female hepatocytes which are naturally resistant to APAP toxicity, to male hepatocytes, which are more susceptible to APAP toxicity, prevented cell death of the male hepatocyte [140]. Cx43 is upregulated during APAP injury, and Cx43 $^{+/-}$ mice had elevated ALT and increased IL-1β and TNFα secretion at 24 hours post APAP injury, suggesting Cx43 protects against APAP injury [141]. Semaphorins are known actin modulators. The actin cytoskeleton transports de novo Cx43 channels from the Golgi to the plasma membrane [281], and stabilises the gap junction formation [131]. Potentially, Sema7a mediates the formation of Cx43 channels to reduce the spread of necrosis during APAP injury.

My second aim for this chapter is that Sema7a promotes the expression of its receptors. In Sema7a KO mice, Plexin C1 expression was significantly reduced at 24 hours post APAP administration. This suggests that Sema7a upregulates Plexin C1 expression in HSCs at peak APAP injury, although this is not seen at the transcript level. Integrin β1 and Plexin C1 expression were unaltered at other time points of APAP injury.

Sema7a signalling regulates the cytoskeleton through Plexin C1 and Integrin β1 to control a delicate balance between cellular adhesion and deadhesion [209]. Cofilin depolymerises F-actin at the slow growing end of the actin filament, providing new actin monomers for polymerization, facilitating cell motility. Cofilin is inhibited by phosphorylation by LIMK I and II [214,215]. In melanocytes, Sema7a signalling through

Integrin β1 and p-FAK causes actin polymerisation and melanocyte spreading [209,217]. Whereas Sema7a - Plexin C1 - LMKII signalling results in the inactivation of cofilin and prevents melanocyte and dendritic cell spreading and adhesion [216–219].

Potentially, Sema7a - Plexin C1 prevents HSCs actin remodelling and spreading during APAP injury. If this were true, Sema7a KO mice would have more elongated HSCs than WT mice, at 24 hours APAP injury. However, as the area of vimentin remained the same in the WT and Sema7a KO mice, this is unlikely to be the mechanism of action.

Sema7a signalling via Plexin C1 and Integrin β1 modulates the actin cytoskeleton, or cytokine secretion from immune cells through p-FAK, p-AKT and p-ERK [209,217,218]. Sema7a can also promote TGFβ signalling and expression through p-FAK and p-AKT in activated HSCs during chronic liver injury [246]. There was no significant difference in the mRNA expression of *FAK, AKT, ERK, TGFβ1* or *TGFβR1* between WT and Sema7a KO mice at 24 hours post APAP administration. Mechanistic studies which examine the protein expression and phosphorylation states of these signalling factors are needed to elucidate the actions of Sema7a signalling during APAP injury.

Sema7a KO mice may have elevated HMGB1 signalling. At 24 hours post APAP overdose, Sema7a KO mice had peri-necrotic hepatocytes with non-nuclear HMGB1 expression, which is indicative of increased cell stress. Active secretion of acetylated HMGB1, or the passive release of HMGB1 by necrotic cells as a DAMP, promotes inflammation [275,276]. In APAP injury, serum HMGB1 correlates with injury [278] and hepatocyte HMGB1 signalling promotes neutrophil infiltration [53]. As Sema7a KO mice have more injury, it is likely they will have elevated serum levels of HMGB1, but this remains to be examined. Sema7a KO mice appeared to have more infiltrating immune cells during APAP injury. A potential theory is that without Sema7a+ hepatocytes to limit the spread of necrosis, the peri-necrotic hepatocytes become more stressed, which results in the secretion of HMGB1, which promotes neutrophil infiltration. The effects of Sema7a in the innate immune system will be investigated in Chapter 5.

Cell cycle arrest, or senescence, is induced in times of cellular stress [143]. Previously, TGFβ signalling been shown to induce cell cycle arrest in peri-necrotic hepatocytes [144]. Sema7a has previously been shown to promote non-canonical TGFβ signalling through a positive feedback loop [246,247]. In Chapter 3, a fifth of the Sema7a+ hepatocytes also expressed p21. Sema3a is now recognised as a senescence marker

[145]. To see if Sema7a could induce cell cycle arrest during APAP injury, p21 expression was examined, however, there was no significant difference WT or Sema7a KO mice. This implies Sema7a does not promote p21 expression. If Sema7a is part of a cell stress response, it is an independent mechanism to the cell cycle arrest pathway.

The final aim for this chapter is that Sema7a promotes hepatocyte proliferation. Proliferative cells were labelled with BrdU. The frequency of BrdU+ nuclei and BrdU+ hepatocytes were not significantly different in the Sema7a KO mice compared to WT mice at 42 hours post APAP administration, showing Sema7a does not have a role in proliferation. The area of necrosis at 42 hours was also the same in the WT and Sema7a KO mice, but Sema7a KO mice have raised ALP levels, suggesting some ongoing damage. Therefore, Sema7a may have an indirect effect in recovery by limiting the spread of damage or by influencing the immune system. To investigate this further Sema7a KO mice should be compared at later time points e.g. 72 hours and one week post APAP administration, to ensure the Sema7a KO mice are completely recovered with no lingering necrosis or inflammation.

To summarise, I have shown a novel role of Sema7a to act as a barrier to necrosis. At 24 hours post APAP overdose, Sema7a is expressed by peri-necrotic hepatocytes, and upregulates Plexin C1 expression. In Sema7a KO mice TUNEL+ necrotic cells are detected in the healthy parenchyma. In addition, a deficiency of Sema7a in the peri-necrotic hepatocytes caused them release HMGB1 from their nuclei, presumably as a stress signal to enhance inflammation. The expression of the cell cycle arrest marker, p21, was not affected in Sema7a KO mice. At 12 hours post APAP overdose Sema7a KO mice have more necrosis. Throughout the APAP time course, Sema7a KO mice had elevated LFTs and were more likely to succumb to APAP injury. Signifying Sema7a has a protective role during APAP injury. During recovery from APAP injury, Sema7a does not have a role in hepatocyte proliferation. However, Sema7a may indirectly influence recovery from APAP injury by preventing the spread of necrosis or influencing inflammation. The next chapter investigates the role of Sema7a in inflammation during APAP injury.

Chapter 5 – Sema7a aids the innate immune system during APAP injury

Introduction

Sema7a deficiency resulted in increased susceptibility to APAP toxicity. Sema7a KO mice had raised LFTs and necrosis at both 12h and 24h post APAP administration, compared to WT mice (Chapter 4). At 24 hours post APAP overdose, TUNEL+ nuclei were detected outside the necrotic area, and HMGB1 negative nuclei were detected in peri-necrotic hepatocytes in Sema7a KO mice. Both events were absent in the WT mice. This suggests that Sema7a+ hepatocytes act as a barrier to contain the spread of necrosis. In Sema7a KO mice, there was an observed increase in the number of small mononuclear cells infiltrating the necrotic area (Chapter 4). This chapter examines the role of Sema7a in inflammation during APAP injury.

Inflammation has both beneficial and detrimental roles during APAP injury. Neutrophils are the first responders to injury in the innate immune system [91]. They are recruited to the liver during APAP injury by DAMPs including HMGB1 and formylated peptides, and cytokines including CXCL1 [52,53,111,282]. The exact role of neutrophils in APAP are unknown. It was originally suggested that neutrophils are detrimental during APAP, as they can release hydrolytic and oxidative enzymes, ROS and NETs, which can cause collateral damage to the tissue [91,110]. However, studies which depleted neutrophils, or blocked their recruitment [60,116], or genetically prevented their ability to release ROS [59,60] showed no protection against APAP injury. Recently, neutrophils have been shown to promote recovery from APAP by secreting ROS to switch monocytes and macrophages to from the Ly6C^{hi} pro-inflammatory phenotype to the Ly6C^{lo} restorative phenotype [60].

Macrophages are professional phagocytes, responsible for phagocytosing cellular debris. Kupffer cells (KCs) become depleted during APAP injury [48,49]. Monocytes infiltrate the injured liver and mature into monocyte derived macrophages and become the dominant hepatic macrophage [48]. Resident and infiltrating macrophages initially have a pro-inflammatory phenotype and release TNFα, IL-6, IL-1a and IL-18 to activate and recruit the innate immune system [4,45]. TNFα also acts to prime hepatocytes for apoptosis, enhancing hepatocyte loss [4]. To reduce the initial wave of inflammation, macrophage depletion studies with liposomal clodronate [61,62] or gadolinium chloride have been performed [55,56]. Macrophage depletion was initially beneficial, but delayed or prevented recovery [21,51]. During recovery, macrophages switch to an anti-inflammatory, pro-restorative phenotype. What initiates this switch is

unknown. Pro-restorative macrophages phagocytose debris, secrete cytokines including IL-10, to reduce inflammation, and promote hepatocyte proliferation by secreting IL-6 and TNFα [34,72,81,84,85].

There is potentially a third macrophage population in the liver during injury. In a model of sterile thermal injury, F4/80+ GATA6+ peritoneal macrophages infiltrated the liver, dismantled necrotic nuclei and promoted regeneration [71]. It is so far unknown how peritoneal macrophages contribute to APAP injury and recovery.

Sema7a has been previously shown as a chemoattractant for monocytes, macrophages and dendritic cells [228–230], mediates neutrophil transmigration across an endothelial barrier [211] and modulates macrophage behaviour in a receptor dependant manner. If macrophages bind to Sema7a on intestinal epithelial cells through their Integrin αvβ1 receptor, they secrete the anti-inflammatory cytokine IL-10 [236]. Equally, if macrophages bind to Sema7a on T cells via their Integrin α1β1 receptor, they secrete the pro-inflammatory cytokines TNFα and IL-6 [231]. *In vivo*, Sema7a KO mice have less PMNs infiltrating the lungs in an acute LPS inhalation model [212], and less CD45+ cells and F4/80+ macrophages in the liver after chronic CCl_4 liver injury [246]. However, after in TGFβ induced pulmonary fibrosis, inflammation was not effected in Sema7a KO mice [247].

In dendritic cells, Sema7a- Plexin C1 signalling prevents cytoskeletal rearrangements required for dendritic cell adhesion, spreading, migration and phagocytosis [218,230]. The herpes and vaccinia poxvirus use this to their advantage. They produce structural Sema7a mimic, which binds to Plexin C1 on dendritic cells. This prevents the dendritic cell from phagocytosing the virus, allowing the virus to thwart the immune system [218,219,239].

It is currently unknown how Sema7a regulates the immune system during APAP injury. Given previous findings, that Sema7a can facilitate neutrophil transmigration across an endothelial barrier, act as a chemoattractant for monocytes and modulate macrophage cytokine secretion. I hypothesise that Sema7a promotes inflammation during APAP injury.

In Chapter 3, F4/80+ macrophages were detected adjacent to the Sema7a+ hepatocytes at 24 hours post APAP overdose, suggesting an interaction between these cells. Specifically, this chapter aims to describe how a deficiency of Sema7a affects the number of F4/80+ macrophages and neutrophils present in the liver, and

their localisation. I will also compare the relative frequencies of macrophages, monocytes and neutrophils systemically, by assessing these population in the blood and peritoneal lavage. Lastly, we examine if Sema7a is required for phagocytosis during APAP injury.

Some of the *in vivo* experiments performed in this chapter required a collaborative effort. The use of 'we' indicates a team effort, with the deserved recognition in the respective figure legend. I performed all IHC staining, imaging and quantification; RNA isolation from the liver and subsequent qRT-PCR; BMDM isolation, differentiation and analysis; protein extraction and quantification; flow cytometry staining and analysis on blood, BMDMs and peritoneal exudate cells. Rhona Aird performed the F4/80 IHC. Jennifer Cartwright helped with staining the APAP time course for Ly6G and the subsequent counting of Ly6G+ cells. The MSD V-Plex was run in conjunction with Philip Starkey Lewis. Tail nicks were performed by Janet Man. APAP experiments were either performed solely by myself, or with help from Jennifer Cartwright or Lara Campana. Jennifer Cartwright performed the liver digest, staining and sample analysis for flow cytometry. Fiona Rossi helped set up the flow cytometry panels and checked the compensation. I performed the subsequent analysis on all flow cytometry data, with technical advice from Lara Campana. Lara Campana also provided technical advice for the *in vitro* and *in vivo* phagocytosis experiments. Technical assistance for confocal imaging was obtained from Matthieu Vermeren.

All data presented was assessed for normality. If required, a Welch test was applied to correct for unequal variances between samples. Each dot represents an individual mouse.

Results

In Chapter 4, Sema7a KO mice appeared to have more small mononuclear cells infiltrating the APAP induced necrotic areas. To test this, the expression of CD45+, a leukocyte marker, was analysed in WT and Sema7a KO mice by flow cytometry and immunofluorescence at 24 hours post APAP overdose. In Figure 5. 1A, CD45+ cells are seen gravitating towards the necrotic area. In both analyses, the frequency of CD45+ cells is the same in the WT and Sema7a KO mice at 24 hours post APAP overdose (Figure 5. 1).

Sema7a KO mice have less F4/80+ macrophages at 12 hours APAP overdose

The CD45+ population examined in Figure 5. 1 consists of neutrophils, monocytes, macrophages, eosinophils and lymphoid cells. I questioned if a deficiency of Sema7a altered the composition of the CD45+ population in the liver during APAP injury. Specifically, we examined the localisation and population dynamics of F4/80+ macrophages during a time course of APAP injury, in WT and Sema7a KO mice. F4/80 is expressed by the resident KCs. During APAP injury, KCs become depleted. They are replaced by self-renewal [48], or by infiltrating CD11b+ F4/80^{lo} macrophages which express F4/80+ [65].

Healthy WT and Sema7a KO mice have similar levels of F4/80+ macrophages in the liver. At 12 hours post APAP overdose, the F4/80+ macrophage population becomes depleted. WT mice had an average of 71 F4/80+ macrophages per 20x field of view. Sema7a KO mice had visibly less F4/80+ macrophages (P=0.0483), with only 42 per 20x field of view, suggesting an enhanced depletion of macrophages in the Sema7a KO mice (Figure 5. 2A).

At 24 hours post APAP overdose, the F4/80+ population drastically increases, to levels above healthy mice as the infiltrating macrophages enter the liver and mature into F4/80+ macrophages (Figure 5. 2B). By this time point, the F4/80+ macrophage population in Sema7a KO mice has been restored to similar levels of WT mice, with 155 and 150 F4/80+ macrophages, per 20x field of view, respectively. During recovery, at 42 hours post APAP injury, the number of F4/80+ macrophages is the same in WT and Sema7a KO mice (Figure 5. 2A). As the mice recover, the number of F4/80+ macrophages in the liver decreases (Figure 5. 2B).

Figure 5. 1 WT and Sema7a KO mice have the same frequency of CD45+ cells at 24 hours post APAP injury

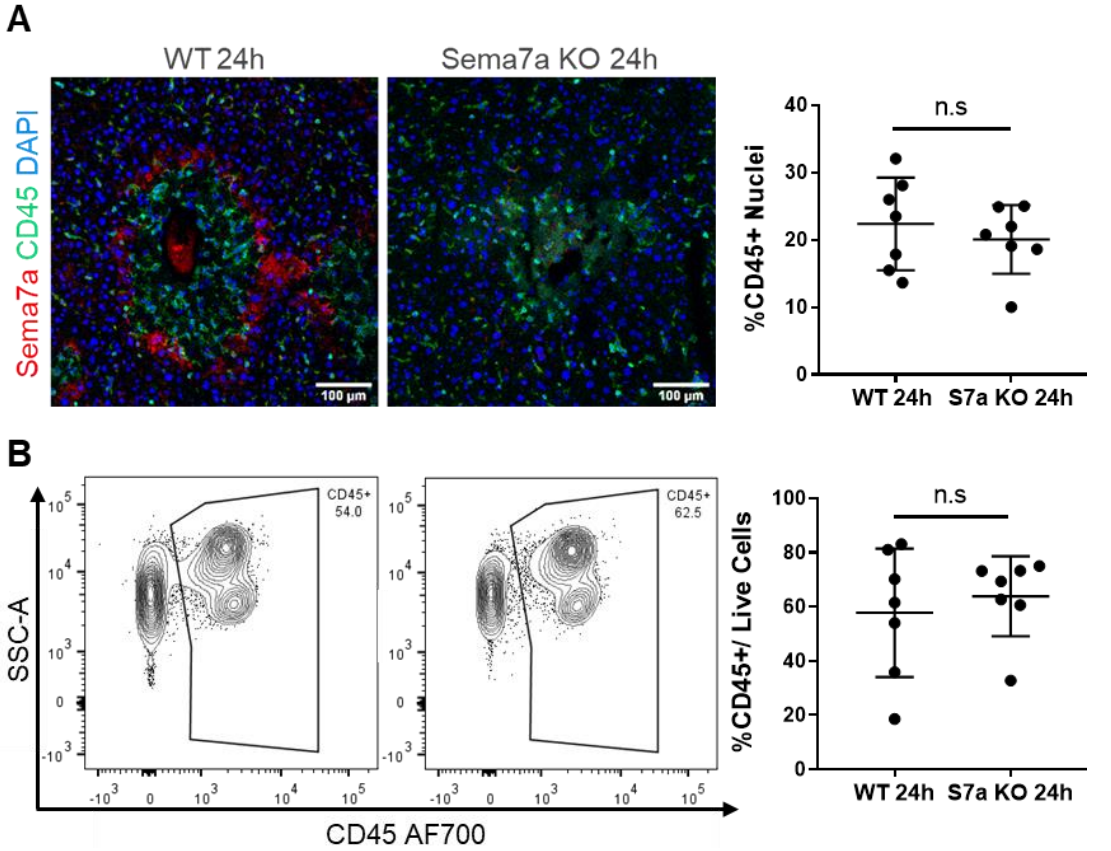

Figure 5. 1

A) Localisation of CD45+ (green) cells in the liver, in relation to Sema7a (red) at 24 hours post APAP administration in WT (top) and Sema7a KO (bottom) mice. DAPI nuclear stain. Quantification shows the percentage of CD45+ nuclei, out of the total nuclei, per field of view.

Unpaired t-test. Scale bars 100µm.

B) Flow cytometry analysis of live, CD45+ cells in the liver at 24 hours post APAP administration in WT (left) and Sema7a KO (centre) mice, quantified (right). Mann Whitney test. Data from three experiments is shown

Each dot represents an individual mouse. Data was checked for normality and equal variance. This applies to every figure henceforth.

This dynamic response of macrophages to APAP injury has been previously reported in mice [48,49,51], and confirms that our model corresponds to those used in the literature. To the best of our knowledge, this is the first time Sema7a KO mice have been shown to have an enhanced depletion of F4/80+ macrophages, at 12 hours post APAP overdose.

During APAP injury, infiltrating macrophages are recruited by CCL2/CCR2 [49,63], and macrophages are directed to the necrotic area by DAMPs and cytokines. Sema7a is a monocyte chemoattractant [228]. In Chapter 3, F4/80+ macrophages were seen in close association with Sema7a+ hepatocytes, suggesting an interaction. To examine if a deficiency of Sema7a prevented the recruitment of F4/80+ macrophages to the necrotic area, the number of F4/80+ macrophages per necrotic area was analysed. Throughout the APAP time course, there was no significant difference between WT and Sema7a KO mice. Interestingly, the number of F4/80+ macrophages in the necrotic area correlates with both the number of F4/80+ macrophages in the liver, and the stage of injury. With the number of F4/80+ macrophages per necrotic area peaking at the height of APAP injury at 24 hours post APAP overdose and decreases as injury resolves (Figure 5. 2C).

Figure 5. 2 Sema7a KO mice have less F4/80 macrophages at 12 hours post APAP administration

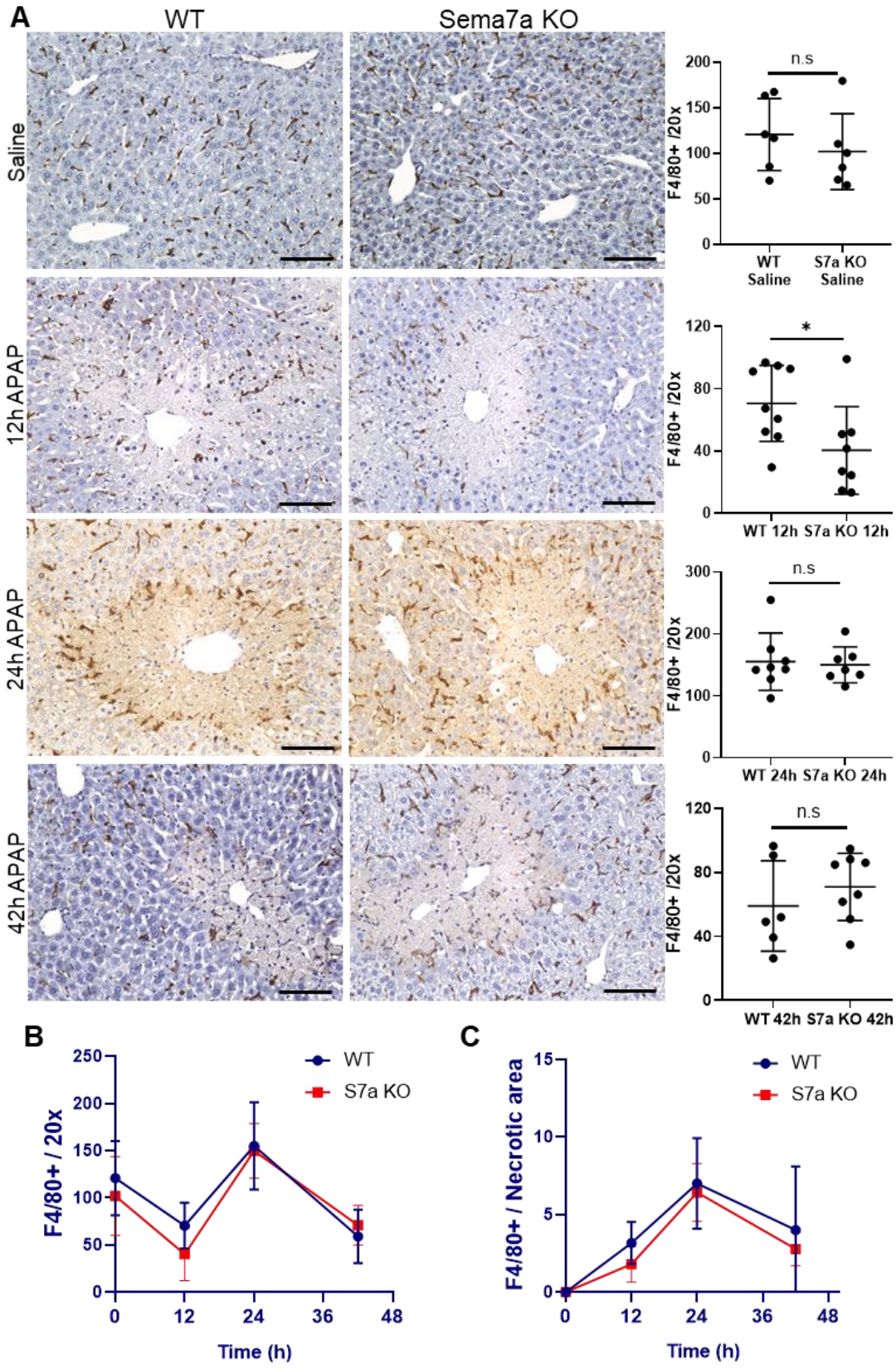

Figure 5. 2

A) F4/80 staining for macrophages in WT (left column) and Sema7a KO mice (centre column) over a time course of APAP. Number of F4/80+ macrophages per 20x field of view is quantified (right). In saline treated (top) or APAP treated mice at 12 (second row), 24 (third row) and 42 (bottom row) hours post administration. Unpaired t-test. Staining was performed by Rhona Aird.
B) Average number of F4/80+ macrophages per 20x field of view, during the APAP injury time course. Two-way ANOVA, n.s.
C) Average number of F4/80+ macrophages in the necrotic area during the time course of APAP injury. Two-way ANOVA, n.s.

Data from eight APAP mice experiments is shown. WT mice, blue. Sema7a KO mice, red. Scale bars 100μm. *p< 0.05.

In Figure 5. 2A, F4/80+ macrophages are detected next to the peri-necrotic hepatocytes, the same location of Sema7a+ hepatocytes at 24 hours post APAP administration. In Sema7a KO mice, the F4/80+ macrophages do not appear to be marginalised to the edge of necrosis. To examine if Sema7a+ hepatocytes cause F4/80+ macrophages to be marginalised to the edge of the necrotic area I separated the necrotic area into two zones, the central necrotic zone and the edge of the necrotic zone, and assessed how many F4/80+ macrophages were present per area (Figure 5. 3B). Sema7a KO mice had significantly less macrophages in the central necrotic zone (P=0.0366), but the same number of F4/80+ macrophages at the edge of necrosis (Figure 5. 3C). This suggests that the Sema7a+ hepatocytes do not marginalise F4/80+ macrophages to the edge of necrosis. However, a Sema7a deficiency either directly or indirectly, prevents F4/80+ macrophages from infiltrating into the central necrotic zone. This could be due to a lack of Sema7a chemoattraction signals, or an inability for the F4/80+ macrophages to migrate through the tissue. Alternatively, as there were less F4/80+ macrophages at 12 hours post APAP overdose in Sema7a KO mice, the reduced number of F4/80+ macrophages in the central necrotic zone many reflect a delay in Sema7a KO F4/80+ macrophages being able to respond to APAP injury.

Figure 5. 3 F4/80+ macrophage localisation at 24 hours post APAP injury

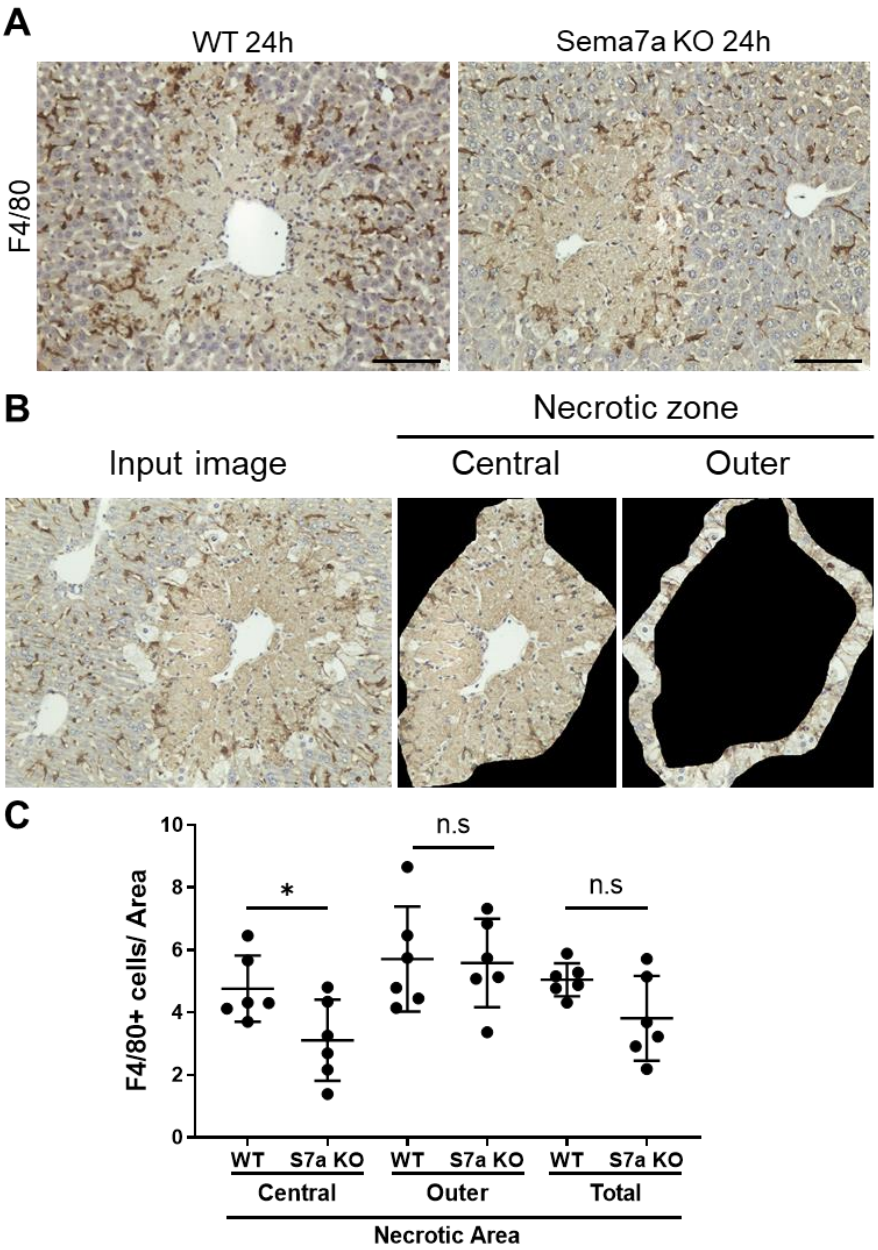

Figure 5. 3

A) F4/80 staining in WT (left) and Sema7a KO mice (right) at 24 hours post APAP overdose.
B) Method used to define areas of necrosis using ImageJ software. The central necrotic zone (centre) and outer necrotic zone (right) was delineated from the input image (left). The number of F4/80+ cells per necrotic area was calculated.
C) Average number of F4/80 macrophages per defined necrotic zone (central, outer or total) in WT and Sema7a KO mice.

Data from three APAP mice experiments is shown. Scale bars 100μm. Unpaired t-test. *p< 0.05

Sema7a KO mice have more neutrophils in the necrotic area at 24 hours post APAP injury

Neutrophils are the first responders of the innate immune system, and are identified by the expression of Ly6G [283]. During sterile injury, neutrophils adhere to ICAM on the LSECs and crawl along the sinusoids towards an increasing concentration of cytokines and DAMPs [52,91]. To leave the sinusoid, neutrophils can exit via a fenestrae, or transmigrate [284]. In a forced ventilation model of lung injury, neutrophils express Plexin C1 which binds to endothelial Sema7a to facilitate transmigration into the alveolar space [211,237]. If Sema7a KO mice have a delay in their innate immune system response to APAP injury, it may be reflected in the neutrophil population.

Neutrophils were examined in WT and Sema7a KO mice during a time course of APAP injury. Healthy WT and Sema7a KO mice had on average two patrolling neutrophils per field of view. By 12 hours post APAP administration, the neutrophil population dramatically increases. Neutrophils continue to accumulate in the liver until 24 hours post APAP administration to a peak of 148 and 132 neutrophils per field of view in WT and Sema7a KO mice respectively. After this time point, the neutrophil population decreases in both the WT and Sema7a KO mice, as seen by the decrease in the number of neutrophils by 42 hours post APAP overdose. Throughout the APAP time course, no statistical difference was detected between the WT and Sema7a KO mice (Figure 5. 4A). Combining this data and comparing it to the F4/80+ macrophage time course (Figure 5. 2B), clearly depicts neutrophils acting as the first responders to injury. At 12 hours post APAP overdose, there is mass infiltration of neutrophils (Figure 5. 4B), before the infiltrating macrophages replenish the F4/80+ macrophage population at 24 hours (Figure 5. 2B). Both the neutrophil and the F4/80+ macrophage population peak at 24 hours post APAP administration, and decrease by 42 hours post APAP administration, as injury resolves.

During APAP injury, neutrophils can be seen homing towards the necrotic area. Whilst analysing the population during the time course in Figure 5. 4, we observed that the Sema7a KO mice had more neutrophils present in the necrotic area. This is confirmed in Figure 5. 5, where Sema7a KO mice have significantly more neutrophils per necrotic area ($P= 0.0182$), but not per field of view at 24 hours post APAP administration.

The increased neutrophil population in the necrotic area could be due to several factors: an increased infiltration of neutrophils into the liver during APAP injury in Sema7a KO mice; a delay in neutrophils and macrophages infiltrating into the necrotic area; a defect in the neutrophils ability to reverse migrate back into the vasculature; or reduced phagocytosis of neutrophils by macrophages. The rest of this chapter investigates why there are more neutrophils in the necrotic area at 24 hours post APAP injury and less F4/80+ macrophages at 12 hours post APAP injury.

Figure 5. 4

A) Ly6G staining for neutrophils in WT (left column) and Sema7a KO mice (centre column). Number of neutrophils per 20x field of view quantified (right column). In saline treated (top) or APAP treated mice at 12 (second row), 24 (third row) and 42 hours (bottom row) post administration. Unpaired t-test. The 12 hours and 24 hours timepoints required a Welch correction.
B) Average number of neutrophils per 20x field of view, during the APAP injury time course. Two-way ANOVA, n.s.

WT mice, blue. Sema7a KO mice, red. Scale bars 100μm. Data from eight APAP mice experiments is shown. Staining and analysis was performed in collaboration with Jennifer Cartwright.

Figure 5. 4 Neutrophils infiltrate the liver during APAP injury

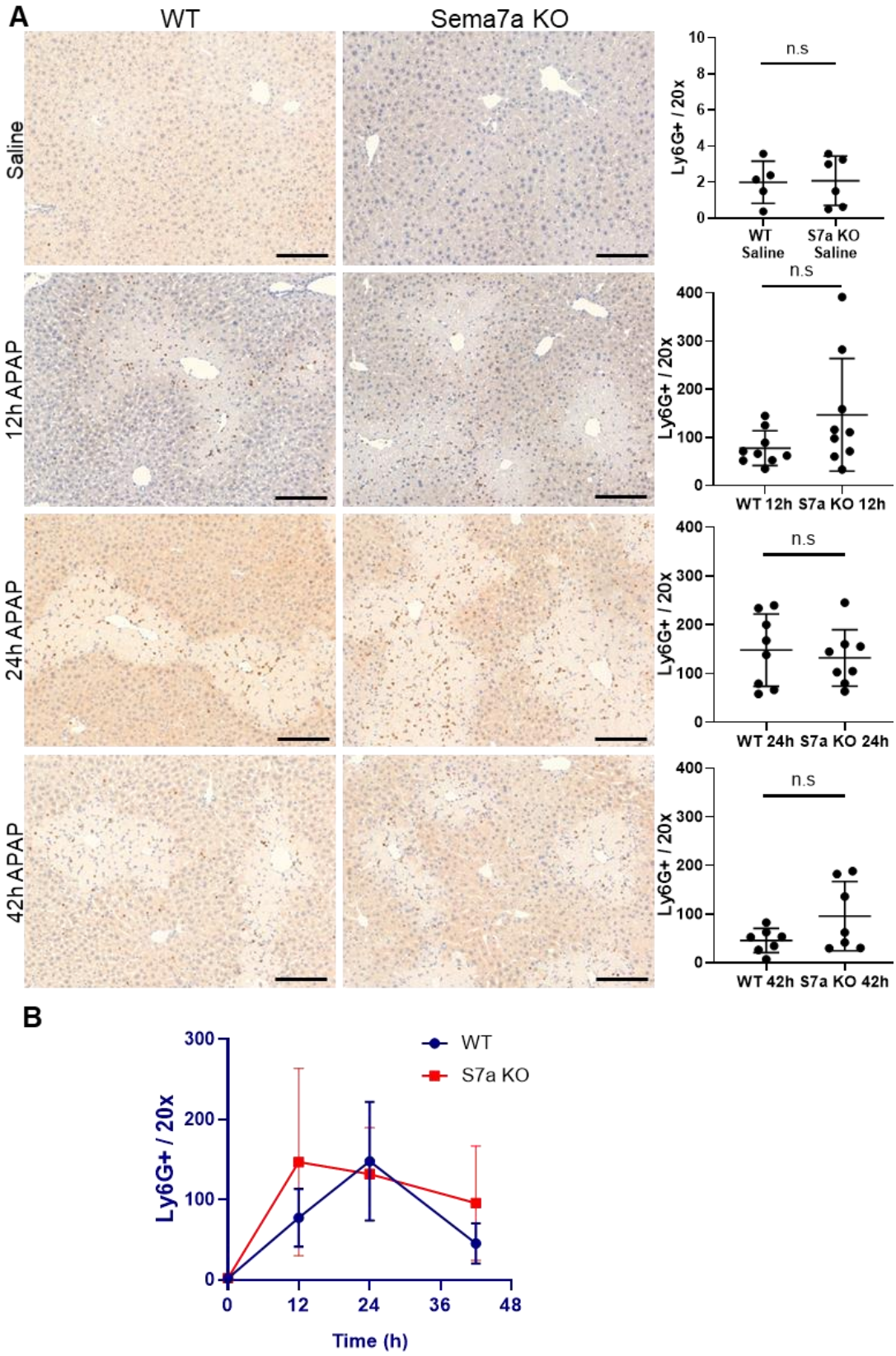

Figure 5. 5 Sema7a KO mice have more neutrophils in the necrotic area at 24 hours post APAP overdose

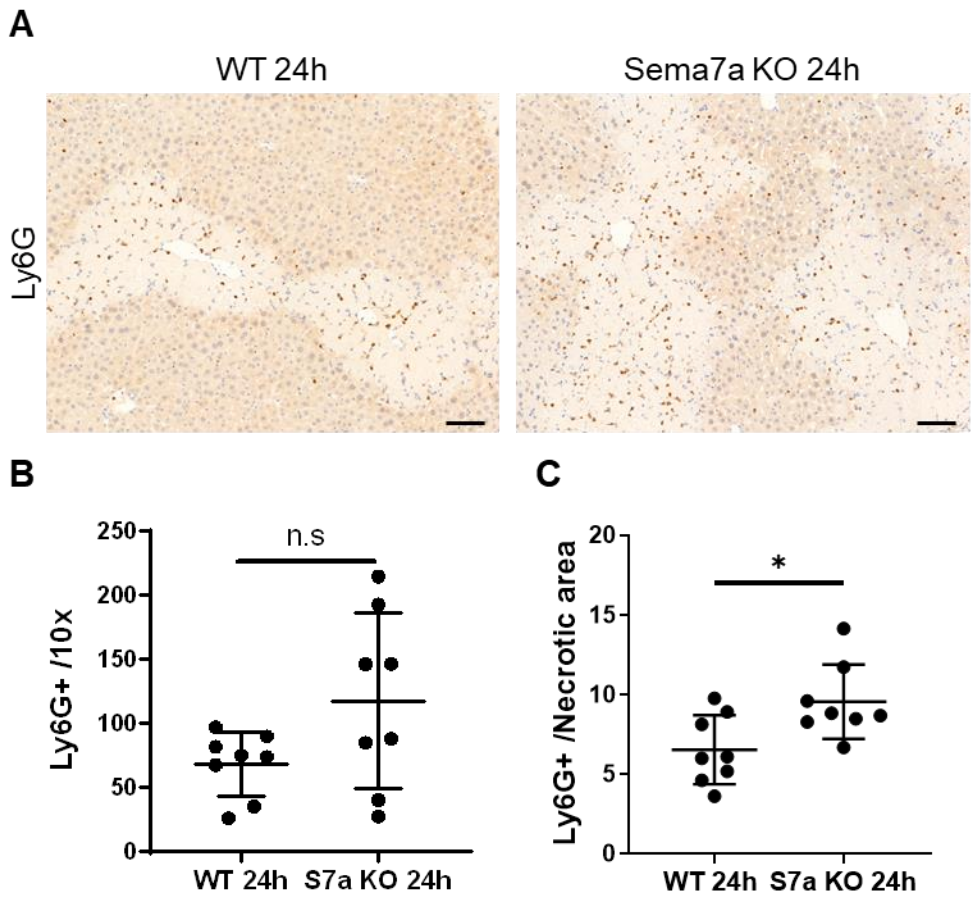

Figure 5. 5

A) Ly6G staining to detect neutrophils in WT (left) and Sema7a KO mice (right) at 24 hours post APAP overdose.
B) Number of Ly6G+ neutrophils per 10x field of view. Unpaired t-test with Welch's correction.
C) Number of Ly6G+ cells per necrotic area. Unpaired t-test.

Data from three APAP mice experiments is shown. *p< 0.05. Scale bars 100μm. Analysis was performed by Jennifer Cartwright.

Healthy Sema7a KO and WT mice have similar numbers of circulating neutrophils and monocytes

Neutrophils and monocytes originate from the bone marrow and circulate the body in search of pathogens or cytokines [48,51,91]. To ensure the increased number of neutrophils in the necrotic area and depleted F4/80+ macrophage population was not due to difference in the frequency of circulating neutrophils or monocytes, these populations were analysed in the peripheral blood of healthy mice.

Peripheral blood was collected by either a tail nick from naive mice, or 12 hours after a saline injection to mimic an APAP experiment. In both scenarios, the frequency of circulating Ly6C+ monocytes (Figure 5. 6B) and neutrophils (Figure 5. 6C) were statistically the same between the WT and Sema7a KO mice. This implies the differences seen during APAP injury are not due to an increase or decrease in the number of available circulating neutrophils or monocytes.

Figure 5. 6 Healthy WT and Sema7a KO mice have the same frequency of circulating neutrophils and monocytes

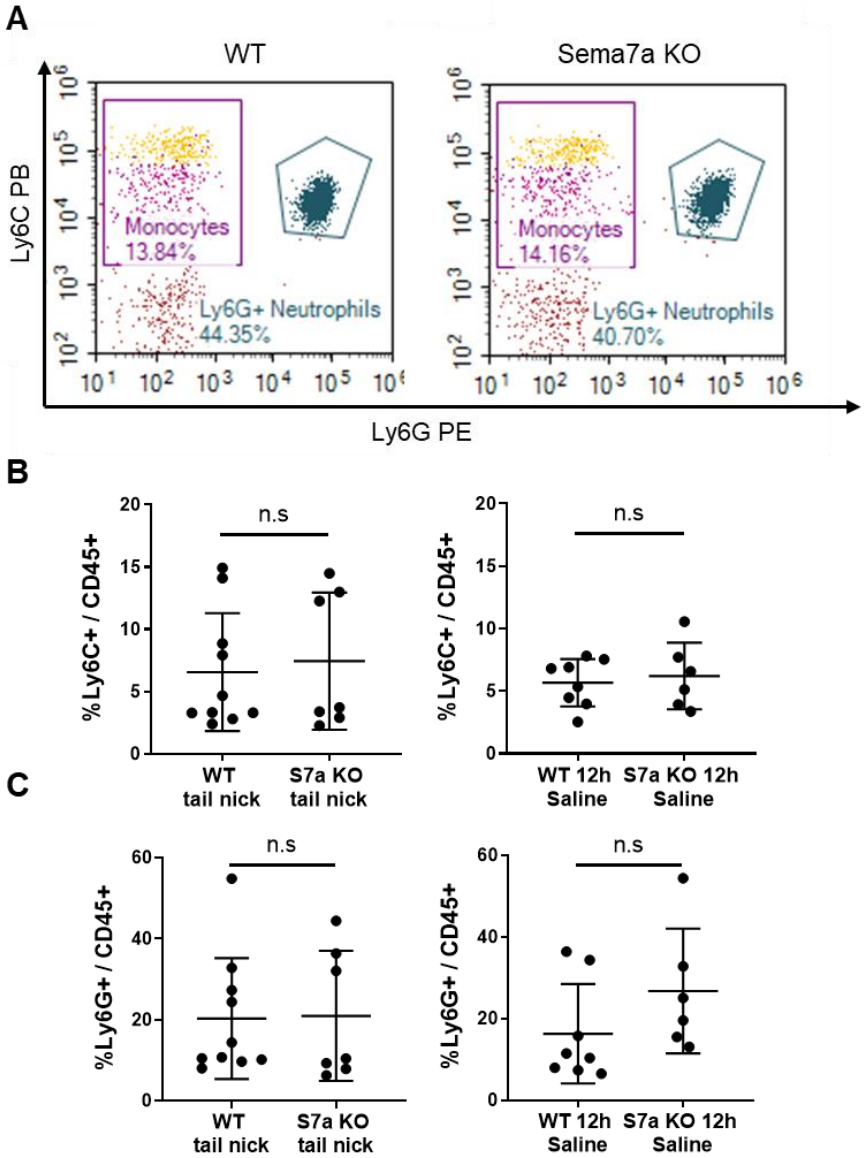

Figure 5. 6

The frequency of blood monocytes and neutrophils in healthy WT and Sema7a KO mice. Blood was obtained via a tail nick, or from mice which had been starved for 12 hours, injected with saline, and sacrificed 12 hours later to mimic an APAP experiment. The experiment was performed twice.

A) Ly6G+ neutrophils and Ly6C+ monocytes populations in blood, from healthy WT (left) and Sema7a KO mice (right). Plots were previously gated for Cells, singlets, live, CD45+, and Lineage-.

B) Frequency of monocytes in blood obtained via a tail nick (left), or cardiac puncture (right). Mann Whitney test.

C) Frequency of neutrophils in blood obtained via a tail nick (left), or cardiac puncture (right). Mann Whitney test.

Neutrophils do not express Sema7a, but both neutrophils and macrophages express the Sema7a receptors

Sema7a is constitutively deleted in the Sema7a KO mice [176]. To ensure the differences seen between the WT and Sema7a KO mice are not due to an intrinsic defect in the neutrophils from a Sema7a deficiency, I examined protein expression of Sema7a in neutrophils with confocal imaging. Neutrophils do not express Sema7a in WT mice (Figure 5. 7A).

The main receptors for Sema7a are: Plexin C1 and Integrin β1, which dimerises with either Integrin α1 or αv. To examine if the changes seen could be due to a lack of Sema7a signalling from other cell types, I examined the expression of the Sema7a receptors on neutrophils. Neutrophils express Plexin C1, as seen by confocal imaging (Figure 5. 7B), and flow cytometry (Figure 5. 8A), as previously reported [218]. Neutrophils also express Integrin β1 and αv, but not Integrin α1 (Figure 5. 8B-D). A deficiency of Sema7a did not affect the frequency of neutrophils which expressed the Sema7a receptors, or the intensity at which the receptors were expressed (Figure 5. 8).

In Chapter 3 Figure 3.17, F4/80+ macrophages were closely associated with Sema7a+ hepatocytes but did not express Sema7a at the protein or transcription level (Figure 3.17). WT BMDMs did express the receptors Integrin β1, α1 and αv (Figure 3.17). To examine if Sema7a KO BMDMs expressed the Sema7a receptors at a similar level to the WT BMDMs, receptor expression was analysed by flow cytometry. Plexin C1, Integrin β1 and α1 were detected at a similar frequency on BMDMs from WT and Sema7a KO mice, and at a similar intensity (Figure 5. 9).

Together, these results imply the differences seen in the neutrophil and F4/80+ macrophage populations during APAP injury is due to a lack of external Sema7a signalling in the Sema7a KO mice, and not an intrinsic defect due to a Sema7a deficiency within these innate immune cells.

Figure 5. 7 Neutrophils express Plexin C1 but not Sema7a

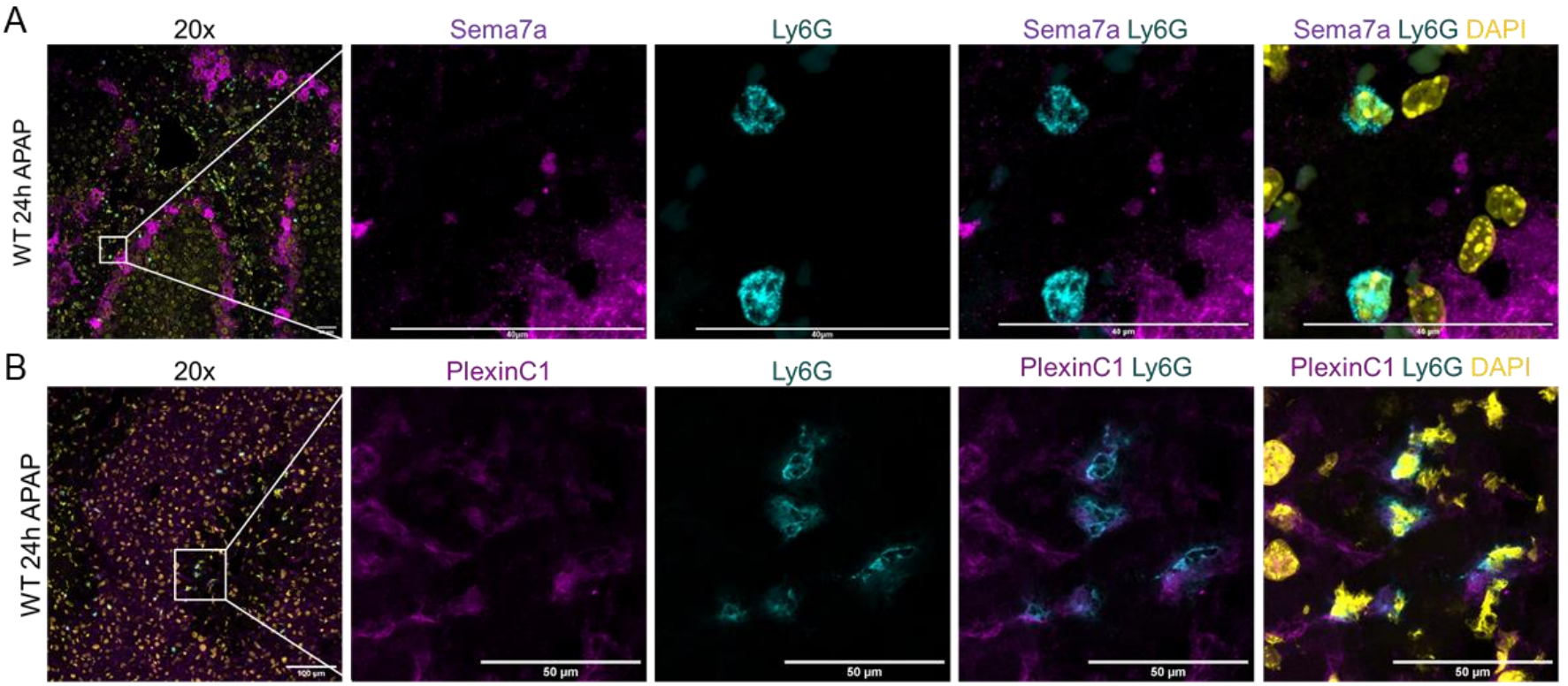

Figure 5. 7

A) Confocal imaging of neutrophils (Ly6G, cyan) and expression of Sema7a (magenta). Scale bars: 40 µm
B) Confocal imaging of neutrophils (Ly6G, cyan) and expression of Plexin C1 (magenta). Scale bars: 50 µm

Images are from WT mice at 24 hours post APAP injection. Nuclear stain, DAPI (yellow). White inset indicates area used for high power images.

Figure 5. 8 Neutrophils express the Sema7a receptors

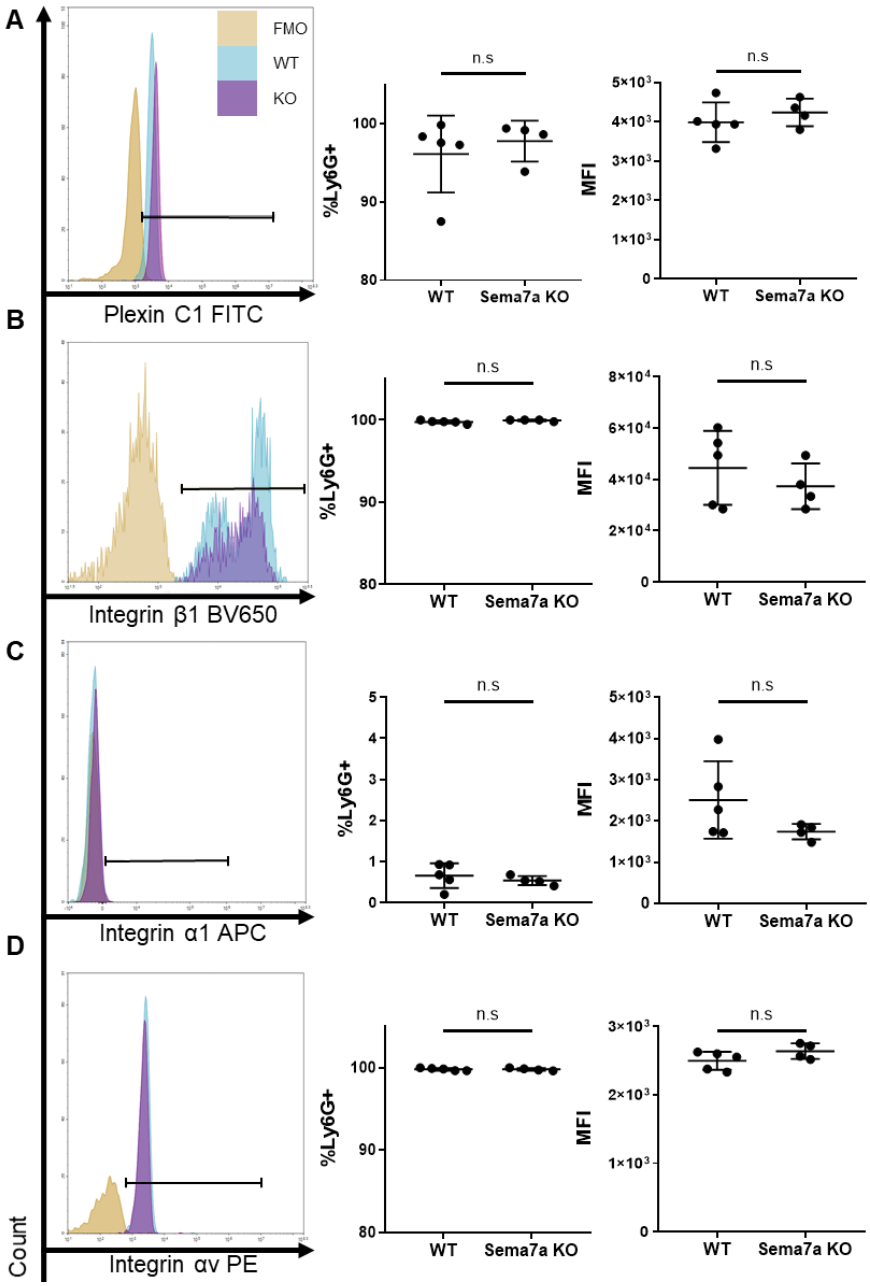

Figure 5. 8

Expression of Sema7a receptors on Live, Lin-, CD45+, Ly6G+ neutrophils from peripheral blood of healthy WT and Sema7a KO mice

A) Plexin C1. Mann Whitney test for %Plexin C1/ Ly6G+.
B) Integrin β1. Mann Whitney test for both quantification graphs.
C) Integrin αv
D) Integrin α1

Left, representative histogram showing neutrophil receptor expression. WT, cyan; Sema7a KO, magenta; FMO, yellow. Centre, frequency of receptor expression. Right, receptor intensity on Ly6G+ cells, assessed by Mean fluorescent intensity (MFI). Unpaired t-test, unless stated otherwise. Data is shown from one experiment.

Figure 5. 9 BMDMs express the Sema7a receptors

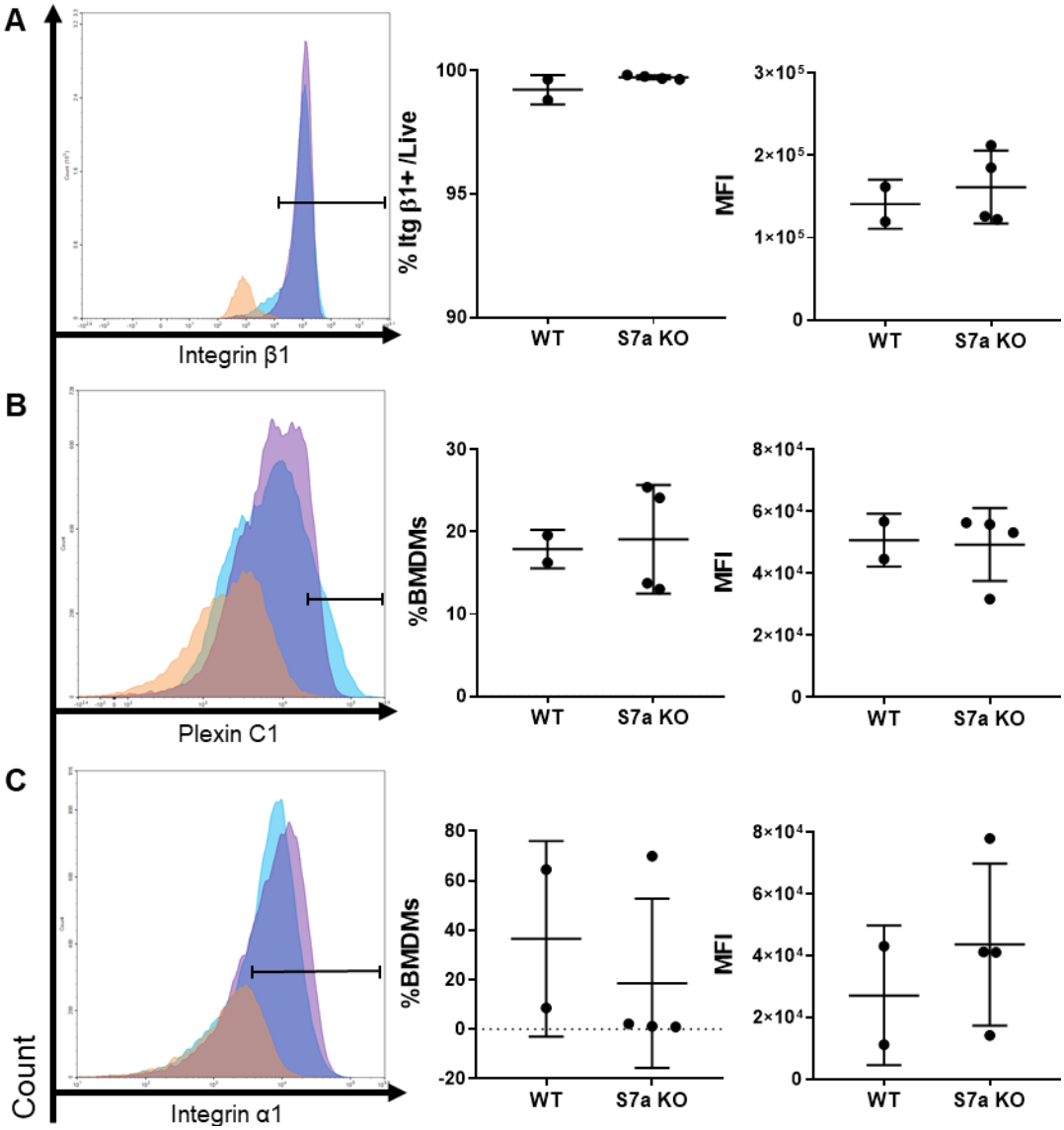

Figure 5. 9

WT and Sema7a KO BMDMs were selected for: singlets, live, then analysed for Integrin β1 (CD11b) expression (A). CD11b+ BMDMs were analysed for the other Sema7a receptors (B&C):

A) Integrin β1
B) Plexin C1
C) Integrin α1

Left, representative histogram showing BMDM receptor expression. WT, cyan; Sema7a KO, magenta; FMO, yellow. Centre, frequency of receptor expression on BMDMs. Right MFI of receptor on BMDMs.

Each dot represents one BMDM sample, with each colour representing a single experiment. Data from four experiments is shown. A higher power is needed for statistical analysis.

Sema7a KO mice have elevated serum levels of IL-6 and CXCL1

During APAP injury, cytokines attract and activate the innate immune system. To examine if the expression of inflammatory cytokines were altered in the Sema7a KO mice, qRT-PCR was utilised. At 24 hours post APAP administration, there was no significant difference in mRNA expression of *IL-1β, IL-6, CXCL1* (mouse homolog to IL-8), *MCP-1* or *IL-10* (Figure 5. 10) in whole liver lysate.

To assess protein cytokine expression, the MSD V-Plex system was employed. IL-6 (P=0.0078), and CXCL1 (P=0.0459) were significantly increased the serum of Sema7a KO mice at 24 hours post APAP administration, compared to WT mice (Figure 5. 11). In the whole liver, there was no significant difference between the WT and Sema7a KO mice in any of the cytokines tested (Figure 5. 11). These results indicate Sema7a KO mice have more systemic inflammation than WT mice. CXCL1 is a neutrophil chemoattractant [52,91]. It may enhance recruitment during APAP injury in Sema7a KO mice.

Figure 5. 10 mRNA expression of pro-inflammatory cytokines in whole liver lysate is similar in WT and Sema7a KO mice

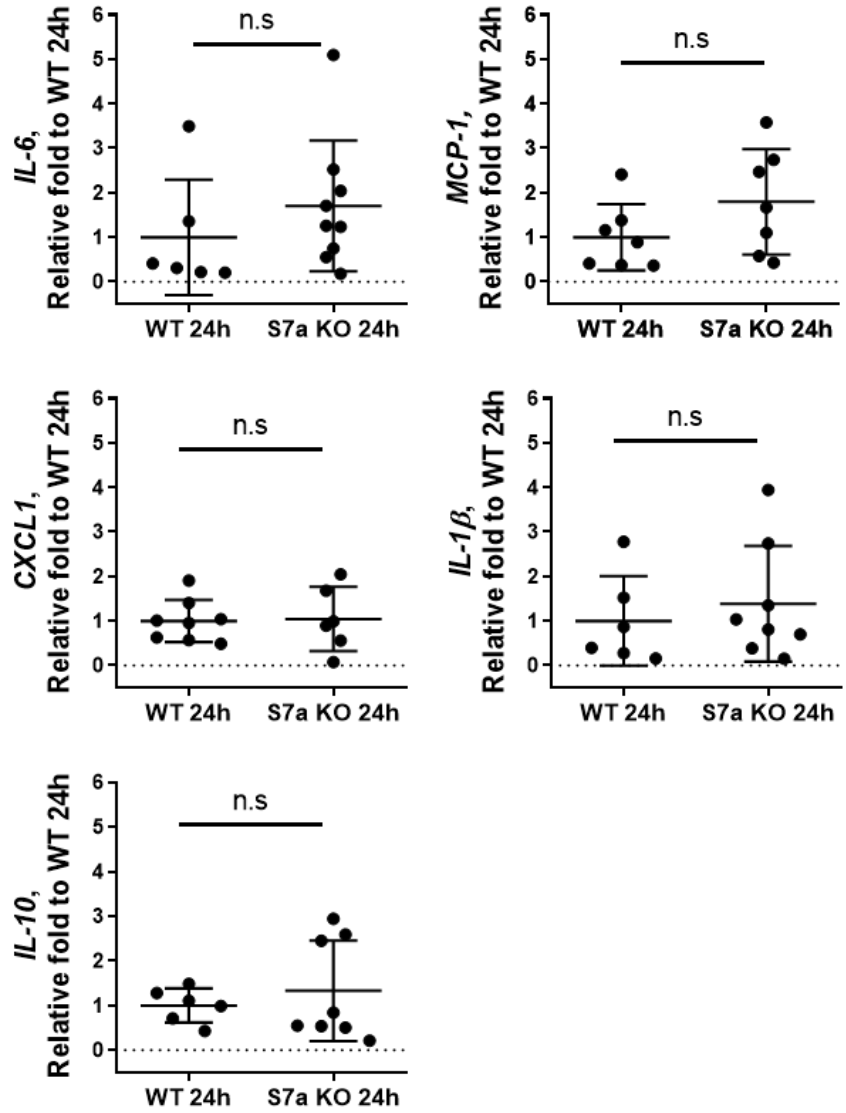

Figure 5. 10
mRNA expression of pro-inflammatory genes at 24 hours post 350 mg/kg APAP injection in WT and Sema7a KO mice, relative to WT mice.
IL-6, IL-10, Mann Whitney test.
Unpaired t-test unless otherwise indicated. Data from three APAP mouse experiments is shown. The ELISA was performed twice.

Figure 5. 11 Sema7a KO mice have elevated IL-6 and CXCL1 in serum at 24 hours post APAP injury

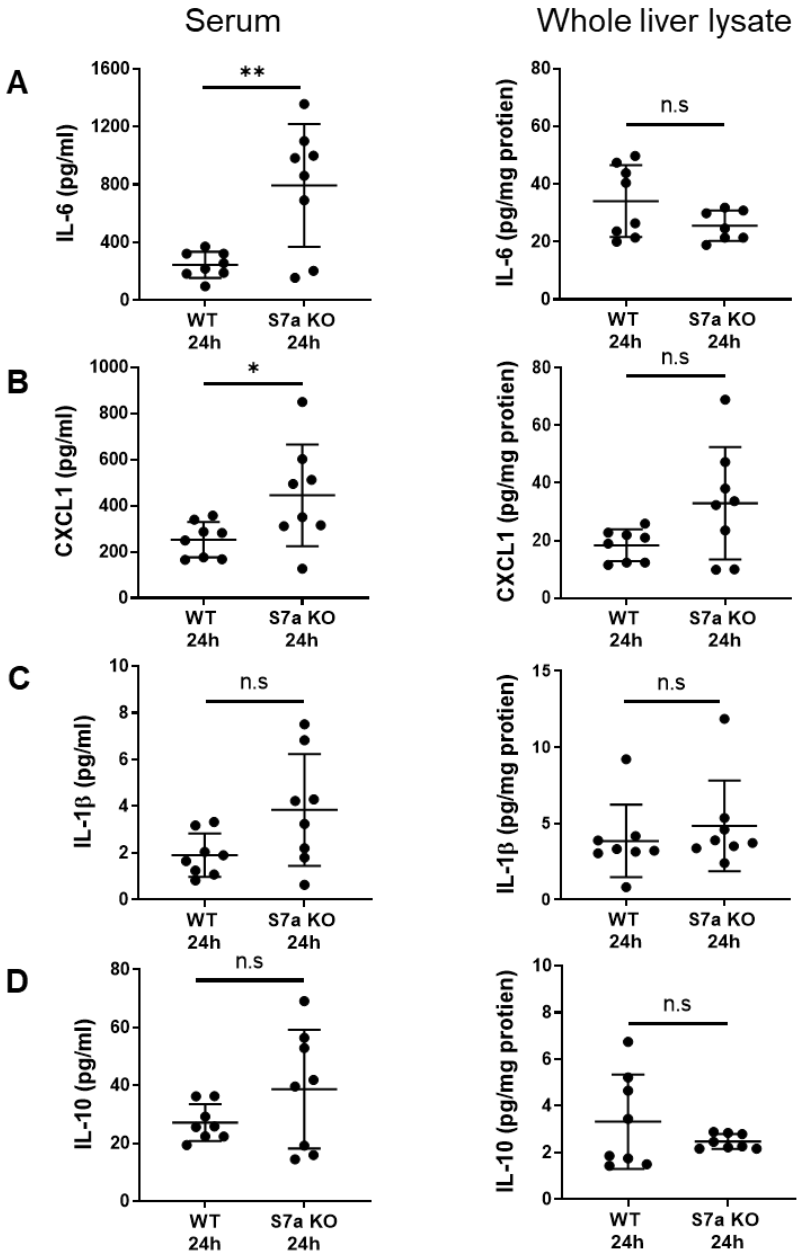

Figure 5. 11

Serum (left column) and whole liver lysate (right column) from WT and Sema7a KO mice at 24 hours post APAP injection, were analysed for the following cytokine expression, with the MSD V-Plex:

A) IL-6. Serum: Unpaired t-test with Welch's correction.
B) CXCL1. Serum and whole liver lysate: Unpaired t-test with Welch's correction.
C) IL-1β. Whole liver lysate Mann Whitney test.
D) IL-10. Whole liver lysate Mann Whitney test.

Unpaired t-test unless otherwise indicated. *p< 0.05, ** p<0.01. Data from three APAP mouse experiments is shown. The ELISA was performed twice

Macrophages and neutrophils are viable during APAP injury

Neutrophils apoptose at the site of injury, and release 'find me' signals that attract monocytes, which then phagocytose the apoptotic neutrophil [91,121,149]. A possible reason for more neutrophils in the necrotic area of Sema7a KO mice is that they are dying and not being cleared by phagocytosis. In our model, the number of neutrophils in the liver decreases after 24 hours post APAP administration (Figure 5. 4B).

To examine if the neutrophils were undergoing apoptosis at 24 hours post APAP injury, a dual stain of Ly6G and active Caspase 3, an apoptosis marker, was performed. In WT mice 1.6% of Ly6G+ neutrophils are dual positive for active caspase 3. Sema7a KO mice had significantly less apoptotic neutrophils (P =0.0129), with only 0.8% of Ly6G+ neutrophils expressing active caspase 3 (Figure 5. 12). This data suggests neutrophils are not undergoing apoptosis at 24 hours post APAP administration. However, it is unknown how long neutrophils maintain their Ly6G expression for when they apoptose. So, we may not be detecting all the apoptotic neutrophils present at 24 hours post APAP overdose. Alternatively, the neutrophils could be being engulfed immediately after they apoptose, making them difficult to detect.

Figure 5. 12 Sema7a KO mice have less apoptotic neutrophils at 24 hours APAP injury

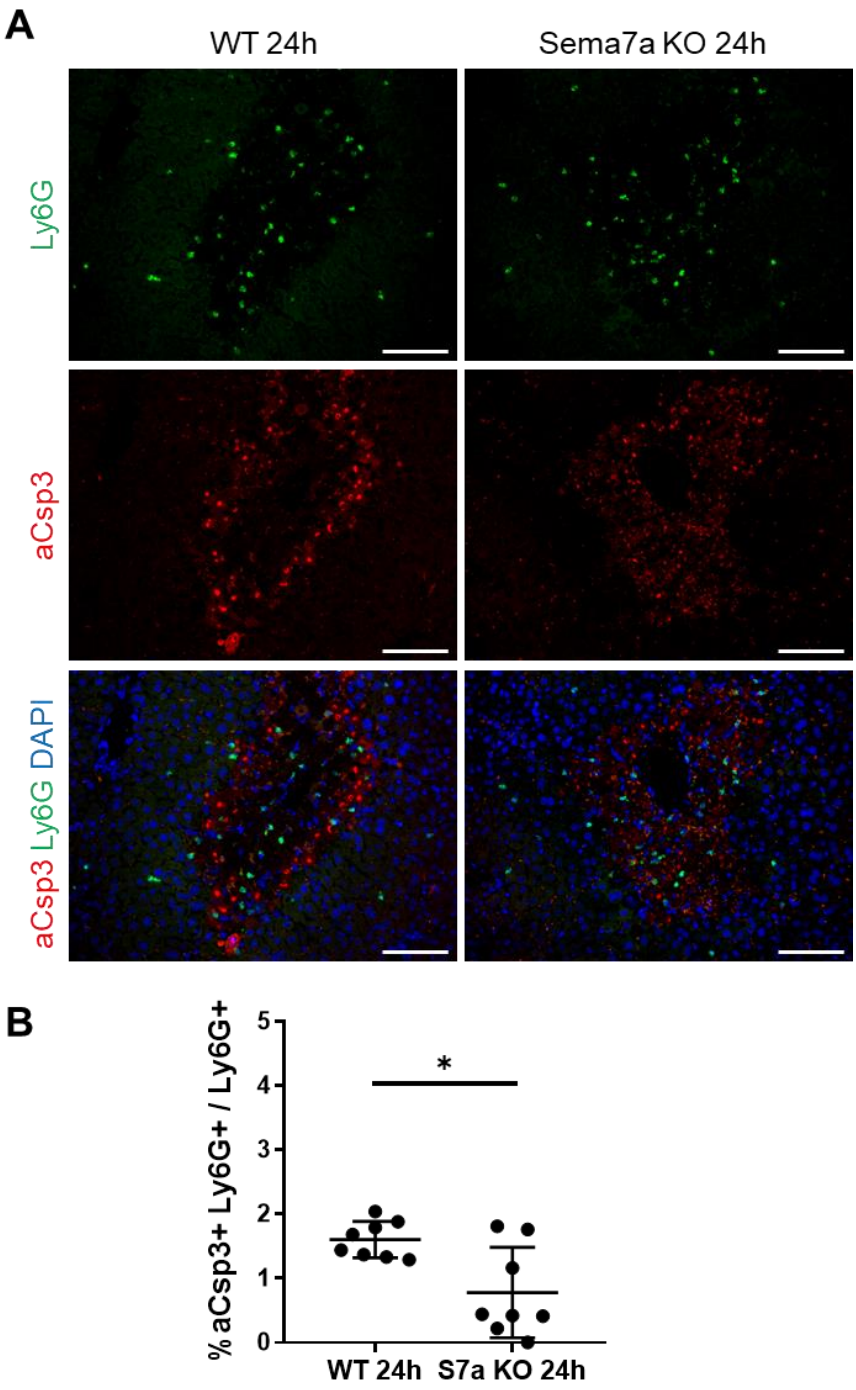

Figure 5. 12

A) Staining for Ly6G+ neutrophils (green) and active Caspase 3 (aCsp3, red), in WT and Sema7a KO mice at 24 hours APAP overdose. Scale bars µm.

B) Percent of apoptotic neutrophils (aCsp3+, Ly6G+) in the total Ly6G population. Unpaired t-test with Welch's correction, $p<0.05$.

aCsp3, active Caspase 3. Data from three APAP mouse experiments is shown.

Resident macrophages become depleted during APAP injury [48,49], as they succumb to APAP toxicity [50]. Sema7a KO mice have less F4/80+ macrophages in the liver at 12 hours post APAP administration. To examine if Sema7a KO F4/80+ macrophages have increased cell death at 12 hours post APAP administration, F4/80+ macrophage viability was examined by flow cytometry.

The non-parenchymal cell (NPC) fraction was isolated from the livers of WT and Sema7a KO mice at 12 hours post APAP administration. Viability was assessed using the Live/Dead (L/D) e780 viability dye. L/D is impermeable to healthy cells. Dying and dead cells have permeable or damaged cell membranes, allowing L/D to covalently bind to intracellular amines. Therefore, dead cells are L/D+, which can be easily separated from viable L/D- cells during flow cytometry [285].

The following populations were examined for viability at 12h post APAP injury: Ly6G+ neutrophils; Ly6G-, F4/80^{hi} CD11b^{lo} resident macrophages; and Ly6G-, F4/80^{lo} CD11b^{hi} infiltrating macrophages, which further subdivided into Ly6C^{lo} macrophages and Ly6C^{hi} monocytes. There was no significant difference in viability in any of these populations between WT and Sema7a KO mice. Resident macrophages and neutrophils both had around 95% viability in WT and Sema7a KO mice (Figure 5. 13). Collectively, resident F4/80+ macrophages and neutrophils are not undergoing cell death at 12 hours post APAP administration. At 24 hours post APAP administration, neutrophils are not apoptotic.

Figure 5. 13 Hepatic neutrophils and macrophages are viable at 12 hours post APAP injury

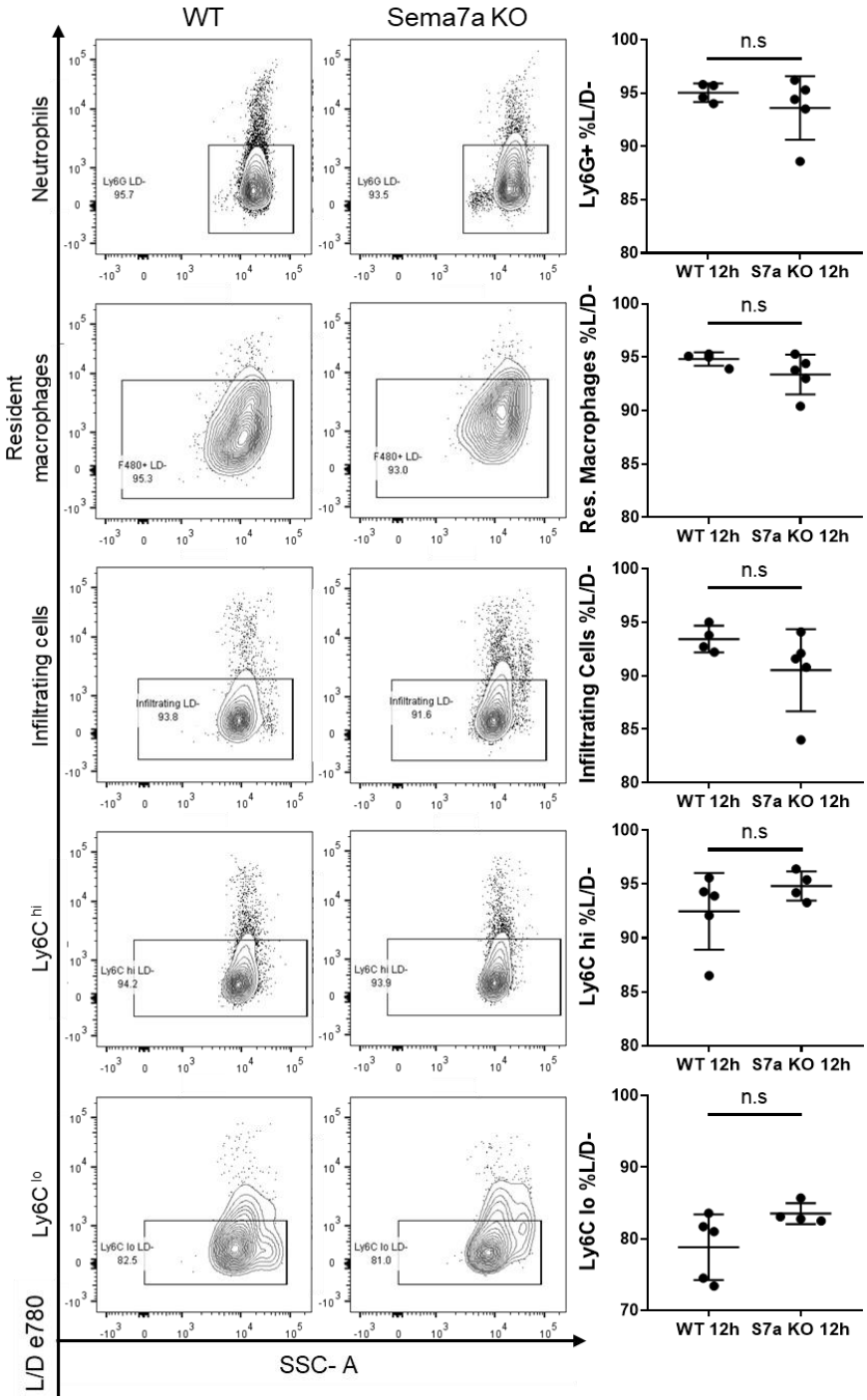

Figure 5. 13

Liver NPCs were isolated from WT (left) and Sema7a KO mice (centre), at 12 hours 350mg/kg APAP. Viability was assessed in the following populations: Neutrophils, resident macrophages, and infiltrating cells, which was separated into Ly6C ^{hi} and Ly6C ^{lo}. Data shown is from one experiment**.** Gates were set using FMOs. Percentage viability is quantified right. Data from three APAP mouse experiments is shown.

Investigating the composition of leukocytes in WT and Sema7a KO mice during APAP injury

Sema7a KO mice have more neutrophils in the necrotic areas at 24 hours APAP post overdose (Figure 5. 5) and a higher expression of CXCL1 in the serum (Figure 5. 11). Could this systemic CXCL1 recruit neutrophils from other compartments in the Sema7a KO mice?

In the IHC analysis, Sema7a KO mice had less F4/80+ macrophages at 12 hours post APAP administration. Whilst at 24 hours APAP, the F4/80+ macrophage population was equivalent to WT mice (Figure 5. 2). Do Sema7a KO mice have more macrophages infiltrating into the liver to restore the F4/80+ macrophage population?

To investigate these questions, flow cytometry was used to analyse specific subsets of neutrophils, monocytes and macrophages, isolated from the liver, blood and peritoneum of WT and Sema7a KO mice, at 12 and 24 hours post APAP administration. For a schematic of the experiment please see Figure 5. 14A and Figure 5. 19A respectively.

At 12 hours post APAP overdose, Sema7a KO mice have a higher frequency of infiltrating macrophages

We first analysed the liver at 12 hours post APAP administration, to see if we could detect an early accumulation of Ly6G+ neutrophils and the enhanced depletion of F4/80+ macrophages in the Sema7a KO mice. Neutrophils were defined as CD45+, lineage (CD3, CD19 & NK1.1) -, Ly6G+. Resident macrophages (Mϕ) were defined as CD45+, lineage-, Ly6G-, F4/80^{hi} CD11b^{lo}. Infiltrating macrophages were defined as CD45+, lineage-, Ly6G-, F4/80^{lo} CD11b^{hi} [72]. This infiltrating macrophage population was further subdivided into Ly6C^{lo} macrophages and Ly6C^{hi} monocytes, which have yet to mature into Ly6C^{lo} macrophages. For the full gating strategy, for all the flow cytometry, please see Chapter 2.

In the liver, the frequency of neutrophils was significantly lower in Sema7a KO mice (P=0.0178) than WT mice at 12 hours post APAP administration (Figure 5. 14B). WT

and Sema7a KO mice had the same frequency of resident macrophages with 3.6% and 3.2% of the NPC CD45+ fraction, respectively (Figure 5. 14C). Infiltrating macrophages were significantly higher (P=0.036) in Sema7a KO mice with 29.0% of CD45+ cells compared to 19.2% of CD45+ cells in WT mice. 86.3% and 86.8% of the infiltrating macrophages are freshly infiltrated Ly6C^{hi} monocytes in WT and Sema7a KO mice, respectively (Figure 5. 14D). This data implies that Sema7a KO mice have a lower frequency of neutrophils but a higher frequency of macrophages infiltrating the liver at 12 hours post APAP administration.

Examining the percentage frequency of a population can be misleading. Large changes in the abundance of a specific population will affect the frequency of other populations cells, but this may not be reflected in the absolute quantity of cells [286]. To examine if the lower frequency of Ly6G+ neutrophils and increased frequency of infiltrating macrophages is reflected in cellular number in the liver, the absolute counts of each population were assessed per gram of liver. At 12 hours post APAP administration, WT and Sema7a KO mice had the same absolute count of neutrophils and resident macrophages per gram of liver. However, Sema7a KO mice had a higher quantity of infiltrating macrophages (P=0.0472) than WT mice, per gram of liver**.** Consistent with this, Sema7a KO mice had significantly more Ly6C^{hi} monocytes, per gram of liver (P=0.0456) compared to WT mice (Figure 5. 15).

These absolute counts per gram of liver confirms that Sema7a KO mice have more infiltrating macrophages at 12 hours post APAP administration than WT mice, with a greater proportion being Ly6C^{hi}. However, WT and Sema7a KO mice have the same quantity of neutrophils. This implies that a Sema7a deficiency does not affect total neutrophil infiltration at 12 hours post APAP administration. The absolute quantity of resident macrophages was also equal in WT and Sema7a KO mice. The different results obtained by flow cytometry and IHC are obtained via different methods and these variations will be considered in the discussion.

Figure 5. 14 Sema7a KO mice have less neutrophils infiltrating the liver than WT mice at 12 hours post APAP injury

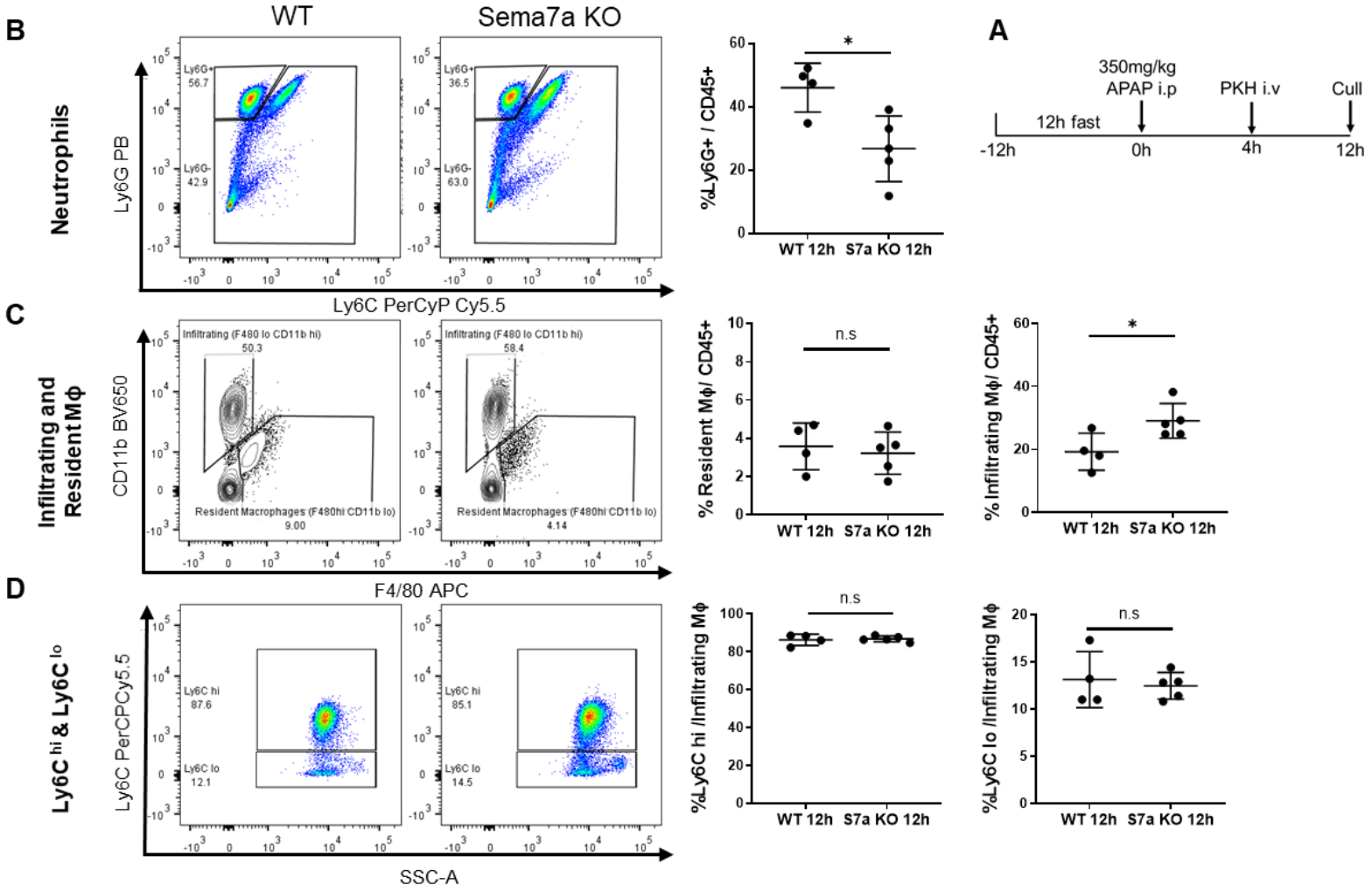

Figure 5. 14

A) Experimental design. After a 12 hour fast, mice were administered with 350 mg/kg APAP. 4 hours later a phagocytic dye (PKH) was injected i.v. Mice were humanely sacrificed at 12 hours APAP.

NPCs were isolated from the livers of WT (left) and Sema7a KO mice (centre). Representative plots from three experiments are shown. The frequency of the following NPC populations in the CD45+ fraction, is quantified (right):

B) Neutrophils

C) Resident macrophages (Mϕ) (quantified left); and infiltrating macrophages (quantified right)

D) Infiltrating macrophages subdivided by $Ly6C^{hi}$ and $Ly6C^{lo}$ (Mann Whitney) expression

Liver digestion and staining was performed by Jennifer Cartwright. Unpaired t-test, unless otherwise stated. *p< 0.05. Data shown is from one experiment.

Figure 5. 15 Absolute counts of NPCs at 12 hours post APAP injury

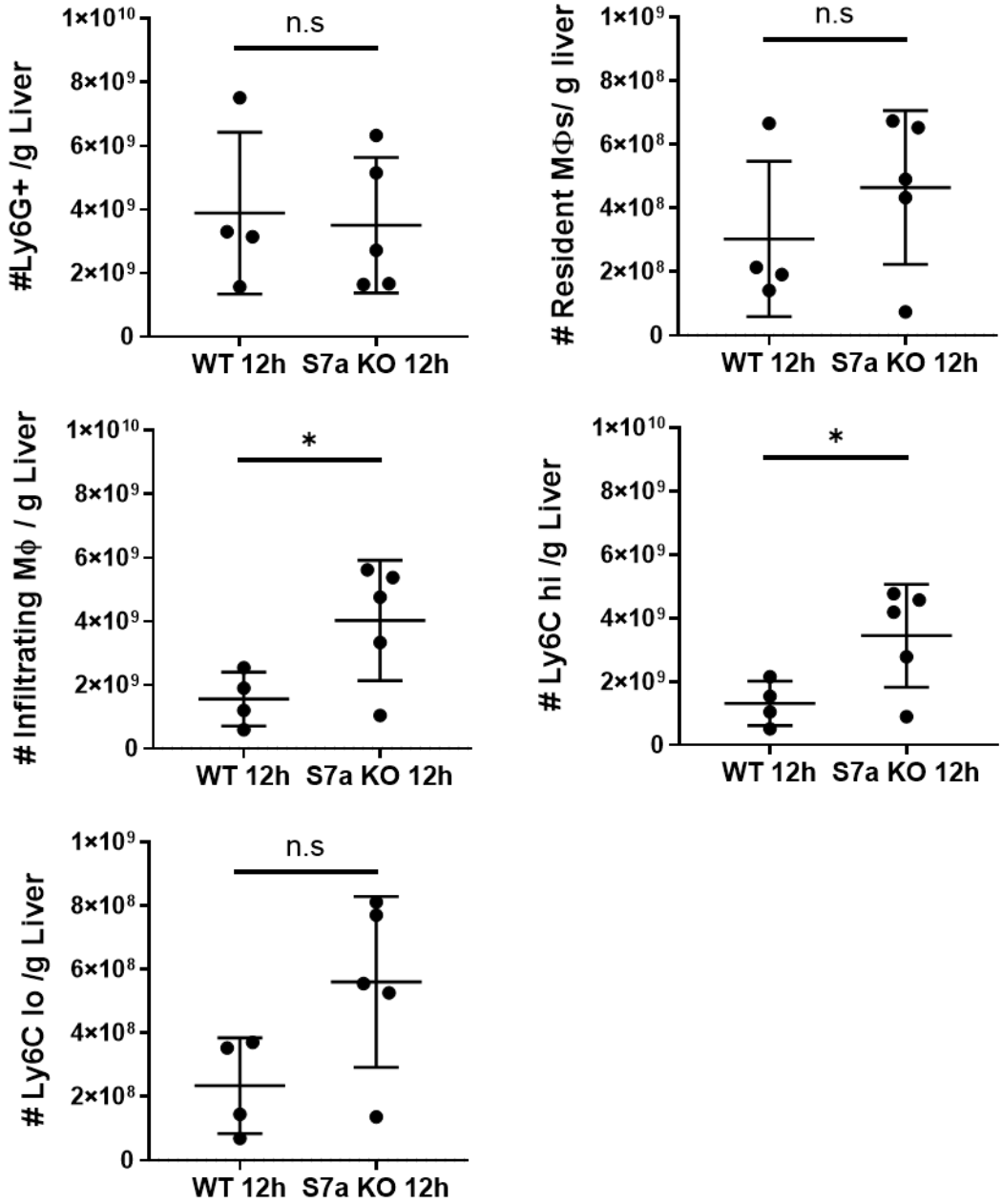

Figure 5. 15

Absolute counts of neutrophils, resident macrophages (Mann Whitney), infiltrating macrophages, Ly6C^{hi} monocytes**,** and Ly6C^{lo} macrophages per gram of liver in WT and Sema7a KO mice at 12 hours post APAP overdose. *p<0.05

Unpaired t-test unless otherwise stated. The experiment was performed once.

Infiltrating neutrophils and monocytes originate from the bone marrow and are delivered to the liver by the circulation [51,52,111,287]. I considered if the increase in infiltrating macrophages and higher neutrophil population was due to an increase in circulating neutrophils and monocytes at 12 hours post APAP administration.

Using flow cytometry, the frequency of circulating: CD45+, lineage + (CD3+, CD19+) B and T cells; CD45+, lineage-, Ly6G+ neutrophils; and CD45+, linage-, Ly6G- monocytes were analysed in WT and Sema7a KO mice at 12 hours post APAP administration. WT and Sema7a KO mice had the same frequency of circulating B and T cells, Ly6G+ neutrophils and Ly6G- monocytes (Figure 5. 16 A & B). Yet, Sema7a KO mice had a significantly higher frequency (P= 0.0297) of $Ly6C^{lo}$ monocytes with 2.3% of CD45+ cells compared to 0.7% of CD45+ cells in WT mice at 12 hours post APAP administration (Figure 5. 16C). Collectively, Sema7a KO mice have more circulating $Ly6C^{lo}$ monocytes, which contribute to the higher levels of infiltrating macrophages of Sema7a KO mice at 12 hours post APAP administration.

GATA6+ peritoneal macrophages infiltrate the liver and promote recovery in a model of sterile thermal injury [71]. If and how these macrophages contribute to inflammation during APAP is currently unexplored. To examine if peritoneal exudate cells (PEC) contribute to enhanced neutrophil or macrophages infiltration, the composition of PEC from WT and Sema7a KO were compared at 12 hours post APAP administration. WT and Sema7a KO mice had the same frequency of: CD11b+ cells, CD11b+ Ly6G+ neutrophils, CD11b+ Ly6G- cells, $Ly6C^{hi}$ monocytes (Figure 5. 17) and F4/80+ mature macrophages, (Figure 5. 18), which have been previously reported to be GATA6+ [70].

Due to time restraints, this experiment was only performed once, and is currently underpowered. With a sample number of 8, there may be a significantly more neutrophils and $Ly6C^{hi}$ monocytes in Sema7a KO mice in the PEC at 12 hours post APAP administration (Figure 5. 17B & C). Therefore, the current conclusion of no significant difference between WT and Sema7a KO mice would be incorrect.

Correction: In the original analysis, the CD11b+ Ly6G- gate was examined as Ly6C monocytes, which was subdivided into the $Ly6C^{hi}$ and $Ly6C^{lo}$ populations. However, this CD11b+ Ly6G- population will include monocytes, macrophages, T cells and B1

cells [70,254]. A lineage negative step should have been included to exclusively examine the peritoneal monocytes.

The MHCII+ F4/80- and MHCII- F4/80- macrophage populations were also examined in live PECs. Again neutrophils, monocytes, T and B1 cells should have been excluded prior to analysis of the macrophage populations. The analysis of: Ly6C monocytes, Ly6C^{lo} monocytes, MHCII+ F4/80- and MHCII- F4/80- macrophages has been removed but are still shown on the flow cytometry plots. As mature macrophages are exclusively F4/80+, they are still included in the analysis [70,254].

Figure 5. 16 Sema7a KO mice have a higher frequency of circulating Ly6C^{lo} monocytes at 12 hours post APAP injury

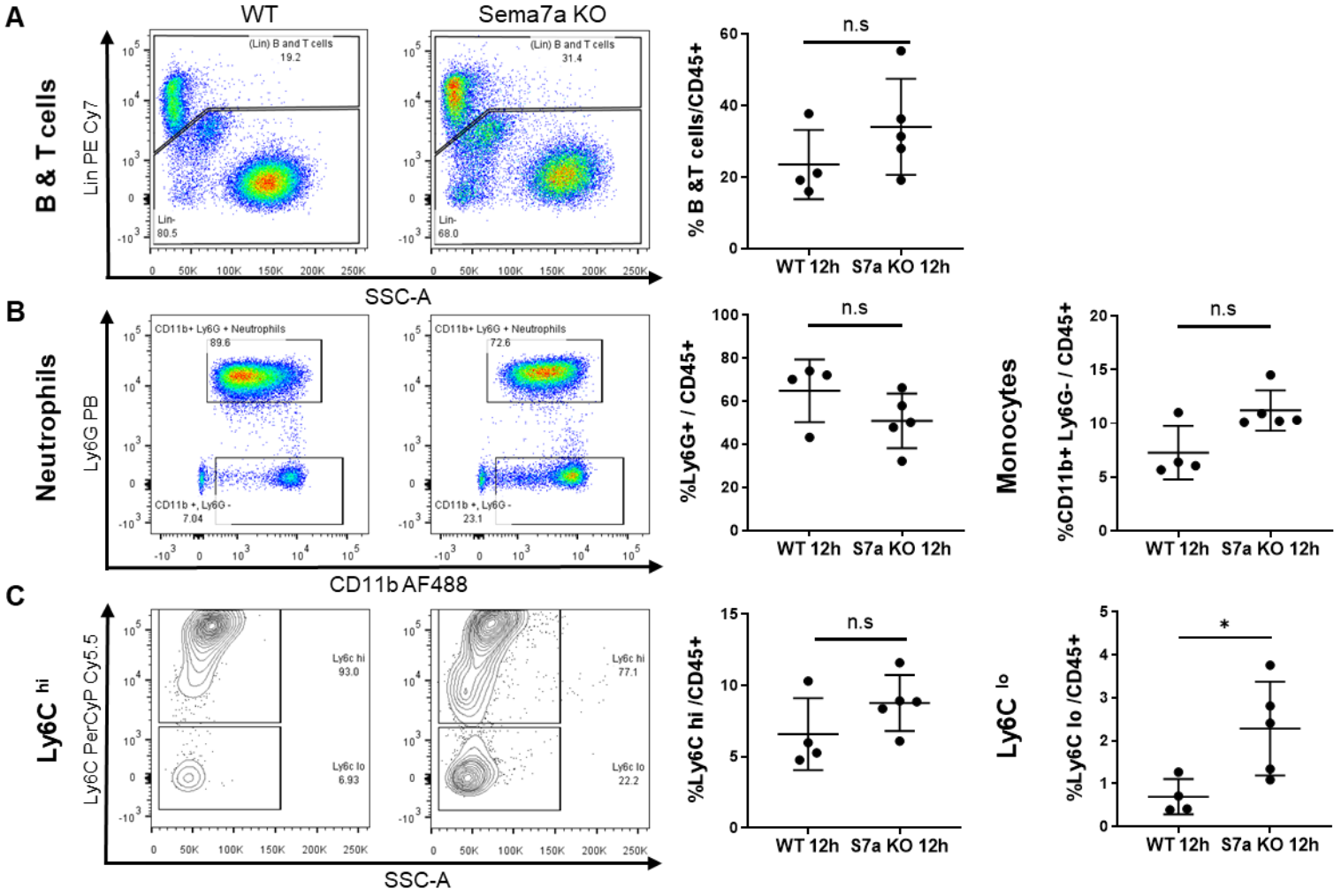

Figure 5. 16
Peripheral blood was collected from WT (left) and Sema7a KO mice (right) at 12 hours post 350mg/kg APAP administration. Representative plots from three experiments are shown. Quantification (right) shows the frequency of CD45+ cells for the following populations:

A) B & T cells (Lin + (CD3+ & CD19+))
B) Neutrophils (quantified left) and monocytes (quantified right)
C) The monocyte population was analysed for $Ly6C^{hi}$ (quantified left); and $Ly6C^{lo}$ monocytes (quantified right).

For the gating strategy see Chapter 2. Unpaired t-test, unless otherwise stated. *p< 0.05. Data shown is from one experiment.

Figure 5. 17
PECs were collected from WT (left) and Sema7a KO (centre) mice at 12 hours post 350mg/kg APAP administration.
Quantification (right) shows the frequency of:

A) CD11b+ cells, in live cells
B) Neutrophils (CD11b+, Ly6G+, quantified left,) and CD11b+ Ly6G- cells as a percentage of live cells
C) $Ly6C^{hi}$ in the Ly6G- fraction.

Mann Whitney tests**.** For the gating strategy see Chapter 2. Data shown is from one experiment.

Figure 5. 17 Sema7a KO mice have the same frequency of neutrophils in the peritoneal exudate as WT mice at 12 hours post APAP overdose

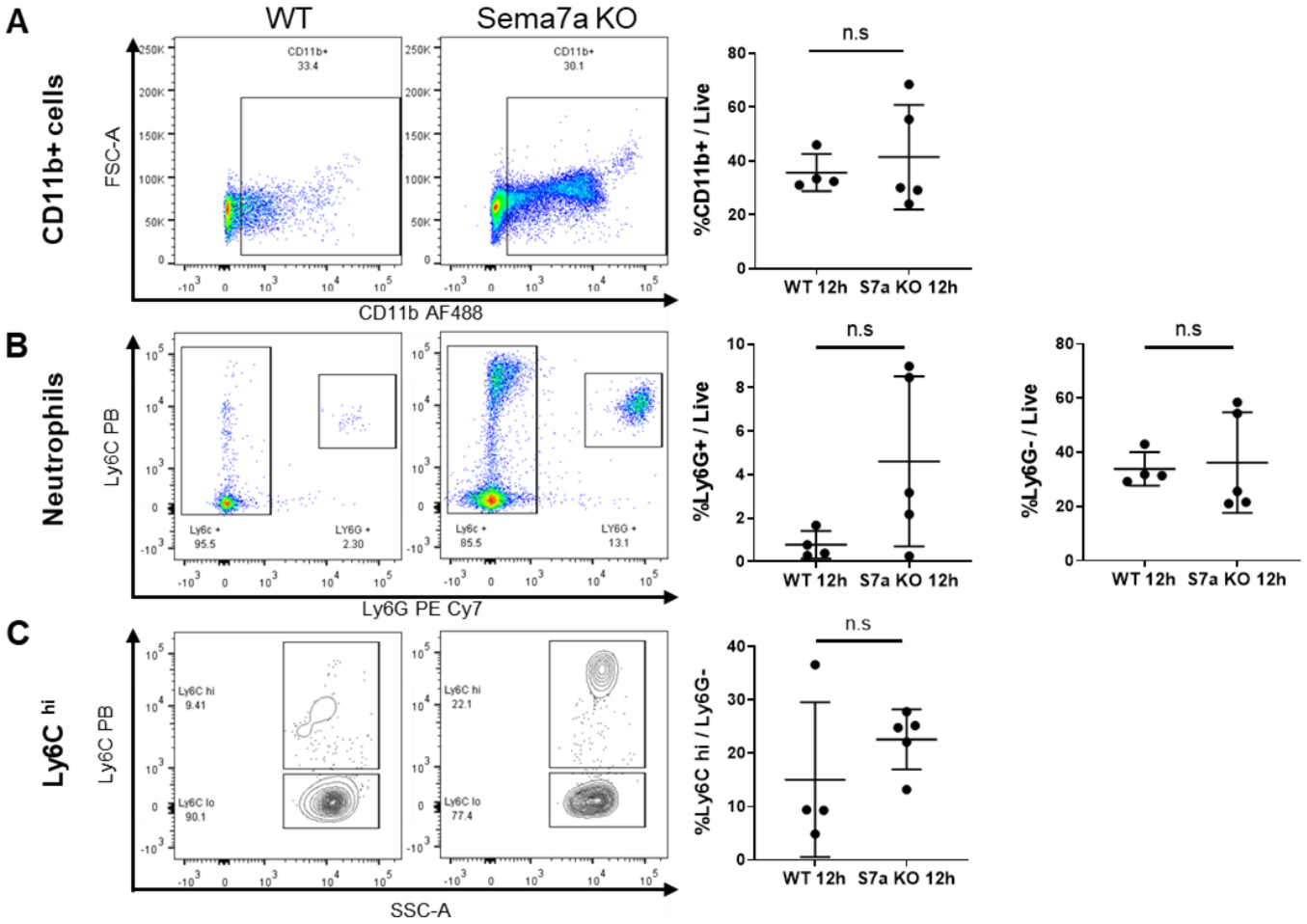

Figure 5. 18 WT and Sema7a KO mice a similar frequency of F4/80+ macrophages in the peritoneal exudate at 12 hours post APAP injury

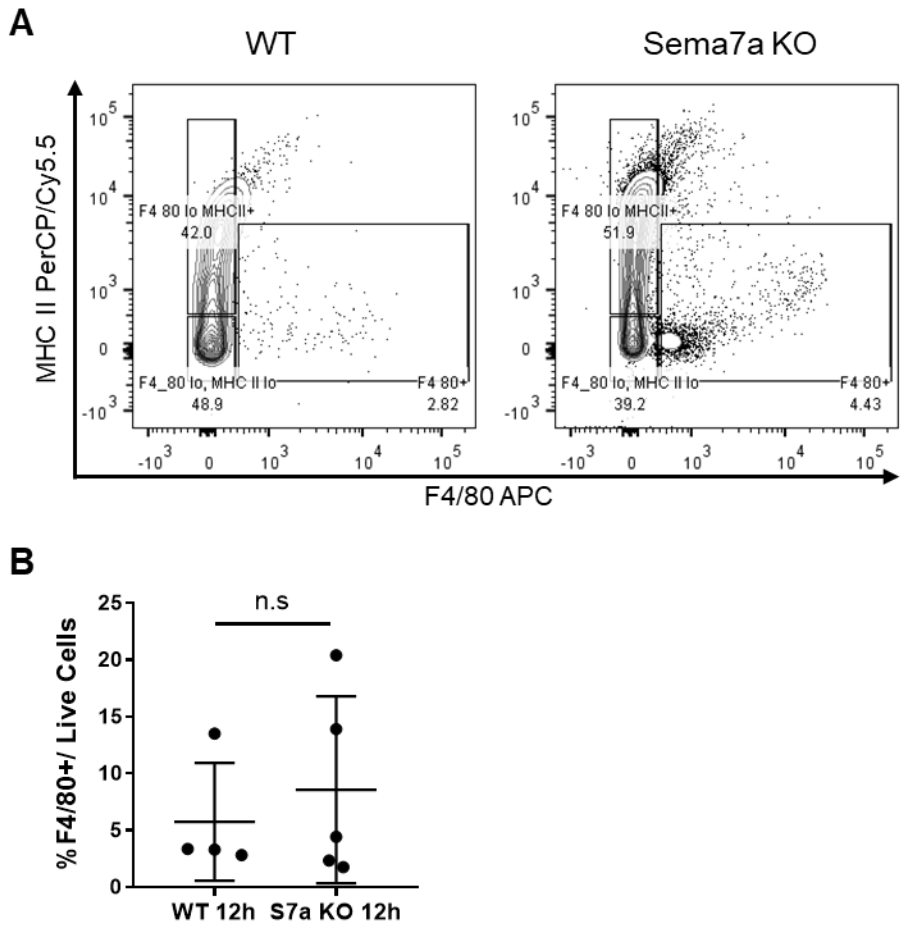

Figure 5. 18

A) Live, Peritoneal macrophages were isolated from WT (left) and Sema7a KO (right) mice, at 12 post hours APAP overdose, and separated by the expression of F4/80 and MHC Class II

B) Frequency of F4/80+. Mann Whitney test

Data shown is from one experiment.

At 24 hours post APAP administration, WT and Sema7a KO mice have similar frequencies of immune cells

Sema7a KO mice have more neutrophils in the necrotic area at 24 hours post APAP injury (Figure 5. 5). Histological analysis also revealed the lower F4/80+ macrophage population at 12 hours post APAP administration is restored by 24 hours (Figure 5. 2). In the flow cytometry experiments, Sema7a KO mice had significantly more Ly6C^{lo} monocytes in the blood and infiltrating macrophages in the liver, but the resident macrophage population was equivalent to WT mice (Figure 5. 14 & Figure 5. 15).

To investigate if the increased neutrophil population in the necrotic areas of Sema7a KO mice was due to an increased neutrophil depletion from other tissues, or a higher or prolonged infiltration of neutrophils, the neutrophil population in the liver, blood and PEC was examined in WT and Sema7a KO mice at 24 hours post APAP administration. The composition of the monocyte/ macrophage populations were also examined in these tissues.

In the NPC CD45+ fraction of the liver, WT and Sema7a KO mice have the same frequency of: neutrophils, resident macrophages, and infiltrating macrophages, which were composed of the same proportions of Ly6C^{hi} and Ly6C^{lo} monocytes (Figure 5. 19). To ensure that this was reflected in the quantity of cells present in the liver, the absolute count was calculated. No significant differences were detected, confirming that WT and Sema7a KO have similar frequencies and abundance of each population analysed in the liver at 24 hours post APAP overdose (Figure 5. 20).

Figure 5. 19 WT and Sema7a KO mice have the same frequency of neutrophils and macrophages in the liver at 24 hours post APAP injury

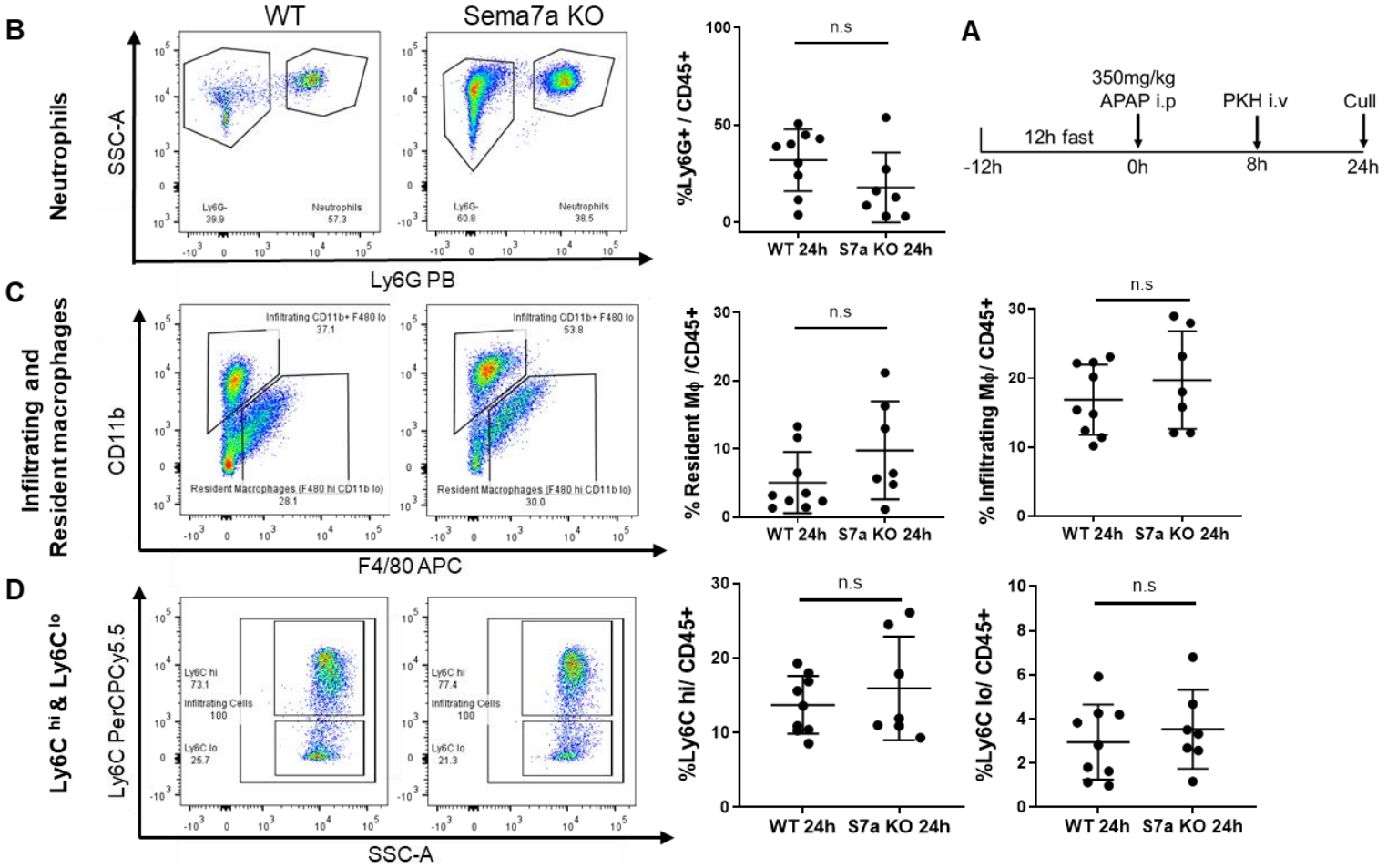

Figure 5. 19

A) Experimental design. After a 12 hour fast, mice were administered with 350 mg/kg APAP. 8 hours later a phagocytic dye (PKH) was injected i.v. Mice were humanely sacrificed at 24 hours APAP.

NPCs were isolated from the livers of WT (left) and Sema7a KO mice (centre). Quantification shows the frequency in CD45+ cells for the following NPC populations:

B) Neutrophils

C) Resident macrophages (quantified left, Mann Whitney test**);** Infiltrating macrophages (quantified right).

D) Infiltrating macrophages were examined for $Ly6C^{hi}$ and $Ly6C^{lo}$ expression

For a gating strategy see Chapter 2. Data from three experiments is shown. Liver digestion and staining was performed by Jennifer Cartwright. Unpaired t-test, unless otherwise stated.

Figure 5. 20 Absolute counts of hepatic immune cells are the same in WT and Sema7a KO at 24 hours post APAP administration

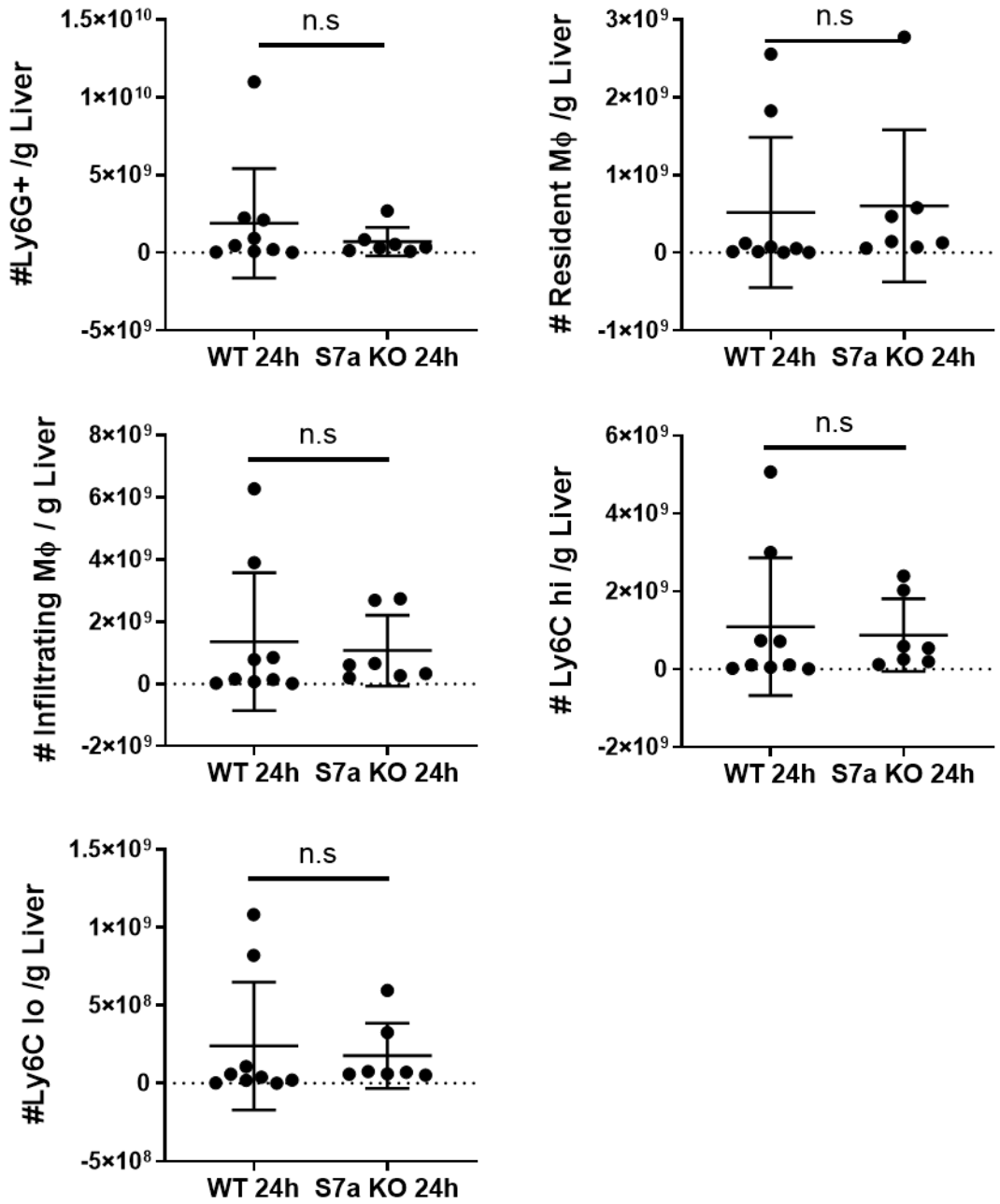

Figure 5. 20

Absolute counts of neutrophils, resident macrophages, infiltrating macrophages**,** Ly6C^{hi} monocytes, and Ly6C^{lo} macrophages per gram of liver in WT and Sema7a KO mice at 24 hours post APAP overdose. Data from three experiments is shown. Mann Whitney test.

Next the frequency of monocytes and neutrophils were examined in the blood from WT and Sema7a KO mice at 24 hours post APAP administration. WT and Sema7a KO mice have similar frequencies of B and T cells, neutrophils, and monocytes in the live, CD45+ population in the blood at 24 hours APAP. In addition, the infiltrating monocytes had the same proportions of $Ly6C^{hi}$ and $Ly6C^{lo}$ monocytes (Figure 5. 21).

The composition of the PEC was also compared between WT and Sema7a KO mice at 24 hours APAP injury. 57% of the live cells were CD11b+ in Sema7a KO mice, which was significantly higher (P=0.0181) than the 34% in WT mice (Figure 5. 22A). CD11b is a marker expressed on B1 cells monocytes, macrophages, natural killer (NK) cells [254,288], and is upregulated on activated neutrophils [289].

WT and Sema7a KO mice had the same frequencies of neutrophils, Ly6G- cells, $Ly6C^{hi}$ monocytes (Figure 5. 22) and F4/80+ mature macrophages in the peritoneal exudate (Figure 5. 23). The increased frequency of CD11b may indicate Sema7a KO mice have a higher proportion of B1 or NK cells not analysed here, or more activated neutrophils.

Overall, by 24 hours APAP post injury and differences in the macrophage compartment have been resolved. WT and Sema7a KO mice have the same frequency and number of macrophages as monocytes in the liver, blood and PEC. The increased neutrophil population the necrotic area at 24 hours post APAP administration in the Sema7a KO mice, is not due to an enhanced infiltration of neutrophils from the blood or peritoneum, as there was no significant difference in the frequency of Ly6G+ neutrophils in the blood or PEC between WT and Sema7a KO mice at both 12 or 24 hours post APAP administration.

Figure 5. 21 WT and Sema7a KO mice have the same frequency of circulating leukocytes at 24 hours post APAP injury

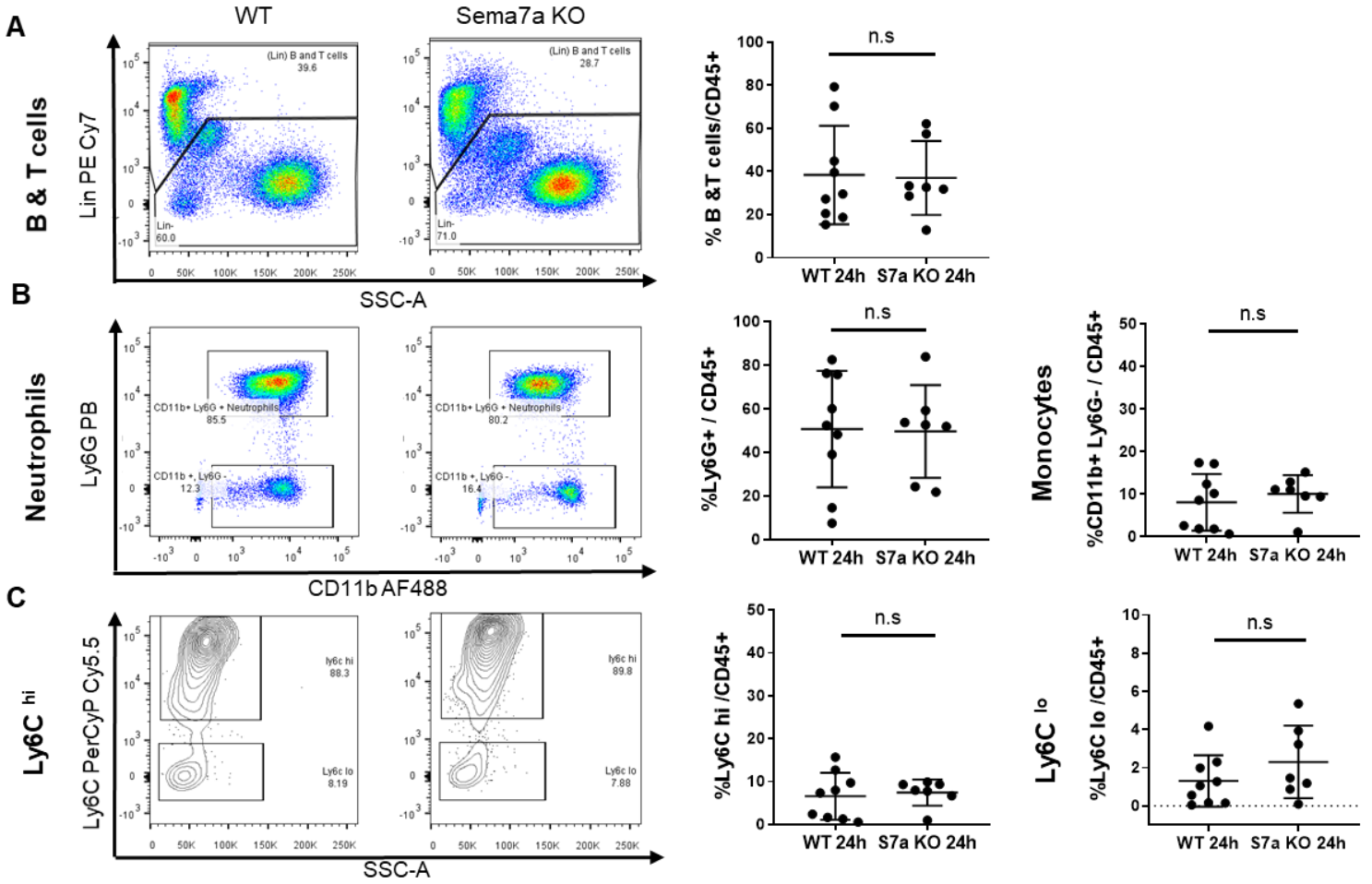

Figure 5. 22 Sema7a KO mice have more peritoneal CD11b+ cells than WT mice at 24 hours APAP post overdose

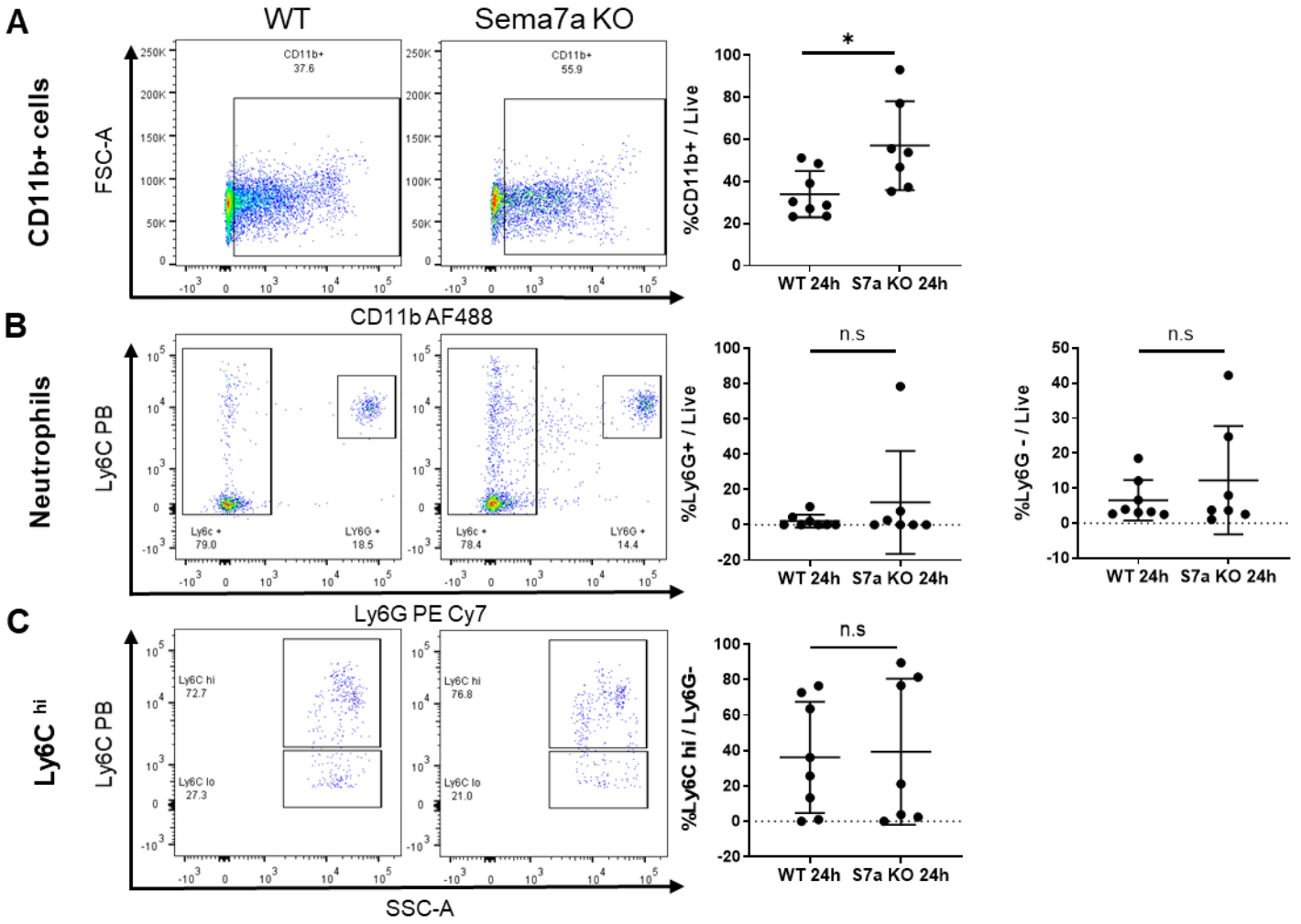

Figure 5. 21

Peripheral blood was collected from WT (left) and Sema7a KO mice (right), treated with 24 hours 350mg/kg APAP. Graphs show the frequency in live, CD45+ cells for the following populations:

A) B & T cells (Lin +, (CD3+ & CD19+));
B) Neutrophils (quantified left); and monocytes (quantified right);
C) Ly6C^{hi} (quantified left, Mann Whitney test**)**; and Ly6C^{lo} monocytes (quantified right)**.**

For a gating strategy see Chapter 2. Data from three experiments is shown. Unpaired t-test, unless otherwise stated.

Figure 5. 22

PECs were collected from WT (left) and Sema7a KO (centre) mice at 24 hours post 350mg/kg APAP administration.

Quantification shows the frequency of:

A) CD11b+ cells.
B) Neutrophils (CD11b+, Ly6G+, quantified left, Mann Whitney test) and CD11b+ Ly6G- cells (quantified right, Mann Whitney test); as a percentage of live cells
C) Ly6C^{hi} in the CD11b+ Ly6G- cell fraction (Mann Whitney test).

Data from three experiments is shown. Unpaired t-test, unless otherwise stated. *p< 0.05.

Figure 5. 23 WT and Sema7a KO mice a have a similar frequency of peritoneal F4/80+ macrophages at 24 hours post APAP injury

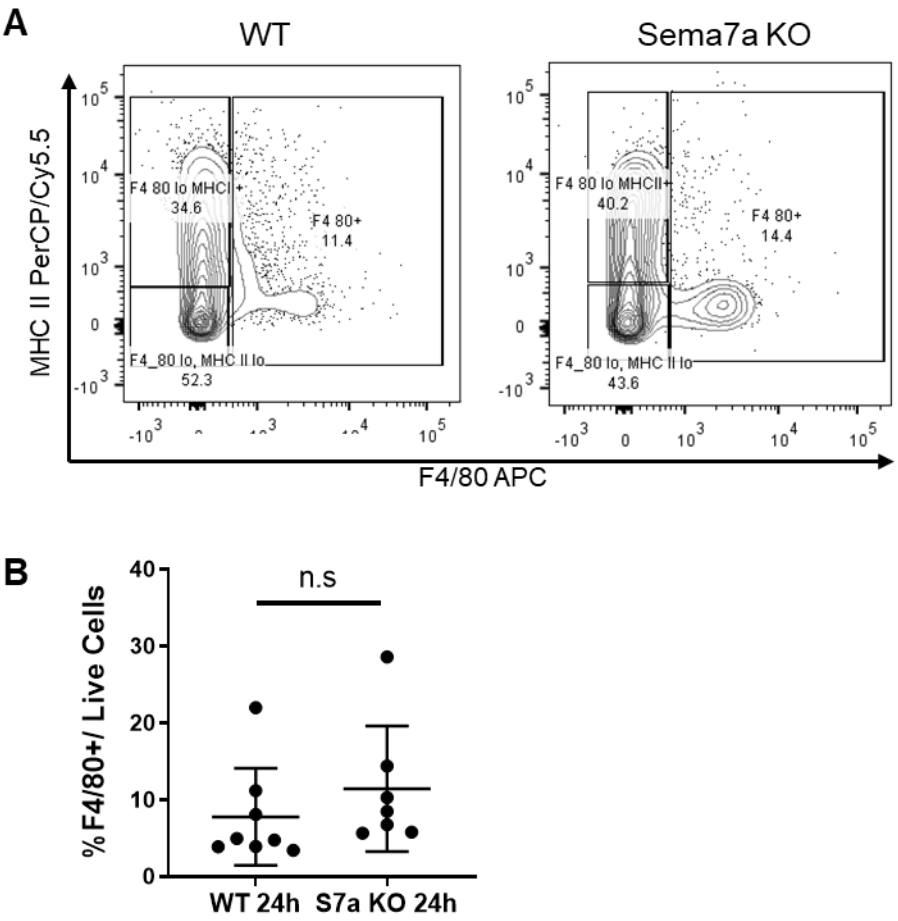

Figure 5. 23

A) Macrophage populations in the peritoneal lavage were separated by the expression of F4/80 and MHC Class II on live cells from WT (left) and Sema7a KO (right) mice, treated with 24 hours APAP.

B) Frequency of F4/80^{hi} mature macrophages. Mann Whitney test.

Data from three experiments is shown.

Comparing leukocyte composition between 12 and 24 hours post APAP overdose

To further analyse the dynamics of the immune system during APAP injury, I compared the frequency of each population present between 12 hours and 24 hours post APAP administration in the WT mice, and separately in the Sema7a KO mice.

In WT mice, the frequency of all NPC populations examined in the liver remained constant between 12 and 24 hours post APAP administration (Figure 5. 24). In our model, resident macrophages become depleted at 12 hours post APAP administration (Figure 5. 2). In Figure 5. 24, the resident macrophages have not significantly increased in frequency from 12 hours to 24 hours post APAP administration. This suggests that the resident macrophage population is not restored by 24 hours post APAP overdose, and the dominant macrophage of the liver is the infiltrating macrophage.

Sema7a KO mice had a significantly lower frequency of infiltrating macrophages ($P=0.0343$) and Ly6C^{hi} monocytes ($P=0.0317$) at 24 hours compared to 12 hours post APAP administration (Figure 5. 24). This reduction may reflect the Sema7a KO macrophage populations returning to normal levels, after the higher influx of infiltrating macrophages seen at 12 hours APAP injury.

Circulatory neutrophils and monocytes remained constant in both the WT and Sema7a KO mice at 12 and 24 hours post APAP administration (Figure 5. 25). Peritoneal F4/80+ GATA6+ macrophages have been previously reported to infiltrate the liver from the peritoneum to promote recovery from a sterile thermal injury [70,71]. This is not seen here between 12 and 24 hours post administration, as the frequency of peritoneal macrophages and neutrophils remained constant between these timepoints (Figure 5. 26).

Figure 5. 24 The frequency of infiltrating macrophages in the liver declines from 12 to 24 hours post APAP in Sema7a KO mice

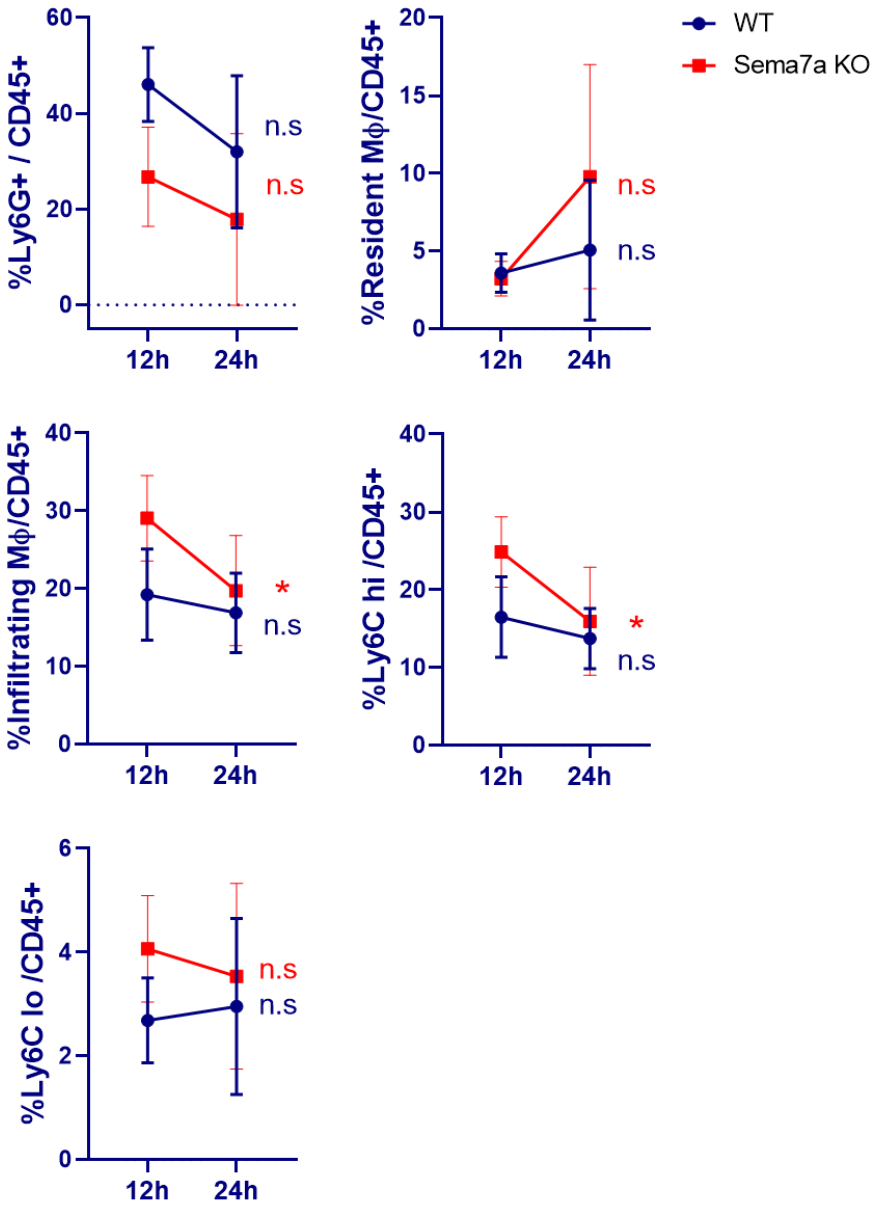

Figure 5. 24

The frequency of NPC cells in the liver was compared between 12 and 24 hours post APAP administration in WT (blue) and Sema7a KO mice (red). Unpaired t-tests, unless otherwise indicated, tested the null hypothesis that there was no change in the frequency of the NPC population between 12 and 24 in WT mice, or Sema7a KO mice in a separate unpaired t-test.

The following NPC populations were analysed: Ly6G+ neutrophils, resident macrophages (WT, Mann Whitney; Sema7a KO, Welch test), infiltrating macrophages, Ly6C^{hi} and Ly6C^{lo} (WT, Mann Whitney) macrophages. *p<0.05. The 12 hour APAP experiment was performed once. The 24 hour APAP experiment was performed three times.

Figure 5. 25 The frequency of neutrophils and monocytes are stable in the blood during APAP injury

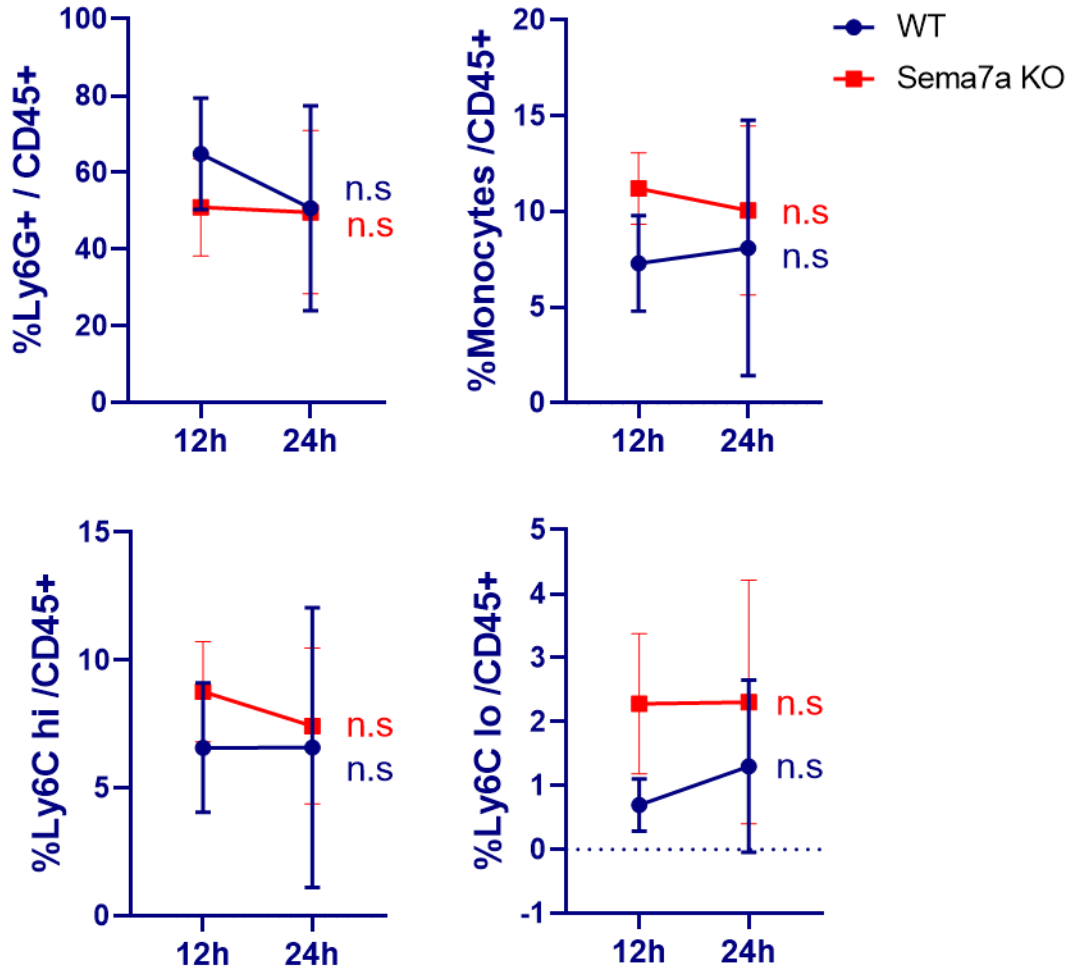

Figure 5. 25

The frequency of circulating immune cells was compared between 12 and 24 hours post APAP administration in WT (blue) and Sema7a KO mice (red). Unpaired t-tests, unless otherwise indicated, tested the null hypothesis that there was no change in the frequency of the NPC population between the 12 hour and 24 hour time point in WT mice, or Sema7a KO mice in a separate unpaired t-test.
The following populations were analysed: Ly6G+ neutrophils (WT, Mann Whitney), monocytes (WT, Mann Whitney), Ly6C^{hi} (Sema7a KO, Mann Whitney) and Ly6C^{lo} monocytes.
The 12 hour APAP experiment was performed once. The 24 hour APAP experiment was performed three times.

Figure 5. 26 The frequencies of PEC populations do not change during APAP injury

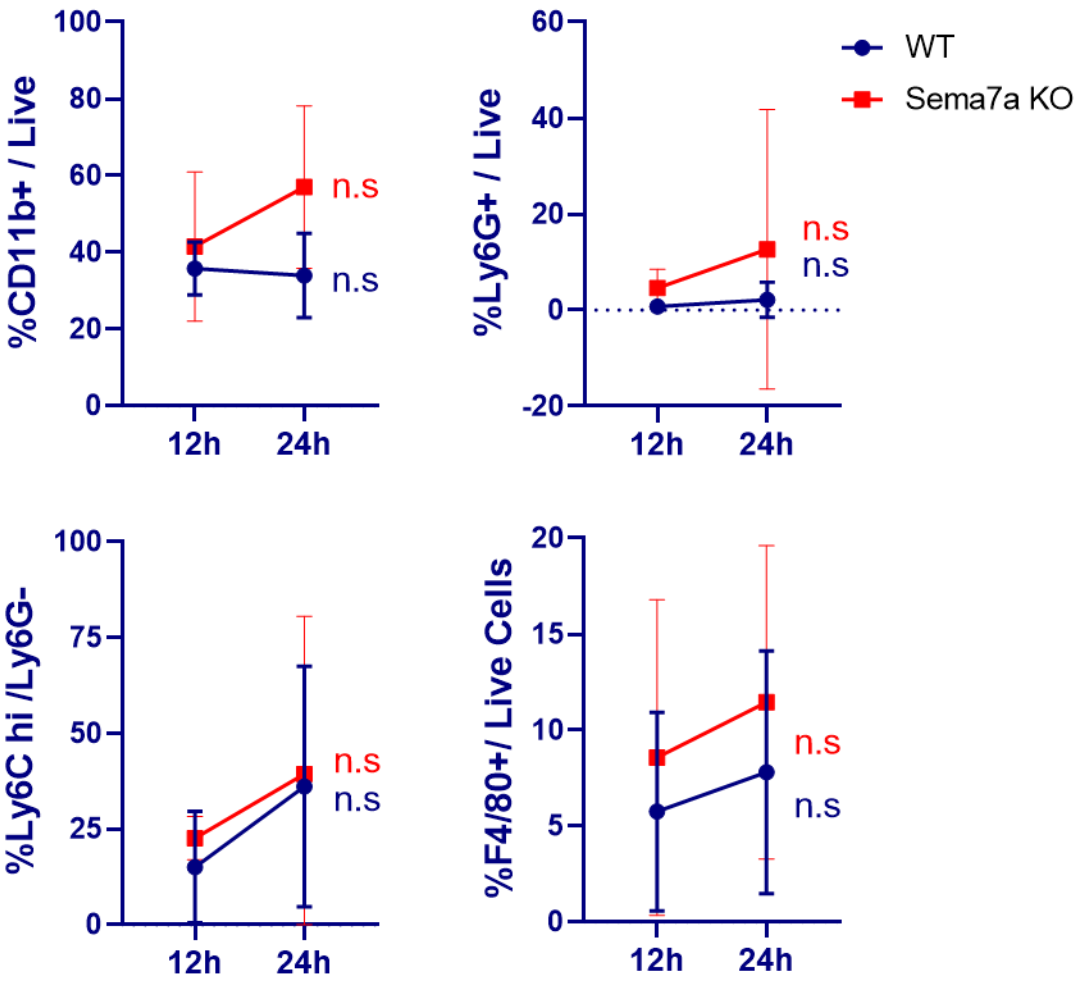

Figure 5. 26

WT (blue) and Sema7a KO mice (red) were compared between 12 and 24 hours post APAP administration for the frequency of the following populations in the peritoneal exudate:
CD11b+ cells (Sema7a KO, Unpaired t-test), Ly6G+ neutrophils, Ly6C^{hi} monocytes and F4/80+ macrophages.
Mann Whitney test unless otherwise stated. The 12 hour APAP experiment was performed once. The 24 hour APAP experiment was performed three times.

Comparing *in vitro* phagocytosis of WT and Sema7a KO BMDMs

Phagocytosis of necrotic debris is required for recovery from APAP injury, and is primarily performed by macrophages [32,51,81]. Phagocytosing macrophages switch from an pro- inflammatory phenotype to a restorative phenotype [72,82,149], and secrete cytokines such as IL-10 [35,62] to reduce inflammation and IL-6 and TNFα to promote hepatocyte proliferation [84,85].

Previously, it has been shown that the herpes and vaccinia poxvirus (A39R) can avoid being phagocytosed by dendritic cells by structurally mimicking Sema7a [218,219]. The viruses bind to Plexin C1 on dendritic cells to prevent the p-FAK dependant cytoskeletal rearrangements required for the dendritic cells to perform phagocytosis [218,219,239]. Therefore, Sema7a mediates phagocytosis through regulation of the cytoskeleton in dendritic cells. To the best of my knowledge, how Sema7a regulates macrophage phagocytosis has not been investigated.

CD11b+ BMDMs were generated from WT and Sema7a KO mice. Apoptotic thymocytes were pre-labelled with the fluorescent CMTMR dye, and fed to BMDMs for two hours, to mimic macrophage phagocytosis of cellular debris during APAP injury. The frequency of phagocytosis (frequency of CD11b+ CMTMR+ BMDMs) was analysed by flow cytometry (Figure 5. 27 A&B).

On average, 15.6% of WT BMDMs had phagocytosed apoptotic T cells after two hours, but only 7.0% Sema7a KO BMDMs had phagocytosed. Unfortunately, there is only 2 repeats of this experiment for the WT BMDMs, due to a fungal infection. With an equal sample number this result may have reached significance (Figure 5. 27C). When visualising the BMDMs by microscopy, the Sema7a KO BMDMs were less smooth in morphology. From each bone marrow isolation, Sema7a KO mice gave a had lower yield of BMDMs compared to their WT counterparts. In summary, Sema7a KO BMDMs had an altered growth, altered morphology and tended to have a lower frequency of phagocytosis.

Figure 5. 27 WT and Sema7a KO BMDMs have the same phagocytic capacity *in vitro*

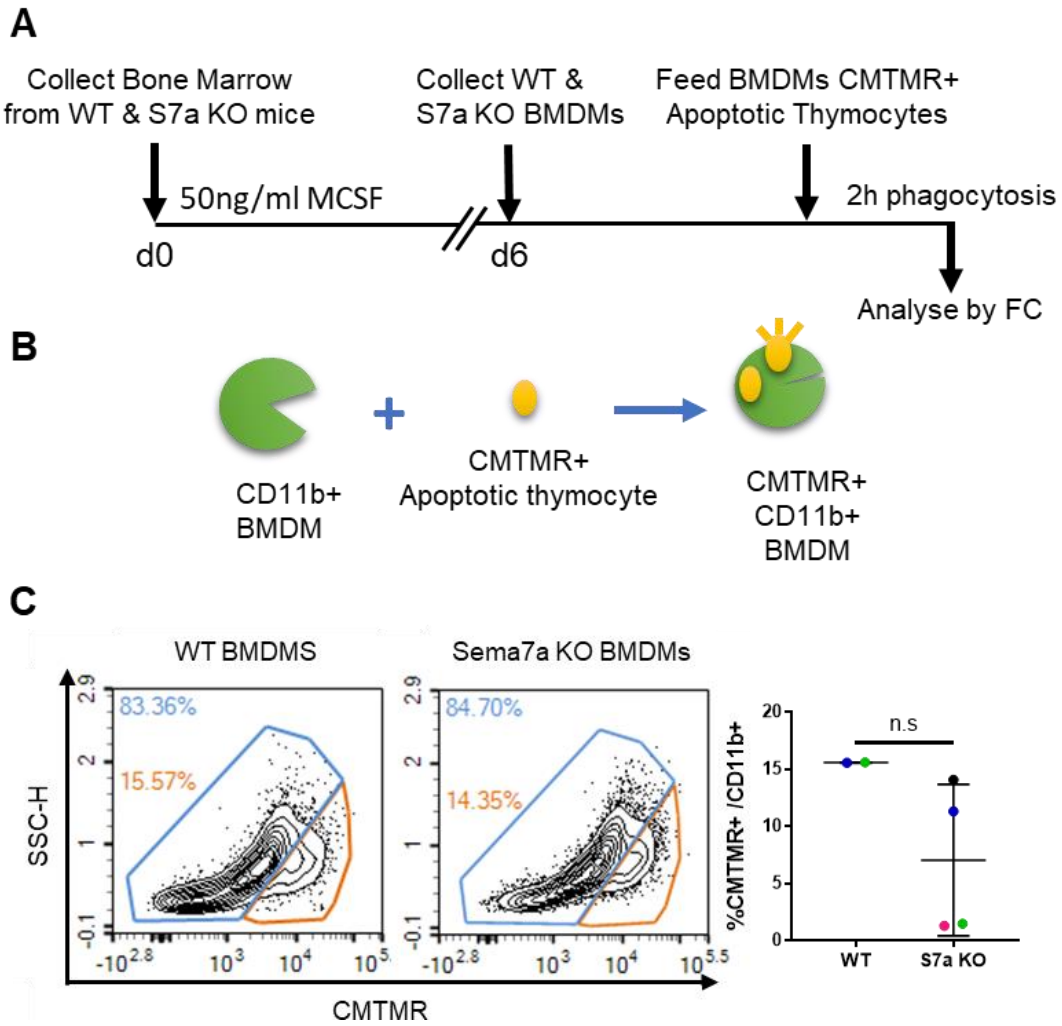

Figure 5. 27

A) Schematic of *in vitro* phagocytosis experiment
B) Diagram of *in vitro* phagocytosis experiment. BMDMs labelled with CD11b are fed 1:5 CMTMR labelled phagocytic thymocytes. BMDMs which have phagocytosed apoptotic thymocytes are CD11b+ CMTMR+.
C) Flow cytometry analysis of *in vitro* phagocytosis experiment. Plots show single, Live CD11b+ cells. CMTMR- BMDMs blue, CMTMR+ BMDMs, orange. WT BMDMs (left) Sema7a KO BMDMs (centre), quantification (right).

Samples were run in triplicate. Each dot represents one BMDM sample, with each colour representing a single experiment. Data from four experiments is shown. Mann Whitney test.

In vivo phagocytosis is unaltered in the Sema7a KO mice at 12 hours post APAP injury

To recover from APAP injury, phagocytosis is required to remove debris. In Figure 5. 27, Sema7a KO BMDMs had the same frequency of phagocytosis as WT BMDMs. However, this study is underpowered. With the correct statistical power, the trend of Sema7a KO BMDMs having a lower frequency of phagocytosis *in vitro*, may be correct.

To examine if defective phagocytosis in Sema7a KO mice caused the increased necrosis seen at 12 hours and raised LFTs at 12 and 24 hours post APAP administration, an *in vivo* phagocytosis assay was performed. A PKH phagocytic dye was injected i.v. 4 hours after APAP administration, mice were euthanised at 12 hours post APAP administration. Phagocytosis was then analysed in the liver, blood and PEC by flow cytometry. For a schematic of this experiment please see Figure 5. 14.

In the liver neutrophils, resident macrophages, infiltrating macrophages and the $Ly6C^{lo}$ and $Ly6C^{hi}$ subpopulations had the same frequency of phagocytosis in WT and Sema7a KO mice at 12 hours post APAP administration (Figure 5. 28). Resident macrophages had the highest frequency of phagocytosis, with 87.0% and 89.7% PKH+ in the WT and Sema7a KO mice, respectively (Figure 5. 28B). Infiltrating macrophages had a low frequency of phagocytosis with 3.7% and 2.8% PKH+ in the WT and Sema7a KO mice, respectively. This may reflect that the infiltrating macrophages are yet to mature into $Ly6C^{lo}$ restorative macrophages. However, I previously detailed no difference in the frequency of $Ly6C^{lo}$ macrophages between 12 and 24 hours post APAP administration (Figure 5. 24).

Figure 5. 28 Liver NPC have the same frequency of phagocytosis in WT and Sema7a KO mice at 12 hours post APAP administration

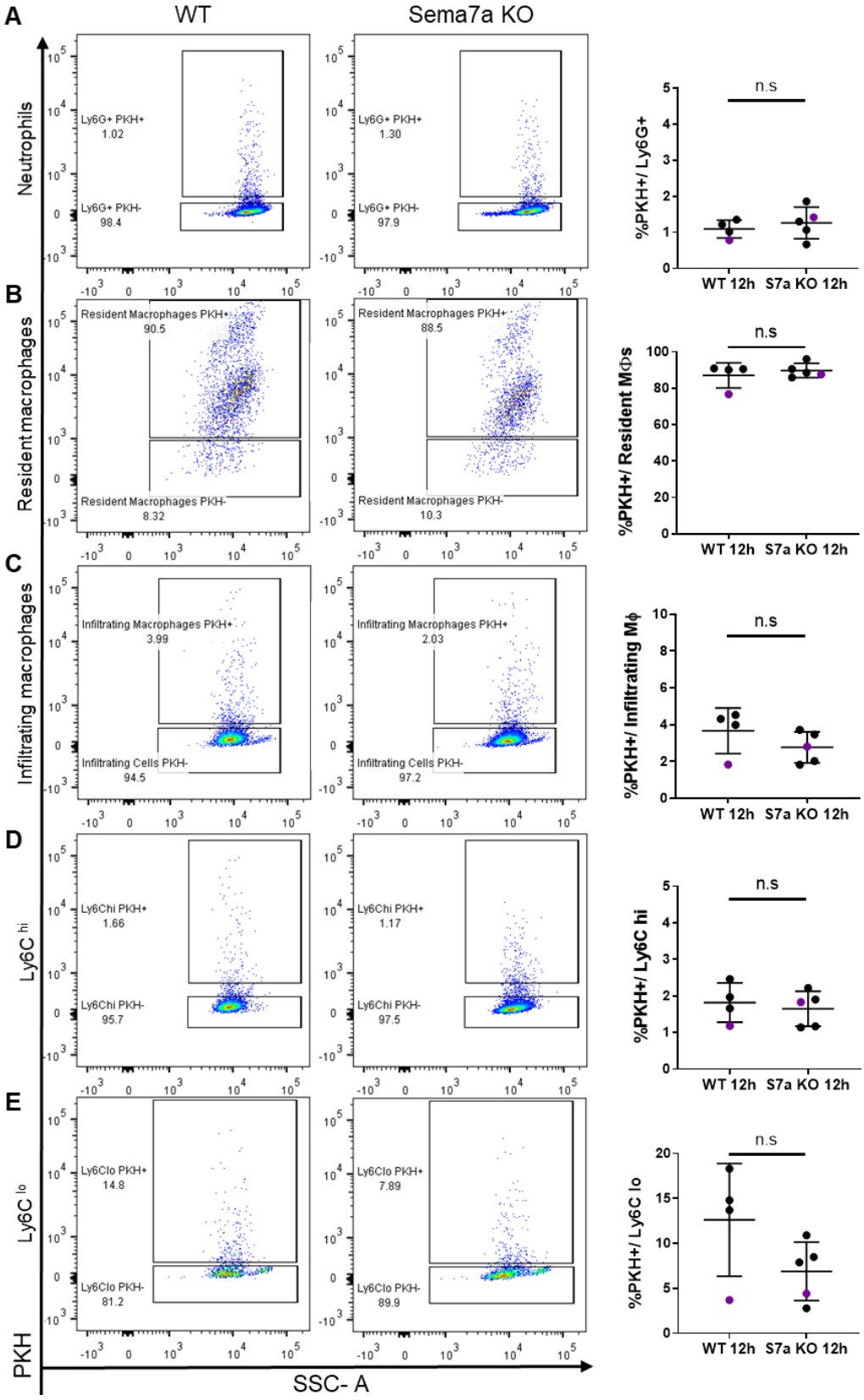

Figure 5. 28

In vivo phagocytosis by liver NPCs isolated from WT (left) and Sema7a KO mice (centre), at 12 hours 350 mg/kg APAP. Quantification (right) show the percentage of phagocytosing cells in each NPC population:

A) Neutrophils,
B) Resident macrophages (Mann Whitney test),
C) Infiltrating macrophages, which was separated into
D) Ly6C^{hi} monocytes
E) Ly6C^{lo} macrophages

Liver digestion and staining was performed by Jennifer Cartwright. Data shown is from one experiment. Each dot represents a single mouse. Purple dot, a mouse which received less PKH i.v.
Unpaired t-test, unless otherwise stated.

Phagocytosis was also examined in the blood. The populations were analysed as before in Figure 5. 16. WT and Sema7a KO mice had the same frequency of phagocytosis in Ly6G+ neutrophils, Ly6G- monocytes, Ly6C^{lo} and Ly6C^{hi} monocytes (Figure 5. 29). Overall, there was very little phagocytosis in the blood with most values below 5% PKH+.

PECs were also analysed for phagocytosis. PEC populations were analysed as before in Figure 5. 17, or Figure 5. 18 specifically for peritoneal macrophages. Peritoneal neutrophils and macrophages had the same phagocytosis in WT and Sema7a KO mice at 12 hours post APAP overdose (Figure 5. 30A & C). However, Ly6C^{hi} monocytes had significantly lower frequency of phagocytosis in Sema7a KO mice with 3.9% PKH+, compared to 22.6% PKH+ in WT mice (P=0.0159, Figure 5. 30B).

Altogether, there was no significant difference in the frequency of PKH phagocytosis between WT and Sema7a KO mice at 12 hours post APAP administration. The exception being peritoneal Ly6C^{hi} monocytes, which had a lower frequency of phagocytosis in Sema7a KO mice. However, this result may be skewed by low cell counts of peritoneal Ly6C^{hi} monocytes in the WT mice.

Figure 5. 29 Circulatory cells have the same phagocytosis in WT and Sema7a KO mice at 12 hours post APAP injury

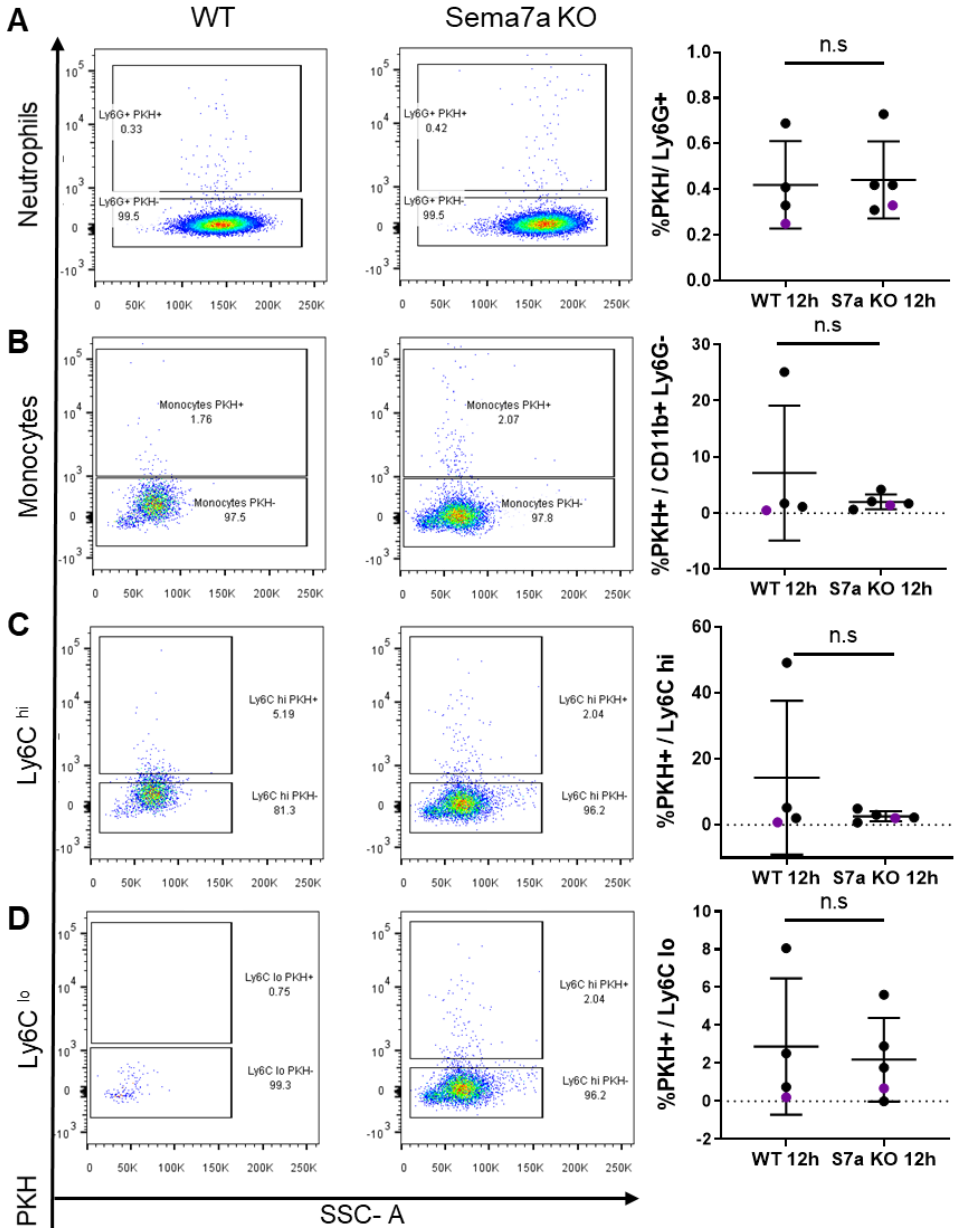

Figure 5. 29

Populations in the peripheral blood from WT (left) and Sema7a KO mice (centre), collected at 12 hours post APAP administration, was analysed for the frequency of phagocytosis (PKH+), quantified (right):

A) Neutrophils
B) Monocytes, which were separated into:
C) Ly6C^{hi} and
D) Ly6C^{lo}

Data from one experiment is shown. Each dot represents a single mouse. Purple dot, a mouse which received less PKH i.v. Unpaired t-test**.**

Figure 5. 30 Sema7a KO Peritoneal Ly6C^{hi} monocytes have a lower frequency of phagocytosis at 12 hours post APAP overdose

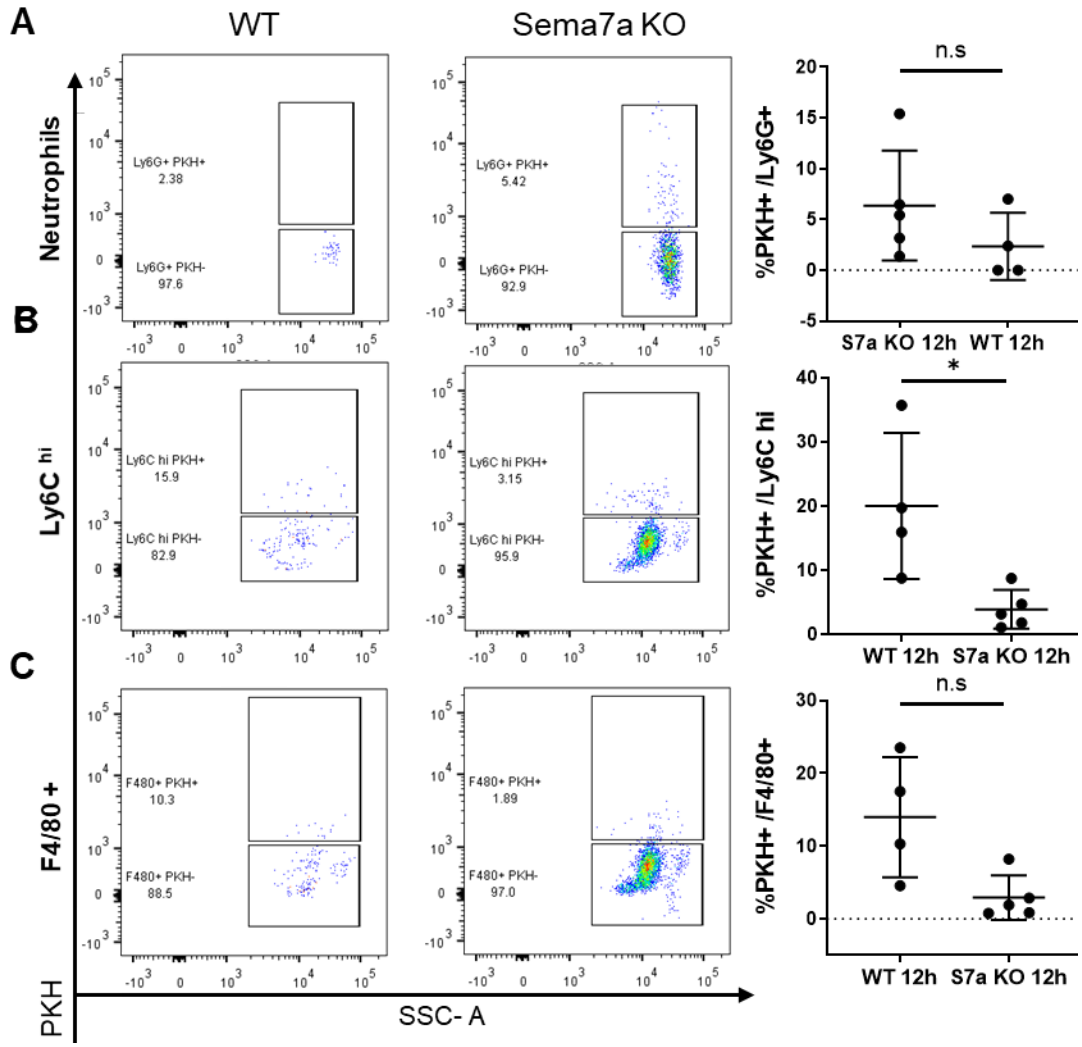

Figure 5. 30

The frequency of PEC phagocytosis was assessed, at 12 hours post APAP overdose in WT and Sema7a KO mice, in the following populations:

A) Neutrophils
B) Ly6C^{hi} monocytes
C) F4/80+ macrophages

Data from one experiment is shown. Mann Whitney test. *p<0.05.

In vivo phagocytosis is unaltered in the Sema7a KO mice at 24 hours APAP injury

After peak injury at 24 hours post APAP administration, mice begin to recover. This requires necrotic material to be removed by phagocytosis. We questioned if *in vivo* phagocytosis was delayed or decreased in Sema7a KO mice. PKH was administered at 8 hours post APAP injection, and mice were sacrificed at 24 hours post APAP administration. For an experimental schematic, please see Figure 5. 19A. Gating for the analysed populations is outlined in Figure 5. 19, and detailed in Chapter 2.

At 24 hours hepatic innate immune cell populations; neutrophils, resident macrophages and infiltrating macrophages, Ly6C^{lo} macrophages and Ly6C^{hi} monocytes, had the same frequency of phagocytosis in WT and Sema7a KO mice, (Figure 5. 31). Resident macrophages still had the highest phagocytic capacity with 64.4% and 63.1% PKH+ in WT and Sema7a KO mice, respectively (Figure 5. 31B).

Infiltrating macrophages had 11.1% and 20.7% PKH+ in WT and Sema7a KO mice, respectively (Figure 5. 31C). Indicating that the infiltrating macrophages are helping the resident macrophages to clear away the debris. Within the infiltrating macrophage population, the Ly6C^{lo} macrophages had a frequency of 17.1% and 28.4% phagocytosis in WT and Sema7a KO mice respectively. This was similar to the frequency of phagocytosis in the Ly6C^{hi} monocytes which had 13.2% and 22.4% PKH+ in WT and Sema7a KO mice, respectively.

Phagocytosis was also analysed in the blood cells. WT and Sema7a KO mice had similar frequencies of phagocytosis in circulating neutrophils, monocytes and in the monocyte subpopulations of Ly6C^{lo} and Ly6C^{hi} (Figure 5. 32).

PECs were also analysed for PKH phagocytosis. Peritoneal neutrophils, Ly6C^{hi} monocytes and F4/80+ macrophages had the same frequency of phagocytosis in WT and Sema7a KO mice (Figure 5. 33).

Figure 5. 31 Liver NPC have the same phagocytosis in WT and Sema7a KO mice at 24 hours post APAP administration

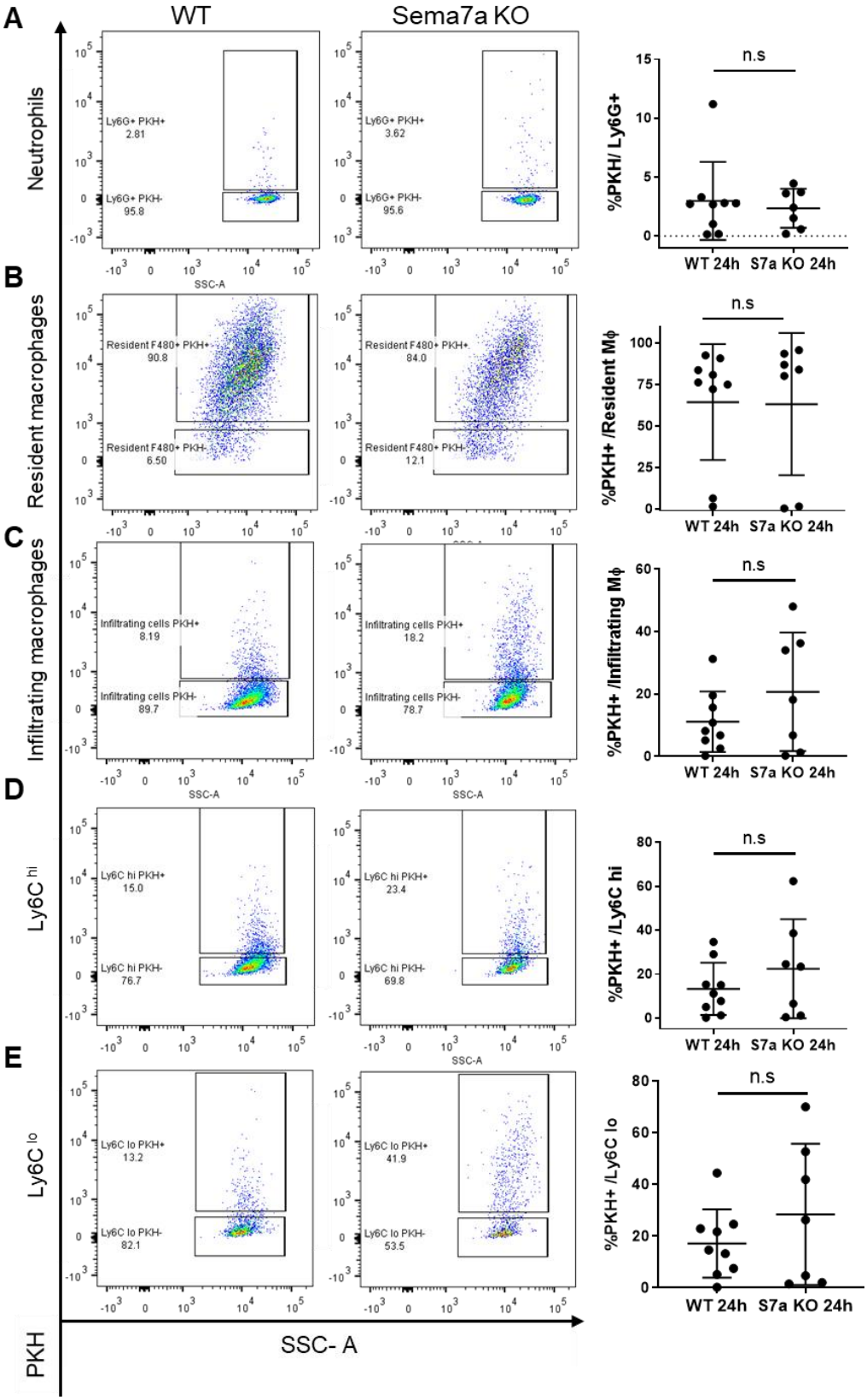

Figure 5. 31
In vivo phagocytosis by liver NPCs isolated in WT (left) and Sema7a KO mice (centre), at 24 hours post APAP injection. Graphs (right) show the frequency of phagocytosing cells in each NPC population:

A) Neutrophils (Mann Whitney test),
B) Resident macrophages (Mann Whitney test),
C) Infiltrating macrophages**,** which was separated into (D) and (E)
D) Ly6C^{hi} infiltrating macrophages
E) Ly6C^{lo} infiltrating macrophages

Data from three experiments is shown. Liver digestion and staining was performed by Jennifer Cartwright. Unpaired t-test, unless otherwise stated.

Figure 5. 32 Circulatory cells have the same phagocytosis in WT and Sema7a KO mice at 24 hours post APAP injury

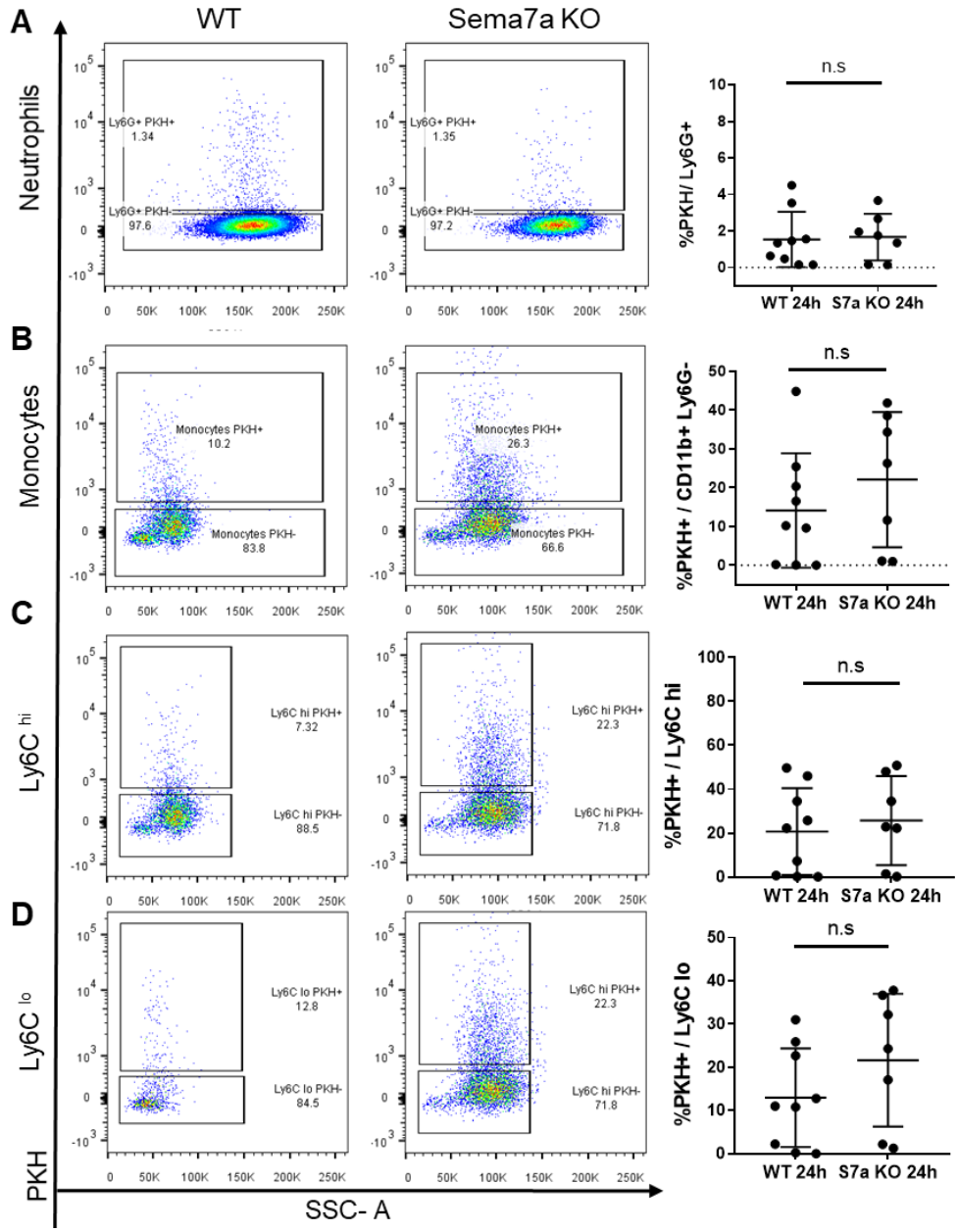

Figure 5. 32

Peripheral blood was collected from WT (left) and Sema7a KO mice (centre) at 24 hours APAP. The following populations were analysed for frequency phagocytosis (PKH+):

A) Neutrophils,
B) Monocytes
C) Ly6C^{hi} monocytes
D) Ly6C^{lo} monocytes

Data is shown from three experiments, and quantified (right). Unpaired t-test, unless otherwise stated.

Figure 5. 33 PECs have the same phagocytosis in WT and Sema7a KO mice at 24 hours post APAP injury

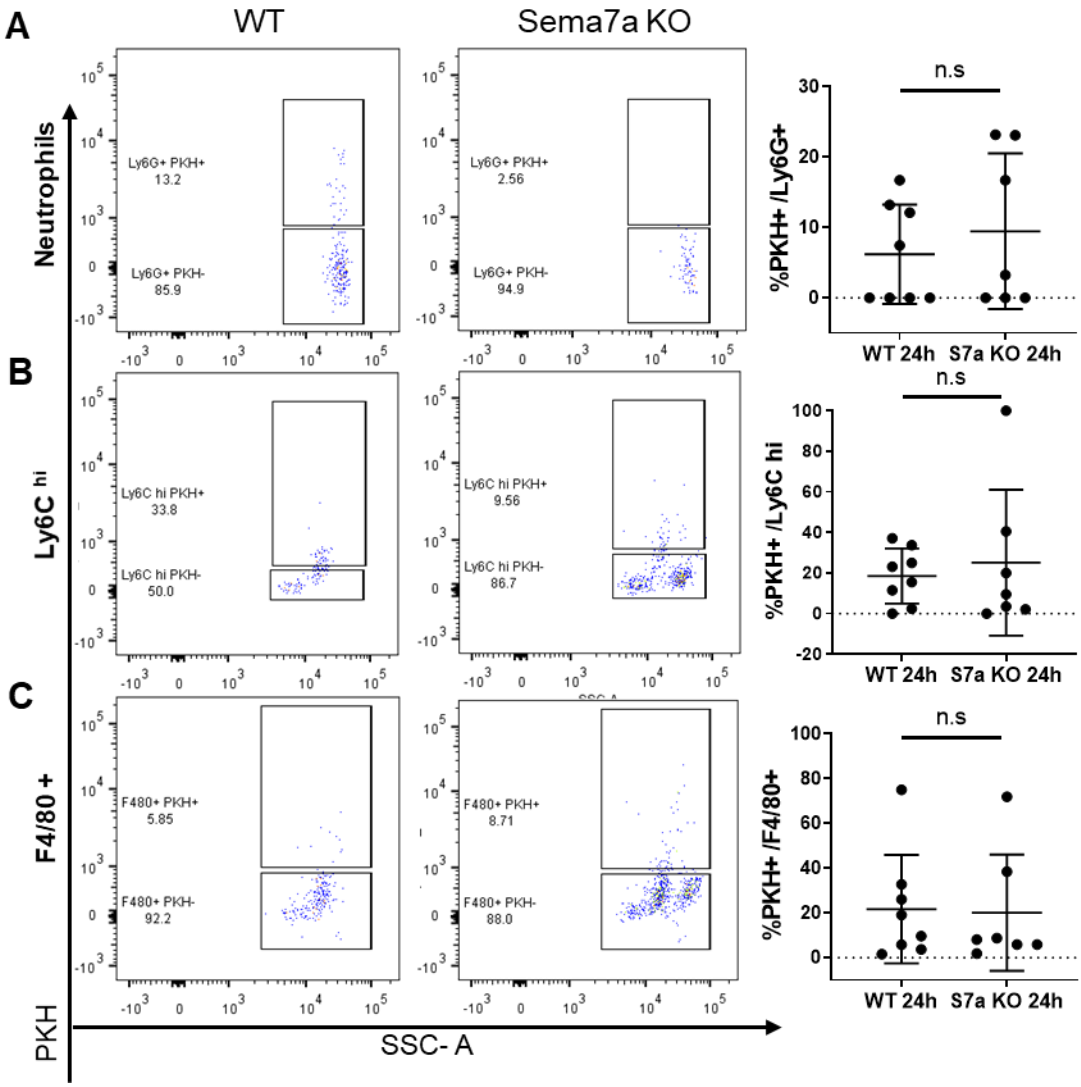

Figure 5. 33

PECs were collected from WT (left) and Sema7a KO mice (centre) at 24 hours post APAP overdose. The following populations were analysed for frequency of phagocytosis (PKH+), quantified (right):

A) Neutrophils
B) Ly6C^{hi} monocytes
C) F4/80+ macrophages

Data is shown from three experiments. Mann Whitney test.

The frequency of monocyte phagocytosis is significantly increased at 24 hours post APAP overdose

At 24 hours post APAP administration, there was trend of increased *in vivo* phagocytosis, compared to 12 hours. To quantify this, the frequency of phagocytosis from each population was compared in the WT between 12 and 24 hours post APAP overdose, and in Sema7a KO mice between 12 and 24 hours post APAP overdose.

The frequency of phagocytosis in infiltrating macrophages in the liver increased from 3.7% at 12 hours to 11.1% at 24 hours post APAP overdose in WT mice. In Sema7a KO mice the frequency of phagocytosis rose significantly (P=0.0467) from 2.8% PKH+ at 12 hours, to 20.7% PKH+ at 24 hours post APAP overdose (Figure 5. 34). In addition, the Ly6C^{hi} monocyte subpopulation of the infiltrating macrophages also had significantly higher %PKH+ (P=0.0206). This increased phagocytosis by infiltrating macrophages will clear debris created by APAP toxicity. The increase in phagocytosis by Ly6C^{hi} monocytes may reflect a switch from a pro inflammatory phenotype to the Ly6C^{lo} restorative phenotype. However, and increase in the percentage of Ly6C^{lo} macrophages was not seen in the Sema7a KO mice at 24 hours post APAP administration. Perhaps 24 hours post APAP administration is the start switch between Ly6C^{hi} and Ly6C^{lo} phenotypes. A significant change may therefore be detected at later timepoints.

In Sema7a KO mice, circulating neutrophils (P=0.0439), monocytes (P=0.0225) and the Ly6C^{hi} (P=0.0232) and Ly6C^{lo} monocytes (P=0.0152) all had increased frequency of phagocytosis at 24 hours compared to 12 hours post APAP administration. In WT mice, these populations had a trend to increase, but only the Ly6C^{lo} population had a significant increase in the frequency of phagocytosis (P=0.0364) (Figure 5. 35).

Peritoneal macrophages, Ly6C^{hi} monocytes and neutrophils did not change their frequency of phagocytosis from 12 to 24 hours post APAP injury in either WT and Sema7a KO. This suggests phagocytosis by PECs is not a major requirement following APAP injury (Figure 5. 36).

On the whole, there is increased phagocytosis at 24 hours post APAP overdose. Sema7a KO mice had significantly more phagocytosis in infiltrating macrophages of the liver, and blood monocytes at 24 hours, compared to 12 hours post APAP administration, underlining the systemic nature of APAP injury.

Figure 5. 34 Infiltrating macrophages significantly increase their frequency of phagocytosis from 12 hours to 24 hours post APAP injury

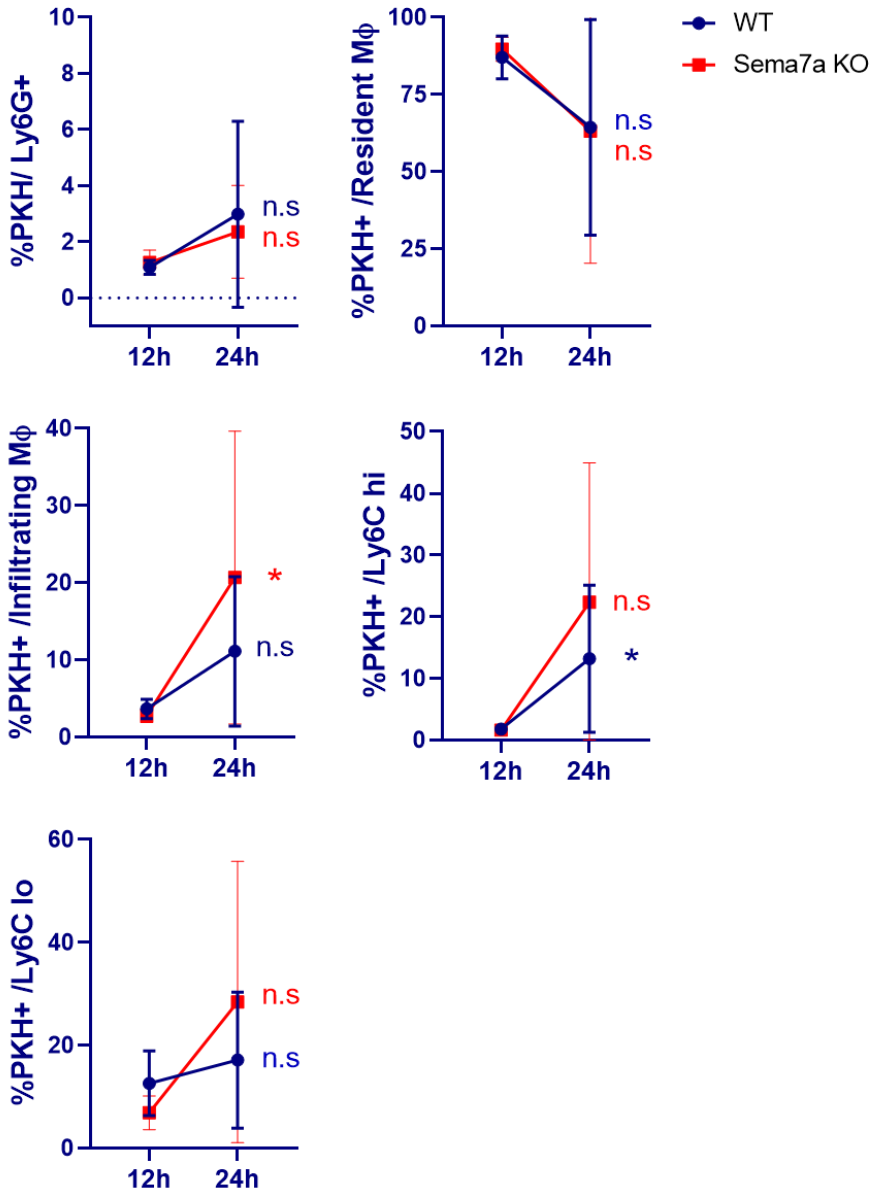

Figure 5. 34

The frequency of liver NPC cells phagocytosis was compared between 12 and 24 hours post APAP administration in WT (blue) and Sema7a KO mice (red).

%PKH+ was analysed in the following NPC populations: Ly6G+ neutrophils (WT, Mann Whitney; Sema7a KO, Welch test), resident macrophages (WT and Sema7a KO, Mann Whitney), infiltrating macrophages (WT and Sema7a KO, Welch test), Ly6C^{hi} (Sema7a KO, Welch test) and Ly6C^{lo} (WT and Sema7a KO, Welch test) macrophages.

Unpaired t-test, unless otherwise indicated, between 12 and 24 hours post APAP in WT or Sema7a KO mice. * $p<0.05$. The 12 hour APAP experiment was performed once. The 24 hour APAP experiment was performed three times.

Figure 5. 35 Monocytes in the blood of Sema7a KO mice significantly increase their frequency of phagocytosis from 12 to 24 hours APAP injury

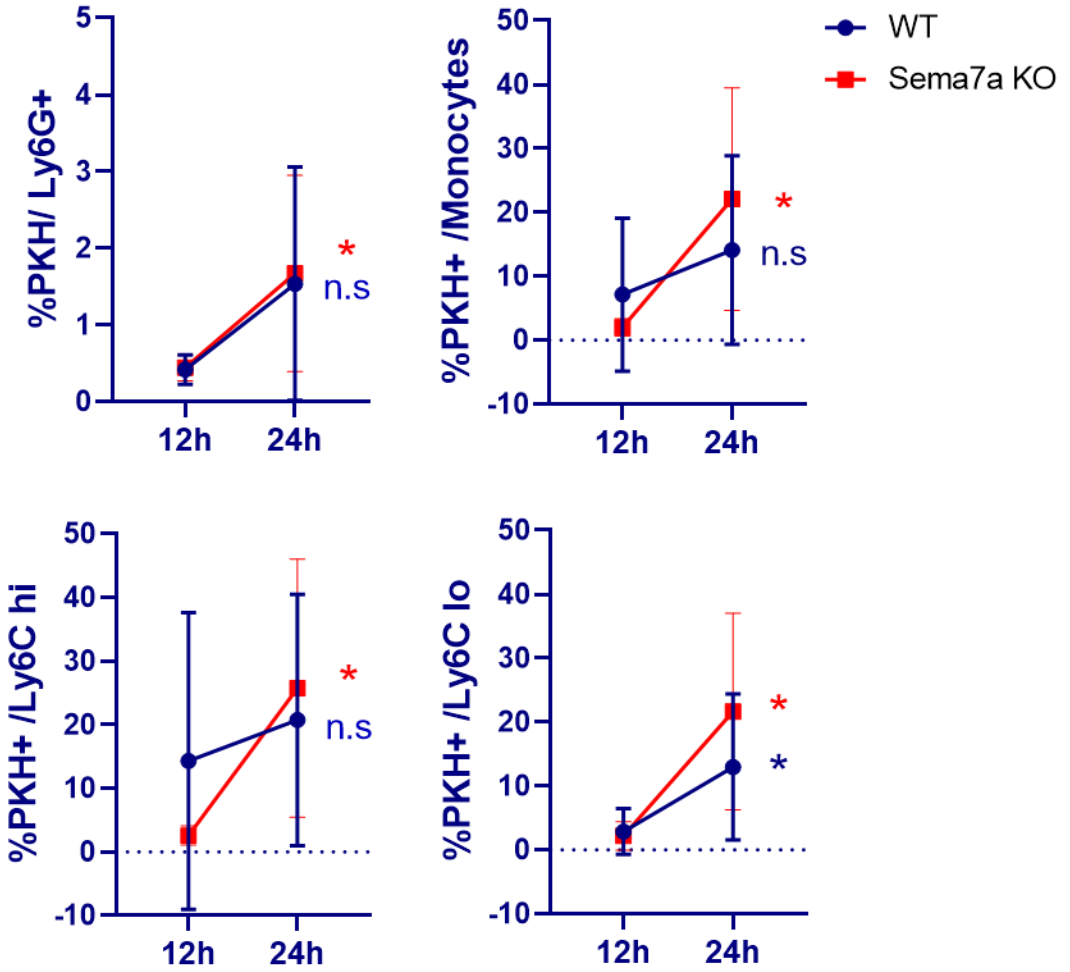

Figure 5. 35

The frequency of phagocytosis in circulating immune cells was compared between 12 and 24 hours post APAP administration in WT (blue) and Sema7a KO mice (red), in the following populations: Ly6G+ neutrophils (WT and Sema7a KO mice, Welch test), monocytes (WT, Mann Whitney; Sema7a KO, Welch test), Ly6C^{hi} (WT, Mann Whitney; Sema7a KO, Welch test) and Ly6C^{lo} (Sema7a KO, Welch test).

Unpaired t-tests, unless otherwise indicated. The 12 hour APAP experiment was performed once. The 24 hour APAP experiment was performed three times.

Figure 5. 36 PECs maintain the same frequency of phagocytosis between 12 and 24 hours APAP injury

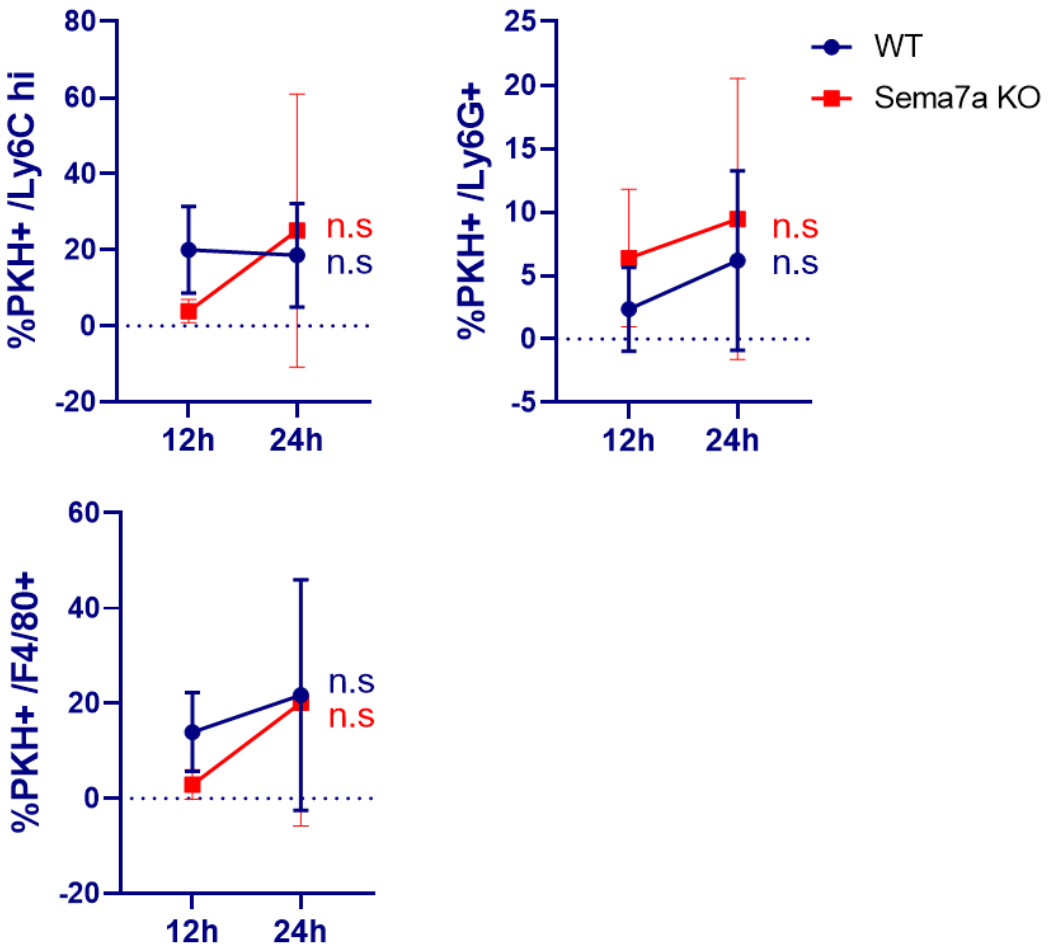

Figure 5. 36

Frequency of phagocytosis (%PKH+) in PECs was compared in WT (blue) and Sema7a KO mice (red) at 12 and 24 hours post APAP administration.
The following PEC populations were analysed: Ly6G+ neutrophils (WT unpaired t-test), Ly6C^{hi} monocytes (WT unpaired t-test) and F4/80^{hi} mature macrophages.

Mann Whitney test unless otherwise stated. The 12 hour APAP experiment was performed once. The 24 hour APAP experiment was performed three times.

Discussion

APAP injury is both enhanced and resolved by the innate immune system [35]. Sema7a has been previously reported as an immunomodulator [151,228,230]. During liver and lung injury Sema7a KO mice have less inflammation [212,246]. In Chapter 4, Sema7a KO mice appeared to have more small mononuclear cells present in the necrotic area. This chapter investigates if Sema7a promotes inflammation during APAP injury.

Firstly, the location of neutrophils and F4/80+ macrophages was examined during a time course of APAP injury. Sema7a KO mice have an enhanced depletion of resident F4/80+ macrophages at 12 hours post APAP challenge. By 24 hours post APAP injury, the number of Sema7a KO F4/80+ macrophages matched the WT mice, but they could not infiltrate the central necrotic zone. In addition, Sema7a KO mice had more neutrophils in the necrotic area.

Secondly, the composition of the liver, blood and peritoneum were examined at 12 and 24 hours post APAP overdose. At 12 hours post APAP overdose, Sema7a KO mice had more infiltrating macrophages, and more blood Ly6C^{lo} monocytes. At 24 hours post APAP injury, there was no difference in the frequency of investigated populations in the liver, blood and peritoneum exudate in WT and Sema7a KO mice.

Thirdly, phagocytosis was compared between the WT and Sema7a KO mice. There was no significant difference in the frequency of phagocytosis *in vitro* or *in vivo*.

Taken together, Sema7a KO mice have more inflammation at 24 hours APAP, but this may be due to compensatory or knock on effects from the increased necrosis at 12 hours post APAP injection. The rest of this discussion examines why there was increased neutrophils in the necrotic area of Sema7a KO mice, and why there were less F4/80+ macrophages at 12 hours post APAP overdose. Within these analyses there are conflicting data. The reasons for this are also debated.

Neutrophils are the first responders of the innate immune system. In our model, neutrophils infiltrated and accumulated in the liver from 12 to 24 hours post APAP overdose. By 42 hours post APAP overdose, the neutrophils had begun to recede. Sema7a KO mice had an increased neutrophil population in the necrotic area at 24 hours post APAP overdose. This was not attributed to a lack of intrinsic Sema7a, or more patrolling neutrophils in the liver or blood of healthy mice.

The increased neutrophil population is not due to an early accumulation or delayed entry to the liver. At 12 hours post APAP administration, Sema7a KO mice had a lower frequency of neutrophils in the CD45+ NPC fraction. However, this was not mirrored in the number of neutrophils per gram of liver, which was equal to WT mice. At 24 hours APAP, WT and Sema7a KO mice had the same frequency and number of neutrophils present in the liver measured by flow cytometry, and at 24 and 42 hours post APAP overdose in the IHC analysis.

The increased neutrophil population was not due to an enhanced infiltration or depletion of neutrophils from the blood or peritoneum. At 12 and 24 hours post APAP overdose, WT and Sema7a KO mice had the same frequency of neutrophils in the blood and peritoneal exudate.

Potentially, the neutrophils are being retained in the necrotic area of the Sema7a KO mice by local signals. In Chapter 4, Sema7a KO mice had peri-necrotic hepatocytes with non-nuclear HMGB1. HMGB1 is normally localised to the nucleus, where it facilitates DNA transcription. During necrosis HMGB1 is passively released to act as a DAMP. Innate immune cells or epithelial cells can actively secrete HMGB1 as a cytokine under stress conditions [275]. During APAP injury, HMGB1 attracts neutrophils to necrotic areas injury via their RAGE receptor. Deletion of hepatocyte HMGB1 resulted in less neutrophil migration during APAP injury [53]. Therefore, the non-nuclear HMGB1 detected in peri-necrotic Sema7a KO hepatocytes in Chapter 4, may act as a local signal to retain neutrophils in the necrotic area.

In addition to localised HMGB1, Sema7a KO mice had more CXCL1 in the serum, at 24 hours post APAP overdose compared to WT mice. CXCL1 is a known chemoattractant of neutrophils [52,282]. This systemic cytokine expression may contribute to the persistent neutrophil population seen in the Sema7a KO mice. However, this was not reflected by an increased circulatory population of neutrophils, or increased presence of neutrophils in the whole liver, as shown by flow cytometry.

An alternative theory for persistent neutrophils in the necrotic area is that they are not being cleared by macrophages. Neutrophils recruit monocytes to areas of injury. Subsequently, the monocyte derived macrophages clear the apoptotic neutrophils through phagocytosis [91,111,121]. However, less than 2% of the neutrophils expressed the apoptotic marker active caspase 3. This suggests the neutrophils are not undergoing apoptosis. However, this analysis does not exclude that neutrophils are undergoing necrosis or NETosis. Neutrophil necrosis could be assessed with a Ly6G and TUNEL dual stain, so far this protocol is not optimised in our lab. At 24 hours post APAP administration there was no difference in the frequency of macrophage phagocytosis in the liver of WT and Sema7a KO mice. Consequently, it is unlikely that neutrophils persist because they are not being cleared by macrophages.

Neutrophils can reverse migrate back into the circulation, and are taken to the bone marrow to apoptose and be recycled [117]. In zebra fish, macrophages “contact ” the neutrophil to induce reverse migration [122]. As there were less macrophages in the central necrotic area of Sema7a KO mice, the contact reverse migration maybe reduced. In addition, endothelial Sema7a binds to Plexin C1 on PMNs to facilitate cell transmigration during hypoxia, or acute lung injury [211,237]. Therefore, neutrophils may persist in the necrotic area due to incumbered reverse migration. Persistent neutrophils can lead to the formation of non-healing wounds, with incessant necrosis, and a delay in vascularisation [117]. To assess this, a neutrophil transmigration study across endothelial cells overexpressing Sema7a or with Sema7a deleted could be performed.

To conclude, neutrophils persist in the necrotic areas of Sema7a KO mice at 24 hours post APAP overdose. This may be a consequence of elevated CXCL1 or secreted HMGB1 signalling or delayed reverse migration.

Sema7a is an attractant for monocytes, and modulates if macrophages secrete pro- or anti-inflammatory cytokines [228,231,232,236]. Macrophages are required for recovery after APAP [4,35]. To investigate a deficiency of Sema7a affected macrophages during APAP injury, the monocyte and macrophages populations of the liver, blood and peritoneum were analysed at 12 and 24 hours post APAP administration in WT and Sema7a KO mice.

Healthy WT and Sema7a KO mice had the same number of F4/80+ macrophages per field of view. In Sema7a KO mice, there were less F4/80+ macrophages in the central necrotic zone at 24 hours post APAP administration. This could be due to a migration

defect in the macrophages of the Sema7a KO mice, as Sema7a acts as a chemoattractant for monocytes and macrophages [228,229]. In dendritic cells, Sema7a regulates migration and adhesion by modulating the cytoskeleton via p-FAK signalling [228,230]. To test macrophage migration, WT and Sema7a KO BMDMs migration towards dying cells could be assessed. To test if Sema7a is acting as a chemoattractant, migration of WT BMDMs could be examined towards a gradient of Sema7a.

Alternatively, the F4/80+ macrophages may be being prevented from entering the central necrotic area by the persistent neutrophils. In a model of sterile thermal injury, invariant natural killer (iNKT) cells are retained at the edge of the necrotic lesion from 4 hours post thermal injury. This is achieved by KC presenting self-antigens to the iNKTs and IL-12 and IL-18 signalling. 48 hours post thermal injury, the iNKT cells entered the necrotic lesion and promote recovery [290]. Perhaps there is a similar spatial- temporal control of innate immune cells during APAP injury, which is delayed in the Sema7a KO mice.

APAP injury induces resident macrophage depletion [48–51]. Subsequently, infiltrating macrophages are recruited to the liver, significantly boosting the liver macrophage population, and become the dominant macrophage population in the liver [48]. This loss and gain of macrophages can been seen in the IHC analysis presented here. At 12 hours post APAP administration the number of F4/80+ macrophages is reduced. Depletion of F4/80+ macrophages was significantly enhanced in the Sema7a KO mice. This was not due to an intrinsic defect, as macrophages did not express Sema7a when examined in Chapter 3. At 12 hours post APAP administration, Sema7a KO mice had more necrosis. This increased injury may have enhanced F4/80+ macrophage depletion, or vice versa.

From 12 to 24 hours post APAP challenge, there is a 2-3 fold increase in the number of F4/80+ macrophages in the liver. By 24 hours post APAP injury, WT and Sema7a KO mice have equivalent levels of F4/80+ macrophages. At this time point there are more F4/80+ macrophages present in the liver than in healthy mice. By 42 hours post APAP injury, the F4/80+ macrophage population is reduced. The resident macrophage population is replenished by self-renewal, or are replaced by the infiltrating macrophages [48,65–67].

The enhanced depletion of F4/80+ macrophages in Sema7a KO mice, and the increase of F4/80+ macrophages in the liver, demonstrated by IHC, is not confirmed by flow cytometry analysis. Flow cytometry analysis of the NPC fraction of the liver

implies that WT and Sema7a KO mice have the same frequency and absolute count of resident macrophages at 12 and 24 hours post APAP overdose. To clarify this, staining for Clec4F, a more specific marker of KCs [65], could be utilised to distinguish between KCs and infiltrating macrophages which can both express F4/80.

Our flow cytometry analysis agrees that the infiltrating macrophages are the most dominant population of the liver. However, the frequency of infiltrating macrophages did not significantly increase from 12 and 24 hours post APAP administration, as shown here in the IHC analysis and previously [48]. As APAP is a highly variable model, a minimum of n=8 is required to reach statistical significance. I would therefore like to repeat the 12 hours flow cytometry experiment and re-examine our findings.

The conflicting results gained reflects the differences in the two techniques. Images taken for IHC focussed on the necrotic centrilobular areas, whereas flow cytometry analyses the NPC fraction from a digest of the whole left lobe. Unlike DAB staining, flow cytometry excludes dying cells and does not amplify the positive signal. Over 90% of resident and infiltrating macrophage populations were viable at 12 hours post APAP administration. On the other hand, dying cells down regulate the expression of their surface antigens [291], without an amplification they may be excluded from the flow cytometry analysis. Therefore, the DAB IHC analysis may be including dying cells which are not detected by flow cytometry.

To assess if the Sema7a KO F4/80+ macrophages are depleted through cell death at 12 hours post APAP administration, I would like to perform an active caspase 3 or TUNEL stain with F4/80. Due to different antigen retrievals required for these stains, I do not yet have a working protocol to examine this.

With these conflicting results, I revisited the F4/80 macrophage slides used for the IHC analysis. There was visibly less F4/80+ macrophages in Sema7a KO mice at 12 hours post APAP administration. At this current point, the IHC data is probably more reliable. There is the required n= 8 in each stain and the loss of F4/80+ macrophages is clearly visible across the liver. Whereas the flow cytometry data is under powered.

Sema7a KO mice had significantly more infiltrating macrophages at 12 hours post APAP administration. This may be a compensatory effect to replace the more depleted resident macrophage compartment. Infiltrating macrophages originate in the bone marrow and travel via the blood to the liver [35,51]. Healthy mice had the same frequency of circulating macrophages, so this increase in infiltrating monocytes is a

direct response to APAP injury. In line with this, Sema7a KO had more circulating Ly6C^{lo} monocytes, which will contribute to the infiltrating macrophage population. Sema7a KO mice have more necrosis at 12 hours post APAP administration, presumably, there will be more DAMPs secreted to recruit innate immune cells, including infiltrating macrophages. Infiltrating macrophages are recruited by CCL2 (MCP1) [49,63], and CSF1. CSF1 has the additional benefit of promoting macrophage infiltration and differentiation into restorative macrophages [32]. It would be interesting to see if CCL2 or CSF1 were upregulated in Sema7a KO mice at 12 hours post APAP overdose.

IL-6 is a highly diverse cytokine with both pro- and anti -inflammatory affects. At 24 hours post APAP administration, the concentration of IL-6 was higher in the serum of Sema7a KO mice, compared to WT. The IL-6 receptor is expressed by hepatocytes, neutrophils, and monocytes [292]. As such it can regulate neutrophil and monocyte recruitment [293]. In combination with CSF1, it can promote monocytes to differentiate into macrophages [294,295]. In APAP injury, IL-6 is required for hepatocyte proliferation [85], and facilitates macrophage phagocytosis [72]. Sema7a signalling induces IL-6 secretion from PMNs and macrophages [231,232,245]. During chronic CCl_4 injury, Sema7a enhances TGFβ induced IL-6 transcription [246]. In alveolar cell lines IL-6 promotes the expression of Sema7a as part of a positive feedback loop [212]. In these studies, it was implied IL-6 has a pro-inflammatory role.

Without studies involving IL-6 deletion and overexpression it is impossible to know its role of elevated IL-6 in the Sema7a KO serum at 24 hours post APAP overdose. It may be an attempt initiate Sema7a production in the Sema7a KO mice, as IL-6 can promote Sema7a expression via NF-κB [212]. It is unlikely to be to enhance recruitment or differentiation of macrophages, as WT and Sema7a KO mice had the same frequency of monocytes and macrophages in the blood, liver and peritoneal exudate. IL-6 might enhance proliferation and phagocytosis in the Sema7a KO mice, but again *in vivo* phagocytosis and proliferation was not affected in the Sema7a KO mice.

Peritoneal F4/80+ GATA6+ macrophages infiltrated the liver within one hour of sterile thermal injury, and aided recovery by dismantling necrotic nuclei and promoted vascular regeneration [71]. Depletion of peritoneal macrophages with liposomal chlodronate prevented mice recovering from CCl_4 injury. It is unknown if peritoneal macrophages contribute to APAP injury and recovery. Here, I examined the frequency of neutrophils, macrophages and Ly6C^{hi} monocytes in the peritoneal exudate. The

frequencies of these populations did not alter between 12 and 24 hours post APAP administration, suggesting they do not contribute to inflammation during APAP injury. However, Wang *et al*. observed these GATA6+ F4/80+ macrophages infiltrating the liver within 1 hour of injury. Perhaps they do contribute to APAP liver inflammation, but before the 12 hour time point.

To recover from APAP injury, phagocytosis is required to remove debris. Sema7a KO BMDMs tended to have lower frequency of phagocytosis, compared to WT BMDMs. These experiments need repeating to be confirmed. *In vivo*, WT and Sema7a KO mice had the same phagocytosis in the liver, blood and PEC in all macrophage, monocyte and neutrophil populations examined. The only exception being peritoneal Ly6C^{hi} monocytes, which had a higher frequency of phagocytosis at 12 hours post APAP administration in WT mice. Phagocytosis can induce a switch from Ly6C^{hi} to Ly6C^{lo}. However, this was not reflected in the frequency of Ly6C^{lo}.

The *in vivo* phagocytosis experiment used a fluorescent bead as phagocytic cargo, whereas the *in vitro* experiment used apoptotic thymocytes. This difference in cargo may explain why there was no difference in phagocytosis *in vivo* between WT and Sema7a KO mice. Sema7a KO mice may therefore have lower phagocytosis of cells, cellular debris or bacteria *in vivo*. *In vivo* LPS phagocytosis can be examined by injecting fluorescent LPS particles. However, as APAP is a sterile injury this experiment would not inform us if phagocytosis of host cellular debris was affected by a lack of Sema7a.

Infiltrating macrophages drastically increased their frequency of phagocytosis in Sema7a KO mice from 12 to 24 hours post APAP overdose. Presumably, this is to remove debris. It is currently unknown what induces the switch from a proinflammatory to a restorative phenotype, and the onset of recovery at a specific time point. Cytokines including IL-10 and IL-4 [296] and phagocytosis [72,149] are known to be important. The resident macrophages had a high rate of phagocytosis at both 12 and 24 hours post APAP injury, but recovery only began after the 24 hour time point. Maybe the infiltrating macrophages needed time to mature, before they could start phagocytosing. Perhaps the APAP induced necrosis and inflammation needs to be contained, before the anti-inflammatory signals could take precedence, and recovery begin.

In this chapter we have shown Sema7a KO mice have persistent neutrophils in the necrotic area at 24 hours post APAP administration. They may be being retained by

local HMGB1 signalling or systemic CXCL1, or due to a delay in their reverse migration.

F4/80+ macrophages were more depleted in Sema7a KO mice, at 12 hours post APAP overdose, with an inability to enter the necrotic area. However, this was not confirmed by flow cytometry, where WT and Sema7a KO mice had the same frequency of resident macrophages at 12 and 24 hours post APAP overdose. Sema7a KO mice had more infiltrating macrophages at 12 hours post APAP overdose, and a greater upregulation in the frequency of phagocytosis from 12 to 24 hours post APAP overdose in the liver and blood. However, a Sema7a deficiency did not affect *in vivo* phagocytosis.

Together, Sema7a aids the innate immune system to combat APAP toxicity. Sema7a KO mice have more inflammation at 24 hours post APAP injury, seen by elevated levels of IL-6 and CXCL1 in the serum and persistent neutrophils in the liver. However, this may be a consequence of the increased necrosis and depleted F4/80+ macrophages at 12 hours post APAP overdose. With this in mind and the conflicting data, more investigations are needed to establish if Sema7a is pro- or anti-inflammatory during APAP injury.

Chapter 6 – Conclusions and future perspectives

APAP overdose causes half of acute liver failure in the UK and the USA [1,2]. NAC is an effective treatment in the first 12 hours following APAP overdose. After this timepoint, 22% of patients require a liver transplant, which is prevented by a scarcity of donors [3]. After a moderate overdose, patients can spontaneously recover [3]. Enhancing endogenous recovery mechanisms after the 12 hour time window of NAC is an attractive approach to treating APAP overdose. These essential recovery mechanisms include: preventing the spread of necrosis, a shift to the anti-inflammatory phenotype, clearance of necrotic debris and proliferation of the remaining hepatocytes to restore the parenchyma.

The innate immune system can perform or promote these recovery processes. Macrophages phagocytose cellular debris, providing space for hepatocytes to proliferate. Phagocytosis causes macrophages to switch from a pro-inflammatory to a restorative phenotype, which secrete anti-inflammatory cytokines such as IL-10 which reduces inflammation [72,256]. Restorative macrophages also secrete TNFα and IL-6 to prime the hepatocytes to proliferate [17]. Depletion of macrophages prevents recovery from APAP injury [21,51]. Macrophages can also delay hepatocyte proliferation by secreting TGFβ to induce hepatocyte senescence [144]. One potential therapeutic avenue is to manipulate the innate immune system to promote recovery. Administration of CSF1-Fc to mice at 12 hours APAP injury promotes recovery by enhancing Ly6C^{hi} monocyte recruitment, KC and infiltrating macrophage proliferation and phagocytosis [32]. In chronic liver injury, injection of BMDMs polarised to the pro-inflammatory phenotype ameliorated liver fibrosis by reducing the number of activated HSCs and enhancing degradation of the collagen scars. The BMDMs also recruited endogenous macrophages which amplified and extended these beneficial effects [87,88]. Therefore, understanding how the immune system promotes recovery, and being able to modulate these pathways will lead to novel therapies.

Semaphorins are known immunomodulators [193]. Sema7a chemoattracts monocytes, macrophages and DCs [228–230]. Sema7a can also modulate if macrophages secrete pro- inflammatory or anti- inflammatory cytokines, in a receptor dependant manner [231,236]. In DCs, Sema7a -Plexin C1 signalling prevents the DC from phagocytosing the herpes and smallpox virus [218,219,239]. Sema7a deficiency *in vivo* either promotes or reduces inflammation. Pulmonary inflammation is reduced during an acute LPS inhalation model in Sema7a KO mice compared to WT mice [212]. In CCl_4 induced liver

fibrosis, Sema7a promotes *IL-6* and *MCP-1* expression, F4/80+ macrophage infiltration and collagen deposition by enhancing the TGFβ - pAKT -pERK pathway [246].

My PhD project therefore investigated the following hypothesis: Sema7a promotes injury and inflammation during APAP injury, by investigating the following aims:

1. Examine if Sema7a+ hepatocytes form a boundary to limit the spread of cell death
2. Examine if Sema7a promotes p21 expression in hepatocytes
3. Define if Sema7a delays proliferation during recovery from APAP injury
4. Investigate if Sema7a has a pro- inflammatory effect during APAP injury

To the best of our knowledge, this is the first investigation of APAP injury in Sema7a KO mice. I discovered that Sema7a becomes expressed on peri – necrotic, non-proliferative, Hnf4α+ hepatocytes during APAP injury. By comparing WT mice to Sema7a deficient mice, I established that Sema7a+ hepatocytes prevent the spread of TUNEL+ cells into the healthy parenchyma, at 24 hours post APAP injection. The Sema7a KO mice succumbed more easily to APAP overdose and elevated LFTs throughout an APAP time course and had significantly more necrosis at 12 hours post APAP injection, compared to WT mice. At 24 hours post APAP injury, Sema7a KO mice had non-nuclear HMGB1 expression in peri-necrotic hepatocytes, indicative of increased cellular stress. p21 expression was not affected in Sema7a KO mice. During APAP recovery, BrdU labelling revealed WT and Sema7a KO mice have the same rate of proliferation. Together, this data shows that Sema7a acts to prevent the spread of necrosis and reduces APAP injury but does not impact hepatocyte proliferation.

At 24 hours post APAP injury Sema7a KO have more inflammation. IL-6 and CXCL1 were elevated in the serum, and there were more neutrophils in the necrotic area. At 12 hours post APAP injury Sema7a KO mice have a greater depletion of F4/80+ macrophages. However, this could be a consequence of the increased necrosis at 12 hours APAP injury. A Sema7a deficiency did not affect the frequency of phagocytosis *in vivo*. Together, I have shown Sema7a prevents the spread of necrosis and reduces inflammation during APAP injury. Sema7a does not directly influence *in vivo* phagocytosis, or hepatocyte proliferation. For a working model see Figure 6. 1.

Figure 6. 1 Working model – Sema7a prevents spread of injury and reduces inflammation during APAP injury

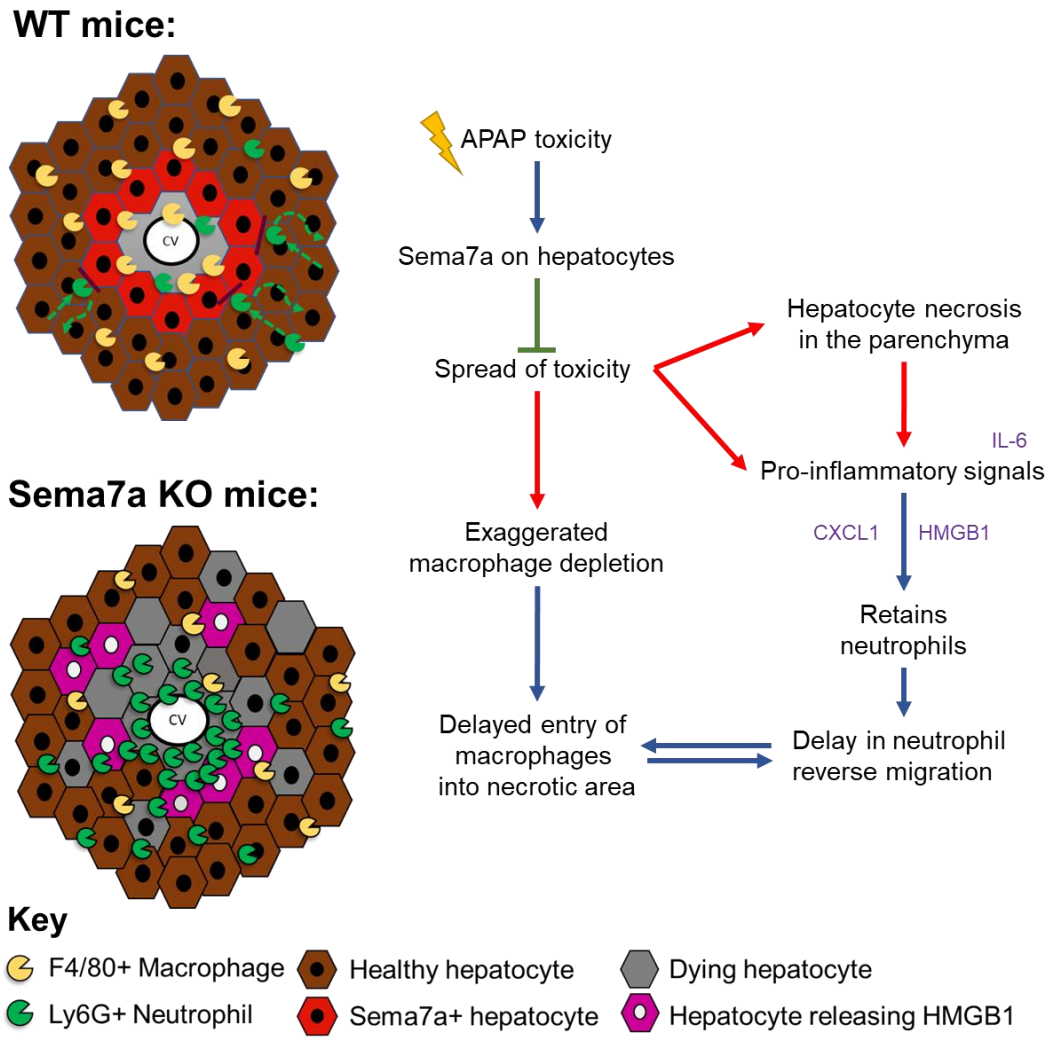

Figure 6. 1
Sema7a becomes expressed peri-necrotic hepatocytes after APAP injury. Which limits the spread of APAP-toxic metabolites, and hepatocyte death in the healthy parenchyma. The Sema7a+ hepatocytes may regulate neutrophil migration into the necrotic area and facilitate neutrophil reverse migration.

In Sema7a KO mice, the APAP induced toxicity spreads into the parenchyma increasing necrosis and exaggerating F4/80+ macrophage depletion and delays their migration into the necrotic area. Augmented cellular stress causes peri-necrotic hepatocytes to release HMGB1 from their nuclei. HMGB1 with CXCL1, may attract and retain neutrophils in the necrotic area. The delay in F4/80+ macrophages may postpone neutrophil clearance.

My first aim examines if Sema7a+ hepatocytes limits the spreads of necrosis. Sema7a is first detected in peri-necrotic hepatocytes at 12 hours post APAP. The peri-necrotic expression of Sema7a peaks at 24 hours post APAP injury. To examine if these Sema7a+ peri-necrotic hepatocytes limited the spread of injury, Sema7a KO mice were compared to WT mice during an APAP time course. At 12 hours post APAP injection, Sema7a KO mice had more necrosis.

In Sema7a KO mice, TUNEL+ cells were detected in the healthy parenchyma, which were not detected in the WT mice, at 24 hours post APAP injury. In the absence of Sema7a, peri-necrotic hepatocytes release HMGB1 from their nuclei, indicative of increased cellular stress or damage. Secreted HMGB1 acts as a cytokine or DAMP to recruit the immune system [275]. This suggests Sema7a+ hepatocytes act as a barrier to contain necrosis during APAP injury.

Epithelial barriers are physically maintained by cellular junctions. Epithelial barriers have been extensively researched in the skin and intestine [297–301]. However, the concept of hepatocytes acting as a physical epithelial barrier against APAP injury has only been briefly examined. The main connexin in the liver is Cx32. Genetic deletion of Cx32, or application of the Cx32 small inhibitor, 2-ABP, prevents the spread of APAP induced necrosis through gap junctions *in vivo* [137]. However, follow up studies indicate the protective effects of 2-ABP were partially mediated by the hepatoprotective vehicle DMSO [24] and a reduction of JNK signalling, and not a block of Cx32 junctions [138]*. In vitro*, two individual hepatocytes were coupled together. Deletion of the Cx32, Cx26 gap junction in coupled hepatocytes prevented synchronised necrotic cell death [140]. With these contradicting studies, further investigations are needed to assess if APAP can spread through Cx32 junctions.

Cx43 is upregulated during APAP injury. At 24 hours post APAP injury, Cx43 $^{+/-}$ mice had elevated ALT and increased IL-1β and TNFα secretion, suggesting Cx43 protects against APAP injury [141], although further work is needed to confirm these results. Sema7a modulates the actin cytoskeleton [176,216–219,227]. The actin cytoskeleton transports de novo Cx43 channels from the Golgi to the plasma membrane [281], and then stabilises the gap junction formation [131]. Potentially, Sema7a mediates the formation of Cx43 channels to reduce the spread of necrosis during APAP injury.

The spread of APAP toxicity may enhance cellular stress and senescence. My second hypothesis examined if Sema7a influenced p21 expression. In WT mice a fifth of the

Sema7a+ hepatocytes co-expressed p21, the senescence marker. It has been shown that macrophages secrete TGFβ to induce p21 expression in peri-necrotic hepatocytes [144]. Sema7a can enhance non-canonical TGFβ signalling and modulate macrophages to secrete cytokines [231,236,246,247]. In addition, Sema3a is now recognised as a senescence marker [145]. To see if Sema7a could induce cell cycle arrest during APAP injury, p21 expression was examined. WT and Sema7a KO mice had the same number or peri-necrotic hepatocytes at 24 hours post APAP injury. This implies Sema7a does not promote p21 expression, either directly or indirectly by enhancing TGFβ signalling.

Plexin C1 expression was significantly reduced at 24 hours post APAP administration in Sema7a KO mice, compared to WT mice. This suggests that Sema7a upregulates Plexin C1 expression in HSCs at peak APAP injury. Sema7a – Plexin C1 – LMKII signalling results in the inactivation of cofilin and induces cell contraction and adhesion and prevents migration in melanocytes, DCs and GnRH neurones [179,216–219,227]. After acute CCl_4 injury, damaged hepatocytes transiently secrete Sema3e which binds to Plexin D1 on LSECs causing the LSECs to contract [186]. The authors suggested that contraction of LSECs might enable the migration of immune cells to the damaged regions, although this was not examined. Potentially, Sema7a – Plexin C1 signalling induces HSCs contraction or prevents HSC migration during APAP injury. In chronic injury, HSCs wrap around the sinusoids and contract, reducing blood flow along the sinusoid [302]. However, the area of vimentin, an HSC marker was the same in WT and Sema7a KO mice at 24 hours APAP injury, suggesting Sema7a does not promoting the contraction of HSCs.

Alternatively, Sema7a – Plexin C1 signalling might induce HSCs to secrete ECM factors required to remodel and regenerate the necrotic area after 24 hours post APAP. In chronic liver injury, activated HSCs produce collagen which drives fibrosis [260,302]. In CCl_4 induced liver fibrosis, Sema7a KO mice had less collagen deposition and reduced expression of αSMA, a marker for activated HSCs [246]. Sema7a KO mice also have reduced TGFβ induced pulmonary fibrosis, with reduced collagen and laminin synthesis [247]. Future work could examine the consequences of Sema7a-Plexin C1 signalling with mechanistic and cell behaviour studies.

Factors secreted by HSCs are protective during APAP injury. One group collected serum free conditioned media from cultured HSCs (HSC-CM) and injected it into mice 2 hours after APAP administration. HSC-CM treatment improved necrosis and the

survival of mice. Mass spectrometry on the HSC-CM and identified 144 proteins [266,267]. However, the authors did not delineate which of these 144 proteins gave protective effects against APAP injury. They also failed to examine mice at later timepoints to ensure the HSC-CM did not trigger fibrosis, prolong the immune response or prevent final resolution of necrosis. Future work is needed to examine the exact roles of HSCs during APAP injury, and to define the protective factors.

My fourth aim examined if Sema7a promotes inflammation during APAP injury. By comparing the macrophage and neutrophil populations in WT and Sema7a KO mice throughout an APAP time course, I demonstrated that F4/80+ macrophages were significantly more depleted in Sema7a KO mice at 12 hours post APAP injury and had more neutrophils in the necrotic area at 24 hours post APAP injury that WT mice. To the best of our knowledge this is the first time Sema7a KO mice have been treated with APAP. In WT mice APAP injury is known to deplete the resident macrophage population, as seen here and previously reported [48–51]. Macrophage depletion is caused by ROS and mitochondrial stress [50]. Possibly, the increased necrosis in Sema7a KO mice enhanced F4/80+ macrophage depletion.

In contrast to this, flow cytometry analysis indicates WT and Sema7a KO mice have the same frequency and absolute count of resident macrophages at 12 hours post APAP overdose, conflicting with the IHC analysis. These conflicting results may reflect the differences between the techniques. The main advantage of flow cytometry is the ability to detect multiple cell markers in a whole tissue, enabling the analysis of immune composition and activation states of a sample. Dead cells or cells with a dim expression of the target antigen are excluded. Here flow cytometry was used to compare the infiltrating and resident macrophages present in the liver. Possibly, dying cells were excluded from the flow cytometry analysis. The 12 hour flow cytometry data is limited by a low sample number. Due to the variability in the APAP model, a sample number of 8 is required. Due to time restraints, the 12 hours experiment was performed once with n=4 WT mice and n=5 Sema7a KO mice, and is therefore underpowered.

The advantages of DAB IHC are its sensitivity and its ability to describe the exact location of cells in a tissue. Here, imaging and quantification of the DAB stain focused

on centrilobular areas. DAB IHC amplifies the positive signal and is therefore more sensitive than flow cytometry but will include dying cells. To assess if the Sema7a KO F4/80+ macrophages are depleted through cell death at 12 hours post APAP administration, I would like to perform an active caspase 3 or TUNEL stain with F4/80.

When the DAB IHC was re-examined Sema7a KO mice had visibly less F4/80+ macrophages at 12 hours post APAP administration across the whole liver slice, compared to WT mice. This IHC analysis also has the required n=8 of WT and n=8 Sema7a KO mice. For these reasons I believe the F4/80 DAB IHC is more reliable.

Sema7a KO mice have significantly more infiltrating macrophages compared to WT mice, at 12 hours post APAP administration. This might be required to restore the enhanced depletion of resident macrophages, so that by 24 hours post APAP injury, Sema7a KO mice have the same frequency and absolute count of macrophages in the liver as WT mice, as measured by both IHC and flow cytometry. During APAP injury infiltrating macrophages are recruited to the liver by CCL2 [49,296] to boost the liver macrophage population. Due to the depletion of resident macrophages, the infiltrating macrophages are the most dominant macrophage population in the liver, in both the WT and Sema7a KO mice at 12 and 24 hours post APAP injury. This agrees with previously published results [48]. Blocking or deletion of CCR2 prevents macrophage infiltration, and delays recovery from APAP injury [21,51].

WT and Sema7a KO mice have the same number of F4/80+ macrophages in the liver at 24 hours post APAP injury. In WT mice the F4/80+ macrophages are seen interacting with the Sema7a + hepatocytes at the edge of necrosis. Some F4/80+ macrophages migrate into the central necrotic zone. In Sema7a KO mice, the F4/80+ macrophages in the outer necrotic zone appear less organised, compared to the WT mice. Possibly the F4/80+ macrophages bind to Sema7a on the hepatocytes to facilitate barrier formation. Recently, macrophages were reported to line the synovial joint capsule in an “epithelial like barrier”. This barrier delayed PMN infiltration during rheumatoid arthritis, and phagocytosed apoptotic bodies [142]. An intriguing idea is that the Sema7a+ hepatocytes prevent the spread of APAP toxicity by binding to HSCs, and by the regulation of macrophages.

Sema7a KO mice have less F4/80+ macrophages in the central necrotic zone at 24 hours post APAP challenge, compared to WT mice. This may indicate that Sema7a facilitates F4/80+ macrophage migration into the necrotic area. Sema7a is a

monocyte and macrophage chemoattractant. Blocking Integrin β1 reduced macrophage migration towards Sema7a, and adherence to endothelial cells *in vitro* [228,229].

Alternatively, Sema7a+ hepatocytes may have a localised effect where they regulate the migration of neutrophils and macrophages into the necrotic area in a temporal manner. Invariant NK T cells (iNKTs) are prevented from entering the necrotic lesion in a temporal manner during a thermal sterile injury. iNKT were kept at the edge of the necrotic area by resident macrophage signalling and IL-12 and IL-18. At 48 hours post thermal injury, the iNKT cells entered the necrotic lesion and promote recovery [290].

Sema7a KO mice had more neutrophils in the necrotic area at 24 hours post APAP overdose. This was not attributed to a lack of intrinsic Sema7a, an increase or a delay in infiltration of neutrophils to the liver. Possibly the neutrophils are being retained in the necrotic area by chemoattractants.

Sema7a KO mice had more non-nuclear HMGB1 expression in peri-necrotic hepatocytes than WT mice, at 24 post APAP administration. HMGB1 is a neutrophil chemoattractant. Specific deletion of hepatocyte HMGB1 reduced neutrophil infiltration and necrosis during APAP injury [53,275]. In addition to localised HMGB1 signalling, Sema7a KO mice had a higher expression of CXCL1 in the serum, at 24 hours post APAP overdose compared to WT mice. CXCL1 is a known chemoattractant of neutrophils [52,282]. This systemic cytokine expression may contribute to the persistent neutrophil population. However, this was not reflected by an increased circulatory population of neutrophils, or increased presence of neutrophils in the whole liver, as shown by flow cytometry.

Alternatively, a deficiency of Sema7a may delay neutrophil transmigration out of the liver. Endothelial Sema7a binds to Plexin C1 on PMNs to facilitate PMN transmigration into the lung during acute ventilation injury [211,237]. ICAM-1+ LSECs were negative for Sema7a, indicating endothelial Sema7a does not facilitate neutrophil reverse transmigration across LSECs in the liver.

In a model of sterile thermal injury, neutrophils remodel the ECM to reverse migrate out of the liver [52,117]. Deletion of cathepsin C, a serine proteinase which can mediate reverse migration through the basement membrane degradation, did not delay neutrophil entry into the necrotic zone, but delayed neutrophil exit. This delayed exit

of neutrophils reduced revascularisation [117]. This indicates a timely exit of neutrophils through the ECM is needed to facilitate regeneration. During lung fibrosis Sema7a KO mice have reduced mRNA expression of the elastase Cathepsin S, and more TIMP-1, a metalloproteinase inhibitor [247,303], causing reduced ECM remodelling. The reduced number of macrophages in the Sema7a KO mice may also delay neutrophil transmigration. In zebra fish, macrophages contact neutrophils to induce neutrophil reverse migration [122]. Collectively, the neutrophils in the Sema7a KO mice may persist due to less reverse migration facilitated by ECM remodelling, or reduced "contact" reverse migration from the decreased population of F4/80 macrophages in the central necrotic zone.

The composition of the blood and peritoneal lavage were also examined. WT and Sema7a KO mice had the same frequency of neutrophils, monocytes and macrophages at 12 and 24 hours post APAP injury. Highlighting the localised effect Sema7a has during APAP injury. The only exception was Ly6C^{hi} monocytes in the blood of Sema7a KO mice at 12 hours post APAP overdose. Presumably, these are the monocytes responsible for increasing the macrophage population in the liver at 12 hours post APAP injury.

To recover from APAP injury, the cellular debris must be cleared, and the hepatocytes must proliferate. Sema7a KO BMDMs tended to have a lower frequency of phagocytosis than WT mice, but more experimental repeats are needed to confirm this. *In vivo,* there was no difference in the frequency of phagocytosis between WT and Sema7a KO mice in the neutrophil, monocyte and macrophage population examined in the blood, peritoneal exudate or liver at 12 and 24 hours post APAP administration. The single exception being Ly6C^{hi} monocytes in the peritoneal lavage, where Sema7a KO mice displayed reduced phagocytosis. However, this data may be skewed due to low cell counts. In the *in vitro* experiments, BMDMs were fed apoptotic thymocytes, whereas in the *in vivo* experiments, the cargo was an injected fluorescent dye. This difference in phagocytic cargo may explain the differences in the *in vitro* and *in vivo* data.

In the liver, infiltrating macrophages quadrupled their frequency of phagocytosis between 12 and 24 hours post APAP overdose, which will facilitate debris removal. The increase in phagocytosis may reflect the maturation of infiltrating macrophages. It may also reflect the switch in the microenvironment from the injury setting to the regeneration phase. The factors which govern this switch are still a mystery.

My third aim examined if Sema7a promotes proliferation. BrdU+ cells did not express Sema7a during APAP recovery, at 42 hours post APAP administration, or in the highly regenerative PHx model. WT and Sema7a KO mice had the same frequency of BrdU+ nuclei, and area of necrosis at 42 hours post APAP injury. This shows Sema7a does not have a direct role in proliferation. However, Sema7a KO mice have raised ALP levels, suggesting some ongoing damage. Therefore, Sema7a may have an indirect effect in recovery by limiting the spread of damage or by modulating the immune system.

In the literature, Sema7a is not considered as a direct mitogen. It has been reported to promote proliferation of human oral squamous cell carcinoma derived cells lines by pERK – pAKT signalling [242], and can indirectly promote T cells proliferation by activating them. Conversely, Sema7a has no effect on HSC cell death or proliferation *in vitro* [246]. Yet, Sema7a – Plexin C1 signalling inhibits melanocyte proliferation and migration in melanoma [243], and proliferation of adult neural progenitors in the SGZ [178]. Together the role of Sema7a in cell proliferation is context and receptor dependant.

One limitation of this PhD project is that we did not examine the recovery of WT and Sema7a KO mice from APAP injury at later time points. Sema7a KO mice had raised ALP at 42 hours APAP and more neutrophils in the necrotic area at 24 hours post APAP. Persistent neutrophils can lead to the formation of non-healing wounds, with incessant necrosis, and a delay in vascularisation [117]. WT mice will recover from APAP by 72 hours post APAP. To be confident of recovery, WT mice are often examined at one week post APAP administration [147,304]. To ensure the Sema7a KO mice do not have lingering necrosis or inflammation, and are completely recovered from APAP injury, they should be examined at 72 hours and one week post APAP administration

Another limitation is the use of a constitutive KO mouse. Sema7a is expressed by T cells and DCs [230–232], and promotes cytokine secretion from macrophages [231,232,236]. Therefore, the increased inflammation at 24 hours post APAP injury may be a due to a lack of Sema7a signalling in the immune system, and not due to a lack of Sema7a expression by hepatocytes. Performing a bone marrow transfer between the WT and Sema7a KO mice will convincingly answer this question.

The question of do macrophages release pro- or anti-inflammatory cytokines after binding to Sema7a + hepatocytes is unanswered. This could be analysed *in vitro* by treating BMDMs with recombinant Sema7a. However, it is likely other signals govern

which macrophage receptor binds Sema7a *in vivo*. Co-culture studies of BMDMs with Sema7a+ primary hepatocytes treated with APAP will reflect what happens *in vivo* more accurately.

The underlying mechanisms which dictate how the Sema7a+ hepatocyte barrier forms have not been described. This is partly due to the localised nature of the Sema7a+ hepatocytes. The mRNA expression of genes reported here was performed on whole liver lysates. In the injury setting this will include all the hepatocytes, biliary cells and immune cells in the liver. Any change detected between the WT and Sema7a KO would indicate a profound change in gene expression, or protein expression if examined by ELISA or western blot. However, small changes in expression will be diluted into insignificance. To delineate the signalling mechanisms underlying Sema7a expression in hepatocytes, laser capture dissection could be performed, followed by mRNA expression profiling, and confirmed at the protein level.

Could Sema7a be upregulated by DAMPs or ROS and therefore act as a stress signal? Sema7a was elevated in mouse serum and correlated with ALT. However, this was not seen in human serum. Possibly, this reflects that Sema7a is active during the early stages of APAP injury.

Future investigations could examine if Sema7a+ hepatocytes prevent the spread of necrosis in other liver diseases. Viral hepatitis and ischemia reperfusion injury both induce necrosis [305]. Sema7a has been shown to be expressed in humans with viral hepatitis C and alcoholics liver injury by western blot [246]. However, the location of Sema7a expression was not examined.

This PhD project discovered Sema7a+ hepatocytes surround the necrotic area during APAP injury, to limit the spread of necrosis. Sema7a deficiency resulted in increased necrosis at 12 hours post APAP administration, and more inflammation at 24 post hours APAP injury. Future work could identify the factors which initiate the formation of the Sema7a+ hepatocyte barrier, and the underlying signalling mechanisms that maintain it during APAP injury, and if it is present in other chronic injuries. Understanding these mechanisms will enable treatments which limit the spread of necrosis and reduce inflammation.

It will be intriguing to see if and how the Sema7a+ hepatocytes regulate the migration of neutrophils and macrophages into the necrotic area. If macrophage migration to injured areas can be enhanced or guided, it may lead to targeted cellular therapies. Understanding these underlying mechanisms may help us find novel ways to contain the spread of damage and modulate the immune system during APAP overdose and chronic liver injury.

References

1. Nourjah, P., Ahmad, S. R., Karwoski, C. & Willy, M. Estimates of acetaminophen (paracetamol)-associated overdoses in the United States. *Pharmacoepidemiol. Drug Saf.* **15**, 398–405 (2006).
2. Office for National Statistics. *Deaths related to drug poisoning in England and Wales: 2015 registrations*. https://www.ons.gov.uk/peoplepopulationandcommunity/birthsdeathsandmarriages/deaths/bulletins/deathsrelatedtodrugpoisoninginenglandandwales/2015registrations (2016).
3. Lee, W. M. Acetaminophen (APAP) hepatotoxicity-Isn't it time for APAP to go away? *J. Hepatol.* **67**, 1324–1331 (2017).
4. Krenkel, O., Mossanen, J. C. & Tacke, F. Immune mechanisms in acetaminophen-induced acute liver failure. *Hepatobiliary Surg. Nutr.* **3**, 331–43 (2014).
5. *Sherlock's Diseases of the Liver and Biliary System*. (Wiley-Blackwell, 2011). doi:10.1002/9781444341294.
6. Planas-Paz, L. *et al.* The RSPO–LGR4/5–ZNRF3/RNF43 module controls liver zonation and size. *Nat Cell Biol* **18**, 467–479 (2016).
7. Mitchell, C. & Willenbring, H. A reproducible and well-tolerated method for 2/3 partial hepatectomy in mice. *Nat. Protoc.* **3**, 1167 (2008).
8. Forbes, S. J. & Rosenthal, N. Preparing the ground for tissue regeneration: from mechanism to therapy. *Nat. Med.* **20**, 857–69 (2014).
9. Birchmeier, W. Orchestrating Wnt signalling for metabolic liver zonation. *Nat. Cell Biol.* **18**, 463–465 (2016).
10. Fontana, R. J. Acute liver failure including acetaminophen overdose. *Med. Clin. North Am.* **92**, 761–94, viii (2008).
11. Yoon, E., Babar, A., Choudhary, M., Kutner, M. & Pyrsopoulos, N. Acetaminophen-Induced Hepatotoxicity: a Comprehensive Update. *J. Clin. Transl. Hepatol.* **4**, 131–142 (2016).
12. Zenger, F. *et al.* Decreased glutathione in patients with anorexia nervosa. Risk factor for toxic liver injury? *Eur. J. Clin. Nutr.* **58**, 238–243 (2004).
13. Schmidt, L. E., Dalhoff, K. & Poulsen, H. E. Acute versus chronic alcohol consumption in acetaminophen-induced hepatotoxicity. *Hepatology* (2002) doi:10.1053/jhep.2002.32148.
14. Karthivashan, G., Arulselvan, P. & Fakurazi, S. Pathways involved in acetaminophen hepatotoxicity with specific targets for inhibition/downregulation. *RSC Adv.* **5**, 62040–62051 (2015).
15. Yan, M., Huo, Y., Yin, S. & Hu, H. Mechanisms of acetaminophen-induced liver injury and its implications for therapeutic interventions. *Redox Biol.* **17**, 274–283 (2018).
16. Hinson, J. A., Pike, S. L., Pumford, N. R. & Mayeux, P. R. Nitrotyrosine-protein adducts in hepatic centrilobular areas following toxic doses of acetaminophen in mice. *Chem. Res. Toxicol.* **11**, 604–607 (1998).
17. Hinson, J. A., Roberts, D. W. & James, L. P. Mechanisms of acetaminophen-induced liver necrosis. *Handb. Exp. Pharmacol.* **196**, 369–405 (2010).
18. Ito, Y., Bethea, N. W., Abril, E. R. & McCuskey, R. S. Early hepatic microvascular injury in response to acetaminophen toxicity. *Microcirculation* **10**, 391–400 (2003).
19. McCuskey, R. S. *et al.* Ethanol binging exacerbates sinusoidal endothelial and parenchymal injury elicited by acetaminophen. *J. Hepatol.* **42**, 371–377 (2005).
20. Gao, S., Silasi-Mansat, R., Behar, A. R., Lupu, F. & Griffin, C. T. Excessive Plasmin Compromises Hepatic Sinusoidal Vascular Integrity After Acetaminophen Overdose. *Hepatology* **68**, 1991–2003 (2018).
21. You, Q. *et al.* Role of hepatic resident and infiltrating macrophages in liver repair after acute injury. *Biochem. Pharmacol.* **86**, 836–843 (2013).
22. Schwabe, R. F. & Luedde, T. Apoptosis and necroptosis in the liver: a matter of life and death. *Nat. Rev. Gastroenterol. Hepatol.* **15**, (2018).
23. Chen, D. *et al.* PUMA induction mediates acetaminophen-induced necrosis and liver injury. *Hepatology* hep.30422 (2018) doi:10.1002/hep.30422.
24. Jaeschke, H., Cover, C. & Bajt, M. L. Role of caspases in acetaminophen-induced liver injury. *Life Sci.* **78**, 1670–1676 (2006).
25. Zhao, H. *et al.* Role of necroptosis in the pathogenesis of solid organ injury. *Cell Death Dis.* **6**, 1–10 (2015).
26. Weinlich, R., Oberst, A., Beere, H. M. & Green, D. R. Necroptosis in development, inflammation

and disease. *Nat. Rev. Mol. Cell Biol.* **18**, 127–136 (2017).

27. Dara, L. *et al.* Receptor interacting protein kinase 1 mediates murine acetaminophen toxicity independent of the necrosome and not through necroptosis. *Hepatology* **62**, 1847–1857 (2015).
28. Takemoto, K. *et al.* Necrostatin-1 protects against reactive oxygen species (ROS)-induced hepatotoxicity in acetaminophen-induced acute liver failure. *FEBS Open Bio* **4**, 777–87 (2014).
29. Schneider, A. T., Gautheron, J., Tacke, F., Vucur, M. & Luedde, T. Receptor interacting protein kinase 1 (RIPK1) in hepatocytes does not mediate murine acetaminophen toxicity. *Hepatology* **64**, 306–308 (2016).
30. Bernal, W. & Wendon, J. Acute Liver Failure. *N. Engl. J. Med.* **369**, 2525–2534 (2013).
31. Balmer, M. L. *et al.* The liver may act as a firewall mediating mutualism between the host and its gut commensal microbiota. *Sci. Transl. Med.* **6**, 1–11 (2014).
32. Stutchfield, B. M. *et al.* CSF1 Restores Innate Immunity after Liver Injury in Mice and Serum Levels Indicate Outcomes of Patients with Acute Liver Failure. *Gastroenterology* **149**, 1896-1909e14 (2015).
33. Racanelli, V. & Rehermann, B. The liver as an immunological organ. *Hepatology* **43**, (2006).
34. Guillot, A. & Tacke, F. Liver Macrophages: Old Dogmas and New Insights. *Hepatol. Commun.* **3**, (2019).
35. Tacke, F. Targeting hepatic macrophages to treat liver diseases. *J. Hepatol.* (2017) doi:10.1016/j.jhep.2017.02.026.
36. Gomez Perdiguero, E. *et al.* Tissue-resident macrophages originate from yolk-sac-derived erythro-myeloid progenitors. *Nature* **518**, 547–551 (2015).
37. Mass, E. *et al.* Specification of tissue-resident macrophages during organogenesis. *Science (80-.).* **353**, aaf4238–aaf4238 (2016).
38. Heymann, F. *et al.* Liver Inflammation Abrogates Immunological Tolerance Induced by Kupffer Cells. *Hepatology* **62**, 279–291 (2015).
39. Robinson, M. W., Harmon, C. & O'Farrelly, C. Liver immunology and its role in inflammation and homeostasis. *Cell. Mol. Immunol.* **13**, 267–276 (2016).
40. Ouyang, W., Rutz, S., Crellin, N. K., Valdez, P. A. & Hymowitz, S. G. Regulation and Functions of the IL-10 Family of Cytokines in Inflammation and Disease. *Annu. Rev. Immunol.* **29**, 71–109 (2011).
41. Uderhardt, S., Martins, A. J., Tsang, J. S., Lämmermann, T. & Germain, R. N. Resident Macrophages Cloak Tissue Microlesions to Prevent Neutrophil-Driven Inflammatory Damage. *Cell* **177**, 541-555.e17 (2019).
42. Tu, Z. *et al.* TLR-dependent cross talk between human Kupffer cells and NK cells. *J. Exp. Med.* **205**, 233–244 (2008).
43. Heymann, F. & Tacke, F. Immunology in the liver - from homeostasis to disease. *Nat. Rev. Gastroenterol. Hepatol.* **13**, 88–110 (2016).
44. Woolbright, B. L. & Jaeschke, H. Role of the inflammasome in acetaminophen-induced liver injury and acute liver failure. *J. Hepatol.* **66**, 836–848 (2017).
45. Brempelis, K. J. J. & Crispe, I. N. N. Infiltrating monocytes in liver injury and repair. *Clin. Transl. Immunol.* **5**, (2016).
46. Shuh, M., Bohorquez, H., Loss, G. E. & Cohen, A. J. Tumor necrosis factor-α: Life and death of hepatocytes during liver ischemia/reperfusion injury. *Ochsner J.* (2013).
47. Laster, S. M., Wood, J. G. & Gooding, L. R. Tumor necrosis factor can induce both apoptic and necrotic forms of cell lysis. *J. Immunol.* (1988).
48. Zigmond, E. *et al.* Infiltrating Monocyte-Derived Macrophages and Resident Kupffer Cells Display Different Ontogeny and Functions in Acute Liver Injury. *J. Immunol.* 1400574 (2014) doi:10.4049/jimmunol.1400574.
49. Mossanen, J. C. *et al.* Chemokine (C-C motif) receptor 2-positive monocytes aggravate the early phase of acetaminophen-induced acute liver injury. *Hepatology* **64**, (2016).
50. Al-Belooshi, T., John, A., Tariq, S., Al-Otaiba, A. & Raza, H. Increased mitochondrial stress and modulation of mitochondrial respiratory enzyme activities in acetaminophen-induced toxicity in mouse macrophage cells. *Food Chem. Toxicol.* **48**, 2624–2632 (2010).
51. Holt, M. P., Cheng, L. & Ju, C. Identification and characterization of infiltrating macrophages in acetaminophen-induced liver injury. *J Leukoc Biol* **84**, 1410–1421 (2008).
52. McDonald, B. *et al.* Intravascular danger signals guide neutrophils to sites of sterile inflammation. *Science* **330**, 362–6 (2010).
53. Huebener, P. *et al.* The HMGB1/RAGE axis triggers neutrophil-mediated injury amplification following necrosis. *J. Clin. Invest.* **125**, 539–550 (2015).

54. George, L., Elizabeth, H. & George, L. The Role of the Reticuloendothelial System in Natural Immunity. in *NeuroImmune Biology* vol. 5 95–101 (2005).
55. Fisher, J. E. *et al.* Role of Kupffer cells and toll-like receptor 4 in acetaminophen-induced acute liver failure. *J. Surg. Res.* **180**, 147–155 (2013).
56. Laskin, D. L., Gardner, C. R., Price, V. F. & Jollow, D. J. Modulation of macrophage functioning abrogates the acute hepatotoxicity of acetaminophen. *Hepatology* (1995) doi:10.1016/0270-9139(95)90253-8.
57. Michael, S. L., Pumford, N. R., Mayeux, P. R., Niesman, M. R. & Hinson, J. A. Pretreatment of mice with macrophage inactivators decreases acetaminophen hepatotoxicity and the formation of reactive oxygen and nitrogen species. *Hepatology* (1999) doi:10.1002/hep.510300104.
58. James, L. P., McCullough, S. S., Knight, T. R., Jaeschke, H. & Hinson, J. A. Acetaminophen toxicity in mice lacking NADPH oxidase activity: Role of peroxynitrite formation and mitochondrial oxidant stress. *Free Radical Research* (2003) doi:10.1080/10715760310001617776.
59. Williams, C. D. *et al.* Neutrophil activation during acetaminophen hepatotoxicity and repair in mice and humans. *Toxicol. Appl. Pharmacol.* **275**, 122–133 (2014).
60. Yang, W. *et al.* Neutrophils promote the development of reparative macrophages mediated by ROS to orchestrate liver repair. *Nat. Commun.* **10**, (2019).
61. Campion, S. N. *et al.* Hepatic Mrp4 induction following acetaminophen exposure is dependent on Kupffer cell function. *Am. J. Physiol. Liver Physiol.* **295**, G294–G304 (2008).
62. Ju, C. *et al.* Protective role of kupffer cells in acetaminophen-induced hepatic injury in mice. *Chem. Res. Toxicol.* **15**, 1504–1513 (2002).
63. Dambach, D. M., Watson, L. M., Gray, K. R., Durham, S. K. & Laskin, D. L. Role of CCR2 in macrophage migration into the liver during acetaminophen-induced hepatotoxicity in the mouse. *Hepatology* (2002) doi:10.1053/jhep.2002.33162.
64. Ju, C. & Tacke, F. Hepatic macrophages in homeostasis and liver diseases: from pathogenesis to novel therapeutic strategies. *Cell. Mol. Immunol.* **13**, 1–12 (2016).
65. Scott, C. L. *et al.* Bone marrow-derived monocytes give rise to self-renewing and fully differentiated Kupffer cells. *Nat. Commun.* **7**, 10321 (2016).
66. Beattie, L. *et al.* Bone marrow-derived and resident liver macrophages display unique transcriptomic signatures but similar biological functions. *J. Hepatol.* **65**, 758–768 (2016).
67. David, B. A. *et al.* Combination of Mass Cytometry and Imaging Analysis Reveals Origin, Location, and Functional Repopulation of Liver Myeloid Cells in Mice. *Gastroenterology* **151**, 1176–1191 (2016).
68. Zhang, C. *et al.* Macrophage-derived IL-1α promotes sterile inflammation in a mouse model of acetaminophen hepatotoxicity. *Cell. Mol. Immunol.* **15**, 973–982 (2018).
69. Bain, C. C. & Jenkins, S. J. The biology of serous cavity macrophages. *Cell. Immunol.* **330**, 126–135 (2018).
70. Bain, C. C. *et al.* Long-lived self-renewing bone marrow-derived macrophages displace embryo-derived cells to inhabit adult serous cavities. *Nat. Commun.* **7**, 1–14 (2016).
71. Wang, J. & Kubes, P. A Reservoir of Mature Cavity Macrophages that Can Rapidly Invade Visceral Organs to Affect Tissue Repair. *Cell* **165**, 668–678 (2016).
72. Campana, L. *et al.* The STAT3–IL-10–IL-6 Pathway Is a Novel Regulator of Macrophage Efferocytosis and Phenotypic Conversion in Sterile Liver Injury. *J. Immunol.* **200**, 1169–1187 (2018).
73. Bourdi, M. *et al.* Protection against acetaminophen-induced liver injury and lethality by interleukin 10: role of inducible nitric oxide synthase. *Hepatology* **35**, 289–98 (2002).
74. Bosurgi, L. *et al.* Macrophage function in tissue repair and remodeling requires IL-4 or IL-13 with apoptotic cells. *Science* **356**, 1072–1076 (2017).
75. Couper, K. N., Blount, D. G. & Riley, E. M. IL-10: The Master Regulator of Immunity to Infection. *J. Immunol.* (2008) doi:10.4049/jimmunol.180.9.5771.
76. Yee, S. B., Bourdi, M., Masson, M. J. & Pohl, L. R. Hepatoprotective role of endogenous interleukin-13 in a murine model of acetaminophen-induced liver disease. *Chem. Res. Toxicol.* (2007) doi:10.1021/tx600349f.
77. Bourdi, M. *et al.* Role of IL-6 in an IL-10 and IL-4 double knockout mouse model uniquely susceptible to acetaminophen-induced liver injury. *Chem. Res. Toxicol.* (2007) doi:10.1021/tx060228l.
78. Ramachandran, P. *et al.* Differential Ly-6C expression identifies the recruited macrophage phenotype, which orchestrates the regression of murine liver fibrosis. *Proc. Natl. Acad. Sci.* **109**, E3186–E3195 (2012).

79. Scher, J. U. & Pillinger, M. H. The anti-inflammatory effects of prostaglandins. in *Journal of Investigative Medicine* (2009). doi:10.2310/JIM.0b013e31819aaa76.
80. Phillipson, M. & Kubes, P. The Healing Power of Neutrophils. *Trends Immunol.* **40**, 635–647 (2019).
81. Triantafyllou, E. *et al.* MerTK expressing hepatic macrophages promote the resolution of inflammation in acute liver failure. *Gut* **67**, 333–347 (2018).
82. Ramachandran, P. *et al.* Differential Ly-6C expression identifies the recruited macrophage phenotype, which orchestrates the regression of murine liver fibrosis. *Proc. Natl. Acad. Sci. U. S. A.* **109**, (2012).
83. Wynn, T. a. & Vannella, K. M. Macrophages in Tissue Repair, Regeneration, and Fibrosis. *Immunity* **44**, 450–462 (2016).
84. Selzner, N. *et al.* ICAM-1 triggers liver regeneration through leukocyte recruitment and Kupffer cell-dependent release of TNF-α/IL-6 in mice. *Gastroenterology* **124**, 692–700 (2003).
85. James, L. P., Lamps, L. W., McCullough, S. & Hinson, J. A. Interleukin 6 and hepatocyte regeneration in acetaminophen toxicity in the mouse. *Biochem. Biophys. Res. Commun.* (2003) doi:10.1016/j.bbrc.2003.08.085.
86. Michalopoulos, G. K. Liver Regeneration. *J. Cell Physiol.* **213**, 286–300 (2007).
87. Thomas, J. a. *et al.* Macrophage therapy for murine liver fibrosis recruits host effector cells improving fibrosis, regeneration, and function. *Hepatology* **53**, 2003–2015 (2011).
88. Ma, P. F. *et al.* Cytotherapy with M1-polarized macrophages ameliorates liver fibrosis by modulating immune microenvironment in mice. *J. Hepatol.* **67**, 770–779 (2017).
89. Forbes, S. J., Gupta, S. & Dhawan, A. Review Cell therapy for liver disease : From liver transplantation to cell factory. *J. Hepatol.* **62**, S157–S169 (2015).
90. Bird, T. G. *et al.* Bone marrow injection stimulates hepatic ductular reactions in the absence of injury via macrophage-mediated TWEAK signaling. *PNAS* **110**, 6542–6547 (2013).
91. Kolaczkowska, E. & Kubes, P. Neutrophil recruitment and function in health and inflammation. *Nat. Rev. Immunol.* **13**, 159–175 (2013).
92. McDonald, B. & Kubes, P. Neutrophils and Intravascular Immunity in the Liver during Infection and Sterile Inflammation. *Toxicol. Pathol.* **40**, 157–165 (2012).
93. De Oliveira, S., Rosowski, E. E. & Huttenlocher, A. Neutrophil migration in infection and wound repair: Going forward in reverse. *Nat. Rev. Immunol.* **16**, 378–391 (2016).
94. Maas, S. L., Soehnlein, O. & Viola, J. R. Organ-specific mechanisms of transendothelial neutrophil migration in the lung, liver, kidney, and aorta. *Frontiers in Immunology* (2018) doi:10.3389/fimmu.2018.02739.
95. Simon, S. I., Hu, Y., Vestweber, D. & Smith, C. W. Neutrophil Tethering on E-Selectin Activates β 2 Integrin Binding to ICAM-1 Through a Mitogen-Activated Protein Kinase Signal Transduction Pathway . *J. Immunol.* (2000) doi:10.4049/jimmunol.164.8.4348.
96. Lawrence, M. B. & Springer, T. A. Neutrophils roll on E-selectin. *J. Immunol.* (1993).
97. Moore, K. L. *et al.* P-selectin glycoprotein ligand-1 mediates rolling of human neutrophils on P-selectin. *J. Cell Biol.* (1995) doi:10.1083/jcb.128.4.661.
98. Guthrie, L. A., McPhail, L. C., Henson, P. M. & Johnston, R. B. Priming of neutrophils for enhanced release of oxygen metabolites by bacterial lipopolysaccharide: Evidence for increased activity of the superoxide-producing enzyme. *J. Exp. Med.* (1984) doi:10.1084/jem.160.6.1656.
99. Vogt, K. L., Summers, C., Chilvers, E. R. & Condliffe, A. M. Priming and de-priming of neutrophil responses in vitro and in vivo. *European Journal of Clinical Investigation* (2018) doi:10.1111/eci.12967.
100. Massena, S. *et al.* Achemotactic gradient sequestered on endothelial heparan sulfate induces directional intraluminal crawling of neutrophils. *Blood* (2010) doi:10.1182/blood-2010-01-266072.
101. Wong, J. *et al.* A minimal role for selectins in the recruitment of leukocytes into the inflamed liver microvasculature. *J. Clin. Invest.* (1997) doi:10.1172/JCI119468.
102. Soehnlein, O. *et al.* Neutrophil secretion products pave the way for inflammatory monocytes. *Blood* **112**, 1461–1471 (2008).
103. Prame Kumar, K., Nicholls, A. J. & Wong, C. H. Y. Partners in crime: neutrophils and monocytes/macrophages in inflammation and disease. *Cell Tissue Res.* **371**, 551–565 (2018).
104. Soehnlein, O. & Lindbom, L. Neutrophil-derived azurocidin alarms the immune system. *J. Leukoc. Biol.* (2009) doi:10.1189/jlb.0808495.
105. Ng, L. G., Ostuni, R. & Hidalgo, A. Heterogeneity of neutrophils. *Nat. Rev. Immunol.* **19**, 255–265 (2019).

106. Silvestre-Roig, C., Hidalgo, A. & Soehnlein, O. Neutrophil heterogeneity: Implications for homeostasis and pathogenesis. *Blood* **127**, 2173–2181 (2016).
107. Pillay, J. *et al.* A subset of neutrophils in human systemic inflammation inhibits T cell responses through Mac-1. *J. Clin. Invest.* **122**, 327–336 (2012).
108. Dotta, L., Tassone, L. & Badolato, R. Clinical and Genetic Features of Warts, Hypogammaglobulinemia, Infections and Myelokathexis (WHIM) Syndrome. *Curr. Mol. Med.* (2011) doi:10.2174/156652411795677963.
109. Zeidler, C., Germeshausen, M., Klein, C. & Welte, K. Clinical implications of ELA2-, HAX1-, and G-CSF-receptor (CSF3R) mutations in severe congenital neutropenia. *British Journal of Haematology* (2009) doi:10.1111/j.1365-2141.2008.07425.x.
110. Marques, P. E. *et al.* Chemokines and mitochondrial products activate neutrophils to amplify organ injury during mouse acute liver failure. *Hepatology* **56**, 1971–82 (2012).
111. McDonald, B. & Kubes, P. Innate Immune Cell Trafficking and Function During Sterile Inflammation of the Liver. *Gastroenterology* **151**, 1087–1095 (2016).
112. Liu, Z. X., Han, D., Gunawan, B. & Kaplowitz, N. Neutrophil depletion protects against murine acetaminophen hepatotoxicity. *Hepatology* **43**, 1220–1230 (2006).
113. Marques, P. E. *et al.* Hepatic DNA deposition drives drug-induced liver injury and inflammation in mice. *Hepatology* **61**, 348–360 (2015).
114. Jaeschke, H. & Liu, J. Neutrophil depletion protects against murine acetaminophen hepatotoxicity: another perspective. *Hepatology* **45**, 1588–9; author reply 1589 (2007).
115. Bautista, A. P., Spolarics, Z., Jaeschke, H., Smith, C. W. & Spitzer, J. J. Antineutrophil monoclonal antibody (1F12) alters superoxide anion release by neutrophils and Kupffer cells. *J. Leukoc. Biol.* (1994) doi:10.1002/jlb.55.3.328.
116. Williams, C. D., Bajt, M. L., Farhood, A. & Jaeschke, H. Acetaminophen-induced hepatic neutrophil accumulation and inflammatory liver injury in CD18-deficient mice. *Liver Int.* **30**, 1280–1292 (2010).
117. Wang, J. *et al.* Visualizing the function and fate of neutrophils in sterile injury and repair. *Science* **358**, 111–116 (2017).
118. Massena, S. *et al.* Identification and characterization of VEGF-A-responsive neutrophils expressing CD49d, VEGFR1, and CXCR4 in mice and humans. *Blood* **126**, 2016–2026 (2015).
119. Christoffersson, G. *et al.* VEGF-A recruits a proangiogenic MMP-9-delivering neutrophil subset that induces angiogenesis in transplanted hypoxic tissue. *Blood* **120**, 4653–4662 (2012).
120. Buckley, C. D., Gilroy, D. W., Serhan, C. N., Stockinger, B. & Tak, P. P. The resolution of inflammation. *Nat. Rev. Immunol.* **13**, 59 (2012).
121. Serhan, C. N. & Savill, J. Resolution of inflammation: The beginning programs the end. *Nat. Immunol.* **6**, 1191–1197 (2005).
122. Tauzin, S., Starnes, T. W., Becker, F. B., Lam, P. ying & Huttenlocher, A. Redox and Src family kinase signaling control leukocyte wound attraction and neutrophil reverse migration. *J. Cell Biol.* **207**, 589–598 (2014).
123. Shin, K., Fogg, V. C. & Margolis, B. Tight Junctions and Cell Polarity. *Annu. Rev. Cell Dev. Biol.* **22**, 207–235 (2006).
124. Butler, M. T. & Wallingford, J. B. Planar cell polarity in development and disease. *Nat. Rev. Mol. Cell Biol.* **18**, 375–388 (2017).
125. Balda, M. S. & Matter, K. Tight junctions at a glance. *J. Cell Sci.* **121**, 3677–3682 (2008).
126. Brückner, B. R. & Janshoff, A. Importance of integrity of cell-cell junctions for the mechanics of confluent MDCK II cells. *Sci. Rep.* **8**, 14117 (2018).
127. Newsome, P. N. *et al.* Serum from patients with fulminant hepatic failure causes hepatocyte detachment and apoptosis by a β1-integrin pathway. *Hepatology* **40**, 636–645 (2004).
128. Gamal, W. *et al.* Low-dose acetaminophen induces early disruption of cell-cell tight junctions in human hepatic cells and mouse liver. *Sci. Rep.* **7**, 37541 (2017).
129. Harris, T. J. C. & Tepass, U. Adherens junctions: from molecules to morphogenesis. *Nat. Rev. Mol. Cell Biol.* **11**, 502 (2010).
130. Dejana, E., Orsenigo, F. & Lampugnani, M. G. The role of adherens junctions and VE-cadherin in the control of vascular permeability. *J. Cell Sci.* (2008) doi:10.1242/jcs.017897.
131. Matsuuchi, L. & Naus, C. C. Gap junction proteins on the move: Connexins, the cytoskeleton and migration. *Biochim. Biophys. Acta - Biomembr.* **1828**, 94–108 (2013).
132. Meşe, G., Richard, G. & White, T. W. Gap junctions: Basic structure and function. *J. Invest. Dermatol.* **127**, 2516–2524 (2007).
133. Contreras, J. E. *et al.* Role of connexin-based gap junction channels and hemichannels in

ischemia-induced cell death in nervous tissue. in *Brain Research Reviews* (2004). doi:10.1016/j.brainresrev.2004.08.002.

134. Nielsen, M. S. *et al.* Gap junctions. *Compr. Physiol.* **2**, 1981–2035 (2012).
135. Sáez, J. C., Retamal, M. A., Basilio, D., Bukauskas, F. F. & Bennett, M. V. L. Connexin-based gap junction hemichannels: Gating mechanisms. *Biochimica et Biophysica Acta - Biomembranes* (2005) doi:10.1016/j.bbamem.2005.01.014.
136. Laird, D. W. & Lampe, P. D. Therapeutic strategies targeting connexins. *Nat. Rev. Drug Discov.* **17**, 905–921 (2018).
137. Patel, S. J. *et al.* Gap junction inhibition prevents drug-induced liver toxicity and fulminant hepatic failure. *Nat. Biotechnol.* **30**, 179–83 (2012).
138. Du, K. *et al.* The gap junction inhibitor 2-aminoethoxy-diphenyl-borate protects against acetaminophen hepatotoxicity by inhibiting cytochrome P450 enzymes and c-jun N-terminal kinase activation. *Toxicol. Appl. Pharmacol.* **273**, 484–491 (2013).
139. Maes, M. *et al.* Connexin32: A mediator of acetaminophen-induced liver injury? *Toxicol. Mech. Methods* (2016) doi:10.3109/15376516.2015.1103000.
140. Saito, C., Shinzawa, K. & Tsujimoto, Y. Synchronized necrotic death of attached hepatocytes mediated via gap junctions. *Sci. Rep.* **4**, 1–8 (2014).
141. Maes, M. *et al.* Involvement of connexin43 in acetaminophen-induced liver injury. *Biochim. Biophys. Acta - Mol. Basis Dis.* **1862**, 1111–1121 (2016).
142. Culemann, S. *et al.* Locally renewing resident synovial macrophages provide a protective barrier for the joint. *Nature* (2019) doi:10.1038/s41586-019-1471-1.
143. Muñoz-Espín, D. & Serrano, M. Cellular senescence: from physiology to pathology. *Nat. Rev. Mol. Cell Biol.* **15**, 482–496 (2014).
144. Bird, T. G. *et al.* TGFβ inhibition restores a regenerative response in acute liver injury by suppressing paracrine senescence. *Sci. Transl. Med.* **10**, eaan1230 (2018).
145. Oubaha, M. *et al.* Senescence-associated secretory phenotype contributes to pathological angiogenesis in retinopathy. *Sci. Transl. Med.* **8**, 362ra144-362ra144 (2016).
146. Ferreira-Gonzalez, S. *et al.* Paracrine cellular senescence exacerbates biliary injury and impairs regeneration. *Nat. Commun.* **9**, 1020 (2018).
147. Bhushan, B. *et al.* Pro-regenerative signaling after acetaminophen-induced acute liver injury in mice identified using a novel incremental dose model. *Am. J. Pathol.* **184**, 3013–3025 (2014).
148. Wynn, T. a, Chawla, A. & Pollard, J. W. Macrophage biology in development, homeostasis and disease. *Nature* **496**, 445–55 (2013).
149. Soehnlein, O. & Lindbom, L. Phagocyte partnership during the onset and resolution of inflammation. *Nature Reviews Immunology* (2010) doi:10.1038/nri2779.
150. Boulter, L. *et al.* Macrophage-derived Wnt opposes Notch signaling to specify hepatic progenitor cell fate in chronic liver disease. *Nat. Med.* **18**, 572–579 (2012).
151. Kumanogoh, A. & Kikutani, H. Immunological functions of the neuropilins and plexins as receptors for semaphorins. *Nat. Rev. Immunol.* **13**, 802–14 (2013).
152. Worzfeld, T. & Offermanns, S. Semaphorins and plexins as therapeutic targets. *Nat. Rev. Drug Discov.* **13**, 603–21 (2014).
153. Alto, L. T. & Terman, J. R. Semaphorins and their Signaling Mechanisms. in *Methods in Molecular Biology* (ed. Terman, J. R.) vol. 1493 1–25 (Humana Press, 2017).
154. Comeau, M. R. *et al.* A poxvirus-encoded semaphorin induces cytokine production from monocytes and binds to a novel cellular semaphorin receptor, VESPR. *Immunity* **8**, 473–482 (1998).
155. Antipenko, A. *et al.* Structure of the Semaphorin-3A Receptor Binding Module. **39**, 589–598 (2003).
156. Love, C. A. *et al.* The ligand-binding face of the semaphorins revealed by the high-resolution crystal structure of SEMA4D. **10**, 843–848 (2003).
157. Nogi, T. *et al.* Structural basis for semaphorin signalling through the plexin receptor. *Nature* **467**, 1123–1127 (2010).
158. Liu, H. *et al.* Structural Basis of Semaphorin-Plexin Recognition and Viral Mimicry from Sema7A and A39R Complexes with PlexinC1. *Cell* **142**, 749–761 (2010).
159. Kruger, R. P., Aurandt, J. & Guan, K.-L. Semaphorins command cells to move. *Nat. Rev. Mol. Cell Biol.* **6**, 789–800 (2005).
160. Kong, Y. *et al.* Structural Basis for Plexin Activation and Regulation. *Neuron* **91**, 1–13 (2016).
161. Neufeld, G. *et al.* The semaphorins and their receptors as modulators of tumor progression. *Drug Resist. Updat.* **29**, 1–12 (2016).

162. Chauvet, S. *et al.* Gating of Sema3E/PlexinD1 Signaling by Neuropilin-1 Switches Axonal Repulsion to Attraction during Brain Development. *Neuron* **56**, 807–822 (2007).
163. Simons, M., Gordon, E. & Claesson-Welsh, L. Mechanisms and regulation of endothelial VEGF receptor signalling. *Nat. Rev. Mol. Cell Biol.* **17**, 611–625 (2016).
164. Glinka, Y. & Prud'homme, G. J. Neuropilin-1 is a receptor for transforming growth factor β-1, activates its latent form, and promotes regulatory T cell activity. *J. Leukoc. Biol.* **84**, 302–310 (2008).
165. Cao, Y. *et al.* Neuropilin-1 mediates divergent R-smad signaling and the myofibroblast phenotype. *J. Biol. Chem.* **285**, 31840–31848 (2010).
166. Sulpice, E. *et al.* Neuropilin-1 and neuropilin-2 act as coreceptors, potentiating proangiogenic activity. *Blood* **111**, 2036–2045 (2008).
167. Swiercz, J. M., Kuner, R., Behrens, J. & Offermanns, S. Plexin-B1 directly interacts with PDZ-RhoGEF/LARG to regulate RhoA and growth cone morphology. *Neuron* (2002) doi:10.1016/S0896-6273(02)00750-X.
168. Zhou, Y., Gunput, R. a F. & Pasterkamp, R. J. Semaphorin signaling: progress made and promises ahead. *Trends Biochem. Sci.* **33**, 161–170 (2008).
169. Piaton, G. *et al.* Class 3 semaphorins influence oligodendrocyte precursor recruitment and remyelination in adult central nervous system. *Brain* **134**, 1156–1167 (2011).
170. Bechara, A. *et al.* FAK-MAPK-dependent adhesion disassembly downstream of L1 contributes to semaphorin3A-induced collapse. *EMBO J.* (2008) doi:10.1038/emboj.2008.86.
171. Gutiérrez-Franco, A. *et al.* Differential expression of sema3A and sema7A in a murine model of multiple sclerosis: Implications for a therapeutic design. *Clin. Immunol.* **163**, 22–33 (2016).
172. Julien, F. *et al.* Dual functional activity of semaphorin 3B is required for positioning the anterior commissure. *Neuron* (2005) doi:10.1016/j.neuron.2005.08.033.
173. Sahay, A., Molliver, M. E., Ginty, D. D. & Kolodkin, A. L. Semaphorin 3F is critical for development of limbic system circuitry and is required in neurons for selective CNS axon guidance events. *J. Neurosci.* (2003).
174. Taniguchi, M. *et al.* Identification and characterization of a novel member of murine semaphorin family. *Genes to Cells* (2005) doi:10.1111/j.1365-2443.2005.00877.x.
175. Matsuoka, R. L. *et al.* Class 5 transmembrane semaphorins control selective mammalian retinal lamination and function. *Neuron* (2011) doi:10.1016/j.neuron.2011.06.009.
176. Pasterkamp, R. J., Peschon, J. J., Spriggs, M. K. & Kolodkin, A. L. Semaphorin 7A promotes axon outgrowth through integrins and MAPKs. *Nature* **424**, 398–405 (2003).
177. Moresco, E. M. Y., Donaldson, S., Williamson, A. & Koleske, A. J. Integrin-mediated dendrite branch maintenance requires Abelson (Abl) family kinases. *J. Neurosci.* **25**, 6105–6118 (2005).
178. Jongbloets, B. C. *et al.* Stage-specific functions of Semaphorin7A during adult hippocampal neurogenesis rely on distinct receptors. *Nat. Commun.* **8**, 14666 (2017).
179. Messina, A. *et al.* Dysregulation of semaphorin7A/B1-integrin signaling leads to defective GnRH-1 cell migration, abnormal gonadal development and altered fertility. *Hum. Mol. Genet.* **20**, 4759–4774 (2011).
180. Schellino, R. *et al.* Opposite-sex attraction in male mice requires testosterone-dependent regulation of adult olfactory bulb neurogenesis. *Sci. Rep.* **6**, 36063 (2016).
181. Ochsenbein, A. M. *et al.* Endothelial cell-derived semaphorin 3A inhibits filopodia formation by blood vascular tip cells. *J. Cell Sci.* **129**, e1.1-e1.1 (2016).
182. Gu, C. *et al.* Semaphorin 3E and plexin-D1 control vascular pattern independently of neuropilins. *Science (80-.).* **307**, 265–268 (2005).
183. Acevedo, L. M., Barillas, S., Weis, S. M. & Göthert, J. R. Semaphorin 3A suppresses VEGF-mediated angiogenesis yet acts as a vascular permeability factor Correspondence should be addressed to : *Online* **2232**, 2674–2681 (2008).
184. Le Guelte, A. *et al.* Semaphorin 3A elevates endothelial cell permeability through PP2A inactivation. *J. Cell Sci.* **125**, 4137–4146 (2012).
185. Hou, S. T. *et al.* Semaphorin3A elevates vascular permeability and contributes to cerebral ischemia-induced brain damage. *Sci. Rep.* **5**, (2015).
186. Yagai, T., Miyajima, A. & Tanaka, M. Semaphorin 3E secreted by damaged hepatocytes regulates the sinusoidal regeneration and liver fibrosis during liver regeneration. *Am. J. Pathol.* **184**, 2250–2259 (2014).
187. Basile, J. R., Barac, A., Zhu, T., Guan, K. L. & Gutkind, J. S. Class IV semaphorins promote angiogenesis by stimulating Rho-initiated pathways through plexin-B. *Cancer Res.* (2004) doi:10.1158/0008-5472.CAN-04-0126.

188. Zhou, H., Binmadi, N. O., Yang, Y. H., Proia, P. & Basile, J. R. Semaphorin 4D cooperates with VEGF to promote angiogenesis and tumor progression. *Angiogenesis* (2012) doi:10.1007/s10456-012-9268-y.
189. Serini, G. *et al.* Class 3 semaphorins control vascular morphogenesis by inhibiting integrin function. *Nature* **424**, 391–7 (2003).
190. Neufeld, G., Sabag, A. D., Rabinovicz, N. & Kessler, O. Semaphorins in Angiogenesis and Tumor Progression. *Cold Spring Harb. Perspect. Med.* **2**, a006718–a006718 (2012).
191. Garcia-Areas, R. *et al.* Semaphorin7A promotes tumor growth and exerts a pro-angiogenic effect in macrophages of mammary tumor-bearing mice. *Front. Physiol.* **5**, 1–13 (2014).
192. Bougeret, C., Schmid, M., Inserm, F., Hdpital, U. & Claude, S. A. Increased surface expression of a newly identified 150-kDa dimer early after human T lymphocyte activation . Bensussan and L Boumsell • Rapid Reviews ! 30 days * from submission to initial decision Information about subscribing to The Journal of Immunolog. *J. Immunol.* **148**, 318–323 (1992).
193. Nishide, M. & Kumanogoh, A. The role of semaphorins in immune responses and autoimmune rheumatic diseases. *Nat. Rev. Rheumatol.* **14**, 91–103 (2018).
194. Ishida, I. *et al.* Involvement of CD100, a lymphocyte semaphorin, in the activation of the human immune system via CD72: Implications for the regulation of immune and inflammatory responses. *Int. Immunol.* **15**, 1027–1034 (2003).
195. Caligaris-Cappio, F. *et al.* CD100/plexin-B1 interactions sustain proliferation and survival of normal and leukemic CD5+ B lymphocytes. *Blood* **101**, 1962–1969 (2003).
196. Nishide, M. *et al.* Semaphorin 4D inhibits neutrophil activation and is involved in the pathogenesis of neutrophil-mediated autoimmune vasculitis. *Ann. Rheum. Dis.* **76**, 1440–1448 (2017).
197. Ishida, I. *et al.* Class IV semaphorin Sema4A enhances T-cell activation and interacts with Tim-2. *Nature* **419**, 629–633 (2002).
198. Constantinescu, C. S., Farooqi, N., O'Brien, K. & Gran, B. Experimental autoimmune encephalomyelitis (EAE) as a model for multiple sclerosis (MS). *Br. J. Pharmacol.* **164**, 1079–1106 (2011).
199. Delgoffe, G. M. *et al.* Stability and function of regulatory T cells is maintained by a neuropilin-1-semaphorin-4a axis. *Nature* **501**, 252–256 (2013).
200. Nkyimbeng-Takwi, E. H. *et al.* Neuroimmune semaphorin 4A downregulates the severity of allergic response. *Mucosal Immunol.* **5**, 409–419 (2012).
201. Mogie, G. *et al.* Neuroimmune semaphorin 4A as a drug and drug target for asthma. *Int. Immunopharmacol.* **17**, 568–75 (2013).
202. Catalano, A. *et al.* Semaphorin-3A is expressed by tumor cells and alters T-cell signal transduction and function. *Blood* **107**, 3321–3329 (2006).
203. Yamamoto, M. *et al.* Plexin-A4 negatively regulates T lymphocyte responses. *Int. Immunol.* **20**, 413–420 (2008).
204. Takamatsu, H. *et al.* Semaphorins guide the entry of dendritic cells into the lymphatics by activating myosin II. *Nat. Immunol.* **11**, 594–600 (2010).
205. Wen, H., Lei, Y., Eun, S.-Y. & P.-Y. Ting, J. Plexin-A4–semaphorin 3A signaling is required for Toll-like receptor– and sepsis-induced cytokine storm. *J. Exp. Med.* **207**, 2943–2957 (2010).
206. Shimizu, I. *et al.* Semaphorin3E-induced inflammation contributes to insulin resistance in dietary obesity. *Cell Metab.* **18**, 491–504 (2013).
207. Movassagh, H. *et al.* Chemorepellent Semaphorin 3E Negatively Regulates Neutrophil Migration In Vitro and In Vivo. *J. Immunol.* 1601093 (2016) doi:10.4049/jimmunol.1601093.
208. Hsieh, C. S. *et al.* Development of T H 1 CD4 + T cells through IL-12 produced by Listeria-induced macrophages. *Science (80-.).* (1993) doi:10.1126/science.8097338.
209. Jongbloets, B. C., Ramakers, G. M. J. J. & Pasterkamp, R. J. Semaphorin7A and its receptors: Pleiotropic regulators of immune cell function, bone homeostasis, and neural development. *Semin. Cell Dev. Biol.* **24**, 129–138 (2013).
210. Sato, Y. & Takahashi, H. Molecular cloning and expression of murine homologue of semaphorin K1 gene. *Biochim. Biophys. Acta - Gene Struct. Expr.* (1998) doi:10.1016/S0167-4781(98)00245-0.
211. Morote-Garcia, J. C. *et al.* Endothelial Semaphorin 7A promotes neutrophil migration during hypoxia. *Proc. Natl. Acad. Sci. U. S. A.* **109**, 14146–51 (2012).
212. Roth, J. M., Köhler, D., Schneider, M., Granja, T. F. & Rosenberger, P. Semaphorin 7A aggravates pulmonary inflammation during lung injury. *PLoS One* **11**, 1–14 (2016).
213. Allegra, M. *et al.* Semaphorin-7a reverses the ERF-induced inhibition of EMT in Ras-dependent mouse mammary epithelial cells. *Mol. Biol. Cell* **23**, 3873–3881 (2012).

214. Bravo-Cordero, J. J., Magalhaes, M. A. O., Eddy, R. J., Hodgson, L. & Condeelis, J. Functions of cofilin in cell locomotion and invasion. *Nat. Rev. Mol. Cell Biol.* **14**, 405–417 (2013).
215. DesMarais, V., Ghosh, M., Eddy, R. & Condeelis, J. Cofilin takes the lead. *J. Cell Sci.* **118**, 19–26 (2005).
216. Scott, G. A., McClelland, L. A. & Fricke, A. F. Semaphorin 7a Promotes Spreading and Dendricity in Human Melanocytes through β1-Integrins. *J. Invest. Dermatol.* **128**, 151–161 (2008).
217. Scott, G. a, McClelland, L. a, Fricke, A. F. & Fender, A. Plexin C1, A Receptor for Semaphorin 7A, Inactivates Cofilin and Is a Potential Tumor Suppressor for Melanoma Progression. *J. Invest. Dermatol.* **129**, 954–963 (2009).
218. Walzer, T., Galibert, L., Comeau, M. R. & De Smedt, T. Plexin C1 Engagement on Mouse Dendritic Cells by Viral Semaphorin A39R Induces Actin Cytoskeleton Rearrangement and Inhibits Integrin-Mediated Adhesion and Chemokine-Induced Migration. *J. Immunol.* **174**, 51–59 (2005).
219. Myster, F. *et al.* Viral Semaphorin Inhibits Dendritic Cell Phagocytosis and Migration but Is Not Essential for Gammaherpesvirus-Induced Lymphoproliferation in Malignant Catarrhal Fever. *J. Virol.* **89**, 3630–3647 (2015).
220. Fukunishi, A. *et al.* The action of Semaphorin7A on thalamocortical axon branching. *J. Neurochem.* **118**, 1008–1015 (2011).
221. Chabrat, A. *et al.* Transcriptional repression of Plxnc1 by Lmx1a and Lmx1b directs topographic dopaminergic circuit formation. *Nat. Commun.* **8**, 933 (2017).
222. Ohsawa, S. *et al.* Caspase-9 activation revealed by semaphorin 7A cleavage is independent of apoptosis in the aged olfactory bulb. *J. Neurosci.* **29**, 11385–92 (2009).
223. Ohsawa, S. *et al.* Maturation of the olfactory sensory neurons by Apaf-1/caspase-9-mediated caspase activity. *Proc. Natl. Acad. Sci. U. S. A.* **107**, 13366–71 (2010).
224. Lee, H., Macpherson, L. J., Parada, C. A., Zuker, C. S. & Ryba, N. J. P. Rewiring the taste system. *Nature* **548**, 330–333 (2017).
225. Kopp, M. a., Brommer, B., Gatzemeier, N., Schwab, J. M. & Prüss, H. Spinal cord injury induces differential expression of the profibrotic semaphorin 7A in the developing and mature glial scar. *Glia* **58**, 1748–1756 (2010).
226. Giacobini, P. & Prevot, V. Semaphorins in the development, homeostasis and disease of hormone systems. *Semin. Cell Dev. Biol.* **24**, 190–198 (2013).
227. Parkash, J. *et al.* Semaphorin7A regulates neuroglial plasticity in the adult hypothalamic median eminence. *Nat. Commun.* **6**, 6385 (2015).
228. Holmes, S. *et al.* Sema7A is a potent monocyte stimulator. *Scand. J. Immunol.* **56**, 270–275 (2002).
229. Elder, A. M. *et al.* Semaphorin 7A promotes macrophage-mediated lymphatic remodeling during postpartum mammary gland involution and in breast cancer. *Cancer Res.* **78**, 6473–6485 (2018).
230. van Rijn, A. *et al.* Semaphorin 7A Promotes Chemokine-Driven Dendritic Cell Migration. *J. Immunol.* **196**, 459–468 (2016).
231. Suzuki, K. *et al.* Semaphorin 7A initiates T-cell-mediated inflammatory responses through alpha1beta1 integrin. *Nature* **446**, 680–4 (2007).
232. Xie, J. & Wang, H. Semaphorin 7A as a potential immune regulator and promising therapeutic target in rheumatoid arthritis. *Arthritis Res. Ther.* **19**, 10 (2017).
233. Fong, K. P. *et al.* Deciphering the human platelet sheddome. *Blood* **117**, 15–27 (2011).
234. Seltsam, A. *et al.* The molecular diversity of Sema7A, the semaphorin that carries the JMH blood group antigens. *Transfusion* **47**, 133–146 (2007).
235. Gras, C. *et al.* Semaphorin 7A protein variants differentially regulate T-cell activity. *Transfusion* **53**, 270–283 (2013).
236. Kang, S. *et al.* Intestinal epithelial cell-derived semaphorin 7A negatively regulates development of colitis via αvβ1 integrin. *J. Immunol.* **188**, 1108–16 (2012).
237. Granja, T. *et al.* Crucial role of Plexin C1 for pulmonary inflammation and survival during lung injury. *Mucosal Immunol.* **7**, 879–91 (2014).
238. König, K. *et al.* The plexin C1 receptor promotes acute inflammation. *Eur. J. Immunol.* **44**, 2648–2658 (2014).
239. Walzer, T., Galibert, L. & De Smedt, T. Poxvirus semaphorin A39R inhibits phagocytosis by dendritic cells and neutrophils. *Eur. J. Immunol.* **35**, 391–398 (2005).
240. Black, S. A. S. A., Nelson, A. C. A. C. A. C. A., Gurule, N. J. N. J. N. J., Futscher, B. W. B. W. B. W. B. W. B. W. B. & Lyons, T. R. T. Semaphorin 7a exerts pleiotropic effects to promote breast tumor progression. *Oncogene* **35**, 1–9 (2016).

241. Garcia-Areas, R. *et al.* Suppression of tumor-derived Semaphorin 7A and genetic ablation of host-derived Semaphorin 7A impairs tumor progression in a murine model of advanced breast carcinoma. *Int. J. Oncol.* **51**, 1395–1404 (2017).
242. Saito, T. *et al.* Semaphorin7A promotion of tumoral growth and metastasis in human oral cancer by regulation of g1 cell cycle and matrix metalloproteases: Possible contribution to tumoral angiogenesis. *PLoS One* **10**, 1–20 (2015).
243. Chen, Y., Soong, J., Mohanty, S., Xu, L. & Scott, G. The neural guidance receptor Plexin C1 delays melanoma progression. *Oncogene* **32**, 4941–9 (2013).
244. Lazova, R., Gould Rothberg, B. E., Rimm, D. & Scott, G. The semaphorin 7A receptor plexin C1 Is lost during melanoma metastasis. *Am. J. Dermatopathol.* (2009) doi:10.1097/DAD.0b013e318196672d.
245. König, K. *et al.* Inhibition of Plexin C1 Protects Against Hepatic Ischemia-Reperfusion Injury. *Crit. Care Med.* **44**, e625-32 (2016).
246. De Minicis, S. *et al.* Semaphorin 7A contributes to TGF-β-mediated liver fibrogenesis. *Am. J. Pathol.* **183**, 820–30 (2013).
247. Kang, H.-R., Lee, C. G., Homer, R. J. & Elias, J. a. Semaphorin 7A plays a critical role in TGF-beta1-induced pulmonary fibrosis. *J. Exp. Med.* **204**, 1083–93 (2007).
248. Lu, S. C. Glutsthione Synthesis. *Biochim Biophys Acta.* **1830**, 3143–3153 (2014).
249. Du, K., Williams, C. D., McGill, M. R. & Jaeschke, H. Lower susceptibility of female mice to acetaminophen hepatotoxicity: Role of mitochondrial glutathione, oxidant stress and c-jun N-terminal kinase. *Toxicol. Appl. Pharmacol.* **281**, 58–66 (2014).
250. Masubuchi, Y., Nakayama, J. & Watanabe, Y. Sex difference in susceptibility to acetaminophen hepatotoxicity is reversed by buthionine sulfoximine. *Toxicology* **287**, 54–60 (2011).
251. Lu, Y. *et al.* Immature mice are more susceptible than adult mice to acetaminophen-induced acute liver injury. *Sci. Rep.* **7**, 1–11 (2017).
252. Harrill, A. H. *et al.* Mouse population-guided resequencing reveals that variants in CD44 contribute to acetaminophen-induced liver injury in humans. *Genome Res.* **19**, 1507–1515 (2009).
253. Lynch, R. W. *et al.* An efficient method to isolate Kupffer cells eliminating endothelial cell contamination and selective bias. *J. Leukoc. Biol.* **104**, 579–586 (2018).
254. Ghosn, E. E. B., Yang, Y., Tung, J., Herzenberg, L. A. & Herzenberg, L. A. CD11b expression distinguishes sequential stages of peritoneal B-1 development. *Proc. Natl. Acad. Sci. U. S. A.* **105**, 5195–5200 (2008).
255. Moore, J. K. *et al.* Patients with the worst outcomes after paracetamol (acetaminophen)-induced liver failure have an early monocytopenia. *Aliment. Pharmacol. Ther.* **45**, 443–454 (2017).
256. Thieblemont, N., Witko-Sarsat, V. & Ariel, A. Regulation of macrophage activation by proteins expressed on apoptotic neutrophils: Subversion towards autoimmunity by proteinase 3. *Eur. J. Clin. Invest.* **48**, 1–10 (2018).
257. Dara, L., Liu, Z.-X. & Kaplowitz, N. Questions and controversies: the role of necroptosis in liver disease. *Cell Death Discov.* **2**, 16089 (2016).
258. Yanger, K. *et al.* Adult Hepatocytes Are Generated by Self-Duplication Rather than Stem Cell Differentiation. *Cell Stem Cell* **15**, 340–349 (2014).
259. Roskams, T. a. *et al.* Nomenclature of the finer branches of the biliary tree: Canals, ductules, and ductular reactions in human livers. *Hepatology* **39**, 1739–1745 (2004).
260. Poisson, J. *et al.* Liver sinusoidal endothelial cells: Physiology and role in liver diseases. *J. Hepatol.* **66**, 212–227 (2017).
261. Kim, W. R., Flamm, S. L., Di Bisceglie, A. M. & Bodenheimer, H. C. Serum activity of alanine aminotransferase (ALT) as an indicator of health and disease. *Hepatology* **47**, 1363–1370 (2008).
262. Tamagnone, L. *et al.* Plexins are a large family of receptors for transmembrane, secreted, and GPI-anchored semaphorins in vertebrates. *Cell* **99**, 71–80 (1999).
263. Van Rossen, E. *et al.* Vinculin and cellular retinol-binding protein-1 are markers for quiescent and activated hepatic stellate cells in formalin-fixed paraffin embedded human liver. *Histochem. Cell Biol.* **131**, 313–325 (2009).
264. Ramadori, G. & Saile, B. Mesenchymal cells in the liver - One cell type or two? *Liver* **22**, 283–294 (2002).
265. Speicher, T. *et al.* Knockdown and knockout of β1-integrin in hepatocytes impairs liver regeneration through inhibition of growth factor signalling. *Nat. Commun.* **5**, 3862 (2014).
266. Chang, W. *et al.* Early activated hepatic stellate cell-derived paracrine molecules modulate acute

liver injury and regeneration. *Lab. Investig.* **97**, 318–328 (2017).

267. Chang, W.-J. Early activated hepatic stellate cell-derived molecules reverse acute hepatic injury. *World J. Gastroenterol.* **21**, 4184 (2015).
268. Campisi, J. & d'Adda di Fagagna, F. Cellular senescence: when bad things happen to good cells. *Nat. Rev. Mol. Cell Biol.* **8**, 729–740 (2007).
269. McMillin, M. *et al.* The TGFβ1 Receptor Antagonist GW788388 Reduces JNK Activation and Protects Against Acetaminophen Hepatotoxicity in Mice. *Toxicol. Sci.* **170**, 549–561 (2019).
270. Gowda, S. *et al.* A review on laboratory liver function tests. *Pan Afr. Med. J.* **3**, 17 (2009).
271. Thapa, B. R. & Walia Anuj. Symposium : Newer Diagnostic Tests Liver Function Tests and their Interpretation. *Indian J. Pediatr.* **74**, 663–671 (2007).
272. McCuskey, R. S. The hepatic microvascular system in health and its response to toxicants. *Anat. Rec.* **291**, 661–671 (2008).
273. Ito, Y., Abril, E. R., Bethea, N. W. & McCuskey, R. S. Inhibition of matrix metalloproteinases minimizes hepatic microvascular injury in response to acetaminophen in mice. *Toxicol. Sci.* **83**, 190–196 (2005).
274. Long, E. O. ICAM-1: Getting a Grip on Leukocyte Adhesion. *J. Immunol.* **186**, 5021–5023 (2011).
275. Bianchi, M. E. *et al.* High-mobility group box 1 protein orchestrates responses to tissue damage via inflammation, innate and adaptive immunity, and tissue repair. *Immunol. Rev.* **280**, 74–82 (2017).
276. Bianchi, M. E. & Manfredi, A. A. How macrophages ring the inflammation alarm. *Proc. Natl. Acad. Sci.* **111**, 2866–2867 (2014).
277. Venereau, E. *et al.* Mutually exclusive redox forms of HMGB1 promote cell recruitment or proinflammatory cytokine release. *J. Gen. Physiol.* **140**, i6–i6 (2012).
278. Antoine, D. J. *et al.* Mechanistic biomarkers provide early and sensitive detection of acetaminophen-induced acute liver injury at first presentation to hospital. *Hepatology* **58**, 777–787 (2013).
279. Lundbäck, P. *et al.* A novel high mobility group box 1 neutralizing chimeric antibody attenuates drug-induced liver injury and postinjury inflammation in mice. *Hepatology* **64**, 1699–1710 (2016).
280. Lee, J. L. & Streuli, C. H. Integrins and epithelial cell polarity. *J. Cell Sci.* **127**, 3217–3225 (2014).
281. Smyth, J. W. *et al.* Actin cytoskeleton rest stops regulate anterograde traffic of connexin 43 vesicles to the plasma membrane. *Circ. Res.* **110**, 978–89 (2012).
282. Lee, J. *et al.* Chemokine binding and activities mediated by the mouse IL-8 receptor. *J. Immunol.* **155**, 2158–64 (1995).
283. Hey, Y. Y., Tan, J. K. H. & O'Neill, H. C. Redefining myeloid cell subsets in murine spleen. *Front. Immunol.* **6**, 1–12 (2016).
284. Mayadas, T. N., Cullere, X. & Lowell, C. A. The Multifaceted Functions of Neutrophils. *Annu. Rev. Pathol. Mech. Dis.* **9**, 181–218 (2013).
285. Perfetto, S. P. *et al.* Amine-reactive dyes for dead cell discrimination in fixed samples. *Curr. Protoc. Cytom.* 1–20 (2010) doi:10.1002/0471142956.cy0934s53.
286. Montes, M., Jaensson, E. A., Orozco, A. F., Lewis, D. E. & Corry, D. B. A general method for bead-enhanced quantitation by flow cytometry. *J. Immunol. Methods* **317**, 45–55 (2006).
287. Shi, C. & Pamer, E. G. Monocyte recruitment during infection and inflammation. *Nat. Rev. Immunol.* **11**, 762–774 (2011).
288. Springer, T. A. Adhesion receptors of the immune system. *Nature* (1990) doi:10.1038/346425a0.
289. Li, N. *et al.* Distinct Binding Affinities of Mac-1 and LFA-1 in Neutrophil Activation. *J. Immunol.* **190**, 4371–4381 (2013).
290. Liew, P. X., Lee, W. Y. & Kubes, P. iNKT Cells Orchestrate a Switch from Inflammation to Resolution of Sterile Liver Injury. *Immunity* **47**, 752-765.e5 (2017).
291. Hart, S. P., Ross, J. A., Ross, K., Haslett, C. & Dransfield, I. Molecular characterization of the surface of apoptotic neutrophils: Implications for functional downregulation and recognition by phagocytes. *Cell Death Differ.* **7**, 493–503 (2000).
292. Barnes, T. C., Anderson, M. E. & Moots, R. J. The many faces of interleukin-6: The role of IL-6 in inflammation, vasculopathy, and fibrosis in systemic sclerosis. *Int. J. Rheumatol.* **2011**, (2011).
293. Hurst, S. M. *et al.* IL-6 and its soluble receptor orchestrate a temporal switch in the pattern of leukocyte recruitment seen during acute inflammation. *Immunity* **14**, 705–714 (2001).
294. Fuster, J. J. & Walsh, K. The good, the bad, and the ugly of interleukin-6 signaling. *EMBO J.* **33**, 1425–1427 (2014).
295. Davoust, J., Palucka, A. K., Chomarat, P. & Banchereau, J. IL-6 switches the differentiation of

monocytes from dendritic cells to macrophages. *Nat. Immunol.* **1**, 510–514 (2000).

296. Dal-Secco, D. *et al.* A dynamic spectrum of monocytes arising from the in situ reprogramming of CCR2+ monocytes at a site of sterile injury. *J. Exp. Med.* **212**, 447–56 (2015).
297. Peterson, L. W. & Artis, D. Intestinal epithelial cells: Regulators of barrier function and immune homeostasis. *Nat. Rev. Immunol.* **14**, 141–153 (2014).
298. Leoni, G., Neumann, P. A., Sumagin, R., Denning, T. L. & Nusrat, A. Wound repair: Role of immune-epithelial interactions. *Mucosal Immunol.* **8**, 959–968 (2015).
299. Proksch, E., Brandner, J. M. & Jensen, J. M. The skin: An indispensable barrier. *Exp. Dermatol.* **17**, 1063–1072 (2008).
300. Pasparakis, M., Haase, I. & Nestle, F. O. Mechanisms regulating skin immunity and inflammation. *Nat. Rev. Immunol.* **14**, 289–301 (2014).
301. Bukhari, S., Mertz, A. F. & Naik, S. Eavesdropping on the conversation between immune cells and the skin epithelium. *Int. Immunol.* **31**, 415–422 (2019).
302. Copple, B. L. Phenotypic Changes in Hepatic Stellate Cells in Response to Toxic Liver Injury. *Curr. Pathobiol. Rep.* **2**, 155–162 (2014).
303. Thiele, N. D. *et al.* TIMP-1 is upregulated, but not essential in hepatic fibrogenesis and carcinogenesis in mice. *Sci. Rep.* **7**, 714 (2017).
304. Wen, Y. *et al.* Metabolic modulation of acetaminophen-induced hepatotoxicity by osteopontin. *Cell. Mol. Immunol.* 1–12 (2018) doi:10.1038/s41423-018-0033-z.
305. Krishna, M. Patterns of necrosis in liver disease. *Clin. Liver Dis.* **10**, 53–56 (2017).